A NEW APPROACH TO VALIDATE SUBGRID MODELS IN COMPLEX HIGH REYNOLDS NUMBER FLOWS

Annual Report for the Period: June, 1994 -May, 1995
Grant Number: N00014-93-1-0342

Suresh Menon
School of Aerospace Engineering
Georgia Institute of Technology
Atlanta, Georgia 30332-0150

E-16-97-82

REPORT DOCUMENTATION PAGE

Form Approved
OMB No. 0704-0188

1. AGENCY USE ONLY (Leave Blank)	2. REPORT DATE	3. REPORT TYPE AND DATES COVERED
	June 1996	Annual Rpt., June 1994 - May 1995

4. TITLE AND SUBTITLE A New Approach to Validate Subgrid Models in Complex High Reynolds Number Flows

5. FUNDING NUMBERS
N00014-93-1-0342

6. AUTHOR(S) Suresh Menon

7. PERFORMING ORGANIZATION NAME(S) AND ADDRESS(ES)
Dr. Suresh Menon
School of Aerospace Engineering
Georgia Institute of Technology
Atlanta, Georgia 30332-0150

8. PERFORMING ORGANIZATION REPORT NUMBER

9. SPONSORING/MONITORING AGENCY NAME(S) AND ADDRESS(ES)
Office of Naval Research
Atlanta Regional Office
101 Marietta Tower
101 Mareitta St., Suite 2805
Atlanta, GA 30323-0008

10. SPONSORING/MONITORING AGENCY REPORT NUMBER

11. SUPPLEMENTARY NOTES COR:

12a. DISTRIBUTION/AVAILABILITY STATEMENT
Unlimited

12b. DISTRIBUTION CODE

13. ABSTRACT *(Maximum 200 words)*

A dynamic subgrid model was developed by using a method that employed the scale similarity concept for validating the behavior of the subgrid models. Since the scale similarity approach can be used directly in the physical space, there was no need to employ spectral space information for implementing the subgrid model (although spectral space analysis was carried out to compare with past models). Thus, the new dynamic approach has potential for application to more complex flows. The key feature of the dynamic model is that it is a truly local model and does not require any type of averaging for a range of flow problems. The flow fields where no averaging was required are: (i) Taylor-Green flow, (ii) decaying isotropic turbulence, (iii) forced isotropic turbulence, iv) temporal mixing layers and, (v) free circular jet with axial entrainment.

14. SUBJECT TERMS	15. NUMBER OF PAGES
Large eddy simulations, Dynamic model, Subgrid model.	200
	16. PRICE CODE

17. SECURITY CLASSIFICATION OF REPORT	18. SECURITY CLASSIFICATION OF THIS PAGE	19. SECURITY CLASSIFICATION OF ABSTRACT	20. LIMITATION OF ABSTRACT
Unclassified	Unclassified	Unclassified	Unlimited

A NEW APPROACH TO VALIDATE SUBGRID MODELS IN COMPLEX HIGH REYNOLDS NUMBER FLOWS

Annual Report for the Period: June, 1994 -May, 1995
Grant Number: N00014-93-1-0342

Suresh Menon
School of Aerospace Engineering
Georgia Institute of Technology
Atlanta, Georgia 30332-0150

1. INTRODUCTION

This second annual report summarizes the progress made in the last year. The overall objectives of this research are to develop new methods to evaluate subgrid models and then to utilize these methods to improve the chosen subgrid models. The subgrid models investigated in this research are chosen primarily for application in high Reynolds number complex flows. A key breakthrough this year was the development of a new localized dynamic subgrid model that no longer requires the Germano's identity; however, it is still dynamic model. This model was developed by using a method that employed the scale similarity concept for validating the behavior of the subgrid models . Since the scale similarity approach can be used directly in the physical space, there was no need to employ spectral space information for implementing the subgrid model (although spectral space analysis was carried out to compare with past models). Thus, the new dynamic approach has potential for application to more complex flows. The key feature of the dynamic model is that it is a truly local model and does not require any type of averaging for a range of flow problems. The flow fields were no averaging was required are: (i) Taylor-Green flow, (ii) Decaying Isotropic turbulence, (iii) Forced isotropic turbulence, (iv) Temporal mixing layers and, (v) free circular jet with axial entrainment. Some modifications (including cross-stream averaging) were required to handle more complex flows such as (vi) turbulent Couette flow. However, preliminary results suggest that the cross-stream averaging for the wall bounded flows may be a limitation of the dissipation term in the one-equation subgrid model and not in the local dynamic modeling concept developed here. These issues are currently being addressed and we believe that it will be possible to develop a truly local dynamic subgrid model for even very complex flows.

The results obtained so far are discussed in detail in the preprints of the papers (Menon et al., 1995; Kim and Menon, 1995a, 1995b; Menon and Kim, 1995; Chakravarty and Menon, 1995) that are included as appendices. For the flows studied so far, the results clearly show that the proposed model is (i) superior to classical eddy viscosity based dynamic model, (ii) can predict the flow accurately using relatively coarse grids, and (iii) is computationally very efficient. In the following, we summarizes the highlights of the research carried out in the last year.

2. DEVELOPMENT OF A NEW LOCALIZED DYNAMIC MODEL

In the earlier studies (Menon and Yeung, 1994; Menon et al., 1995) various subgrid models were analyzed to investigate their behavior in predicting the subgrid stresses and energy transfer. Using cross-correlation analysis, it was determined that classical subgrid models (such as the Smagorinsky's eddy viscosity model and the constant coefficient model for the subgrid kinetic energy) are not able to reproduce accurately the subgrid stresses. On the other hand, dynamic models such as the Germano's dynamic model and a new dynamic model for the subgrid kinetic energy (Menon et al., 1994; 1995) clearly showed superior ability to reproduce the subgrid stresses and the energy transfer. More interestingly, the dynamic model for the subgrid kinetic energy appeared to have the potential for modeling the subgrid terms accurately even when relatively coarse grids were employed. Since the one equation model for the subgrid kinetic energy was chosen for simulating high Reynolds number LES, this result was particularly encouraging. It is expected that for high Reynolds number LES of complex flows, the grid resolution practically possible (due to resource constraints) will be limited. Therefore, simple dissipative models (even with dynamic evaluations) may not be sufficient for practical LES. In addition, the assumption of local equilibrium between the production and dissipation of the kinetic energy (an assumption implicit in all algebraic eddy viscosity models) is violated (as shown in Kim and Menon, 1995a). It was therefore, important that the ability of the kinetic energy model be demonstrated for high Reynolds number flows. This was accomplished recently using simple flows but at relatively high Reynolds number flows (e.g., $Re_\lambda = 250$) using very coarse grids (e.g., 32^3). These results are reported in Menon and Kim (1995) and Kim and Menon (1995b).

A limitation of the Germano's method was that some form of local or global averaging was required to ensure stability of the simulation. This averaging was required due to the inherent deficiencies of the Germano's dynamic method such as the mathematical inconsistent derivation and ill-conditioning problem of the dynamic formulation and the prolonged presence of negative model coefficient. These limitations were removed by Carati et al. (1995) recently using a localized model; however, their model required solution of the subgrid kinetic energy to constraint the coefficient and furthermore, two additional equations had to be solved. The computational cost was quite severe for this approach. The limitations with the Germano's approach have been overcome in the present formulation using a different approach based on local scale similarity and a new truly local (in both time and space) evaluation of the coefficients has been constructed for the one-equation subgrid model for the subgrid kinetic energy. Moreover, the new approach no longer requires application of the Germano's identity which was the cause of the ill-conditioning problem and, the localized model coefficients obtained from this model have been shown to be Galilean-invariant and very realizable. In addition, the computational cost for the new model is minimal compared to other techniques.The properties of this model has been studied by applying it to various flows and comparing its prediction with DNS and experimental data. It has been shown that very high Re flows can be simulated relatively accurately using very coarse grids provided the scale-similarity requirements are satisfied. The predictions have also been compared to the predictions using the Germano's model (which is unstable without averaging) and the results suggest that the proposed new local model is capable of predicting results using coarser grid and without using any global or local averaging.

3. DEVELOPMENT OF A METHOD FOR COMPLEX FLOWS WITH AND WITHOUT CHEMICAL REACTIONS ON A NON-STAGGERED GRIDS

A new method for solving the time dependent Navier-Stokes equations has been recently developed using the low-Mach number approximation. The low Mach number approximation allows the study of reacting flows where the effect of acoustics is negligible. This methodology was developed to study complex flows with and without chemical reactions. The key feature of this method is the non-staggered formulation (unlike the staggered methods) used within the fractional step scheme. The non-staggered formulation was developed to address some fundamental issues in LES modeling. For example, when staggered grids are employed, the flow velocity components are defined at half-points that are not coincident. Thus, when filtering is carried out (specially for dynamic approach), the filtered variables are not at the same physical location. In the past studies using staggered grids (e.g., Carati et al., 1995) this issue has been ignored. However, it is not clear if this issue is not important for complex flows, specially when coarse grids are employed. A non-staggered scheme is required to remove this problem. In addition to this capability another interesting feature of the non-staggered method is that it allows the same scheme to work without any modifications for flow with and without chemical reactions. An implicit scheme is used for time advancement and a multigrid solver is used to solve the Poisson equation for pressure. The scheme has been validated for a variety of flows using both DNS and LES. The flows studied so far include: (i) isotropic turbulence, (ii) temporal mixing layers with and without heat release, (iii) plane Couette flow and (iv) laminar and turbulent round jets. The last two flows are considered the building blocks for analyzing the subgrid models in flows with walls and in more complex flows such as the turbulent, swirling free jet. Preliminary studies (reported in Chakravarty and Menon, 1995) show that the dissipation term in the subgrid kinetic energy needs to be modified to handle flows near walls. A modification was devised and tested recently with apparent success. Further study is underway to investigate the issue of local evaluation near walls.

These results are summarized in Chakravarty and Menon (1995) which is included as an Appendix to this report.

4. PLANS FOR THE NEXT YEAR

The study carried out so far has established that the baseline local dynamic model can be used without any modification for a variety of flow fields even when the Reynolds number is high. The studies also showed that some modifications are required to handle flows with walls. However, preliminary results in wall-bounded flows showed that the modification to the dissipation term is required to develop a local subgrid model for wall-bounded flows. The validation of the local model for wall bounded flows and for more complex flows will be the primary focus of the next year's work. Currently, four parallel research studies are underway to address these issues. These studies are:

(a) Demonstration of the local subgrid model for rotating isotropic turbulence and rotating free shear flows

This study is directed towards determining the behavior of the new subgrid model in flows where external rotation is imposed. It is well known that with rotation, the energy transfer from

the large scales to the small scales is modified. An accurate subgrid model specially such as the one currently being investigated (based on the subgrid kinetic energy) must adjust to the global rotation imposed on the flow field. The behavior of the dissipation term in the subgrid model is key to this adjustment. Therefore, this study is being carried out first using a rotating isotropic field and then later with a rotating shear flow to investigate the modifications needed for simulating such flows using the new local subgrid model. This study should also provide guidelines regarding the implementation of the LES approach to more complex flows such as the swirling jets.

(b) Demonstration of the local subgrid model for wall bounded flows

Past study of Couette flow has shown that the current model is quite accurate; however, there are some more issues that remains to be resolved such as: (i) the effect of grid stretching, (ii) the effect of grid anisotropy (i.e., when the grid spacing is different in the spatial directions), and the effect of filtering on the governing equations when the grid is highly stretched. These issues has to be resolved for studies of complex wall-bounded flows where is grid stretching is mandatory and since, the resolution in the three spatial dimensions cannot be the same.

(c) Development of the next generation local subgrid models for more complex flows

For flows with large scale and unsteady separation such as flows past rearward facing steps, application of the Germano's algebraic model has shown good predictive capability. However, to achieve good agreement, relatively low Reynolds number flows were simulated using relatively very high grid resolution. Both this limits are considered unacceptable for developing practical LES methods for complex high Reynolds number flows. We have begun a new study of the rearward facing step flow using the new subgrid model to study high Reynolds number flow (Re = O(100000)) using practical grid resolution. Past calculations has shown reasonable agreement for flow for Re = O(1000) but it is expected that even the present model will be unable to simulate such flows accurately. Modifications to the dissipation terms are expected to improve the model; however, some new thinking is required to handle such flows. A key issue to be addressed is the behavior of the energy transfer in complex flows. Local and global backscatter needs to be addressed in a more general manner than studied before. Anisotropic eddy viscosity concepts (i.e., eddy viscosity that is a function of spatial directions) are being investigated to improve the basic method of representing the subgrid stresses in terms of an eddy viscosity model. We are also exploring a new approach whereby the local energy transfer and subgrid stresses are modeled by more complex non-linear closures which contains other terms in addition to the eddy viscosity term.These issues will be investigated in the coming year.

(d) Application of local subgrid models for free jets with and without swirl

This study was initiated recently to study free jets using the current model. Preliminary results are encouraging. This study will be extended to handle jets with swirl in the next year. The study of rotating flows (case (b) above) should shed light on the modifications necessary to handle such flows.

References

Carati, D., Ghosal, S., and Moin, P. (1995) "On the Representation of Backscatter in Dynamic Localization Models," *Phys. Fl.*, Vol., 7, pp. 606-613.

Chakravarty, K. and Menon, S. (1995) "A New Semi-Implicit Fractional Step Method for Simulation of Turbulent Flows on a Non-Staggered Grid," under preparation, to be submitted to the *Journal of Computational Physics*.

Germano, M., Piomelli, U., Moin, P., and Cabot, W. H. (1991) "A Dynamic Subgrid-Scale Eddy Viscosity Model", *Physics of Fluids A*, Vol. 3.

Kim, W.-W., and Menon, S. (1995a) "A New Dynamic One-Equation Subgrid Model for Large-Eddy Simulations", AIAA 95-0356, 33rd AIAA Aerospace Sciences Meeting, January 9-12, Reno, NV.

Kim, W.-W. and Menon, S. (1995b) "On the Properties of a Localized Dynamic Subgrid-Scale Model for Large-Eddy Simulations," under preparation, to be submitted to *Journal of Fluid Mechanics*.

Menon, S., and Yeung, P.-K. (1994a) "Analysis of Subgrid Models using Direct and Large-Eddy Simulations of Isotropic Turbulence" 74th AGARD Fluid Dynamics Panel Symposium on "Application of Direct and Large Eddy Simulation to Transition and Turbulence" AGARD CP-450.

Menon, S., Yeung, P.-K. and Kim, W.-W. (1994b) "Effect of Subgrid Models on the Computed Interscale Energy Transfer in Isotropic Turbulence" AIAA Paper No. 94-2387, AIAA 94-2387, AIAA 25th Fluid Dynamics Conference, June 20-23, 1994, Colorado Springs, CO.

Menon, S. and Kim, W.-W. (1994) "Analysis of Dynamic Subgrid Models Using Simulated Isotropic Turbulence Data", presented at the 1994 Meeting of the Division of Fluid Dynamics, American Physical Society, November 20-22, 1994, Atlanta, Georgia.

Menon, S. and Kim, W.-W. (1995) "High Reynolds Number Simulations using a New Localized Subgrid Model," submitted for presentation at the 34th Aerospace Sciences Meeting, Reno, NV.

Menon, S., Yeung, P.-K. and Kim, W.-W. (1995) "Effect of Subgrid Models on the Computed Interscale Energy Transfer in Isotropic Turbulence" to appear in *Computer and Fluids*.

ON THE PROPERTIES OF A LOCALIZED DYNAMIC SUBGRID-SCALE MODEL FOR LARGE-EDDY SIMULATIONS

Won-Wook Kim and Suresh Menon*
School of Aerospace Engineering
Georgia Institute of Technology
Atlanta, Georgia, 30332-0150

Submitted to

Journal of Fluid Mechanics

July 1995

*Corresponding Author
Associate Professor
(404)-853-9160
(404)-894-2760 (Fax)
menon@falcon.ae.gatech.edu

On the properties of a localized dynamic subgrid-scale model for large-eddy simulations

Won-Wook Kim and Suresh Menon

School of Aerospace Engineering

Georgia Institute of Technology

Atlanta, Georgia

Abstract

A new dynamic model that provides localized (both in time and space) determination of the model coefficients has been constructed with the base on the subgrid-scale kinetic energy equation model for large-eddy simulations of turbulent flows. In this model, the deficiencies of Germano *et al.*'s dynamic subgrid-scale model, such as the mathematically inconsistent derivation and ill-conditioning problem of the dynamic formulation and the prolonged presence of negative model coefficient, have been overcome. Moreover, the localized model coefficients obtained from this model are proved to be Galilean-invariant and very realizable. The properties of the model have been studied by applying it to large-eddy simulations of Taylor-Green vortex flow, and decaying and forced isotropic turbulence. The results are compared to experiments, direct numerical simulations and large-eddy simulations using the previously developed dynamic subgrid-scale models. Finally, it is demonstrated that the simplicity of the proposed model makes it computationally very efficient.

1. Introduction

The dynamic subgrid-scale (SGS) model which was introduced by Germano *et al.* (1991) has been successfully applied to various types of flow fields (Moin *et al.*, 1991; Akselvoll & Moin, 1993; Piomelli, 1993; Zang *et al.*, 1993; El-Hady *et al.*, 1994). Two desirable features make this model especially attractive. First, the model coefficient is determined as a part of the solution, thus, removing

the major limitation of the conventional eddy-viscosity type SGS models (e.g., the Smagorinsky model) which was the inability to parameterize accurately the unresolved SGS stresses in different turbulent flows with a single *universal* constant. Second, as a result of the dynamic determination, the model coefficient can become negative in certain regions of the flow field and, thus, appears to have the capability to mimic backscatter of energy from the subgrid-scales to the resolved scales.

Although it has been shown that Germano *et al.*'s dynamic model is superior to the conventional fixed-coefficient model, the dynamic procedure, as developed earlier, still has some deficiencies. These deficiencies originate from a weakness of the Smagorinsky model used in Germano *et al.*'s dynamic model, as well as, from the mathematically inconsistent derivation and the ill-conditioning of the dynamic formulation itself. The Smagorinsky time-independent, algebraic eddy-viscosity model is derived by assuming the equilibrium between the SGS energy production and dissipation. However, the validity of this assumption in general turbulent flows is still questionable. Furthermore, in actual implementation of the Smagorinsky model, the isotropic part of the SGS stress tensor (which is equivalent to 2/3 of the SGS kinetic energy) is added to the pressure and treated as a pressure head resulting in the grid-scale total pressure. Consequently, the velocity field is determined from the direct influence of this grid-scale total pressure instead of the pressure alone (Yoshizawa & Horiuti, 1985). These are considered to be limitations of the Smagorinsky model. Also, as noted by the original authors, the dynamic model employing Germano *et al.*'s mathematical identity cannot guarantee stable numerical simulations. A popular approach to stabilize the simulations is spatial-averaging of the model coefficient in directions of flow homogeneity. This has been quite successful in simple flows such as isotropic turbulence. However, since complex flows do not possess any direction of flow homogeneity, more complex local-averaging procedures are required and have been recently proposed (e.g., Zang *et al.*, 1993; Meneveau *et al.*, 1994; Kim & Menon, 1995). Although good results have been demonstrated using these methods, local-averaging approaches are still, in general, unacceptable because averaging itself is carried out only to avoid numerical instability, and has nothing to do with the dynamic procedure. Therefore, a truly robust dynamic model must be able to yield a stable and accurate solution using *local* values of the model coefficients that vary both in time and space.

In this paper, a transport equation for the SGS kinetic energy incorporated with the dynamic procedure has been investigated. The direct computation of the SGS kinetic energy implemented in the present approach is expected to account for some local details of the flow structure and history effects of the turbulence evolution. Also, this separately evaluated SGS kinetic energy makes it possible that the velocity is determined directly from the pressure. To remove the mathematical inconsistency and the ill-conditioning problem of Germano *et al.*'s dynamic formulation without employing spatial-averaging, a new localized dynamic formulation associated with the one-equation SGS model has been developed. This model provides a straightforward localized determination of the model coefficients and does not cause numerical instability. The properties of this model have been studied using data obtained from experiments, direct numerical simulations (DNS), and large-eddy simulations (LES) of Taylor-Green vortex flows, and decaying and forced isotropic turbulence. The localized dynamic SGS model is developed for applications to LES of complex, high Reynolds number flows in arbitrary geometry. Hence, studying this model in isotropic turbulent flows is not sufficient enough to fully demonstrate its capabilities. However, successful prediction of simple turbulent flows is a necessary step toward model validation because the simplicity of these flows makes it easy to study the properties of a model thoroughly.

In section 2, various dynamic SGS models are described with the basic equations indicating their advantages and limitations. Also, a new model that overcomes the deficiencies of the previously developed dynamic models is introduced with some basic properties being studied. In section 3, the numerical methods employed in this study are described. In section 4, the new model is applied to Taylor-Green vortex flow and decaying and force isotropic turbulence. Conclusions are presented in section 5.

2. Subgrid-scale modeling

In physical space, the incompressible Navier-Stokes equations for LES are achieved by low-pass filtering of a computational mesh (hence, the characteristic length of this filter is the grid width $\overline{\Delta}$) as follows,

$$\frac{\partial \overline{u}_i}{\partial x_i} = 0 \tag{1}$$

$$\frac{\partial \overline{u}_i}{\partial t} + \overline{u}_j \frac{\partial \overline{u}_i}{\partial x_j} = -\frac{\partial}{\partial x_j}\left(\overline{p}\delta_{ij} + \tau_{ij}\right) + \nu \frac{\partial^2 \overline{u}_i}{\partial x_j \partial x_j} \tag{2}$$

where $\overline{u}_i(x_i,t)$ is the resolved velocity field and the SGS stress tensor τ_{ij} is defined as

$$\tau_{ij} = \overline{u_i u_j} - \overline{u}_i \overline{u}_j. \tag{3}$$

In order to close equations (1) and (2), one needs to model τ_{ij} in terms of the resolved velocity field $\overline{u}_i$. By decomposing the full scale velocity u_i into the large scale quantity $\overline{u}_i$ and the small scale quantity u_i', τ_{ij} can be shown to contain three components: the Leonard stress $L_{ij} \equiv \overline{\overline{u}_i \overline{u}_j} - \overline{u}_i \overline{u}_j$, the cross stress $C_{ij} \equiv \overline{\overline{u}_i u_j'} - \overline{\overline{u}_j u_i'}$, and the SGS Reynolds stress $R_{ij} \equiv \overline{u_i' u_j'}$. In earlier studies (e.g., Moin & Kim, 1982), the Leonard stress was calculated directly while the cross and SGS Reynolds stresses were typically modeled. Speziale (1985) pointed out that the cross stress is not Galilean-invariant while the typical models for this term are invariant and, hence, this approach of separating the exact SGS stress into three components results in the LES equations of motion that are not Galilean-invariant. Consequently, this approach cannot have general applicability since it is inconsistent with the basic physics of the problem, which requires that the description of the turbulence be the same in all inertial frames of reference. An alternate approach, which is properly invariant, is modeling τ_{ij} as a whole. This approach is adopted in this study.

Eddy-viscosity models assume proportionality between the anisotropic part of the SGS stress tensor $\tau_{ij} - \frac{1}{3}\delta_{ij}\tau_{kk}$ and the resolved scale strain rate tensor $\overline{S}_{ij}$:

$$\tau_{ij} - \frac{1}{3}\delta_{ij}\tau_{kk} = -2\nu_T \overline{S}_{ij} \tag{4}$$

where ν_T is the eddy viscosity and

$$\overline{S}_{ij} = \frac{1}{2}\left(\frac{\partial \overline{u}_i}{\partial x_j} + \frac{\partial \overline{u}_j}{\partial x_i}\right). \tag{5}$$

Simple dimensional arguments suggest that the eddy viscosity ν_T should be given by the product of a velocity scale and a length scale. In LES, the length scale is usually related to the filter size ($\overline{\Delta}$), however, various models differ in their prescription for the velocity scale which can be estimated from the smallest resolved scales. In the Smagorinsky model, an algebraically described velocity scale is obtained by assuming that an equilibrium exists between energy production and dissipation in the small scales. One-equation SGS model (Schumann, 1975; Yoshizawa & Horiuti, 1985; Menon *et al.*, 1994) solves a transport equation for the SGS kinetic energy to provide the velocity scale.

The eddy-viscosity models for spatial-filtered LES have almost the same forms as used for Reynolds-averaged Navier-Stokes computations. Another class of SGS models, which are often called similarity models, has also been developed (Bardina *et al.*, 1980; Liu *et al.*, 1994). These models assume the similarity of turbulent stresses in consecutive scales or resolutions (e.g., similarity between the smallest resolved scale stress and the largest unresolved SGS stress). Although these models reproduce the structure of the SGS stress rather well, they do not dissipate sufficient energy and must be combined with the eddy-viscosity model in order to have all of the desired properties. The resulting models are usually called the mixed models. In the mixed models, the major role of the similarity part is to cause backscattering of SGS energy (Horiuti, 1989).

Dynamic SGS models have recently received the most attention. This type of SGS models uses the eddy-viscosity model as a base model and incorporates the similarity concept to dynamically determine the model coefficients. To date, two typical dynamic models have been suggested. One is a dynamic algebraic SGS model (Germano *et al.*, 1991) which is incorporated with the Smagorinsky model, and the other is a dynamic one-equation SGS model (Ghosal *et al.*, 1995; Kim and Menon, 1995) based on the SGS kinetic energy.

This paper is restricted to the study of the dynamic SGS models (see Menon *et al.*, 1994 for a detailed study of the eddy-viscosity and similarity models).

2.1. Dynamic Algebraic Subgrid-Scale (DASGS) Model

The simplest model which predicts the global energy transfer with acceptable accuracy is the algebraic eddy-viscosity model originally proposed by Smagorinsky (1963):

$$\tau_{ij} = -2c_A \overline{\Delta}^2 |\overline{S}| \overline{S}_{ij} + \tfrac{1}{3}\delta_{ij}\tau_{kk} \tag{6}$$

where the model coefficient c_A is equivalent to the square of the Smagorinsky constant and $|\overline{S}| = (2\overline{S}_{ij}\overline{S}_{ij})^{\frac{1}{2}}$. In classical approach, c_A requires adjustment for different flows. A large number of studies have been devoted to fine-tuning c_A for various flows of interest. This problem was circumvented by using a dynamic procedure (Germano *et al.*, 1991) which implements a direct evaluation of c_A. In the dynamic modeling approach, a mathematical identity between the SGS stresses resolved at the grid filter level characterized by $\overline{\Delta}$ and the test filter characterized by $\hat{\Delta}$ (typically, $\hat{\Delta} = 2\overline{\Delta}$) is used to determine the model coefficient c_A. Piomelli *et al.* (1988) showed that the proper choice of filter is essential to maintain model consistency for conventional SGS models. Furthermore, the nature of the test filter should be similar to that of the grid filter to conserve the similarity of the SGS stresses defined on these two filter levels. Various types of filtering operations have been studied, such as, top-hat, Gaussian, and Fourier cut-off. In the present study, we employ the top-hat filter for

the test filtering which is considered appropriate for finite-difference methods in physical space. Thus, if the application of the test filter on any variable ϕ is denoted by $\hat{\phi}$ or $<\phi>$, it can be shown that,

$$L_{ij} = T_{ij} - \hat{\tau}_{ij} = \left\langle \overline{u}_i \overline{u}_j \right\rangle - \hat{\overline{u}}_i \hat{\overline{u}}_j . \tag{7}$$

where

$$T_{ij} = \left\langle \overline{u_i u_j} \right\rangle - \hat{\overline{u}}_i \hat{\overline{u}}_j \tag{8}$$

is the SGS stress tensor defined at the test filter level. Assuming self-similarity of the subgrid-scale stresses, one can model T_{ij} in the same way as τ_{ij}:

$$T_{ij} = -2c_A \hat{\Delta}^2 \left|\hat{\overline{S}}\right| \hat{\overline{S}}_{ij} + \tfrac{1}{3}\delta_{ij} T_{kk} . \tag{9}$$

Combining (6), (7), and (9), an equation for c_A can be obtained;

$$L_{ij} - \tfrac{1}{3}\delta_{ij} L_{kk} = 2c_A M_{ij} \tag{10}$$

where

$$M_{ij} = -\left(\hat{\Delta}^2 \left|\hat{\overline{S}}\right| \hat{\overline{S}}_{ij} - \overline{\Delta}^2 \left\langle \left|\overline{S}\right| \overline{S}_{ij} \right\rangle \right). \tag{11}$$

Equation (10) is a set of five independent equations for one unknown c_A. To minimize the error that can occur solving this over-determined system, Lilly (1992) proposed a least-square method which yields

$$c_A = \frac{1}{2} \frac{L_{ij} M_{ij}}{M_{ij} M_{ij}} . \tag{12}$$

While Germano *et al.*'s dynamic model has been used successfully, some drawbacks are worth noting. First, in spite of a large spatial variation of the model coefficient, it is taken out of the spatial-filtering operation, as shown in (10), as if it were a constant in space. Local values of the model coefficient as a function of space are then sought. This mathematical inconsistency decreases the accuracy of the

dynamic model. Second, the resulting equation (12) for c_A is ill-conditioned because the denominator of this expression (i.e. M_{ij}) comes from the algebraic manipulation of two base models defined at different filtering levels and, hence, it can become very small causing numerical instability. These two drawbacks are directly related to Germano *et al.*'s mathematical identity (7). The final drawback is the prolonged occurrence of negative model coefficient in some locations of the flow field which has also been known to cause numerical instability (Lund *et al.*, 1993). This drawback appears to result from the nature of the Smagorinsky model used as a base model in Germano *et al.*'s dynamic formulation.

In this paper, we refer to Germano *et al.*'s dynamic formulation incorporated with the Smagorinsky algebraic model as the dynamic algebraic subgrid-scale (DASGS) model.

2.2. Dynamic k-Equation Subgrid-Scale (DKSGS) Model

A one-equation model for the subgrid-scale kinetic energy,

$$k_{sgs} = \tfrac{1}{2}\left(\overline{u_i^2} - \overline{u}_i^2\right), \tag{13}$$

in the following form (e.g. Yoshizawa, 1993),

$$\frac{\partial k_{sgs}}{\partial t} + \overline{u}_i \frac{\partial k_{sgs}}{\partial x_i} = -\tau_{ij}\frac{\partial \overline{u}_i}{\partial x_j} - \varepsilon + \frac{\partial}{\partial x_i}\left(\nu_T \frac{\partial k_{sgs}}{\partial x_i}\right) \tag{14}$$

has been studied recently (Menon & Yeung, 1994; Menon *et al.*, 1994). Here, the three terms on the right-hand-side of (14) represent, respectively, the production, dissipation and diffusion of k_{sgs}. In the model of the diffusion term, the direct effect of ν has been dropped. In the original model of this term, ν_T / σ_k is used in place of ν_T. However, since $\sigma_k = 1$ is usually adopted (Bradshaw *et al.*, 1981; Yoshizawa, 1993), σ_k has been dropped from (14). Note that the dynamic procedure might need to be used to determine σ_k (or a diffusion model coefficient defined in different way such as in appendix A). It is especially expected that the dynamic procedure for σ_k (or a diffusion model coefficient) is

worthwhile in the flow where the diffusion term becomes important, such as, in jets and wakes, and in the vicinity of walls in channel and boundary layer flows. This dynamic formulation of a diffusion model coefficient is presented in appendix A. The SGS stress tensor τ_{ij} is modeled in terms of the SGS eddy viscosity ν_T and k_{sgs} as:

$$\tau_{ij} = -2\nu_T \overline{S}_{ij} + \tfrac{2}{3}\delta_{ij} k_{sgs} \tag{15}$$

where

$$\nu_T = c_\tau k_{sgs}^{\frac{1}{2}} \overline{\Delta}. \tag{16}$$

Here, c_τ is an adjustable coefficient that is determined dynamically, as shown below. As shown in (16), ν_T has the form which is used in a standard one-equation model for Reynolds-averaged Navier-Stokes computations. Equation (14) is closed by providing a model for the dissipation rate term, ε. Using simple scaling arguments, ε is usually modeled as

$$\varepsilon = c_\varepsilon \frac{k_{sgs}^{\frac{3}{2}}}{\overline{\Delta}} \tag{17}$$

where, c_ε is another coefficient that is also obtained dynamically. An important feature of this model is that no assumption of the equilibrium between the SGS energy production and dissipation has been made. Moreover, the direct evaluation of the SGS kinetic energy implemented in this model allows the velocity to be directly determined from the pressure (i.e., the pressure and the velocity are directly coupled) unlike in the Smagorinsky model where the velocity is determined by the grid-scale total pressure which includes both the pressure and the isotropic part of the SGS stress (Yoshizawa & Horiuti, 1985).

The dynamic modeling method is applied to the *k*-equation subgrid-scale model to obtain appropriate values of the coefficients c_τ and c_ε. To implement this method, the SGS kinetic energy at the test filter level is obtained from the trace of (7);

$$K = L_{ii}/2 + \hat{k}_{sgs}. \tag{18}$$

Using a procedure similar to that outlined in Section 2.1, an equation for c_τ can be derived,

$$L_{ij} - \tfrac{1}{3}\delta_{ij}L_{kk} = 2c_\tau N_{ij} \tag{19}$$

where

$$N_{ij} = -\left(\hat{\Delta}K^{\frac{1}{2}}\hat{\bar{S}}_{ij} - \overline{\Delta}\left\langle k_{sgs}^{\frac{1}{2}}\bar{S}_{ij}\right\rangle\right). \tag{20}$$

Since (19) has the same form as (10), c_τ can be determined in a similar manner using the least-square method which yields

$$c_\tau = \frac{1}{2}\frac{L_{ij}N_{ij}}{N_{ij}N_{ij}}. \tag{21}$$

A mathematical identity similar to (7) between the dissipation rate resolved at the grid filter level, ε, and the test filter level, E, can be obtained as;

$$F = E - \hat{\varepsilon} = \nu\left(\left\langle\frac{\partial\bar{u}_i}{\partial x_j}\frac{\partial\bar{u}_i}{\partial x_j}\right\rangle - \frac{\partial\hat{\bar{u}}_i}{\partial x_j}\frac{\partial\hat{\bar{u}}_i}{\partial x_j}\right) \tag{22}$$

where

$$\varepsilon = \nu\left(\overline{\frac{\partial u_i}{\partial x_j}\frac{\partial u_i}{\partial x_j}} - \frac{\partial\bar{u}_i}{\partial x_j}\frac{\partial\bar{u}_i}{\partial x_j}\right) \tag{23}$$

$$E = \nu\left(\left\langle\overline{\frac{\partial u_i}{\partial x_j}\frac{\partial u_i}{\partial x_j}}\right\rangle - \frac{\partial\hat{\bar{u}}_i}{\partial x_j}\frac{\partial\hat{\bar{u}}_i}{\partial x_j}\right). \tag{24}$$

This identity is used to evaluate the dissipation rate model coefficient c_ε by employing the model for ε, (17), and the similar model for E at the test filter level;

$$F = c_\varepsilon\left(\frac{K^{\frac{3}{2}}}{\hat{\Delta}} - \left\langle\frac{k_{sgs}^{\frac{3}{2}}}{\overline{\Delta}}\right\rangle\right). \tag{25}$$

Note that (25) is a scalar equation for a single unknown and, hence, an exact value c_ε can be obtained without applying any approximation.

In this type of dynamic formulation, Germano *et al.*'s mathematical identity and its variant (22) are still adopted. Hence, the mathematical inconsistent derivation and the ill-conditioning problem remain. The advantage of this model is that by introducing the k-equation SGS model as a base model for the dynamic formulation, the prolonged presence of negative model coefficient (i.e., c_ε) is no longer the source of numerical instability. Unfortunately, however, this formulation does generate another drawback by introducing the identity (22). That is, the equation (25) for c_ε has the unphysical property of vanishing at high Reynolds numbers. This is due to the fact that the effective viscosity for E in (24) is not the same as the molecular viscosity for ε in (23). Since E is the dissipation characterized by a larger scale than the characteristic scale of ε, the effective viscosity for E should include the energy transfer (to the smaller scale) at that larger scale. Furthermore, the scale separation between E and ε increases as Reynolds number increases. Thus, as Reynolds number increases, the modeled expression for E, (24), becomes worse, resulting in poor prediction of the coefficient c_ε and, hence, the actual dissipation ε. To resolve this problem, the molecular viscosity in (24) should be replaced by the effective viscosity for E which is larger than the molecular viscosity. However, deriving an expression for the effective viscosity is not possible due to a lack of information on the characteristic scale of the test-filter-level SGS kinetic energy dissipation.

2.3 Localized Dynamic k-Equation Subgrid-Scale (LDKSGS) Model

As explained in the preceding sections, the dynamic formulations using Germano *et al.*'s mathematical identity suffer from numerical instability caused by the ill-conditioned expression for model coefficient and by the prolonged presence of negative model coefficient at some locations in the computational domain. This problem has been circumvented by spatial-averaging the expression for the model coefficient in directions of flow homogeneity (e.g., Germano *et al.*, 1991; Moin *et al.*, 1991). Recently, Meneveau *et al.* (1994) suggested a Lagrangian-averaging scheme applied along particle trajectories rather than directions of homogeneity. This model is based on the hypothesis that the SGS model coefficient at a given point should depend in some way on the history of the flow along the trajectory leading to that point because turbulent eddies are expected to evolve along this pathline. This model was tested in homogeneous and channel turbulent flows. In homogeneous flows, the results were as good as the volume-averaged dynamic model; while in channel flows, the predictions were superior to those of the conventional plane-averaged dynamic model. It was reported that this model required about 10% more computational time than the conventional spatial-averaged dynamic model. Kim & Menon (1995) also developed a simple local-averaging scheme which is based on the assumption that the main dynamic mechanism determining the local property of the turbulent flow occurs inside local structures. These local structures were defined in terms of vorticity since turbulent flow is characterized by three-dimensional vorticity fluctuations caused by both the large scale and the small scale eddies. They obtained slightly better results than the volume-averaged dynamic model in the simulation of Taylor-Green vortex flows and demonstrated the potential of the scheme for application to complex flows.

Although the local-averaged dynamic models might lead to accurate results and have the potential for application to complex flows, the concept of local-averaging (whether based on local structures or along particle trajectories) is still an artifact that is employed primarily to control the numerical instability. Furthermore, since the implementation of any averaging method necessarily accompany with it an ambiguity in choosing the domain over which averaging is to be applied, the local-averaging method is inconsistent with the dynamic procedure which is attempting to adjust the model without any

ambiguity. A true dynamic model should evaluate the model coefficients locally without any *ad hoc* averaging. In the following, we describe two different localized dynamic models that do not employ (nor require) any form of averaging.

Ghosal *et al.* (1995) developed the dynamic localization model based on the SGS kinetic energy, DLM(k), which is applicable to inhomogeneous flows. This model introduces a variational formulation to rigorously derive integral equations for the model coefficient as a function of position and time and is mathematically consistent. Also, by solving the integral equations iteratively, the numerical instability resulting from the ill-conditioning problem was effectively prevented (note that, since this model used the SGS kinetic energy equation as a base model, the prolonged presence of negative model coefficient is not a source for numerical instability). However, this was achieved at an additional price (Carati et al. (1995) reported that DLM(k) required 67% more CPU time than the standard Smagorinsky model while the conventional spatial-averaged dynamic model spent 4% more CPU time) due to the complicated and expensive procedure required to solve two more integral equations iteratively, as well as, one transport equation. This model has been tested in isotropic turbulence and in the flow over a backward-facing step and demonstrated its capability by showing a good agreement with experiments for both cases.

In this study, we propose a simpler, mathematically consistent, and numerically stable formulation of localized dynamic model. Before describing this model, some characteristic scales and flow properties at the grid and test filter levels need to be defined as shown in table 1. The following discussion will attempt to demonstrate the features of the new model using reasoning based in physical space (rather than in spectral space). At the grid filter level, there are two energy levels characterized by $\overline{u_i u_i}$ and $\overline{u}_i\overline{u}_i$ (the factor ½ is neglected in the following discussion for brevity). The SGS kinetic energy k_{sgs} is then determined by the difference between these two energy levels, i.e., $2k_{sgs} = \overline{u_i u_i} - \overline{u}_i\overline{u}_i$. Since the energy $\overline{u}_i\overline{u}_i$ is resolved at the grid filter level, the only meaningful length scale characterizing this energy level is the grid resolution $\overline{\Delta}$. However, the characteristic length scale (say l^*) for the energy level $\overline{u_i u_i}$ is unknown. Since $\overline{u_i u_i} > \overline{u}_i\overline{u}_i$, it can be deduced that the characteristic length scale for $\overline{u_i u_i}$ lies in the unresolved range of scales (i.e., $l^* < \overline{\Delta}$). It is also known that the length scale characterizing the

production of the SGS kinetic energy is much larger than the length scale characterizing the dissipation of the SGS kinetic energy and, hence, it is reasonable to state that the length scale characterizing the production of the SGS kinetic energy is $\overline{\Delta}$ while l^* represents a characteristic length scale for the dissipation of the SGS kinetic energy. The separation between the scales where the SGS kinetic energy is produced and where it is dissipated explains why the model for $\varepsilon\ (\propto k_{sgs}^{3/2}/\overline{\Delta})$ is poor (i.e., the dissipation model uses $\overline{\Delta}$ as a length scale, which is inappropriate). To properly model the production and the dissipation of the SGS kinetic energy, it is necessary to have additional information on the energy transfers at these two length scales. However, the information on the energy transfer characterized by the smaller scale (e.g., dissipation by the molecular viscosity) is not available. Therefore, an additional assumption (similar to that used in the Reynolds-averaged Navier-Stokes turbulence models) that the energy transfer which occurs at the smaller scale is essentially controlled by *the energy transfer at the larger scale* and *the energy determined by both energy transfers* (e.g. k_{sgs}) is required. Finally, the length scale and the strain rate tensor (to parameterize the energy transfer) of the larger scale, and the energy determined by both energy transfers are sufficient to model not only the production rate of the SGS kinetic energy (or the SGS stress tensor on which the SGS kinetic energy production depends, e.g., the production rate of $k_{sgs} \equiv -\tau_{ij}\overline{S}_{ij}$) but also the dissipation rate of the SGS kinetic energy.

The definitions and relations employed at the grid filter level can be extended to the test filter level as long as the scales are defined in a similar manner. The energy level $\hat{\overline{u}}_i\hat{\overline{u}}_i$ is resolved at the test filter level and characterized by $\hat{\Delta} = 2\overline{\Delta}$ whereas the characteristic length scale (say l^{**}) for the energy $\langle\overline{u_iu_i}\rangle$ is unknown, and again $\langle\overline{u_iu_i}\rangle > \hat{\overline{u}}_i\hat{\overline{u}}_i$ and $l^{**} < 2\overline{\Delta}$. However, at the test filter level, an additional scale can be defined. Since the SGS kinetic energy, $2k_{sgs} = \overline{u_iu_i} - \overline{u}_i\overline{u}_i$, is obtained by filtering the total turbulent energy u_iu_i at the grid filter level, a (similarly defined) energy at the test filter level, $\langle\overline{u}_i\overline{u}_i\rangle - \hat{\overline{u}}_i\hat{\overline{u}}_i$, is obtained by applying the test filter to $\overline{u}_i\overline{u}_i$. This energy is dissipated at the scale characterized by the energy level $\langle\overline{u}_i\overline{u}_i\rangle$ while being produced at the characteristic length scale $\hat{\Delta} = 2\overline{\Delta}$ which corresponds to the energy level $\hat{\overline{u}}_i\hat{\overline{u}}_i$, since $\langle\overline{u}_i\overline{u}_i\rangle > \hat{\overline{u}}_i\hat{\overline{u}}_i$. However, since this dissipative scale lies in the resolved range of scales, the energy is dissipated due to the SGS eddy viscosity as well as the molecular viscosity. Therefore, the effective viscosity for the dissipation of the energy $\langle\overline{u}_i\overline{u}_i\rangle - \hat{\overline{u}}_i\hat{\overline{u}}_i$ is $(\nu + \nu_T)$.

Using the assumption and the parameters defined above, we obtain three different SGS stress tensors and dissipation rates. One is at the grid filter level and the other two are at the test filter level:

the SGS stress tensor at the grid filter level,

$$\begin{aligned} \tau_{ij} &= \overline{u_i u_j} - \overline{u}_i \overline{u}_j \\ &= -2c_t \overline{\Delta} \left[\tfrac{1}{2} \left(\overline{u_i u_i} - \overline{u}_i \overline{u}_i \right) \right]^{\frac{1}{2}} \overline{S}_{ij} + \tfrac{2}{3} \delta_{ij} \left[\tfrac{1}{2} \left(\overline{u_i u_i} - \overline{u}_i \overline{u}_i \right) \right] \end{aligned} \tag{26a}$$

the SGS stress tensors at the test filter level,

$$\begin{aligned} T_{ij} &= \left\langle \overline{u_i u_j} \right\rangle - \hat{\overline{u}}_i \hat{\overline{u}}_j \\ &= -2c_t \hat{\Delta} \left[\tfrac{1}{2} \left(\left\langle \overline{u_i u_i} \right\rangle - \hat{\overline{u}}_i \hat{\overline{u}}_i \right) \right]^{\frac{1}{2}} \hat{S}_{ij} + \tfrac{2}{3} \delta_{ij} \left[\tfrac{1}{2} \left(\left\langle \overline{u_i u_i} \right\rangle - \hat{\overline{u}}_i \hat{\overline{u}}_i \right) \right] \end{aligned} \tag{26b}$$

$$\begin{aligned} t_{ij} &= \left\langle \overline{u}_i \overline{u}_j \right\rangle - \hat{\overline{u}}_i \hat{\overline{u}}_j \\ &= -2c_t \hat{\Delta} \left[\tfrac{1}{2} \left(\left\langle \overline{u}_i \overline{u}_i \right\rangle - \hat{\overline{u}}_i \hat{\overline{u}}_i \right) \right]^{\frac{1}{2}} \hat{S}_{ij} + \tfrac{2}{3} \delta_{ij} \left[\tfrac{1}{2} \left(\left\langle \overline{u}_i \overline{u}_i \right\rangle - \hat{\overline{u}}_i \hat{\overline{u}}_i \right) \right] \end{aligned} \tag{26c}$$

the dissipation rate at the grid filter level,

$$\begin{aligned} \varepsilon &= \nu \left(\overline{\frac{\partial u_i}{\partial x_j} \frac{\partial u_i}{\partial x_j}} - \frac{\partial \overline{u}_i}{\partial x_j} \frac{\partial \overline{u}_i}{\partial x_j} \right) \\ &= c_e \left[\tfrac{1}{2} \left(\overline{u_i u_i} - \overline{u}_i \overline{u}_i \right) \right]^{\frac{3}{2}} \Big/ \overline{\Delta} \end{aligned} \tag{27a}$$

the dissipation rates at the test filter level,

$$\begin{aligned} E &= \nu \left(\left\langle \overline{\frac{\partial u_i}{\partial x_j} \frac{\partial u_i}{\partial x_j}} \right\rangle - \frac{\partial \hat{\overline{u}}_i}{\partial x_j} \frac{\partial \hat{\overline{u}}_i}{\partial x_j} \right) \\ &= c_e \left[\tfrac{1}{2} \left(\left\langle \overline{u_i u_i} \right\rangle - \hat{\overline{u}}_i \hat{\overline{u}}_i \right) \right]^{\frac{3}{2}} \Big/ \hat{\Delta} \end{aligned} \tag{27b}$$

$$e = (\nu+\nu_T)\left(\left\langle\frac{\partial\overline{u}_i}{\partial x_j}\frac{\partial\overline{u}_i}{\partial x_j}\right\rangle-\frac{\partial\hat{\overline{u}}_i}{\partial x_j}\frac{\partial\hat{\overline{u}}_i}{\partial x_j}\right). \qquad (27c)$$
$$= c_\epsilon\left[\tfrac{1}{2}\left(\langle\overline{u}_i\overline{u}_i\rangle-\hat{\overline{u}}_i\hat{\overline{u}}_i\right)\right]^{\frac{3}{2}}\Big/\hat{\Delta}$$

As long as both the grid and the test filter levels are located in the range where the similarity assumption is valid, c_t and c_e in (26) and (27) remain the same. Note that (26a) and (27a) represent, respectively, the actual SGS stress tensor and the dissipation rate which must be modeled. These two expressions contain the two unknown model coefficients c_t and c_e. Previously (see section 2.2) the expressions for T_{ij} and E, (26b) and (27b), were adopted to dynamically determine these unknowns. However, this procedure introduced additional unknowns, $\langle\overline{u_iu_j}\rangle$ and $\left\langle\overline{\frac{\partial u_i}{\partial x_j}\frac{\partial u_i}{\partial x_j}}\right\rangle$. Therefore, to close the model, the other independent relations (e.g. Germano *et al.*'s mathematical identity, (7), and its variant, (22)) were needed. These additionally introduced relations become the source of both the mathematical inconsistency and the ill-conditioning problems. In this study, we adopt the expressions for t_{ij} and e, (26c) and (27c), (which do not contain any additional unknowns) instead of T_{ij} and E, respectively. Therefore, Germano *et al.*'s mathematical identity and its variant are *no longer needed to close the model.* Both c_t and c_e can be determined in the same manner as was done earlier for c_τ and c_ε (in section 2.2). Thus,

$$c_t = \frac{1}{2}\frac{t_{ij}\sigma_{ij}}{\sigma_{ij}\sigma_{ij}} \qquad (28)$$

where

$$\sigma_{ij} = -\hat{\Delta}\left[\tfrac{1}{2}\left(\langle\overline{u}_i\overline{u}_i\rangle-\hat{\overline{u}}_i\hat{\overline{u}}_i\right)\right]^{\frac{1}{2}}\hat{\overline{S}}_{ij} \qquad (29)$$

and

$$c_e = \frac{(\nu+\nu_T)\left(\left\langle\frac{\partial\overline{u}_i}{\partial x_j}\frac{\partial\overline{u}_i}{\partial x_j}\right\rangle-\frac{\partial\hat{\overline{u}}_i}{\partial x_j}\frac{\partial\hat{\overline{u}}_i}{\partial x_j}\right)}{\left[\tfrac{1}{2}\left(\langle\overline{u}_i\overline{u}_i\rangle-\hat{\overline{u}}_i\hat{\overline{u}}_i\right)\right]^{\frac{3}{2}}\Big/\hat{\Delta}}. \qquad (30)$$

As shown above, no mathematically inconsistent procedure is involved in this dynamic formulation. Furthermore, the denominators of (28) and (30) contain the energy information within the resolved

scale which is well-defined (note that in (12), (21), and (25), the denominators contain algebraically manipulated parameters, hence, the resulting expressions can not be well-defined). Therefore, the ill-conditioning problem (observed in the dynamic models using Germano *et al.*'s mathematical identity) is not considered serious here. Furthermore, the expression for c_ϵ, (30), does not have the unphysical property of vanishing at high Reynolds numbers unlike (25) since the effective viscosity $(\nu+\nu_T)$ is used instead of just ν. The existence of the similarity between the SGS stress $\overline{u_iu_j}-\overline{u}_i\overline{u}_j$ and the resolved stress $\langle\overline{u_iu_j}\rangle-\hat{\overline{u}}_i\hat{\overline{u}}_j$ is supported by Liu *et al.*'s (1994) analysis of experimental data in the far field of a round jet at a reasonably high Reynolds number ($Re_\lambda \approx 310$). In their work, a high correlation between the two stresses is obtained. Therefore, the basic assumption of the proposed localized model has some validity from experimental observation. The proposed LDKSGS model can be in a more general form if the dynamic procedure is applied to the diffusion model. This dynamic formulation is presented in appendix A. Finally, the computational cost of the LDKSGS model was evaluated and compared to the cost of the volume-averaged DKSGS and DASGS models in the simulations of Taylor-Green vortex flow (the detailed description of this flow will be presented in section 4.1). It was observed that to reach the same (physical) time level, the LDKSGS model required the same computational efforts as the volume-averaged DASGS model, while the volume-averaged DKSGS model required 40% more computational cost than the volume-averaged DASGS model. The simplicity of the dynamic formulation in the LDKSGS model (it can be easily observed that both the volume-averaged DKSGS and DASGS models need much more information to determine the model coefficients than the LDKSGS requires) appears to compensate for the additional expense involved in the solution procedure of the SGS kinetic energy transport equation.

2.4 Basic Properties of LDKSGS Model

Before applying the LDKSGS model to various flow fields of interest, it is worthwhile to examine the basic properties of the model from a theoretical point of view. Recently, Vreman *et al.* (1994) argued that SGS models should share some basic properties with the exact SGS stress τ_{ij} to successfully predict this unresolved quantity. They presented three properties of τ_{ij} that SGS models should fulfill as a necessary condition. First, τ_{ij} is a symmetric tensor, therefore, the model of τ_{ij} should be symmetric. Second, the filtered Navier-Stokes equations are Galilean-invariant. They should retain this property even after τ_{ij} is replaced by the model. Finally, the property that τ_{ij} is positive for positive filters (i.e., the filter kernel is positive over the domain applied) must be satisfied. Therefore, the model for τ_{ij} is required to be positive as well, if positive filter is employed. Actually, the first requirement is true for all existing SGS models. However, the latter two requirements need to be checked especially when a new SGS model is being considered. The ability of the proposed LDKSGS model to satisfy these requirements is discussed below.

The Navier-Stokes equations, as well as their filtered LES form (2), exhibit Galilean-invariance. As Speziale (1985) has argued, the SGS stress must be modeled with terms which are Galilean-invariant so that the resulting LES equations of motion for the large eddies retain the same form in all inertial frames of reference. In other words, the proposed SGS model should be properly Galilean-invariant, otherwise, the model loses its general applicability. The Galilean-invariance of the SGS model can be examined by employing the following transformations,

$$x_i^* = x_i + Ut + C \tag{31a}$$

$$t^* = t \tag{31b}$$

where U and C are any constant vectors. This transformation yields a frame of reference in which the motion differs by a constant translational velocity. Hence, if x_i constitutes an inertial frames of reference, then x_i^* will represent the class of inertial frames of reference. By differentiating (31), we obtain

$$u_i^* = u_i + U \tag{32a}$$

$$\frac{\partial}{\partial x_i^*} = \frac{\partial}{\partial x_i} \tag{32b}$$

$$\frac{\partial}{\partial t^*} = \frac{\partial}{\partial t} - U_j \frac{\partial}{\partial x_j}. \tag{32c}$$

Substituting (32a) into the definition of the SGS kinetic energy (13), we derive $k_{sgs}^* = k_{sgs}$. Since U is constant, the strain rate tensor $\overline{S}_{ij}$ is invariant. Consequently, it is clear that the models for τ_{ij}, (26a), and for ε, (27a), are invariant. The direct substitution of these results and (32) into (14) yields,

$$\frac{\partial k_{sgs}^*}{\partial t^*} + \overline{u}_i^* \frac{\partial k_{sgs}^*}{\partial x_i^*} = -\tau_{ij}^* \frac{\partial \overline{u}_i^*}{\partial x_j^*} - \varepsilon^* + \frac{\partial}{\partial x_i^*}\left(\nu_T^* \frac{\partial k_{sgs}^*}{\partial x_i^*}\right) \tag{33}$$

and, hence, the SGS kinetic energy equation, (14), is Galilean-invariant. This analysis can be extended to the test filter level to show that the trace $\langle \overline{u}_i \overline{u}_j \rangle - \hat{\overline{u}}_i \hat{\overline{u}}_j$, the test-filter-level strain rate tensor $\hat{\overline{S}}_{ij}$, t_{ij} in (26c), and e in (27c) are all Galilean-invariant. Finally, by direct substitution of these results, it can be shown that

$$c_t^* = c_t \tag{34a}$$

$$c_e^* = c_e. \tag{34b}$$

Vreman et al. (1994) have shown that the realizability conditions for the Reynolds stress in the statistical approach are also valid for the SGS stress τ_{ij} in the spatial-filtering approach. They proved that the tensor τ_{ij} forms a Grammian matrix which is always positive semidefinite. Hence, τ_{ij} is positive semidefinite and the realizability conditions given by the following inequalities hold,

$$\tau_{ii} \geq 0 \tag{35a}$$

$$\tau_{ij}^2 \leq \tau_{ii}\tau_{jj}. \tag{35b}$$

However, this proof is only valid if positive filters such as the top-hat or Gaussian filters are employed. If the spectral cut-off filter is applied, this proof does not hold. (It is worthwhile to note here that in the dynamic SGS modeling approach, grid-filtering is usually implemented by the low-pass filter of a computational mesh which is believed to be a positive filter, therefore, the resulting SGS stress τ_{ij} is positive. In this case, if the spectral cut-off filter is used for test-filtering, the SGS stress at the test filter level can locally be negative. Therefore, the dynamic SGS modeling approach loses its consistency.) The use of the low-pass filter of a computational mesh makes τ_{ij} positive and, hence, it is consistent to require that the model of τ_{ij} should be positive as well. In the LDKSGS modeling approach, the base model (i.e., the SGS kinetic energy equation model) is formulated in such a way that the SGS kinetic energy remains positive during the simulation. This was briefly proved by Ghosal *et al.* (1995). Thus, this base model for the LDKSGS formulation is realizable. The key question that remains to be answered here is that whether the dynamically determined model coefficients are reliable enough to guarantee that the model for τ_{ij} satisfies the realizability conditions expressed by the two inequalities in (35). The first inequality (35a) expresses the realizability condition for the diagonal elements of the stress. Therefore, this inequality is not sufficient to demonstrate a complete realizability condition. Including the second inequality provides a more general set of the realizability conditions. (Note that one may need other inequalities such as $\det(\tau_{ij}) \geq 0$ to complete the set of realizability conditions.) These inequalities give upper and lower bounds for the model coefficient. We will first examine the inequality in (35a). By rewriting (26a) for the diagonal elements of τ_{ij}, we obtain

$$\tau_{\alpha\alpha} = -2c_l\overline{\Delta}k_{sgs}^{\frac{1}{2}}\overline{S}_{\alpha\alpha} + \tfrac{2}{3}k_{sgs} \tag{36}$$

where $\alpha = \{l,m,n\}$ and $\overline{S}_{\alpha\alpha}$ denote the eigenvalues of the strain rate tensor which are assumed to have an arrangement of $\overline{S}_{ll} \geq \overline{S}_{mm} \geq \overline{S}_{nn}$ (here, repeated indices ($\alpha\alpha$, *ll*, *mm*, and *nn*) are used to indicate the eigenvalues of the strain rate tensor, therefore, the summation rule is not implied) for convenience. Furthermore, the signs of these eigenvalues of the strain rate tensor are determined from the incompressibility condition ($\overline{S}_{ll} + \overline{S}_{mm} + \overline{S}_{nn} = 0$) so that the largest eigenvalue $\overline{S}_{ll} \geq 0$, the smallest eigenvalue $\overline{S}_{nn} \leq 0$, and $\overline{S}_{mm}$ can have either sign. The direct substitution of these results into the first realizability condition (35a) gives the following condition:

$$\frac{k_{sgs}^{\frac{1}{2}}}{3\overline{\Delta S}_{nn}} \le c_l \le \frac{k_{sgs}^{\frac{1}{2}}}{3\overline{\Delta S}_{ll}} \tag{37}$$

where $\overline{S}_{nn}$ has negative sign and, hence, the lower bound is also negative. This condition implies the realizability of the diagonal elements of the SGS stress model (i.e., consequently, the positivity of the SGS kinetic energy). However, it does not automatically imply that the off-diagonal elements of the SGS stress model are also realizable. Another expression of upper and lower bounds for c_l which includes the off-diagonal elements is obtained by substituting (15) into the second realizability condition (35b) (for generality, the sum of all three off-diagonal elements is considered),

$$\nu_T^2(\overline{S}_{12}^2 + \overline{S}_{23}^2 + \overline{S}_{31}^2) \le \nu_T^2(\overline{S}_{11}\overline{S}_{22} + \overline{S}_{22}\overline{S}_{33} + \overline{S}_{33}\overline{S}_{11}) + \frac{1}{3}k_{sgs}^2. \tag{38}$$

This expression can be rewritten using a simple algebraic treatment as follows,

$$\nu_T^2(\overline{S}_{12}^2 + \overline{S}_{23}^2 + \overline{S}_{31}^2) \le -\frac{1}{2}\nu_T^2(\overline{S}_{11}^2 + \overline{S}_{22}^2 + \overline{S}_{33}^2) + \frac{1}{3}k_{sgs}^2. \tag{39}$$

Combining the terms which contain the strain rate tensor and substituting the definition $|\overline{S}| = (2\overline{S}_{ij}\overline{S}_{ij})^{\frac{1}{2}}$ yields

$$\nu_T^2|\overline{S}|^2 \le \frac{4}{3}k_{sgs}^2. \tag{40}$$

Finally, the upper and the lower bounds for c_l are obtained by the substitution of the definition for ν_T:

$$-\frac{2}{\sqrt{3}}\frac{k_{sgs}^{\frac{1}{2}}}{\overline{\Delta}|\overline{S}|} \le c_l \le \frac{2}{\sqrt{3}}\frac{k_{sgs}^{\frac{1}{2}}}{\overline{\Delta}|\overline{S}|}. \tag{41}$$

The two conditions, (37) and (41), give the realizable range for the dynamically determined model coefficient c_l. The model coefficient c_l should, therefore, fall inside this range for the LDKSGS model

to become a realizable model of the SGS stress. Unfortunately, it is difficult to analytically prove that these realizability conditions hold for the LDKSGS model. Numerical experiments are the only feasible way to prove these realizability conditions. Decaying isotropic turbulence (the detailed description of this flow field will be presented in the section 4.2) is used for the numerical verification. It is observed that more than 99.9% (for the 48^3 grid resolution), 99.8% (for the 32^3 grid resolution), and 99.6% (for the 24^3 grid resolution) of the grid points satisfy both the realizability conditions, (37) and (41), at the same time during the entire simulation. Therefore, it can be said that the LDKSGS model satisfies the realizability conditions even in a strict sense. However, this statement may not be true for other types of flow fields, especially, when the model is applied to complex, high Reynolds number flows. In that case, it is recommended that both the realizability conditions given by (37) and (41) be adopted as constraints for the dynamically determined model coefficient. This will ensure a more realizable and stable implementation of the dynamic model. Ghosal *et al.* (1995) reported that the DLM(k) model satisfies the realizability condition at about 95% of the grid points for the simulation of decaying isotropic turbulence using a 48^3 grid resolution. Thus, it appears that, unlike the present LDKSGS model, the DLM(k) is not quite realizable even for a simple isotropic turbulence. Furthermore, to examine the realizability, they used only the condition (37). According to our numerical experiments, the satisfaction of the condition (37) does not automatically guarantee the satisfaction of the condition (41). For definite realizability, both conditions, (37) and (41), should be used for accurate verification.

3. Numerical method

To date, most reliable simulations of turbulent flows have been performed using spectral methods because of their extremely high accuracy. However, spectral methods are relatively complicated and, moreover, they cannot be used for simulations of flows in complex geometry. For complex flows, numerical methods defined in the physical space like finite-difference methods (FDM) and finite-volume methods (FVM) are more appropriate. The major shortcoming of these physical space methods is that their accuracy is inadequate for turbulence simulations. Rai and Moin (1991) suggested a high-order accurate, upwind-biased finite-difference method as a good candidate for highly accurate simulations of turbulent flows associated with complex geometry. Their approach used a non-conservative form of the

unsteady, incompressible Navier-Stokes equations, (1) and (2), and, hence, it is appropriate only for simulations of flow fields without discontinuities (i.e., it can be applied to simulations of most incompressible flow fields and some compressible flow fields which do not include eddy-shocklets). The present study is limited to such flows and, therefore, a similar methodology is adopted here. Similar to Rai and Moin (1991), the convective terms are approximated using fifth-order-accurate, upwind-biased finite-differences with a seven-point stencil. For example, the first term in the u-momentum equation, $u\frac{\partial u}{\partial x}$, is evaluated as (in the following, the filtering operator '-' is dropped for simplicity);

$$(uu_x)_{i,j,k} = (u)_{i,j,k}(-6(u)_{i+2,j,k} + 60(u)_{i+1,j,k} + 40(u)_{i,j,k} - 120(u)_{i-1,j,k} + 30(u)_{i-2,j,k} - 4(u)_{i-3,j,k})/120\Delta \quad (42a)$$

if $(u)_{i,j,k} > 0$, and

$$(uu_x)_{i,j,k} = (u)_{i,j,k}(4(u)_{i+3,j,k} - 30(u)_{i+2,j,k} + 120(u)_{i+1,j,k} - 40(u)_{i,j,k} - 60(u)_{i-1,j,k} + 6(u)_{i-2,j,k})/120\Delta \quad (42b)$$

if $(u)_{i,j,k} < 0$, on a uniform grid. Here, subscript x indicates differentiation with respect to x. The remaining convective terms are evaluated in a similar manner. The viscous terms are computed using central differences. By applying the fourth-order-accurate, half-points differencing, the first viscous term in the u-momentum equation, $\frac{\partial}{\partial x}\left(\nu\frac{\partial u}{\partial x}\right)$, is discretized as

$$((\nu u_x)_x)_{i,j,k} = (-(\nu u_x)_{i+3/2,j,k} + 27(\nu u_x)_{i+1/2,j,k} - 27(\nu u_x)_{i-1/2,j,k} + (\nu u_x)_{i-3/2,j,k})/24\Delta \quad (43)$$

Also, u_x which is defined at the half-points is computed using the same fourth-order-accurate finite-difference given as

$$(u_x)_{i+1/2,j,k} = (-(u)_{i+2,j,k} + 27(u)_{i+1,j,k} - 27(u)_{i,j,k} + (u)_{i-1,j,k})/24\Delta \quad (44)$$

As shown, the discretization of the viscous terms (the second derivatives) uses seven grid points, hence, the viscous terms are approximated to sixth-order accuracy on uniform grids. The physical time derivatives in the momentum equations are differenced using a second-order backward-difference formula,

$$\frac{3u^{n+1} - 4u^{n} + u^{n-1}}{2\Delta t} = -\mathrm{Res}(u^{n+1}) \tag{45}$$

where the superscript n denotes the quantities at the physical time level n and 'Res' represents the residual in the momentum equations. Note that, in this study, a non-staggered grid is used with the velocities and the pressure defined at the grid points.

For incompressible flows, the continuity equation ($\partial u_i / \partial x_i = 0$) is essentially a time independent velocity constraint imposed on the momentum equations. This means that the system of incompressible Navier-Stokes equations possesses a singularity in time which makes the well-developed methods for the computation of compressible flows inefficient for the incompressible case. This singularity is removed in the present study by introducing the method of artificial compressibility, originally proposed by Chorin (1967). In this approach, a pseudo-time derivative of the pressure is added to the continuity equation making the resulting equation hyperbolic,

$$\frac{1}{\beta^2}\frac{\partial p}{\partial \tau} + \frac{\partial u_i}{\partial x_i} = 0 \tag{46}$$

where β is a prescribed parameter, which correspond to an artificial speed of sound, with a typical value of 5 to 10 as used by many researchers and τ is the pseudo-time variable which is not related to the physical time t. The time-accurate solution capability is obtained by adding pseudo-time velocity derivatives to the momentum equations (e.g., Rogers *et al.*, 1991). In this unsteady formulation, the governing equations are marched in the pseudo-time (i.e., subiterated) until the divergence-free flow field is obtained. Therefore, the artificial compressibility does not corrupt the physical time solution as long as the pseudo-time solution converges to a steady state at each physical time level.

The integration in the pseudo-time is carried out by an explicit method based on a Runge-Kutta time-stepping scheme. A 5-stage scheme was employed with the coefficients (0.059, 0.145, 0.273, 0.5, 1.0). Local time-stepping (in the pseudo-time), determined by the local stability limit, is also adopted to accelerate the convergence to a steady-state solution. A significant improvement in convergence is achieved by incorporating the full approximation scheme (FAS) multigrid method proposed by Brandt (1981). Details of the multigrid algorithm is given by Brandt (1981) and is omitted here for brevity.

In practice, a solution is considered converged if the root-mean-square of the pressure and velocity changes decrease less than 10^{-6} since, in most cases, further iterations to reduce these quantities do not noticeably change the solution. Both the eddy viscosity and the model coefficients are computed at each pseudo-time step. Usually, the model coefficients adjust themselves quickly and remain almost constant during pseudo-time iterations.

The code used in this study was validated earlier (Menon and Yeung, 1994) by carrying out direct numerical simulations of decaying isotropic turbulence and comparing the resulting statistics with the predictions of a well-known pseudo-spectral code (Rogallo, 1981). Further validation of this code is demonstrated in this paper by comparison with experiments as shown in section 4.2.

4. Results and Discussion

The proposed LDKSGS model has been applied to Taylor-Green vortex flow (section 4.1), and decaying (section 4.2) and forced (section 4.3) isotropic turbulence. Due to their inherent simplicity, these flows are considered necessary test flows where the properties of the SGS models can be investigated in detail. The behavior of the LDKSGS model near solid walls and for anisotropic grids is currently being investigated and will be reported in the near future.

4.1. Taylor-Green vortex flow

To investigate the properties of SGS models, one popular approach is to compare the predicted LES results with the results of DNS predictions. However, since DNS require a significant amount of computer resources (both memory and execution time), it can be applied only to a limited low range of Reynolds numbers. This Reynolds number range can be increased by simulating a flow that has spatial symmetries (which are preserved in time as the flow evolves), because the information in a fractional part of the periodic box is sufficient to describe the whole flow field using these symmetries. This idea was exploited by Brachet *et al.* (1983) who simulated a Taylor-Green vortex flow and reduced the necessary memory by 1/64 compared to that required for a general non-symmetric periodic flow. In this study, simulation in the so-called impermeable box ($0 \le x,y,z \le \pi$) of the Taylor-Green vortex flow is carried out. The flow field develops from the initial condition,

$$\begin{aligned} u &= \sin(x)\cos(y)\cos(z) \\ v &= -\cos(x)\sin(y)\cos(z). \\ w &= 0 \end{aligned} \tag{47}$$

At time $t = 0$, the flow is two-dimensional but becomes three-dimensional for all times $t > 0$. This flow is considered a simple flow field in which the generation of small scales and the resulting turbulence can be studied.

In this study, an effectively 128^3 DNS in a 2π-box (actually simulated using the 64^3 grid resolution in a π-box) has been carried out. The results are then used to evaluate LES predictions (obtained using coarse grid resolutions). Figure 1 shows the unscaled energy and dissipation spectra of the 128^3 DNS data at t=29. At this time, turbulence is well developed and no energy is left in the range of wavenumbers $k \leq 1$. The Taylor microscale Reynolds number Re_λ is approximately 32. We obtain a value of about 1.5 for the Kolmogorov constant, C_K. This value of C_K is in a good agreement with the value obtained from experiments at high Reynolds number (Monin and Yaglom, 1975), however, it is a smaller than the values determined directly from spectra in the high resolution DNS (e.g., Vincent and Meneguizzi, 1991) which estimate C_K to be around 2. In the range of wave numbers $k \leq 10$, the energy spectrum conforms to the inertial $k^{-5/3}$ law with the dissipation spectrum having a peak at $k \approx 10$. At this resolution and for the chosen molecular viscosity $\nu = 0.001$, the energy containing range and the dissipation range have a significant overlap (at very high Reynolds number, the energy and dissipation range should be widely separated). However, the present result is similar to the results of Domaradzki *et al.* (1993) which was obtained at $\mathrm{Re}_\lambda \approx 70$. Therefore, the Reynolds number used in the present simulation belongs to the range where the Reynolds number is just high enough to capture the beginning of the inertial range dynamics but too low to separate it from the effects of the dissipation range dynamics, as claimed by Domaradzki *et al.* (1993).

Figures 2 and 3 show the energy spectra of the 64^3 and 32^3 LES, respectively, which are compared with the energy spectra of the 128^3 DNS and the filtered 128^3 DNS (filtering was performed using the top-hat filter) at $t = 29$. All LES (using the LDKSGS model, the volume-averaged DKSGS model and the volume-averaged DASGS model) are performed by first filtering the 128^3 DNS flow field down to the LES resolution using the top-hat filter at $t = 9$ (at which time turbulence starts to decay by the viscous damping and realistic turbulence is about to develop). Thus, at $t = 9$, all flow variables (e.g., velocities and pressure) are highly correlated with the DNS data in the physical space. However, as observed in other studies, the subsequent evolution of the flow field in the LES becomes uncorrelated with the DNS data. Therefore, point-to-point correlation between the data resulted from DNS and those predicted by LES is not expected to be high. However, if the dynamic models guarantee the accurate prediction of the turbulent energy transfer, then it is expected that the energy spectra

computed from DNS and LES will be closely located. This is clearly observed in figures 2 and 3. A more interesting observation obtained from these figures is that the LES energy spectra are closer to the filtered 128^3 DNS spectrum than the 128^3 DNS energy spectrum itself. The difference (at the wavenumber range below the cut-off wavenumber, k_c) between the 128^3 DNS data and the filtered 128^3 DNS data is the result of using the top-hat filter which yields a significant contribution to the subgrid-scale energy from the lower wavenumbers than k_c (when the Fourier cut-off filter is employed, the subgrid-scale energy is entirely due to the higher wavenumbers than k_c). Therefore, it is consistent that the LES data compare well with the filtered DNS data since the LES performed by the current FDM code is implicitly adopting the top-hat filter in the numerical implementation. It can be deduced from this observation that a more meaningful comparison between LES predictions and DNS data can be achieved by filtering DNS data down to the same resolution as LES.

Although in this study, some information from the spectral space (e.g., energy spectrum) is used for comparison purposes, in most cases, the analysis of the properties of the proposed LDKSGS model will be carried out in the physical space. To determine whether the SGS stress tensors in consecutive resolutions (e.g., 64^3 and 32^3) have some similarity (which is the basic assumption adopted in the dynamic models using two filter levels), the ratio of the dissipation rate ($D \equiv \nu\left(\overline{\frac{\partial u_i}{\partial x_j}\frac{\partial u_i}{\partial x_j}} - \frac{\partial \overline{u}_i}{\partial x_j}\frac{\partial \overline{u}_i}{\partial x_j}\right)$) to the production rate ($P \equiv -\left(\overline{u_i u_j} - \overline{u}_i \overline{u}_j\right)\overline{S}_{ij}$) of the SGS kinetic energy, (D/P), is investigated. This ratio is expected to characterize the energy cascade mechanism inside the range of scales bracketed by these two energy transfers (the dissipation and production of the SGS kinetic energy). Furthermore, this energy cascade mechanism uniquely determines the property of the corresponding SGS stress tensor. Therefore, (D/P) is an appropriate parameter to investigate the existence of similarity in consecutive resolutions. Figure 4 shows the time evolution of (D/P) at three different resolutions (64^3, 32^3 and 16^3) as computed from the 128^3 DNS data. As noted earlier, the inertial range dynamics are not separated from the effects of the dissipation range dynamics, hence, the value of (D/P) is not equal to unity even in the inertial range. It is observed that the similarity of (D/P) exists between 32^3 and 16^3 grid resolutions (i.e., the (D/P) predictions from DNS data for these grid resolutions remain approximately same) while the similarity of (D/P) between 64^3 and 32^3 grid resolutions appears to be nonexistent,

especially, as time evolves. (The rapid change of (D/P) in the 64^3 grid resolution occurs since all length scales, including the Kolmogorov dissipation length scale, grow as the turbulent kinetic energy decays. Therefore, the 64^3 grid resolution becomes to lie under a larger influence of the Kolmogorov dissipation length scale and shows a higher (D/P) ratio.) Thus, the similarity of the SGS stresses in consecutive resolutions is not guaranteed for the 64^3 grid resolution. Therefore, the dynamic model in the 64^3 LES (which uses the 32^3 grid resolution as a test filter level) may result in the reduced accuracy. This will be demonstrated in the following figures.

To evaluate the performance of the SGS models, the time evolution of the velocity derivative (here, we use $\partial w/\partial z$) skewness S and flatness F factors computed from DNS and LES data are compared. Since the statistics of velocity derivative are the property of the relatively small scales, which are available in the corresponding grid resolution, the comparison between DNS and LES data should be performed at the same grid resolution. That is, before comparing statistics, DNS data should be filtered down to the same grid resolution as the LES. Usually, the velocity derivative statistics are considered strict standards for LES to match because they are determined by the small scales existing at that grid resolution and the small scales are largely dependent on the SGS model employed. Therefore, these statistics can be a direct measure of a quality of the SGS model. The skewness and flatness are defined as follows:

$$S = \frac{\left\langle (\partial w/\partial z)^3 \right\rangle}{\left\langle (\partial w/\partial z)^2 \right\rangle^{\frac{3}{2}}} \tag{48a}$$

$$F = \frac{\left\langle (\partial w/\partial z)^4 \right\rangle}{\left\langle (\partial w/\partial z)^2 \right\rangle^{2}}. \tag{48b}$$

Note that, here $<\cdot>$ denotes ensemble-averaging instead of test-filtering. Figures 5 and 6 show, respectively, the time evolution of skewness and flatness at the 64^3 grid resolution. This grid resolution has the cut-off wave number at $k \approx 30$ which is located inside the dissipation range (see figure 1). Thus, for simulations using this grid resolution, the role of the SGS models is not important since a significant

range of dissipation scales is resolved by the grid resolution. Without indicating any obvious superiority, all dynamic SGS models contribute in a favorable manner since the low resolution simulations adequately reproduce the higher resolution results. It can be seen from both figures that the curves for all 64^3 LES are always located between the curves for the 128^3 and 64^3 DNS. All the LES results begin to deviate from the filtered 128^3 DNS results at $t \approx 21$ (this is approximately the same time when the 32^3 (*D/P*) curve starts to largely deviate from the 64^3 (*D/P*) curve in figure 4). Also after $t \approx 21$, the 64^3 DNS results deviate from the filtered 128^3 DNS results due to the following reason. In the 64^3 DNS, the Kolmogorov dissipation length scale is not fully resolved and, hence, the turbulent energy is under-dissipated. As a result, the influence of the Kolmogorov dissipation length scale growth is not properly included in the 64^3 DNS even when this length scale becomes comparable to the 64^3 grid resolution in the 128^3 DNS.

In figures 7 and 8, the modeled production and dissipation rates of k_{sgs} using the 64^3 LES are compared to the exact values computed from DNS data. While the production rates are reasonably approximated by both models, there is relatively poor agreement between the exact and the modeled dissipation rates (as mentioned earlier, the poor prediction of the dissipation rate is caused by an inappropriate use of $\overline{\Delta}$ as a length scale). As time evolves, the decay of the dissipation rate of k_{sgs} (the slope of *D* in figure 8) computed from the 128^3 DNS becomes less steeper since the Kolmogorov dissipation length scale grows and becomes comparable to the characteristic length scale of the dissipation rate of k_{sgs}. However, the effect of the Kolmogorov dissipation length scale growth is not properly accounted for in the dissipation rate computed from both models. As a result, the difference between the exact and the modeled dissipation rates becomes more amplified after $t \approx 19$. The decay of the production rate of k_{sgs} (the slope of *P* in figure 8) computed from the 128^3 DNS also becomes less steeper after $t \approx 24$ indicating that the Kolmogorov dissipation length scale becomes comparable to the characteristic length scale of the production rate of k_{sgs}. This fact can be considered a rough proof for the existence of the scale separation between the length scales characterizing the production rate and the dissipation rate of k_{sgs}.

Figures 9 and 10 show, respectively, the velocity derivative skewness and flatness computed from the 32^3 LES and the filtered 128^3 DNS. There is now a clear difference in the results of the different subgrid-scale models; the one-equation models (both the volume-averaged DKSGS model and the LDKSGS model) are behaving better than the algebraic model. More interestingly, it can be seen that the localized dynamic model predicts a more accurate flow field than the volume-averaged dynamic model. According to these figures, an overall agreement between DNS and LES results (even the most accurate LES results using the LDKSGS model) becomes noticeably worse than the 64^3 grid resolution case. However, it should be noted that a (somewhat) poor prediction of the velocity derivative statistics by LES does not necessarily mean that the velocity statistics are also poorly predicted. This issue will be addressed in more detail in section 4.3.

Figures 11 and 12 show, respectively, the exact and the modeled production and dissipation rates of k_{sgs} at the 32^3 grid resolution. From the comparison with the 64^3 grid resolution (figures 7 and 8), it can be observed that the LES prediction of the production rate becomes worse as the grid resolution becomes coarse. However, the dissipation rate is rather well predicted at the coarser grid resolution. In both grid resolutions, the LDKSGS model shows an improved prediction of the dissipation rate from the volume-averaged DKSGS model predictions. This improvement seems to originate from the fact that, in the LDKSGS model, the local turbulent intermittency effects can be retained by not employing spatial-averaging. Since the dissipation mechanism is dominated by the scales smaller than the scales characterizing the production, it has a higher level of intermittency than the production mechanism. Therefore, the LDKSGS model improves the prediction of the dissipation more noticeably.

Figures 13 and 14 show the temporal variation of the dynamically determined coefficients. In the actual simulations of the LDKSGS model, the local values of the coefficients are used. However, to simplify the comparison, the volume-averaged values are shown in figures 13 and 14. It is observed during the simulations that the model coefficients can become negative even in volume-averaged values. In the LES using the dynamic one-equation models (the volume-averaged DKSGS model and the LDKSGS model), negative coefficients (i.e. $c_\epsilon < 0$ and $c_l < 0$) do not cause numerical instability (we have shown in section 2.4 that the LDKSGS model is realizable even when $c_l < 0$). However, the LES using the

volume-averaged DASGS model sometimes becomes unstable when $c_A < 0$ (Lund *et al.*, 1993). Therefore, the DASGS model is constrained to have non-negative coefficients (as shown at the zero-valued flat region of c_A-plot in figure 13). When the model coefficients become negative (e.g., $c_\epsilon < 0$ and $c_\epsilon < 0$), the model predicts backscatters. To correctly model this backscatter, we require information about the energy contained in the subgrid-scale. Thus, when the subgrid kinetic energy vanishes, backscatters should vanish. This is automatically satisfied with one-equation models since the eddy viscosity is modeled in terms of the subgrid kinetic energy; however, in the algebraic model, backscatters may occur (due to $c_A < 0$) even when there is no energy left in the subgrid scale thereby resulting in numerical instability. Another interesting observation from figures 13 and 14 is that the coefficient computed using the LDKSGS model is usually smaller in magnitude than the coefficient computed using the volume-averaged DKSGS model. The dissipation model coefficient of the LDKSGS model is more sensitive to a grid resolution change than that of the volume-averaged DKSGS model.

4.2. Decaying isotropic turbulence

The experiment of decaying isotropic turbulence of Comte-Bellot and Corsin (1971) is simulated to demonstrate the capability of the LDKSGS model in predicting the decay of the turbulent energy. Another reason for this test is to compare the results with those of Ghosal *et al.*'s DLM(k) (1993; 1995) which is the only other existing localized dynamic model formulated without employing the *ad hoc* (averaging) procedure. They simulated this experiment using both 32^3 and 48^3 grid resolutions. In predicting the energy decaying rate, a good agreement with the experimental data was obtained using a 48^3 grid resolution (see figure 1 in Ghosal *et al.*, 1995). However, relatively poor results were obtained using a 32^3 grid resolution (see figure 1 in Ghosal *et al.*, 1993). This made them conclude that the 48^3 grid resolution is the smallest possible resolution for LES since the 32^3 grid resolution is not fully consistent with the basic assumption of LES that the resolved scales should contain most of the energy. To investigate this issue, we computed the resolved energy at each grid resolution by numerically integrating the spectrum given by Comte-Bellot & Corsin(1971) between wavenumbers zero to the maximum wavenumber resolved by the grid resolution. The results are summarized in table 2. As

shown, 32^3 and 48^3 grid resolutions resolve 59.3% and 70.3% of the total turbulent kinetic energy, respectively. Strictly speaking, both resolutions are, therefore, not fully consistent with the basic assumption of LES. For these grid resolutions, a significant number of energy-containing eddies resides in the unresolved scales and the quality of the SGS model becomes much more important. Therefore, the simulation of this experiment especially using the grid resolution coarser than 48^3 (i.e., when the subgrid scales contain more than 30% of total turbulent kinetic energy) is a good test case to measure the quality of the SGS model. For this purpose, three grid resolutions (48^3, 32^3, and 24^3) are used for the large-eddy simulations implemented here.

In the experiment, measurements of the energy spectra were carried out at three locations downstream of the mesh (which generated the turbulence in the wind tunnel). At the first measuring station, the Reynolds number based on the Taylor microscale and based on the integral scale were, respectively, 71.6 and 187.9 (these values decreased to 60.7 and 135.7, respectively, at the last measuring station). Using the assumption of a constant mean velocity across the cross section of the wind tunnel, the elapsed time for the turbulent field traveling at the mean velocity from the mesh (that is, proportional to the downstream distance) can be obtained. That is, the spatial evolution of turbulence in the experiment can be converted to a temporally evolving state. Therefore, this (spatially evolving) problem can be thought of as a decaying isotropic turbulence inside a cubical box which is moving with the mean flow velocity. The size of the box is chosen to be greater than the integral scale of the measured real turbulence. The statistical properties of turbulence inside the box are believed to be realistic even after applying periodic boundary condition for numerical implementation. All experimental data is nondimensionalized by the reference length scale $10M/2\pi$ (where $M = 5.08cm$ is the wind-tunnel mesh spacing) and the reference time scale 0.1 sec for computational convenience. (By this nondimensionalization, the three measuring locations correspond to the three dimensionless time levels, $t^* = 2.13$, 4.98 and 8.69, respectively.)

The initial velocity field (primarily the amplitudes of the velocity Fourier modes) is chosen to match the three-dimensional energy spectrum obtained at the first experimental measuring station. The phases of Fourier modes are chosen to be random so that the initial velocity field satisfy Gaussian statistics. The

initial pressure is assumed to be uniform throughout the flow field and the initial SGS kinetic energy is roughly estimated by assuming the similarity between the SGS kinetic energy and the resolved energy at the test filter level, i.e.,

$$k_{sgs} \approx \frac{c_k}{2}(\langle \overline{u}_i \overline{u}_i \rangle - \hat{\overline{u}}_i \hat{\overline{u}}_i) \tag{49}$$

where a constant c_k is determined by matching the magnitude of the SGS kinetic energy to the exact SGS kinetic energy calculated by integrating the experimental spectrum at the first measuring station. (In situations where the information about the magnitude of the exact SGS kinetic energy is not known, a value of c_k given by Liu *et al.* (1994) for the stress-similarity model, $\overline{u_i u_j} - \overline{u}_i \overline{u}_j = c_k(\langle \overline{u}_i \overline{u}_j \rangle - \hat{\overline{u}}_i \hat{\overline{u}}_j)$, can be used; that is $c_k = 0.45 \pm 0.15$. The initial SGS kinetic energy can be estimated more consistently with the dynamic procedure by adopting the similarity concept used in the dynamic procedure. This formulation is presented in appendix B.) Although the above procedure generating the initial condition looks reasonable, the initial turbulent field generated by it may not be sufficiently realistic. Carati *et al.* (1995) suggested that a practical way to make the initial field more realistic, is to let the flow evolve for a few physical time steps and then multiply all Fourier modes by an appropriate real number to scale the velocity field to be consistent with the experimental spectrum. This additional procedure for initial conditions ensures that the randomly chosen phase information, the pressure and the SGS kinetic energy becomes more realistic. This procedure is also adopted in this study.

Figure 15 shows the decay of the resolved turbulent kinetic energy computed using the LDKSGS model at three grid resolutions, 48^3, 32^3, and 24^3. The results are compared with the predictions of the volume-averaged DASGS model at the 48^3 grid resolution and the experimental data of Comte-Bellot and Corsin (1971). The predictions of both models (at the 48^3 grid resolution) are in good agreement with the experiment. As is well known (Huang and Leonard, 1994), the turbulent kinetic energy undergoes a power law decay, i.e., $E \sim (t^*)^n$, in the asymptotic self-similar regime. The experimental data roughly confirms the existence of the power law by lying on a straight line on a log-log plot. The decay exponent n is obtained from a least-square fit to each data as given in table 2. The value of n predicted by the DLM(k) is used as given in Carati *et al.* (1995). (Actually, $n = -1.28$ was given for the

DLM(k) in Carati *et al.* (1995). However, this value seems to be misprinted by accidentally switching with the value for their stochastic dynamic localization model since the energy decay plot in their paper clearly shows that the decay predicted by the DLM(k) is slower than that of the stochastic dynamic localization model.) These results confirm the agreement between the predictions of LES and the experiment. More importantly, the results of the LDKSGS model at all three grid resolutions used (even for the 24^3 grid resolution where about a half of the turbulent kinetic energy is not resolved) show consistency in predicting the energy decay. This property of the model is a fascinating feature especially when the model is (to be) applied to complex and high Reynolds number flows where a significant amount of turbulent energy possibly lies in the unresolved scales. Without a self-consistent behavior, the SGS model can not simulate high Reynolds number flows in complex geometries reliably. Therefore, the proposed LDKSGS model seems to have a promising potential for application to complex, high-Reynolds number flows.

The computed and experimental three-dimensional energy spectra resolved at the three different grid resolutions, 48^3, 32^3 and 24^3, are shown in figures 16 (at $t^* = 4.98$) and 17 (at $t^* = 8.69$). Both of the LDKSGS and volume-averaged DASGS models predict the spectra reasonably well. Especially, the LDKSGS model predicts the spectra consistently well for all three grid resolutions. Some discrepancy between the experimental and LES-predicted energy spectra is observed around the cut-off wavenumber. This discrepancy is due to the fact that the FDM code used in this study implicitly adopts the top-hat filter for its discretized numerical implementation, as explained in section 4.1 (see figures 2 and 3). Direct comparison between experimental and LES-predicted energy spectra is meaningful only when the full-resolution experimental flow filed is filtered down to the LES grid resolution to compare using the top-hat filter (to be more consistent, the initial flow field for LES also should be obtained from the experimental flow field using the top-hat filter).

Figures 18 and 19 show the time evolution of the model coefficient c_t and the dissipation model coefficient c_ϵ, respectively (locally evaluated coefficients are volume-averaged for quantitative presentation). Even though a seemingly reasonable method to generate the realistic initial velocity field described earlier was employed, the coefficients (both c_t and c_ϵ) remain small for an initial period of

time during which the more realistic turbulent fields develop. However, the final results appear to be not much affected by this initial evolution period. It can be deduced from these figures that for same flow conditions (e.g., same kinematic viscosity), larger value of the coefficients (both c_t and c_ϵ) are required for LES if the grid resolution becomes coarse in the simulation of (decaying) isotropic turbulence.

4.3 Forced isotropic turbulence

A statistically stationary isotropic turbulence is simulated using a 32^3 grid resolution. The main purpose of this simulation is to determine whether a low resolution LES using the LDKSGS model can reproduce the statistics (of the large scale structures) of a realistic, high Reynolds number turbulent field. The results are compared with the existing high resolution DNS data by Vincent and Meneguizzi (1991) and Jimenez *et al.* (1993) obtained at $\mathrm{Re}_\lambda \approx 150$ and $\mathrm{Re}_\lambda \approx 170$, respectively.

A statistically stationary turbulent field is obtained by forcing the large scales as was done by Kerr (1985). In this study, the initial value of all Fourier modes with wave number components equal to 1 is kept fixed. The initial condition is obtained by generating a random realization of the energy spectrum (e.g., Briscolini and Santangelo, 1994),

$$E(k) = C\frac{k^4}{1+(k/k_0)^{5/3+4}} \tag{50}$$

where $k_0 = 1$ and C is a constant which normalizes the initial total energy to be 0.5. In isotropic turbulence, there are some generally accepted parameters characterizing the flow such as the Taylor microscale Reynolds number, the integral scale Reynolds number, and the large-eddy turnover time. For an accurate estimate of these parameters, the full resolution DNS data are required. Strictly speaking, there is no way to exactly evaluate these quantities from LES data. Therefore, the characteristic parameters are computed here in an approximate manner. The energy dissipation rate ε can be computed accurately using the property of the forced turbulence since in the forced isotropic

turbulence, the energy dissipation rate is balanced with the energy injection rate by the external force. The energy injection rate can be easily determined from the external force added into the field and the velocity at the wavenumber component equal to 1 where the external force is applied. The total energy E_t involved in the cascade process is estimated by assuming that the energy spectrum obeys the Kolmogorov law $E(k) = C_K \varepsilon^{2/3} k^{-5/3}$ (where $C_K \approx 1.5$ is the Kolmogorov constant),

$$E_t = \int_{k_0}^{\infty} E(k)dk = C_K \varepsilon^{2/3} \int_{k_0}^{\infty} k^{-5/3} dk = \frac{3}{2} C_K \varepsilon^{2/3} k_0^{-2/3}. \tag{51}$$

The root-mean-square velocity u_{rms} is defined by

$$u_{rms}^2 = \frac{2}{3} E_t, \tag{52}$$

and the Taylor microscale λ is defined by

$$\lambda^2 = 15 \nu_{eff} u_{rms}^2 / \varepsilon \tag{53}$$

where ν_{eff} denotes the use of the effective viscosity $(\nu + \nu_T)$ instead of the molecular viscosity. The integral scale l is

$$l = \frac{\pi}{2u_{rms}^2} \int_{k_0}^{\infty} k^{-1} \left(C_K \varepsilon^{2/3} k^{-5/3} \right) dk = \frac{3\pi}{10} \frac{C_K \varepsilon^{2/3} k_0^{-5/3}}{u_{rms}^2}. \tag{54}$$

Finally, the Taylor microscale Reynolds number is defined as $\mathrm{Re}_\lambda = u_{rms} \lambda / \nu_{eff}$, the integral scale Reynolds number as $\mathrm{Re}_l = u_{rms} l / \nu_{eff}$, and the large-eddy turnover time as $\tau = l / u_{rms}$. In this study, LES are implemented under two different flow conditions. One is characterized by $\mathrm{Re}_\lambda \approx 260$, $\mathrm{Re}_l \approx 2400$, and $\tau \approx 3.7$; the other is characterized by $\mathrm{Re}_\lambda \approx 80$, $\mathrm{Re}_l \approx 220$, and $\tau \approx 4$. The simulations have been run for 27 and 25 large-eddy turnover times, respectively. To ensure statistical independence, 20 fields are used in statistical analysis for both cases (i.e., the time interval between successive fields is larger than (or at least same as) one large-eddy turnover time).

Figure 20 shows the temporal evolution of the mean turbulent kinetic energy. After an initial decaying period (i.e., after $t \approx 20$), the mean turbulent kinetic energy remains at almost the same level, reflecting a balance between forcing at the large scales (the energy injection rate) and dissipation at the small scales (the energy dissipation rate). Only this energy equilibrium period of time is used in statistical analysis because it is closer to a statistically steady state.

Figure 21 shows the probability distribution of velocity differences, $\delta u(r) = u(x+r) - u(r)$, for various values of r (note that all values of r used here are comparable with the inertial range scales). For generality, δu is normalized so that $\sigma^2 = <\delta u^2> = 1$. The LES results (using the LDKSGS model at $Re_\lambda \approx 260$) clearly show that the distribution changes from a non-Gaussian (which has the wings) to a Gaussian, as r increases. The same behavior of the distribution was observed in the high resolution DNS of Vincent and Meneguizzi (1991). In addition to the basic agreement regarding the development of the non-Gaussian statistics, the LES accurately predicts the probability for each bin. Figure 22 shows an agreement between the distributions for $r = 0.39$ obtained from the LES and the DNS except for some deviation in the wing region. However, as is well known, the wings of the non-Gaussian distribution develop mainly due to small-scale fluctuations. Therefore, the deviation between the LES and the DNS results in the wings is somewhat natural; since in LES, most small scales are not resolved and even the resolved portion of small scales lies under strong influence of the top-hat filter implicitly implemented in FDM code.

The statistics of velocity and its derivatives are also investigated. While the statistics of velocity are the property of the large scales which are mostly resolved in LES, the statistics of velocity derivative are the property of the dissipation range scales which are not resolved by LES. Therefore, the direct comparison of LES and DNS using the statistics of velocity derivative may be meaningless. A more useful comparison can be achieved by filtering the DNS field down to the same resolution as the LES. For the same grid resolution and flow conditions, the statistics of the LES and the filtered DNS should match well. However, the velocity derivative statistics of the filtered DNS data are not available, therefore, the DNS statistics of velocity derivative obtained from the full resolution simulation (shown

in the table 4) is being used only as a qualitative measure for the LES results. We computed the nth-order moments of the velocity and its derivative distributions using

$$S_n = \frac{< x^n >}{< x^2 >^{n/2}} \tag{55}$$

here, $<\cdot>$ denotes ensemble-averaging instead of test-filtering. The results of this calculation is summarized in table 4. The results of the 512^3 DNS ($Re_\lambda \approx 170$), the 240^3 DNS ($Re_\lambda \approx 150$), and the 64^3 LES ($Re_\lambda \approx 140$) are obtained from Jimenez *et al.* (1993), Vincent and Meneguizzi (1991), and Briscolini and Santangelo (1994), respectively. (Note that different authors use a definition of Re_λ in different form, however, we use the original value provided by the authors without any correction.) The 64^3 LES was implemented using the Kraichnan's eddy viscosity where the small scales are parameterized reproducing a self-similar range of energy in spectral space. We simulated two different Reynolds number cases using the same grid resolution to investigate the effect of the Reynolds number on the statistics. As shown in the table, the velocity statistics appear not to depend on either the grid resolution or the Reynolds number simulated. However, the velocity derivative statistics were highly influenced by the grid resolution employed (it can be observed from the table that those values of the velocity derivative statistics are consistently decreased as the grid resolution becomes coarse from 512^3 to 32^3). In the LES, the effect of the Reynolds number on the velocity derivative statistics is not captured (in the DNS of Jimenez *et al.* (1993), consistent increase in the velocity derivative statistics with Reynolds number increase was observed), since the velocity derivative statistics are strongly determined by the grid resolution employed.

Figure 23 shows that the fraction of grid points where the model coefficient c_l is negative. In the LES using the LDKSGS model, regardless of the Reynolds number simulated, about 20% fraction of grid points have negative model coefficient throughout the simulation. Carati *et al.* (1995) reported that the DLM(k) predicts negative model coefficient in about 13% fraction of grid points for a similar forced isotropic simulation. Therefore, the LDKSGS permits backscattering in larger fraction of grid points than the DLM(k).

Figures 24 and 25 show the temporal evolution of the model coefficient c_t and the dissipation model coefficient c_ϵ (locally evaluated coefficients are volume-averaged for quantitative presentation). The LDKSGS model predicts $c_t \approx 0.056$ and $c_\epsilon \approx 0.33$ for higher Reynolds number case ($\mathrm{Re}_\lambda \approx 260$) and $c_t \approx 0.05$ and $c_\epsilon \approx 0.44$ for lower Reynolds number case ($\mathrm{Re}_\lambda \approx 80$). These values for c_t are pretty well matched with that suggested by Yoshizawa & Horiuti (1985); they recommended $c_t \approx 0.05$ from the framework of the two-scale direct-interaction approximation (TSDIA). (Note that, in the Reynolds-averaged turbulence models, a generally adopted value for c_t is about 0.09; that is significantly larger than that for LES.) However, there are some discrepancies between c_ϵ values dynamically determined and suggested by Yoshizawa & Horiuti ($c_\epsilon \approx 1$). From the observation of these figures, it can be roughly concluded that in LES of (forced) isotropic turbulence using the fixed grid resolution, a larger value of the model coefficient c_t and a smaller value of the dissipation model coefficient c_ϵ is required as higher Reynolds number flows are simulated.

5. Conclusions

In this paper, the properties of a new dynamic localized model (the LDKSGS model) have been studied. This model is formulated using the subgrid-scale kinetic energy equation model as a base model. As was done in the other dynamic models, two different filter levels are introduced to dynamically determine the model coefficient. However, this model has a unique feature which distinguishes it from the previously developed dynamic models; that is, in the present model, Germano *et al.*'s mathematical identity is not employed. This feature allows the LDKSGS model to overcome some of the inherent deficiencies in the dynamic procedures using Germano *et al.*'s mathematical identity, such as, the mathematically inconsistent derivation and ill-conditioning problem. The instability caused by the prolonged presence of negative model coefficients is also prevented in the LDKSGS model by the use of the subgrid-scale kinetic energy to model the subgrid-scale stress tensor. Another advantage obtained by avoiding Germano *et al.*'s mathematical identity is that the LDKSGS model has a relatively simple structure which makes the model computationally very efficient. As a result, the additional expense involved in the solution procedure of the subgrid-scale kinetic energy transport equation (when compared to the DASGS model) has been greatly compensated. Moreover, the localized model coefficients obtained from the LDKSGS model are shown to be Galilean-invariant and very realizable. Especially, the realizability of the model provides a means to obtain a numerically stable and a physically accurate solution.

The LDKSGS model has been successfully applied to three different types of homogeneous turbulent flows. In the simulations of Taylor-Green vortex flow, the results obtained from the LDKSGS model were compared with those of two existing dynamic models. It was demonstrated that the LDKSGS model yields a better agreement with the high-resolution DNS than other dynamic models tested. The capability of the LDKSGS model in predicting the energy decay rate has been demonstrated by simulating the decaying isotropic turbulence and comparing the results to the experimental data (the LES results confirmed the power law decay which was observed in the experimental data). Furthermore, three different resolutions LES (at the coarsest resolution, about a half of the kinetic energy was not resolved) showed consistency in predicting the energy decay. This property of the

LDKSGS model is very attractive, especially when the model is (to be) applied to complex and high Reynolds number flows where a significant amount of turbulent energy possibly lies in the unresolved scales. The application of the present model to forced (statistically stationary) isotropic turbulence also proves the capability of the LDKSGS model in reproducing the statistics (of the large scale structures) of a realistic, high Reynolds number turbulent field. The LES results, when compared to the high resolution DNS data, clearly show the accurate prediction of velocity statistics and the development of the non-Gaussian statistics (which was observed in the high resolution DNS).

To complete the study on the properties of the proposed model, the model behavior near solid walls and for anisotropic grid should be included. This issue is currently being investigated. According to the preliminary results obtained from the large-eddy simulation of turbulent, plane Couette flow, the present model can be applied to the wall-bounded flow simulations in a straightforward manner. The detailed results of this study will be reported in the near future.

The authors are grateful for the financial support from the Fluid Dynamics Division of the Office of Naval Research under grant N00014-93-1-0342 (monitored by Dr. P. Purtell). This work was also supported in part by a grant of HPC time from the DoD HPC Center; we used "vlsc" (Cray C-90) at the Naval Oceanographic Office (NAVO) and "pk" (Cray C-90) at the USAE Waterways Experiment Station (CEWES).

Appendix A. The dynamic determination of the diffusion model coefficient

The diffusion term in the transport equation for k_{sgs}, (14), can be rewritten as;

$$\frac{\partial}{\partial x_i}\left(D_i + \nu\frac{\partial k_{sgs}}{\partial x_i}\right). \qquad \text{(A 1)}$$

Here, the exact expression and the model of D_i at the grid filter level are given by

$$D_i = -\left(\overline{pu_i} - \overline{p}\,\overline{u_i}\right) - \left(\overline{u_i k_{tot}} - \overline{u_i}\,\overline{k_{tot}}\right) + \overline{u_j}\left(\overline{u_i u_j} - \overline{u_i}\,\overline{u_j}\right)$$
$$= c_d k_{sgs}^{\frac{1}{2}} \overline{\Delta} \frac{\partial k_{sgs}}{\partial x_i} \qquad \text{(A 2)}$$

where $k_{tot} = \frac{1}{2} u_i u_i$ and $c_d = c_t/\sigma_k - \nu/k_{sgs}^{\frac{1}{2}}\overline{\Delta}$ which is defined here as a diffusion model coefficient. Using the logic described in section 2.3, the following expression for the diffusion flux at the test filter level is obtained,

$$d_i = -\left(\langle \overline{p u_i} \rangle - \hat{\overline{p}}\,\hat{\overline{u}}_i\right) - \left(\langle \overline{u_i} \overline{k}_{tot} \rangle - \hat{\overline{u}}_i \hat{\overline{k}}_{tot}\right) + \hat{\overline{u}}_j \left(\langle \overline{u_i u_j} \rangle - \hat{\overline{u}}_i \hat{\overline{u}}_j\right)$$
$$= c_d k_{res}^{\frac{1}{2}} \hat{\Delta} \frac{\partial k_{res}}{\partial x_i} \qquad \text{(A 3)}$$

where $\overline{k}_{tot} = \frac{1}{2}\overline{u_i u_i} = \frac{1}{2}\overline{u}_i \overline{u}_i + k_{sgs}$ and $k_{res} = \frac{1}{2}\left(\langle \overline{u_i u_i} \rangle - \hat{\overline{u}}_i \hat{\overline{u}}_i\right)$. (A 3) does not include any other unknowns except c_d, hence, c_d can be determined directly from (A 3). However, since (A 3) is a set of three independent equations for one unknown c_d, the least-square method is needed to solve this over-determined system as was done to determine c_t; this approach gives

$$c_d = \frac{d_i \dfrac{\partial k_{res}}{\partial x_i}}{k_{res}^{\frac{1}{2}} \hat{\Delta} \dfrac{\partial k_{res}}{\partial x_i} \dfrac{\partial k_{res}}{\partial x_i}}. \qquad \text{(A 4)}$$

Appendix B. The dynamic estimate of the initial k_{sgs}

As shown by Yoshizawa (1985), the usual Smagorinsky model can be derived from the SGS kinetic energy model by assuming the equilibrium of the SGS energy production and dissipation. Upon this assumption, the SGS energy is described in terms of the grid width and the resolved scale strain rate tensor without employing a transport equation for k_{sgs}. This description is easily obtained by comparing (6) with (15) and (16),

$$k_{sgs} = \frac{1}{2}\left(\overline{u_i u_i} - \overline{u}_i \overline{u}_i\right) \approx C\overline{\Delta}^2 \left|\overline{S}\right|^2. \qquad \text{(B 1)}$$

The test-filter-level energy is also described in a similar manner,

$$k_{res} = \tfrac{1}{2}\left(\langle \overline{u}_i \overline{u} \rangle - \hat{\overline{u}}_i \hat{\overline{u}}_i\right) \approx C\hat{\Delta}^2 \left|\hat{\overline{S}}\right|^2. \qquad \text{(B 2)}$$

Now, a dimensionless coefficient C can be evaluated from (B 2),

$$C \approx \frac{k_{res}}{\hat{\Delta}^2 \left|\hat{\overline{S}}\right|^2}. \qquad \text{(B 3)}$$

By substituting (B 3) into (B 1), we get

$$k_{sgs} \approx \frac{\overline{\Delta}^2 \left|\overline{S}\right|^2}{\hat{\Delta}^2 \left|\hat{\overline{S}}\right|^2} k_{res}. \qquad \text{(B 4)}$$

(B 4) can provide a dynamic estimate of k_{sgs} when the initial k_{sgs} is not known. Interestingly, the description for k_{sgs} in (B 4) is same as in (49) except that (B 4) contains a variable coefficient while (49) contains a fixed coefficient c_k. By analogy between (B 4) and (49), c_k can be evaluated from the resolved scale information in LES data,

$$c_k \approx \frac{\overline{\Delta}^2 \left|\overline{S}\right|^2}{\hat{\Delta}^2 \left|\hat{\overline{S}}\right|^2}. \qquad \text{(B 5)}$$

Using the LES data of the forced isotropic turbulence (section 4.3), (B 5) predicts $c_k \approx 0.49$ for higher Reynolds number case ($\mathrm{Re}_\lambda \approx 260$) and $c_k \approx 0.45$ for lower Reynolds number case ($\mathrm{Re}_\lambda \approx 80$). These values are in very good agreement with that given by Liu *et al.* (1994). In their work, $c_k = 0.45 \pm 0.15$ was obtained from a high Reynolds number ($\mathrm{Re}_\lambda \approx 310$) experimental data for a free jet.

References

Akselvoll, K. & Moin, P. 1993 Application of the dynamic localization model to large-eddy simulation of turbulent flow over a backward facing step. In *Engineering Applications of Large Eddy Simulations* (ed. U. Piomelli & S. Ragab). ASME-FED, **162**, 1.

Bardina, J., Ferziger, J. H. & Reynolds, W. C. 1980 Improved subgrid scale models for large eddy simulation. *AIAA Paper* 80-1357.

Brachet, M. E., Meiron, D. I., Orszag, S. A., Nickel, B. G., Morf, R. H. & Frisch, U. 1983 Small-scale structure of the Taylor Green Vortex. *J. Fluid Mech.* **130**, 411.

Bradshaw, P., Cebeci, T. & Whitelaw, J. H. 1981 *Engineering Calculation Methods for Turbulent Flow*. Academic Press, London.

Brandt, A. 1981 Guide to multigrid development. In *Lecture Notes in Mathematics* **960**, 220. Springer-Verlag, Berlin.

Briscolini, M. & Santangelo, P. 1994 The non-Gaussian statistics of the velocity field in low-resolution large-eddy simulations of homogeneous turbulence. *J. Fluid Mech.* **270**, 199.

Chorin, A. J. 1967 A numerical method for solving incompressible viscous flow problems. *J. Comput. Phys.* **2**,12.

Carati, D., Ghosal, S. & Moin, P. 1995 On the representation of backscatter in dynamic localization models. *Phys. Fluids* **7**, 606.

Domaradzki, J. A., Liu, W. & Brachet, M. E. 1993 An analysis of subgrid-scale interactions in numerically simulated isotropic turbulence. *Phys. Fluids* A **5**, 1747.

El-Hady, N. M., Zang, T. A. & Piomelli, U. 1994 Application of the dynamic subgrid-scale model to axisymmetric transitional boundary layer at high speed. *Phys. Fluids* **6**, 1299.

Germano, M., Piomelli, U., Moin, P. & Cabot, W. H. 1991 A dynamic subgrid-scale eddy viscosity model. *Phys. Fluids* A **3**, 1760.

Ghosal, S., Lund, T. S. & Moin, P. 1993 A local dynamic model for large eddy simulation. *CTR Annual Research Briefs* 1992, 3.

Ghosal, S., Lund, T. S., Moin, P. & Akselvoll, K. 1995 A dynamic localization model for large-eddy simulation of turbulent flows. *J. Fluid Mech.* **289**, 229.

Huang, M.-J. & Leonard, A. 1994 Power-law decay of homogeneous turbulence at low Reynolds numbers. *Phys. Fluids* **6**, 3765.

Horiuti, K. 1989 The role of the Bardina model in large eddy simulation of turbulent channel flow. *Phys. Fluids* A **1**, 426.

Jimenez, J., Wray, A. A., Saffman, P. S. & Rogallo, R. S. 1993 The structure of intense vorticity in isotropic turbulence. *J. Fluid Mech.* **255**, 65.

Kerr, R. M. 1985 Higher order derivative correlations and the alignment of small-scale structures in isotropic numerical turbulence. *J. Fluid Mech.* **153**, 31.

Kim, W.-W. & Menon, S. 1995 A new dynamic one-equation subgrid-scale model for large eddy simulations. *AIAA Paper* 95-0356, *AIAA 33rd Aerospace Sciences Mtg, Reno, NV.*

Lilly, D. K. 1992 A proposed modification of the Germano subgrid-scale closure method. *Phys. Fluids* **4**, 633.

Liu, S., Meneveau, C. & Katz, J. 1994 On the properties of similarity subgrid-scale models as deduced from measurements in a turbulent jet. *J. Fluid Mech.* **275**, 83.

Lund, T. S., Ghosal, S. & Moin, P. 1993 Numerical experiments with highly-variable eddy viscosity models. In *Engineering Applications of Large Eddy Simulations* (ed. U. Piomelli & S. Ragab). ASME-FED, **162**, 7.

Meneveau, C., Lund, T. S. & Cabot, W. 1994 A Lagrangian dynamic subgrid-scale model of turbulence. *Proc. CTR Summer Program* 1994, 271.

Menon, S. & Yeung, P.-K. 1994 Analysis of subgrid models using direct and large-eddy simulations of isotropic turbulence. *Proc. AGARD 74th Fluid Dynamics Symp. on Application of Direct and Large Eddy Simulation to Transition and Turbulence, AGARD-CP*-551, 10-1.

Menon, S., Yeung, P.-K. & Kim, W.-W. 1994 Effect of subgrid models on the computed interscale energy transfer in isotropic turbulence. *AIAA Paper* 94-2387, *AIAA 25th Fluid Dynamics Conf., Colorado Springs, CO.*

Moin, P. & Kim, J. 1982 Numerical investigation of turbulent channel flow. *J. Fluid Mech.* **118**, 341.

Moin, P., Squires, K., Cabot, W. & Lee, S. 1991 A dynamic subgrid-scale model for compressible turbulence and scalar transport. *Phys. Fluids* A **3**, 2746.

Monin, A. S. & Yaglom, A. M. 1975 *Statistical Fluid Mechanics*, **2**. MIT Press, Cambridge, MA.

Piomelli, U., Moin, P. & Ferziger, J. H. 1988 Model consistency in large eddy simulation of turbulent channel flows. *Phys. Fluids* **31**, 1884.

Piomelli, U. 1993 High Reynolds number calculations using the dynamic subgrid-scale stress model. *Phys. Fluids* A **5**, 1484.

Rai, M. M. & Moin, P. 1991 Direct simulations of turbulent flow using finite-difference schemes. *J. Comput. Phys.* **96**, 15.

Rogallo, R. S. 1981 Numerical experiments in homogeneous turbulence. *NASA Tech. Memo.* 81315.

Rogers, S. E., Kwak, D. & Kiris, C. 1991 Steady and unsteady solutions of the incompressible Navier-Stokes equations. *AIAA J.* **29**, 603.

Schumann, U. 1975 Subgrid scale model for finite difference simulations of turbulent flows in plane channels and annuli. *J. Comput. Phys.* **18**, 376.

Smagorinsky, J. 1963 General circulation experiments with the primitive equations. I. The basic experiment. *Month. Wea. Rev.* **91**, 99.

Speziale, C. G. 1985 Galilean invariance of subgrid-scale stress models in the large-eddy simulation of turbulence. *J. Fluid Mech.* **156**, 55.

Vincent, A. & Meneguzzi, M. 1991 The spatial structure and statistical properties of homogeneous turbulence. *J. Fluid Mech.* **225**, 1.

Vreman, B., Geurts, B. & Kuerten, H. 1994 Realizability conditions for the turbulent stress tensor in large-eddy simulation. *J. Fluid Mech.* **278**, 351.

Yoshizawa, A & Horiuti, K. 1985 A statistically-derived subgrid-scale kinetic energy model for the large-eddy simulation of turbulent flows. *J. Phys. Soc. Jpn.* 54, 2834.

Yoshizawa, A. 1993 Bridging between eddy-viscosity-type and second-order models using a two-scale DIA. *Proc. 9th Symp. on Turbulent Shear Flows*, 23-1-1.

Zang, Y., Street, R. L. & Koseff, J. R. 1993 A dynamic mixed subgrid-scale model and its application to turbulent recirculating flows. *Phys. Fluids* A 5, 3186.

Table Captions

Table 1. Characteristic scales and flow properties at the grid and test filter levels.

Table 2. Resolved energy at various grid resolutions. This data is obtained from numerically integrating the spectrum given by Comte-Bellot & Corsin (1971).

Table 3. Decay exponent n of the power law decay $E \sim (t^*)^n$. The experimental data is obtained from a least-square fit to the resolved energy data which is computed by numerically integrating the spectrum of Comte-Bellot & Corsin (1971).

Table 4. Higher-order moments for a velocity component, u, and its longitudinal and transverse gradients, $\partial u/\partial x$ and $\partial u/\partial y$. The nth-order moments are denoted by S_n. The DNS statistics of velocity derivative are obtained from the full resolution field. Therefore, the direct comparison of LES and DNS using the statistics of velocity derivative may be meaningless.

Figure Captions

Figure 1. Energy spectrum, $E(k)$, and dissipation spectrum, $D(k) = 2\nu k^2 E(k)$, computed from 128^3 DNS data at $t = 29$.

Figure 2. Energy spectra computed from 128^3 DNS and 64^3 LES using various dynamic SGS models at $t = 29$.

Figure 3. Energy spectra computed from 128^3 DNS and 32^3 LES using various dynamic SGS models at $t = 29$.

Figure 4. Time evolution of the ratio of the dissipation rate of the SGS kinetic energy (D) to the production rate of the SGS kinetic energy (P) computed from 128^3 DNS data at three different grid resolutions.

Figure 5. Time evolution of the velocity derivative skewness computed from 128^3 DNS and 64^3 LES using various dynamic SGS models.

Figure 6. Time evolution of the velocity derivative flatness computed from 128^3 DNS and 64^3 LES using various dynamic SGS models.

Figure 7. Time evolution of the production rate of the SGS kinetic energy computed from 128^3 DNS and 64^3 LES using dynamic one-equation SGS models.

Figure 8. Time evolution of the dissipation rate of the SGS kinetic energy computed from 128^3 DNS and 64^3 LES using dynamic one-equation SGS models.

Figure 9. Time evolution of the velocity derivative skewness computed from 128^3 DNS and 32^3 LES using various dynamic SGS models.

Figure 10. Time evolution of the velocity derivative flatness computed from 128^3 DNS and 32^3 LES using various dynamic SGS models.

Figure 11. Time evolution of the production rate of the SGS kinetic energy computed from 128^3 DNS and 32^3 LES using dynamic one-equation SGS models.

Figure 12. Time evolution of the dissipation rate of the SGS kinetic energy computed from 128^3 DNS and 32^3 LES using dynamic one-equation SGS models.

Figure 13. Time evolution of the model coefficients determined by various dynamic SGS models.

Figure 14. Time evolution of the dissipation model coefficients determined by dynamic one-equation SGS models.

Figure 15. Decay of turbulent kinetic energy resolved in three different resolution LES; compared to the experimental data by Comte-Bellot & Corsin (1971).

Figure 16. Energy spectra predicted by three different resolution LES at $t^* = 4.98$; compared to the experimental data by Comte-Bellot & Corsin (1971).

Figure 17. Energy spectra predicted by three different resolution LES at $t^* = 8.69$; compared to the experimental data by Comte-Bellot & Corsin (1971).

Figure 18. Time evolution of the model coefficients determined from three different resolution LES.

Figure 19. Time evolution of the dissipation model coefficients determined from three different resolution LES.

Figure 20. Time evolution of mean kinetic energy resolved in 32^3 LES at two different Reynolds numbers.

Figure 21. Probability distribution of normalized velocity difference for five different scales (r) predicted by 32^3 LES at $Re_\lambda = 260$.

Figure 22. Probability distribution of normalized velocity difference for $r = 0.39$; compared to the high resolution DNS results by Vincent & Meneguizzi (1991).

Figure 23. Time evolution of negative model coefficient fraction resulted from 32^3 LES at two different Reynolds numbers.

Figure 24. Time evolution of the model coefficients determined from 32^3 LES at two different Reynolds numbers.

Figure 25. Time evolution of the dissipation model coefficients determined from 32^3 LES at two different Reynolds numbers.

	Grid filter level		Test filter level		
	Dissipation range	Production range	Dissipation range		Production range
Characteristic length scale	Not available	$\overline{\Delta}$	Not available	Not available	$\hat{\Delta} = 2\overline{\Delta}$
Energy level	$\overline{u_i u_i}$	$\overline{u}_i \overline{u}_i$	$\langle \overline{u_i u_i} \rangle$	$\langle \overline{u}_i \overline{u}_i \rangle$	$\hat{\overline{u}}_i \hat{\overline{u}}_i$
Stress tensor	$\overline{u_i u_j}$	$\overline{u}_i \overline{u}_j$	$\langle \overline{u_i u_j} \rangle$	$\langle \overline{u}_i \overline{u}_j \rangle$	$\hat{\overline{u}}_i \hat{\overline{u}}_j$
Dissipation rate	$\overline{\frac{\partial u_i}{\partial x_j} \frac{\partial u_i}{\partial x_j}}$	$\frac{\partial \overline{u}_i}{\partial x_j} \frac{\partial \overline{u}_i}{\partial x_j}$	$\left\langle \overline{\frac{\partial u_i}{\partial x_j} \frac{\partial u_i}{\partial x_j}} \right\rangle$	$\left\langle \frac{\partial \overline{u}_i}{\partial x_j} \frac{\partial \overline{u}_i}{\partial x_j} \right\rangle$	$\frac{\partial \hat{\overline{u}}_i}{\partial x_j} \frac{\partial \hat{\overline{u}}_i}{\partial x_j}$
Strain rate tensor	Not available	$\overline{S}_{ij}$	Not available	Not available	$\hat{\overline{S}}_{ij}$
Effective viscosity	ν		ν	$\nu + \nu_T$	

(Here, "Not available" implies that this information can not be obtained from the LES.)

Table 1. Characteristic scales and flow properties at the grid and test filter levels.

Grid resolution	512^3	384^3	256^3	192^3	128^3	96^3	64^3	48^3	32^3	24^3	16^3	12^3	8^3
Resolved energy (%)	99.8	99.5	98.4	96.6	92.2	87.3	78.3	70.3	59.3	49.7	35.1	24.4	10.5

Table 2. Resolved energy at various grid resolutions. This data is obtained from numerically integrating the spectrum given by Comte-Bellot & Corsin (1971).

Grid resolution	Experiment	LDKSGS	DLM(k)	DASGS
48^3	-1.20	-1.17	-1.17	-1.20
32^3	-1.16	-1.13		
24^3	-1.12	-1.09		

Table 3. Decay exponent n of the power law decay $E \sim (t^*)^n$. The experimental data is obtained from a least-square fit to the resolved energy data which is computed by numerically integrating the spectrum of Comte-Bellot & Corsin (1971).

	u		$\partial u/\partial x$				$\partial u/\partial y$			
	S_4	S_6	S_3	S_4	S_5	S_6	S_3	S_4	S_5	S_6
512^3 DNS	2.80	12.5	-0.525	6.1	-12.0	125		9.4		370
240^3 DNS			-0.5	5.9	-9	90	-0.04	8.0		
64^3 LES			-0.35				0.06	4.5		
32^3 LDKSGS ($Re_\lambda \approx 260$)	2.78	11.9	-0.317	3.47	-3.48	23.4	-0.005	4.87	-0.109	49.9
32^3 LDKSGS ($Re_\lambda \approx 80$)	2.80	12.1	-0.302	3.59	-3.57	25.8	0.028	4.93	0.233	51.3
Gaussian	3.0	15.0	0.0	3.0	0.0	15.0	0.0	3.0	0.0	15.0

Table 4. Higher-order moments for a velocity component, u, and its longitudinal and transverse gradients, $\partial u/\partial x$ and $\partial u/\partial y$. The nth-order moments are denoted by S_n. The DNS statistics of velocity derivative are obtained from the full resolution field. Therefore, the direct comparison of LES and DNS using the statistics of velocity derivative may be meaningless.

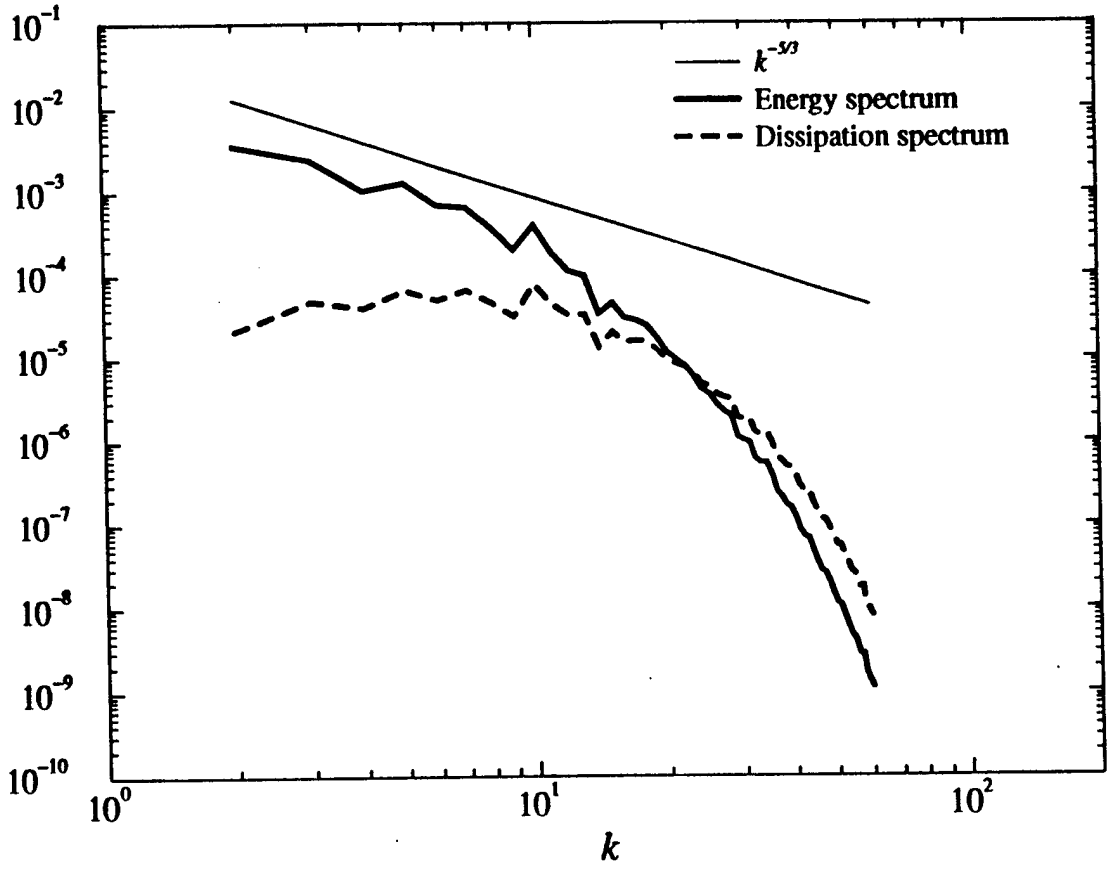
10^{-1}
10^{-2}
10^{-3}
10^{-4}
10^{-5}
10^{-6}
10^{-7}
10^{-8}
10^{-9}
10^{-10}
10^{0}
10^{1}
10^{2}
k
$k^{-5/3}$
Energy spectrum
Dissipation spectrum

Figure 1.

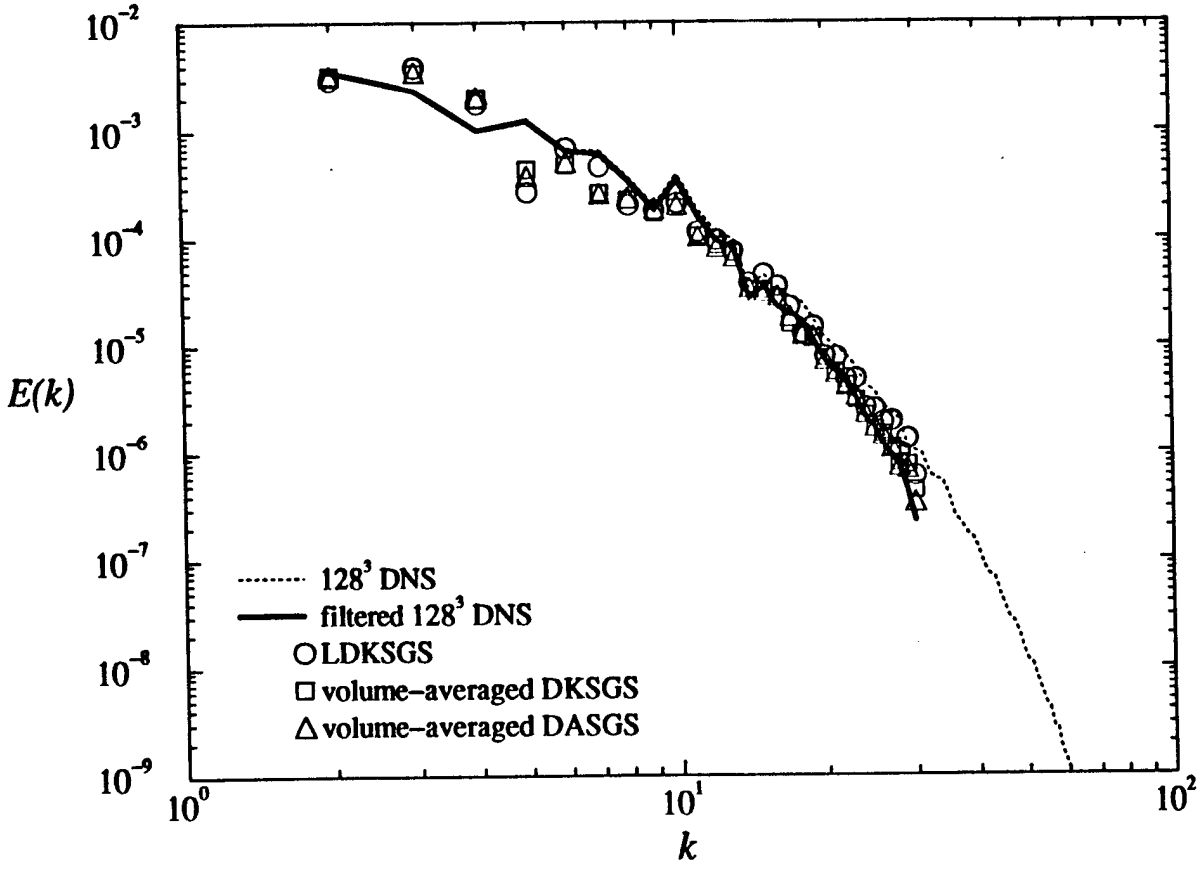
10^{-2}
10^{-3}
10^{-4}
10^{-5}
10^{-6}
10^{-7}
10^{-8}
10^{-9}
E(k)
10^{0}
10^{1}
10^{2}
k
128³ DNS
filtered 128³ DNS
LDKSGS
volume–averaged DKSGS
volume–averaged DASGS

Figure 2.

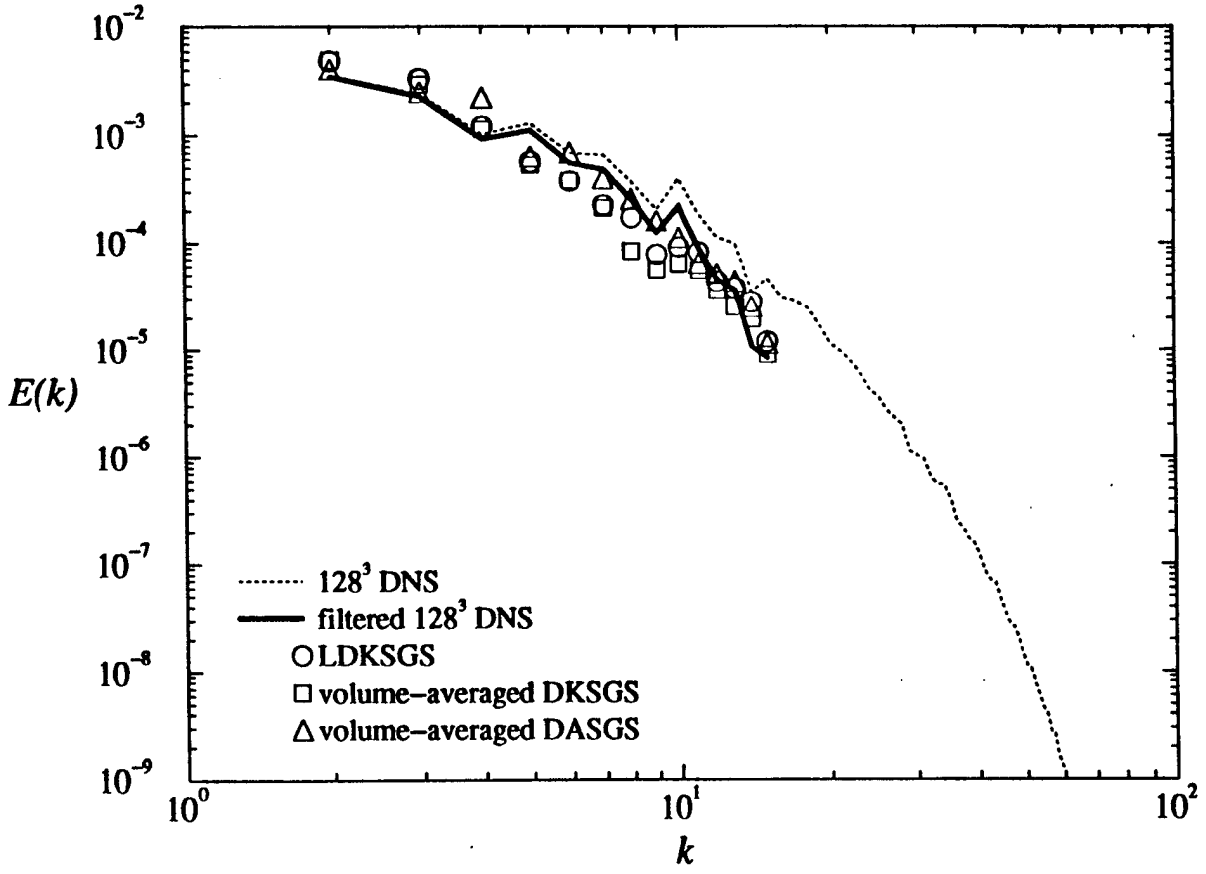
10^{-2}
10^{-3}
10^{-4}
10^{-5}
10^{-6}
10^{-7}
10^{-8}
10^{-9}
E(k)
10^{0}
10^{1}
10^{2}
k
128^3 DNS
filtered 128^3 DNS
LDKSGS
volume–averaged DKSGS
volume–averaged DASGS

Figure 3.

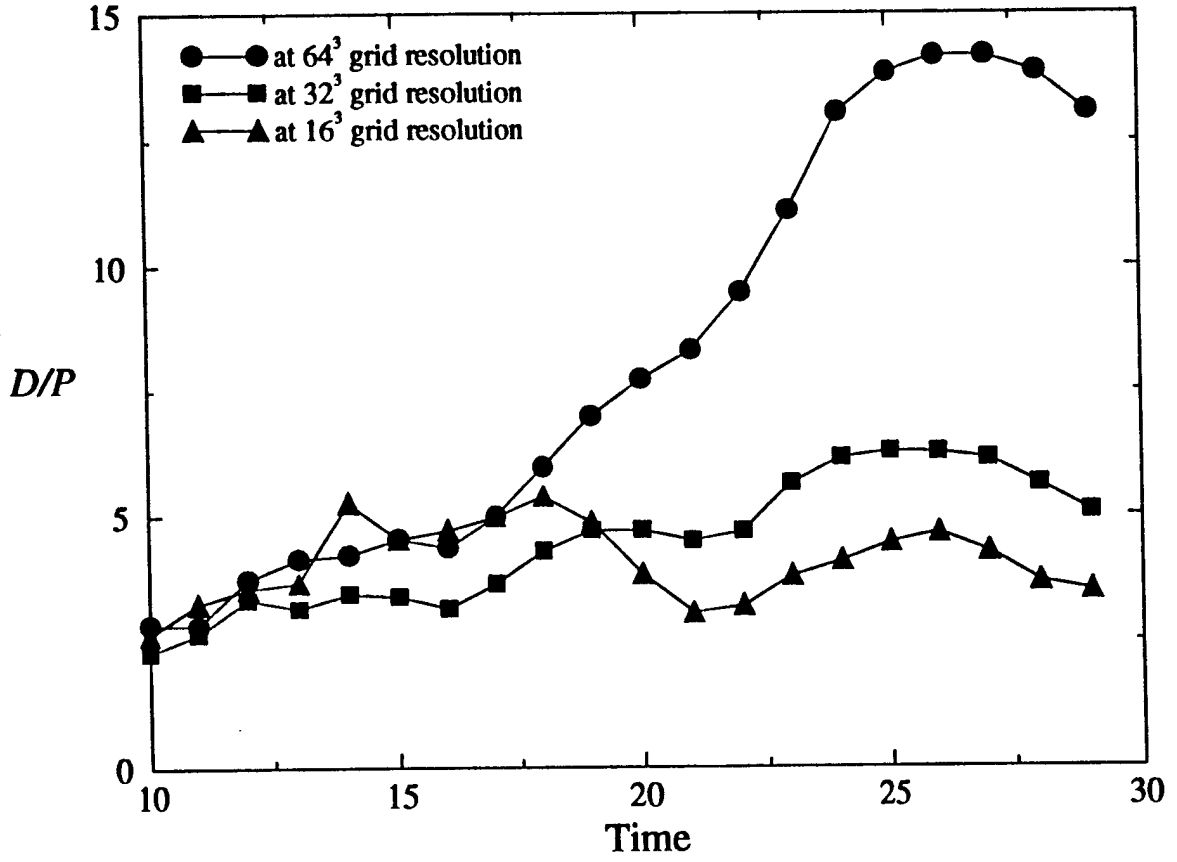
15
10
5
0
D/P
at 64³ grid resolution
at 32³ grid resolution
at 16³ grid resolution
10
15
20
25
30
Time

Figure 4.

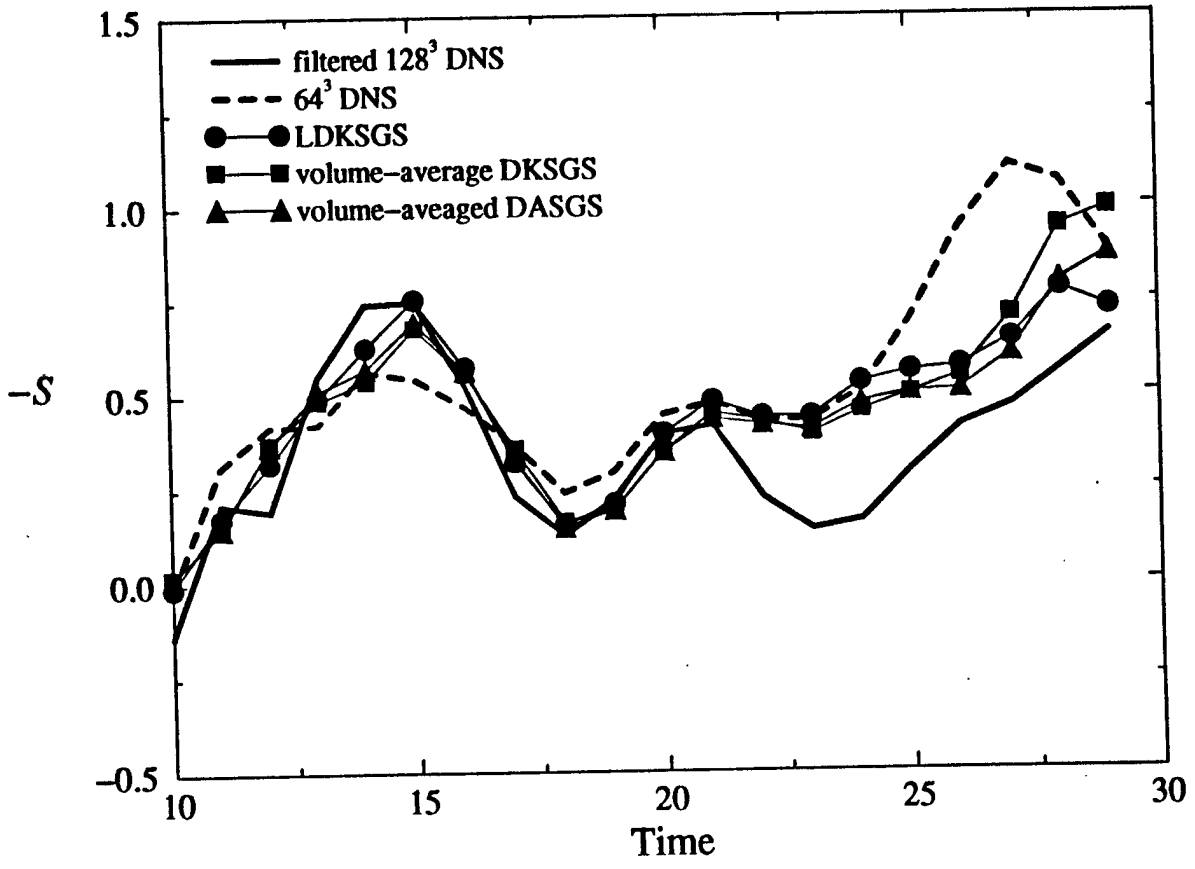
filtered 128³ DNS
64³ DNS
LDKSGS
volume–average DKSGS
volume–aveaged DASGS
1.5
1.0
0.5
0.0
−0.5
−S
10
15
20
25
30
Time

Figure 5.

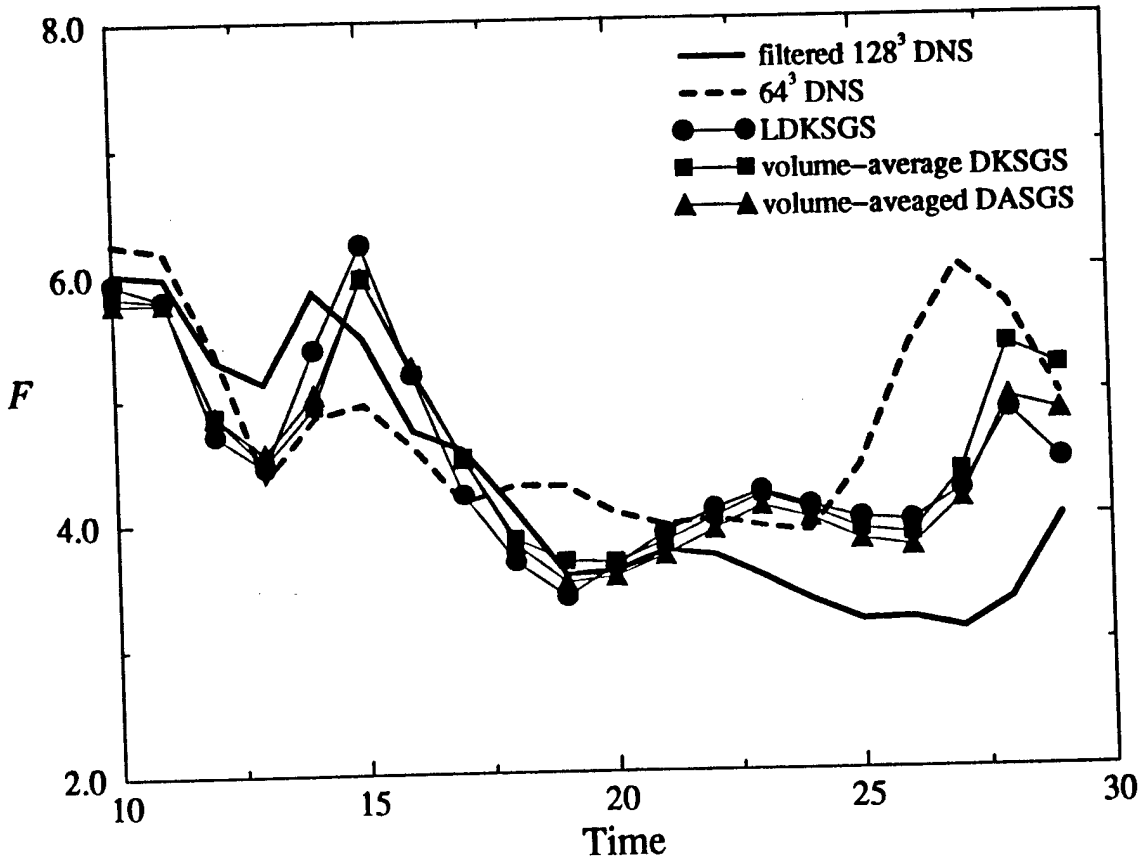
8.0
6.0
4.0
2.0
F
10
15
20
25
30
Time
filtered 128³ DNS
64³ DNS
LDKSGS
volume–average DKSGS
volume–aveaged DASGS

Figure 6.

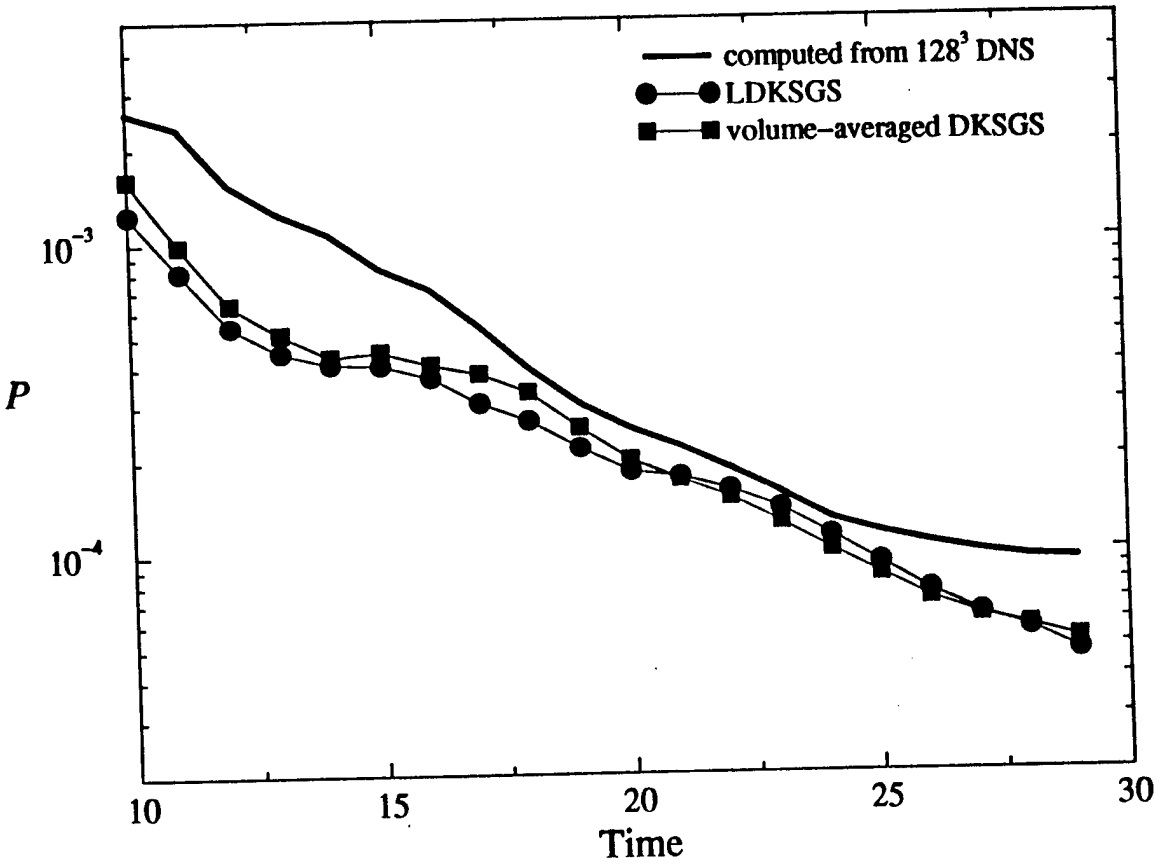
computed from 128³ DNS
LDKSGS
volume–averaged DKSGS
10^{-3}
10^{-4}
P
10
15
20
25
30
Time

Figure 7.

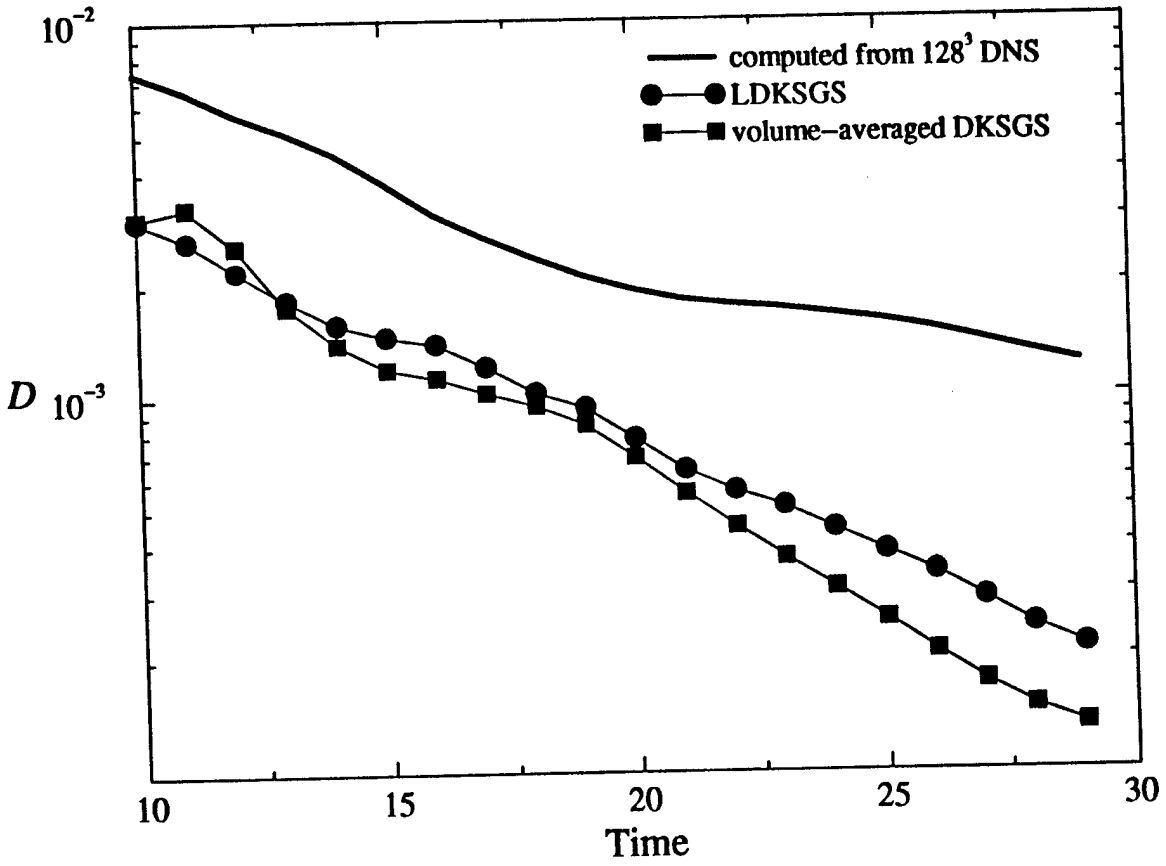
10^{-2}
D 10^{-3}
computed from 128^3 DNS
LDKSGS
volume–averaged DKSGS
10
15
20
25
30
Time

Figure 8.

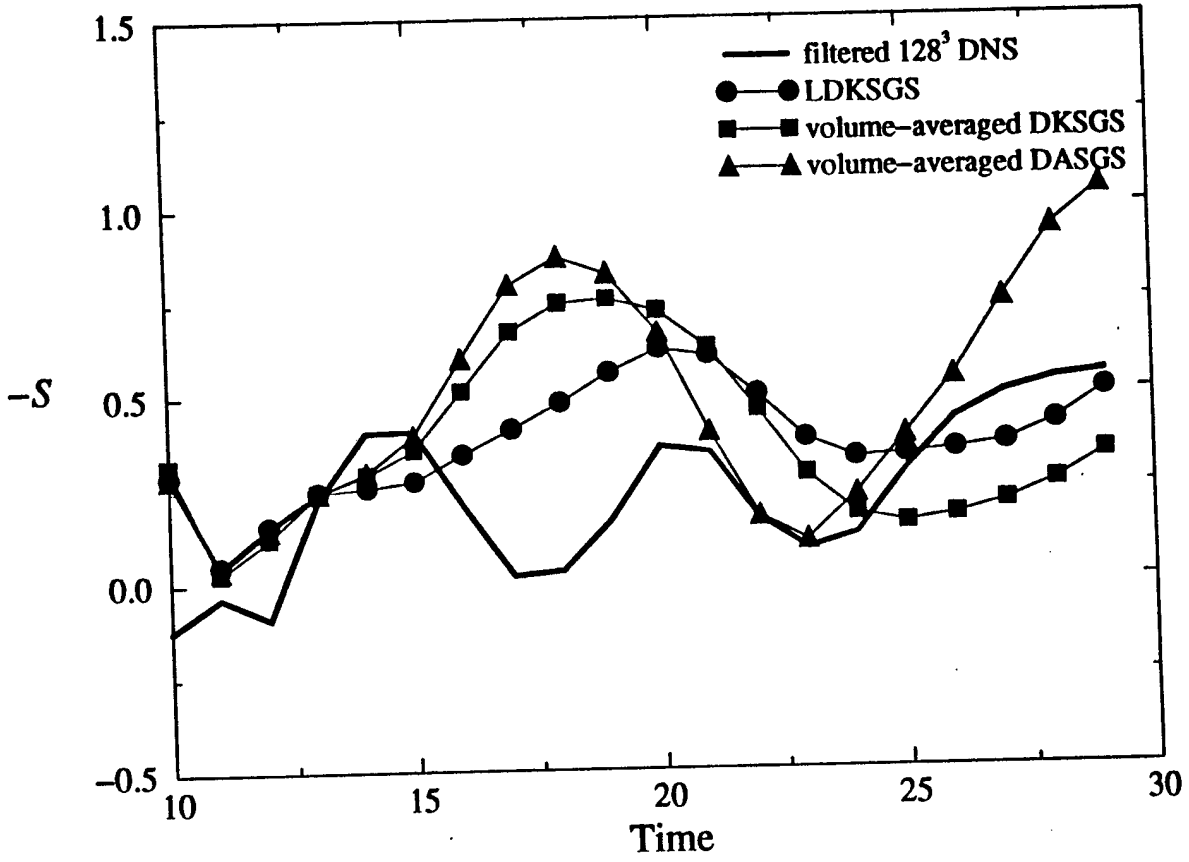
filtered 128³ DNS
LDKSGS
volume–averaged DKSGS
volume–averaged DASGS
1.5
1.0
0.5
0.0
−0.5
−S
10
15
20
25
30
Time

Figure 9.

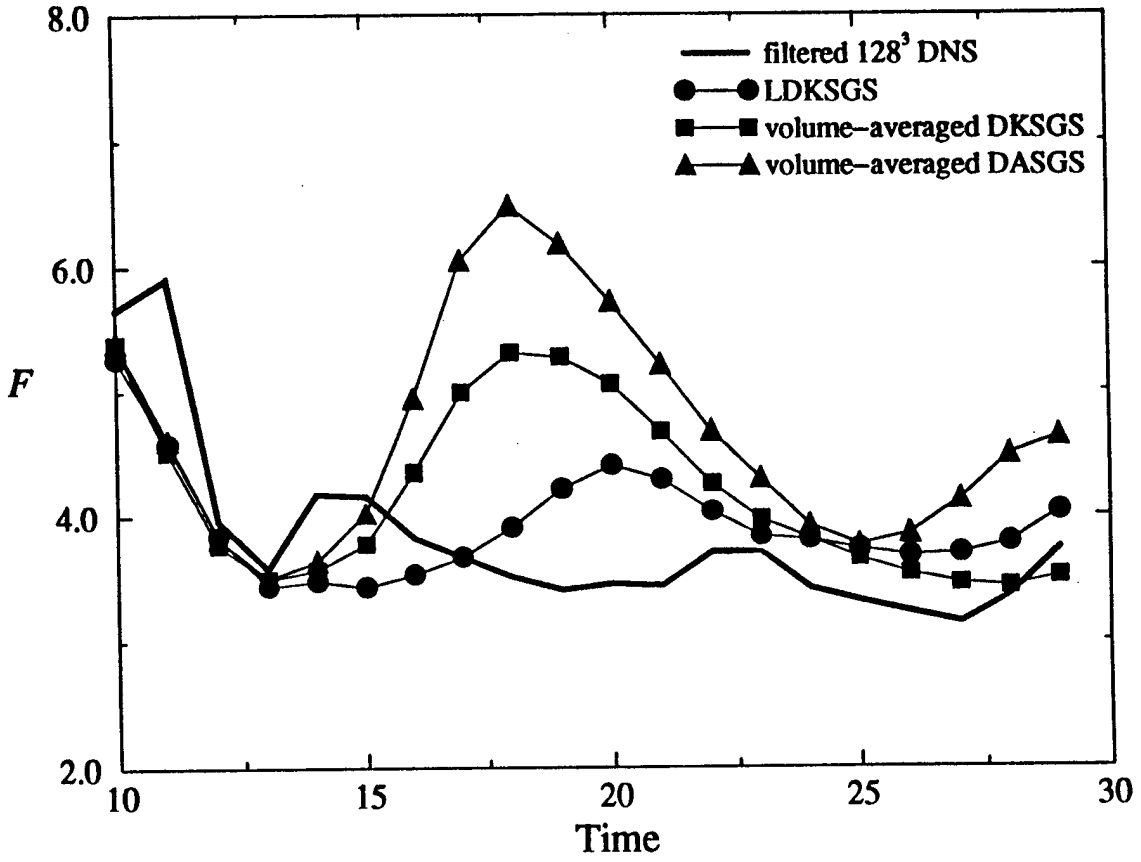
8.0
6.0
4.0
2.0
F
10
15
20
25
30
Time
filtered 128³ DNS
LDKSGS
volume–averaged DKSGS
volume–averaged DASGS

Figure 10.

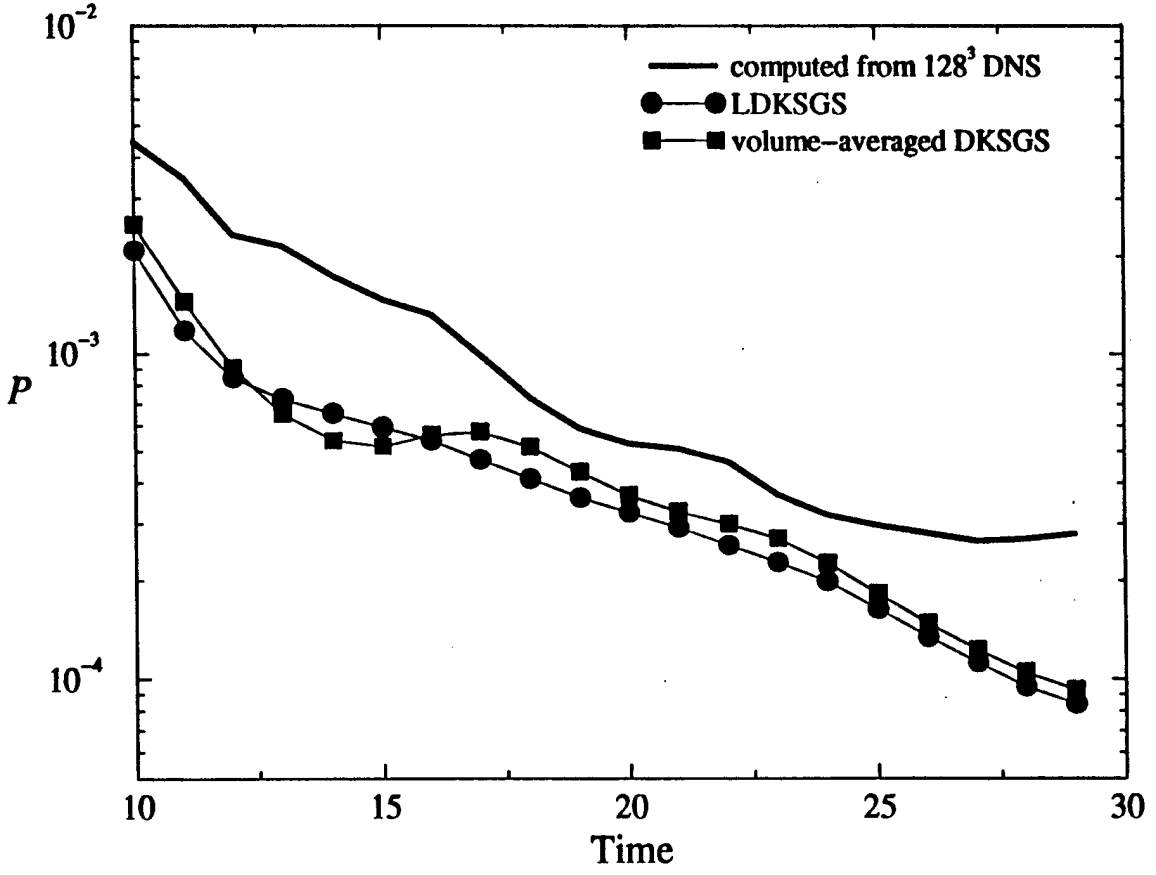
computed from 128³ DNS
LDKSGS
volume–averaged DKSGS
10^{-2}
10^{-3}
10^{-4}
P
10
15
20
25
30
Time

Figure 11.

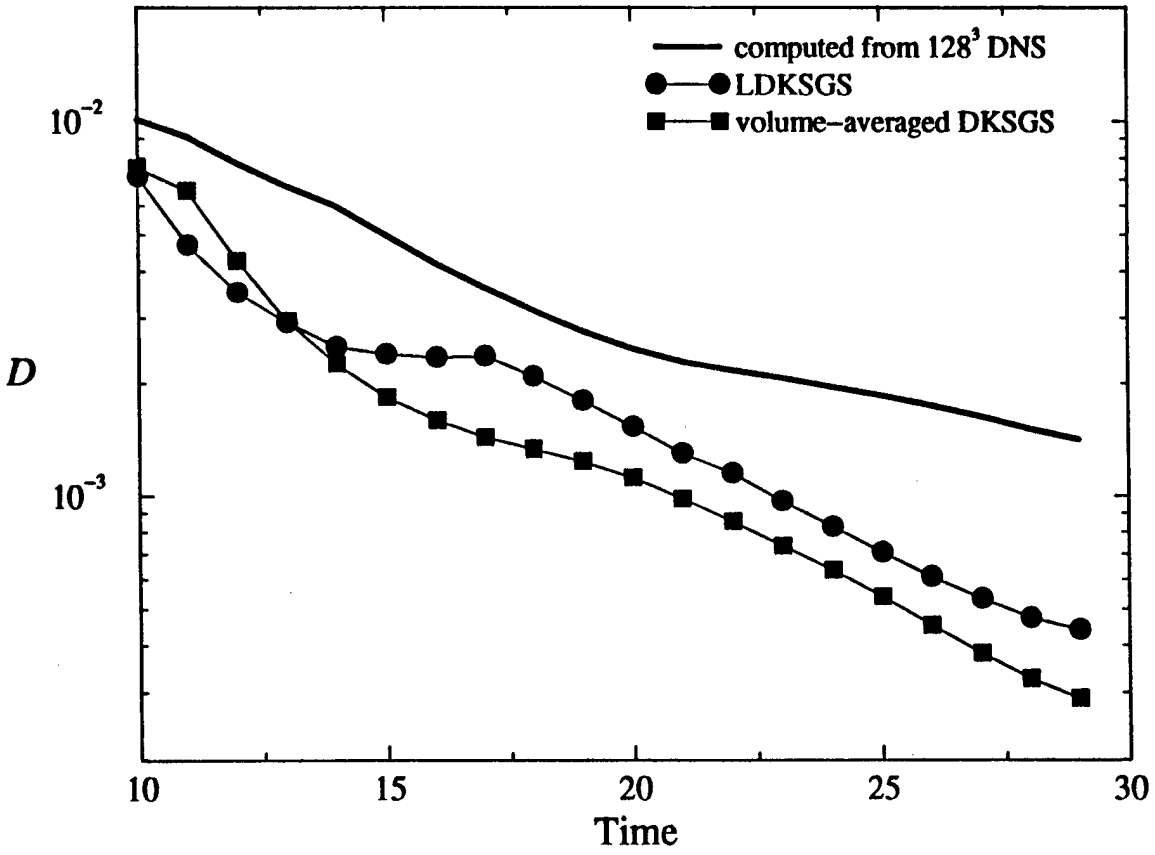
computed from 128³ DNS
LDKSGS
volume–averaged DKSGS
10^{-2}
10^{-3}
D
10
15
20
25
30
Time

Figure 12.

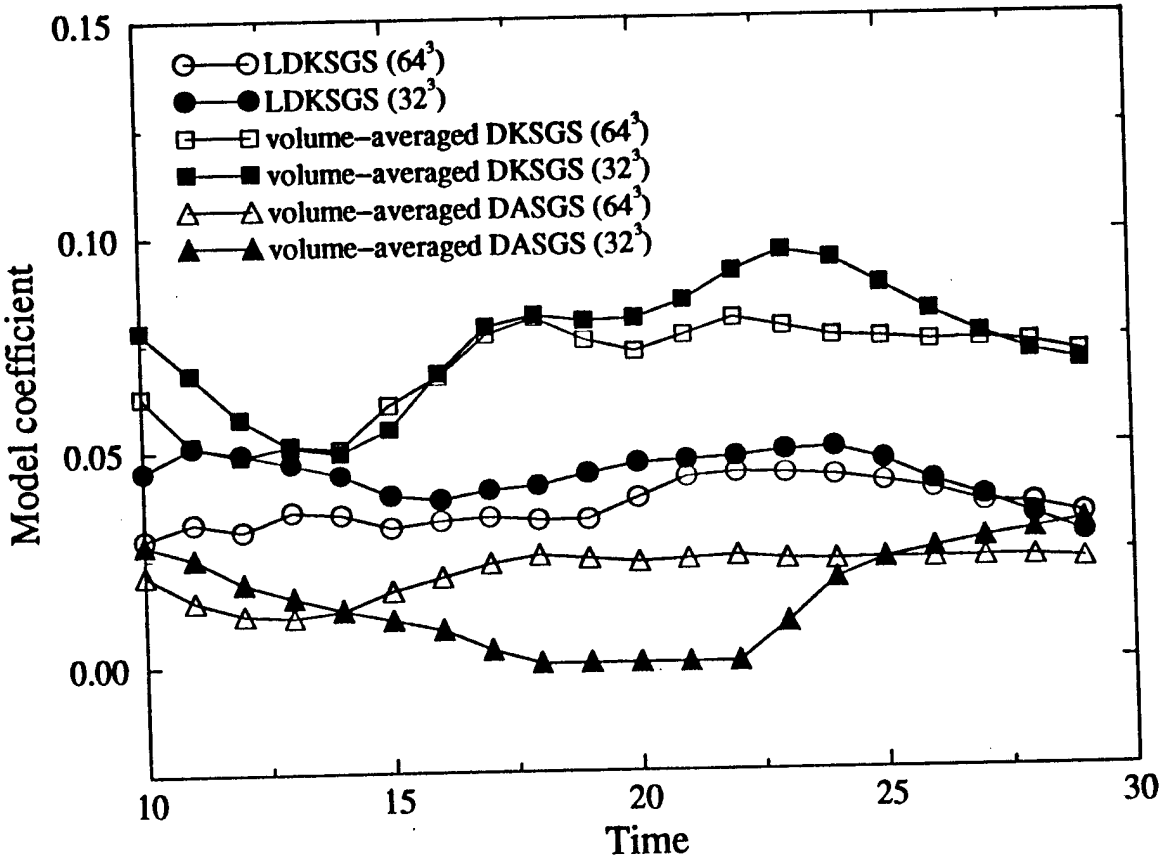
0.15
0.10
0.05
0.00
Model coefficient
LDKSGS (64³)
LDKSGS (32³)
volume–averaged DKSGS (64³)
volume–averaged DKSGS (32³)
volume–averaged DASGS (64³)
volume–averaged DASGS (32³)
10
15
20
25
30
Time

Figure 13.

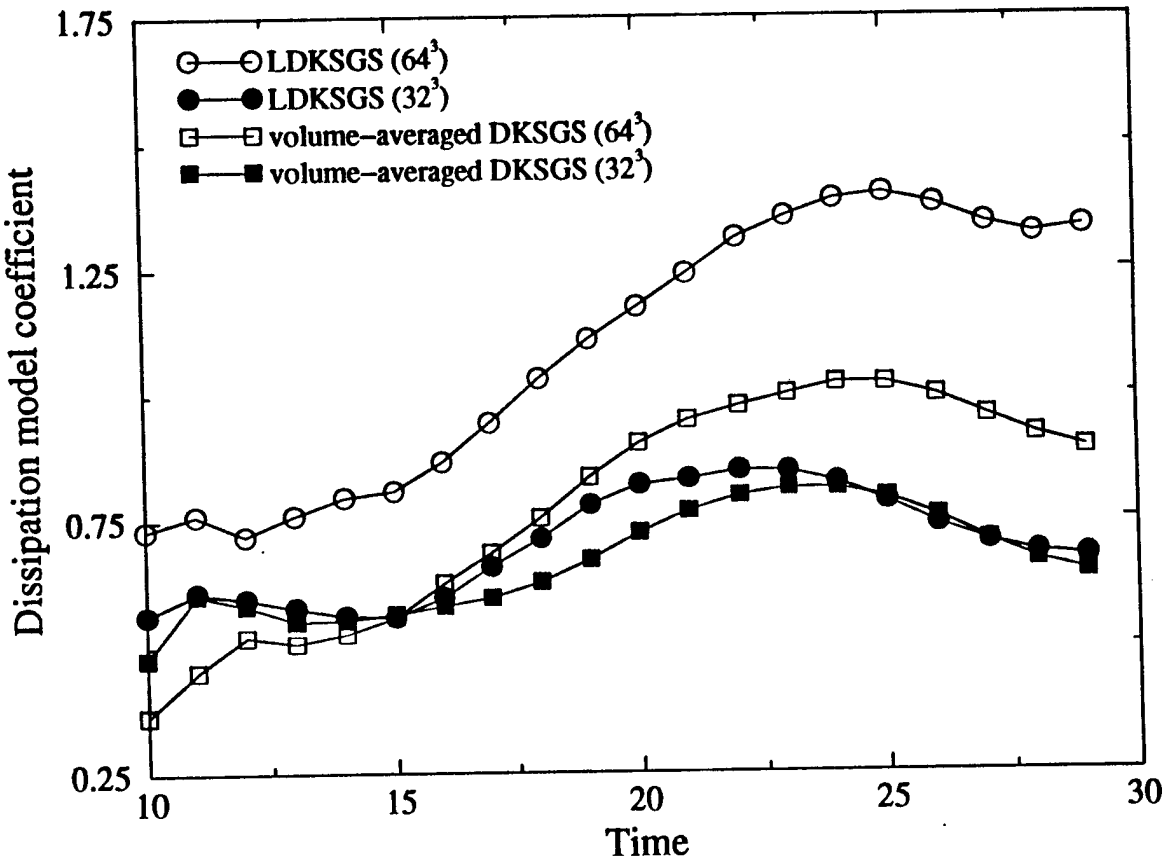
LDKSGS (64³)
LDKSGS (32³)
volume–averaged DKSGS (64³)
volume–averaged DKSGS (32³)
Dissipation model coefficient
1.75
1.25
0.75
0.25
10
15
20
25
30
Time

Figure 14.

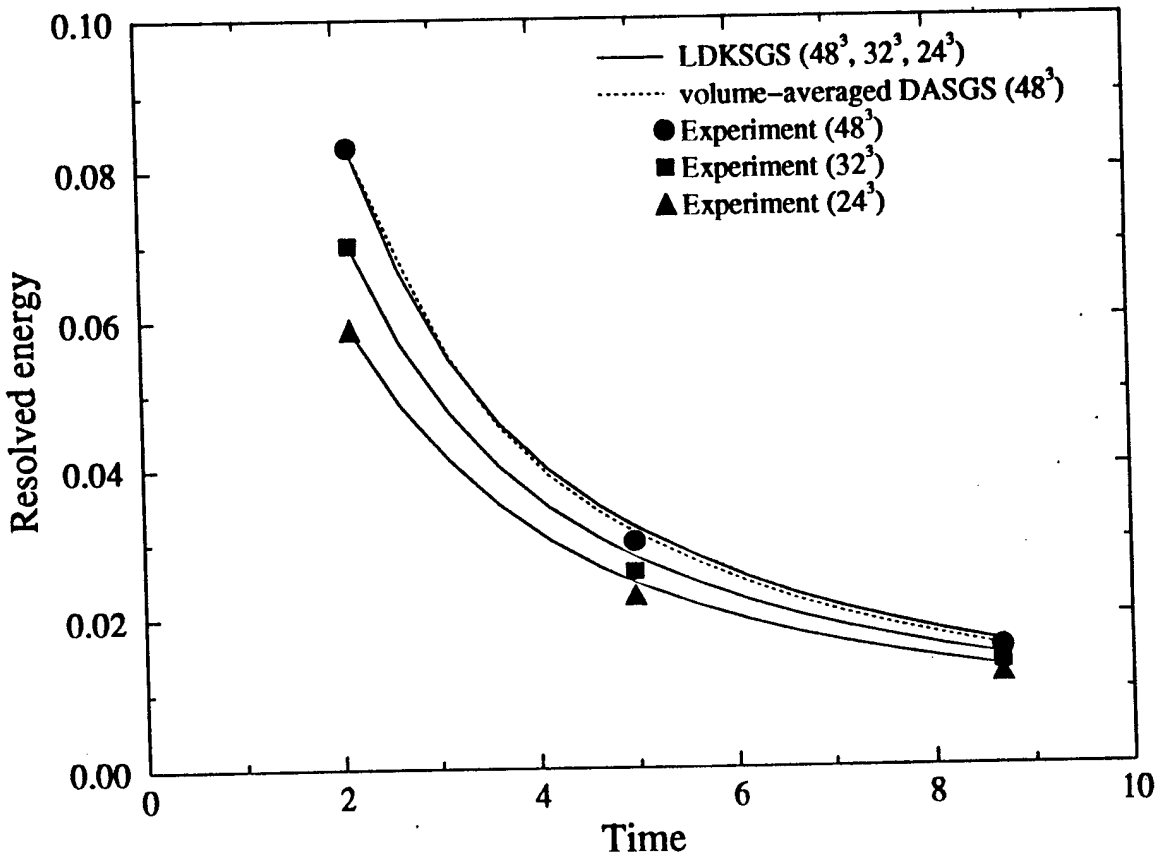
LDKSGS (48³, 32³, 24³)
volume-averaged DASGS (48³)
Experiment (48³)
Experiment (32³)
Experiment (24³)
Resolved energy
0.10
0.08
0.06
0.04
0.02
0.00
0
2
4
6
8
10
Time

Figure 15.

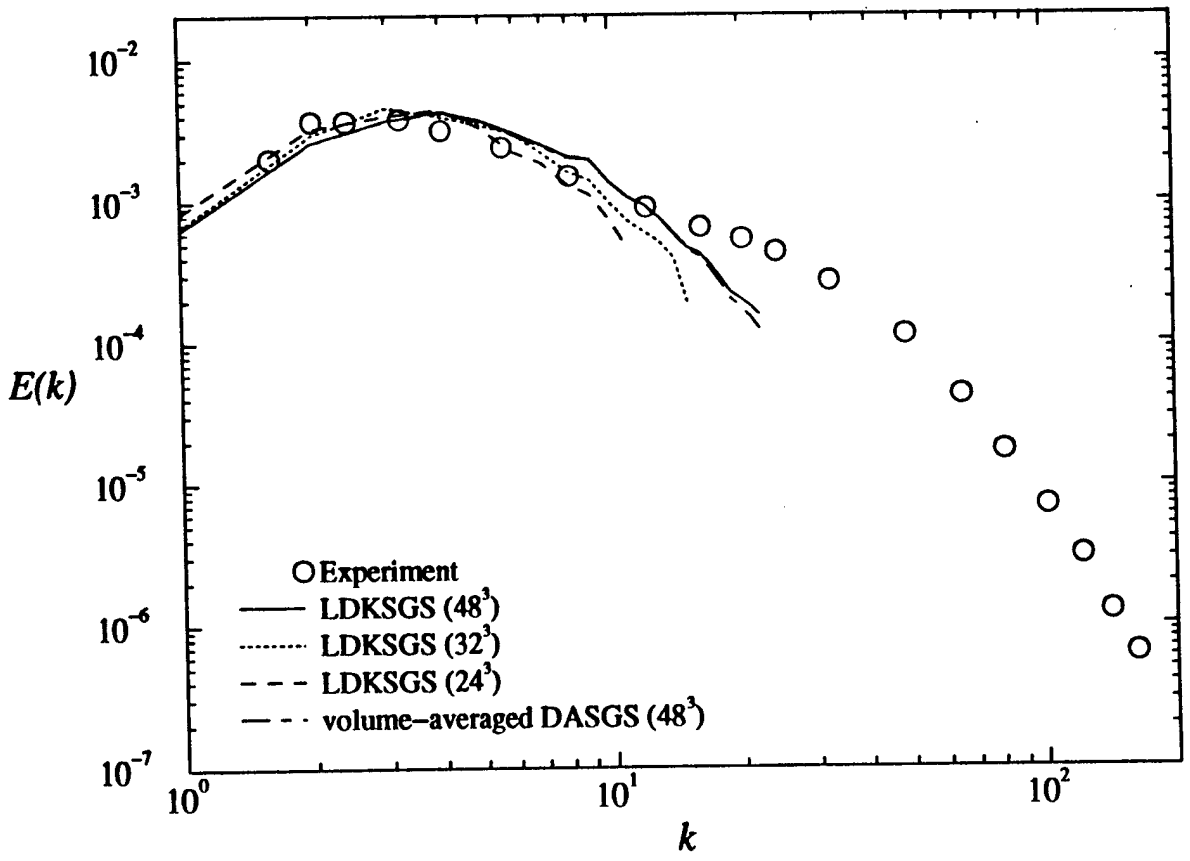
10^{-2}
10^{-3}
10^{-4}
10^{-5}
10^{-6}
10^{-7}
$E(k)$
10^{0}
10^{1}
10^{2}
k
Experiment
LDKSGS (48^3)
LDKSGS (32^3)
LDKSGS (24^3)
volume–averaged DASGS (48^3)

Figure 16.

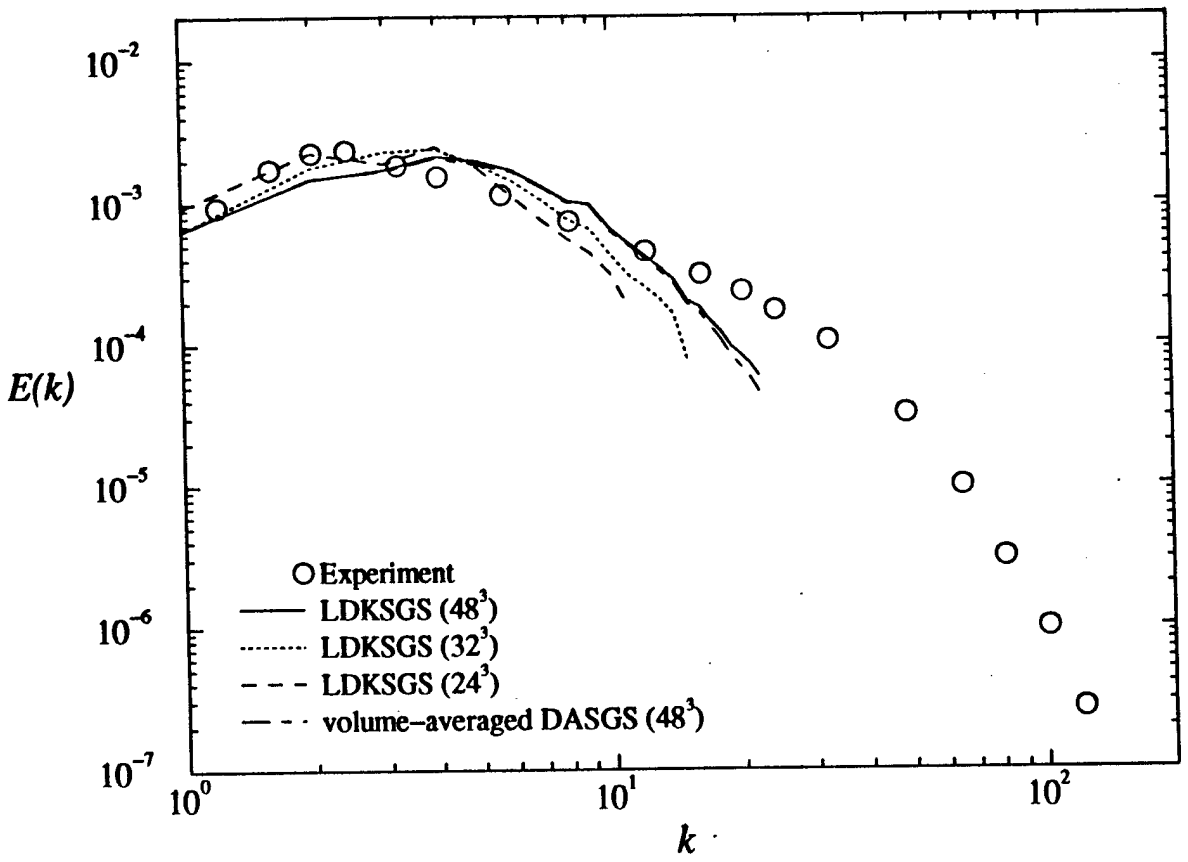
10^{-2}
10^{-3}
10^{-4}
10^{-5}
10^{-6}
10^{-7}
$E(k)$
10^{0}
10^{1}
10^{2}
k
Experiment
LDKSGS (48^3)
LDKSGS (32^3)
LDKSGS (24^3)
volume–averaged DASGS (48^3)

Figure 17.

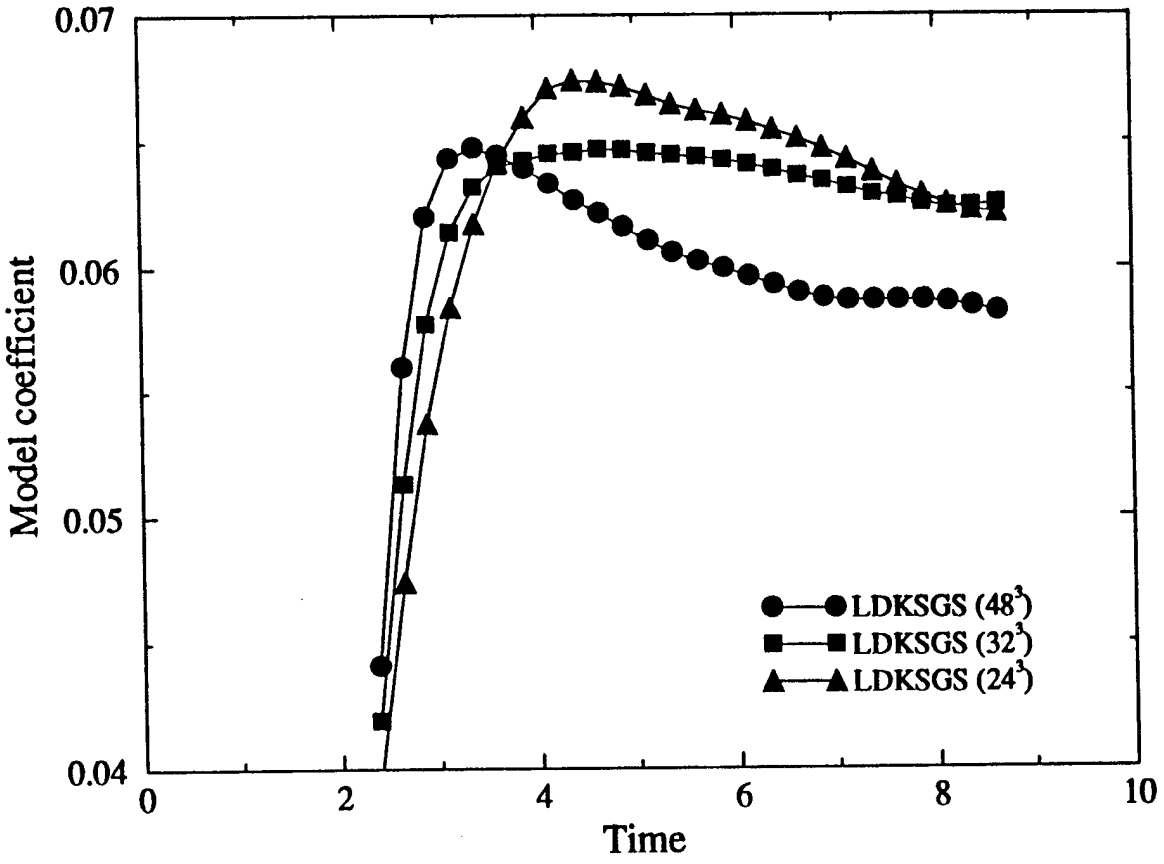
0.07
0.06
0.05
0.04
Model coefficient
0
2
4
6
8
10
Time
LDKSGS (48³)
LDKSGS (32³)
LDKSGS (24³)

Figure 18.

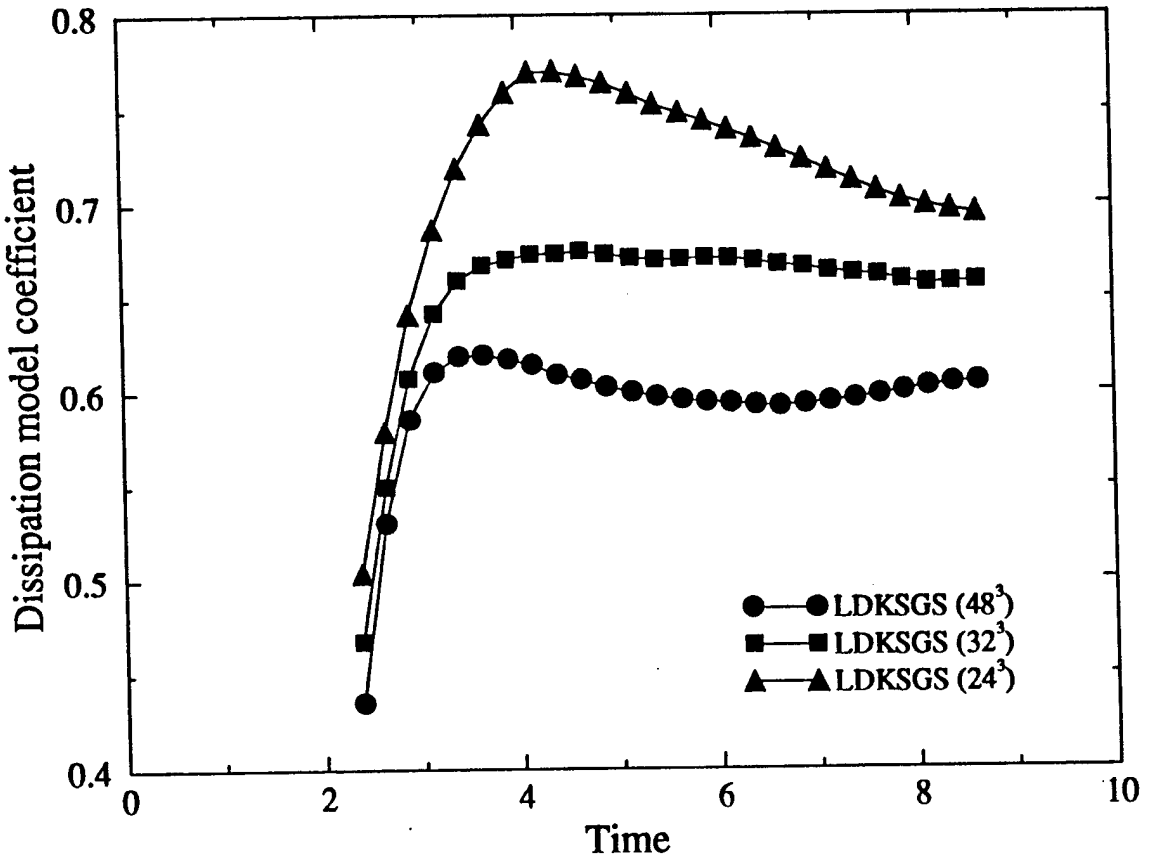
0.8
0.7
0.6
0.5
0.4
Dissipation model coefficient
0
2
4
6
8
10
Time
LDKSGS (48³)
LDKSGS (32³)
LDKSGS (24³)

Figure 19.

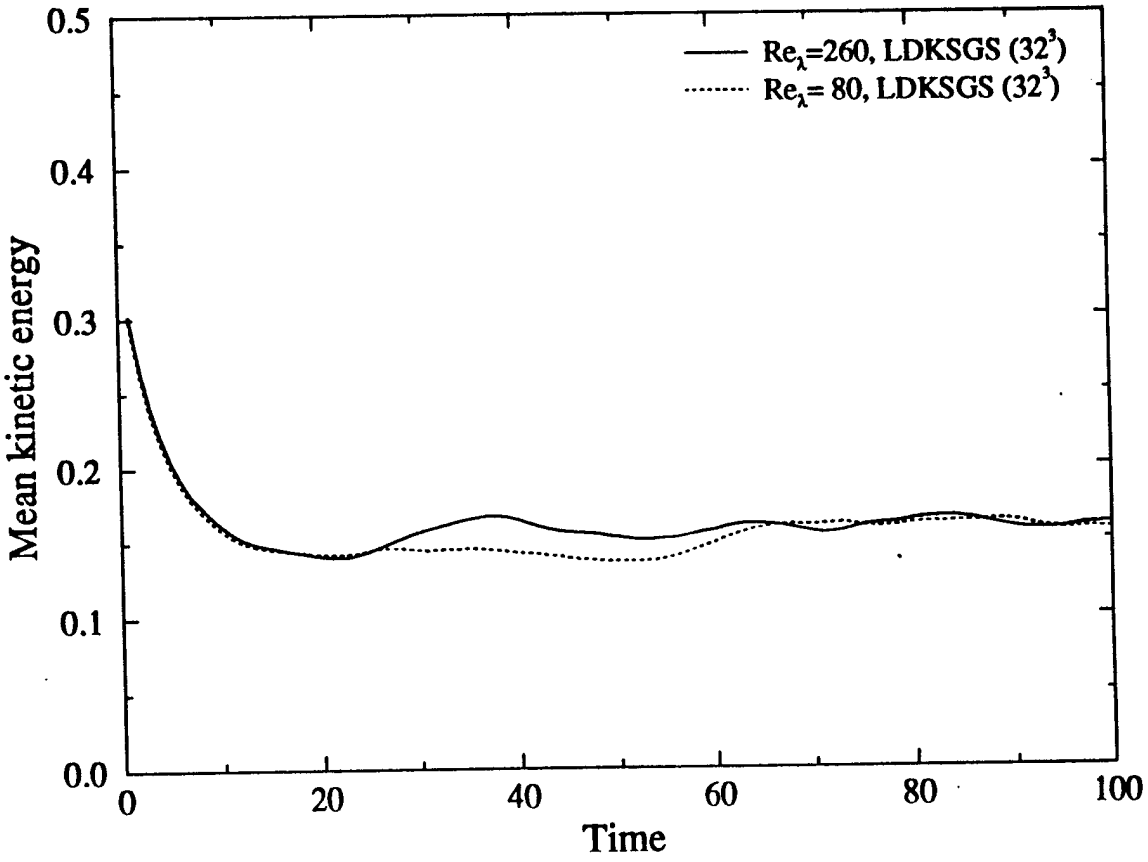
0.5
0.4
0.3
0.2
0.1
0.0
Mean kinetic energy
0
20
40
60
80
100
Time
Re$_\lambda$=260, LDKSGS (32^3)
Re$_\lambda$= 80, LDKSGS (32^3)

Figure 20.

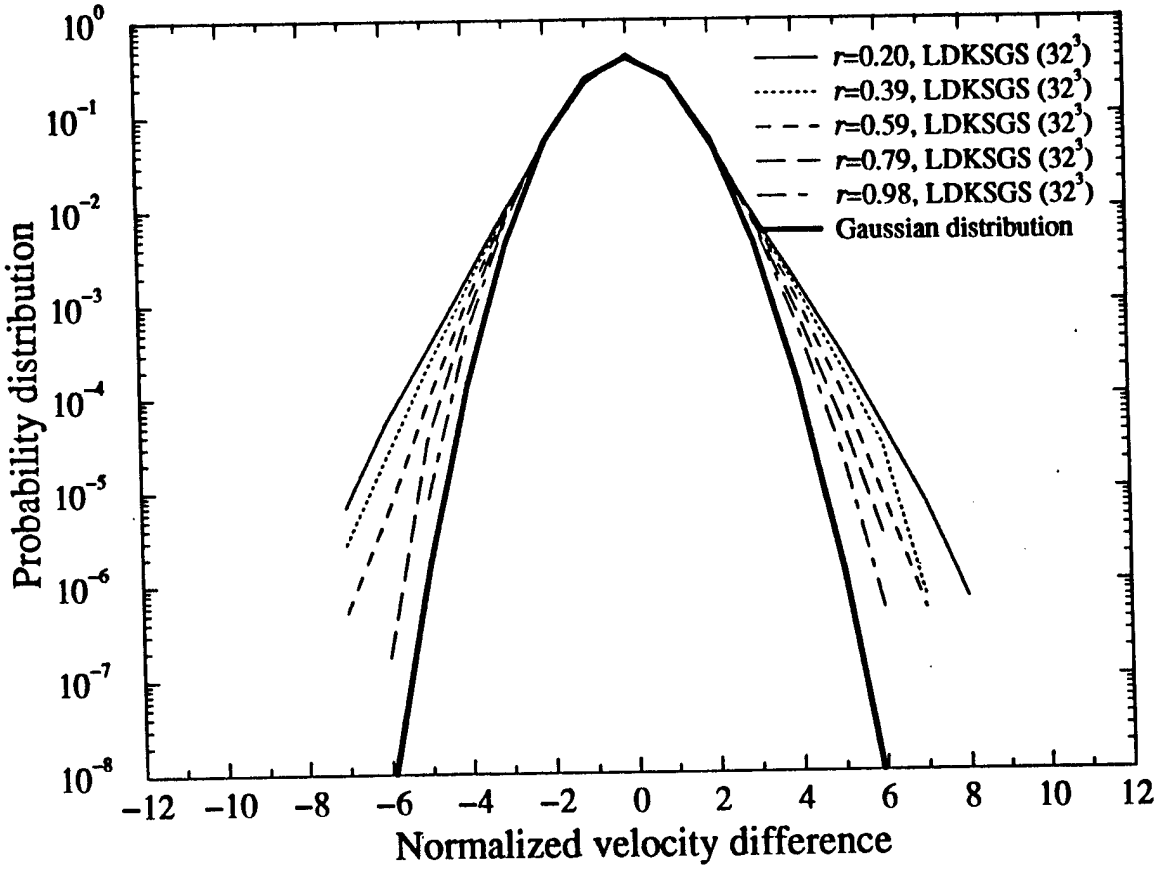
Probability distribution
Normalized velocity difference
r=0.20, LDKSGS (32^3)
r=0.39, LDKSGS (32^3)
r=0.59, LDKSGS (32^3)
r=0.79, LDKSGS (32^3)
r=0.98, LDKSGS (32^3)
Gaussian distribution
10^0
10^-1
10^-2
10^-3
10^-4
10^-5
10^-6
10^-7
10^-8
-12 -10 -8 -6 -4 -2 0 2 4 6 8 10 12

Figure 21.

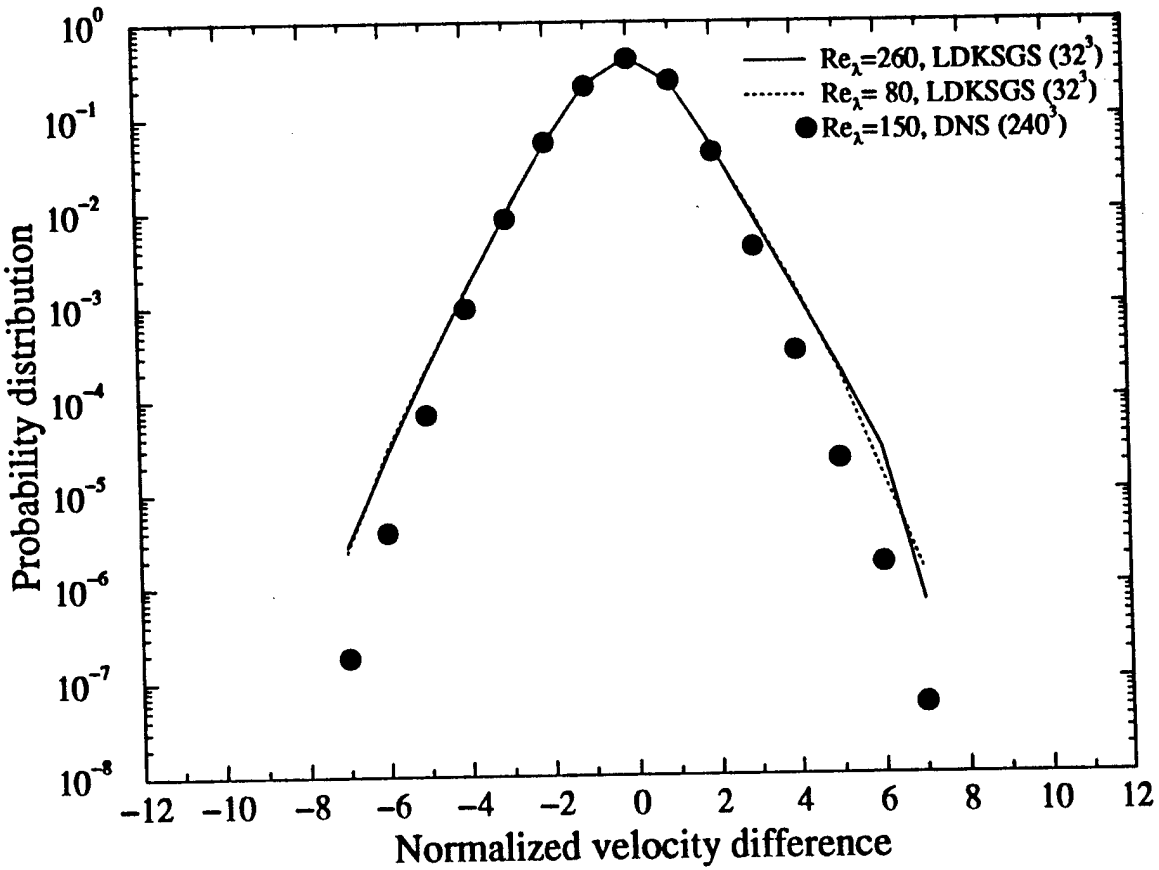
Probability distribution
Normalized velocity difference
Re_λ=260, LDKSGS (32^3)
Re_λ= 80, LDKSGS (32^3)
Re_λ=150, DNS (240^3)
10^0
10^{-1}
10^{-2}
10^{-3}
10^{-4}
10^{-5}
10^{-6}
10^{-7}
10^{-8}
−12 −10 −8 −6 −4 −2 0 2 4 6 8 10 12

Figure 22.

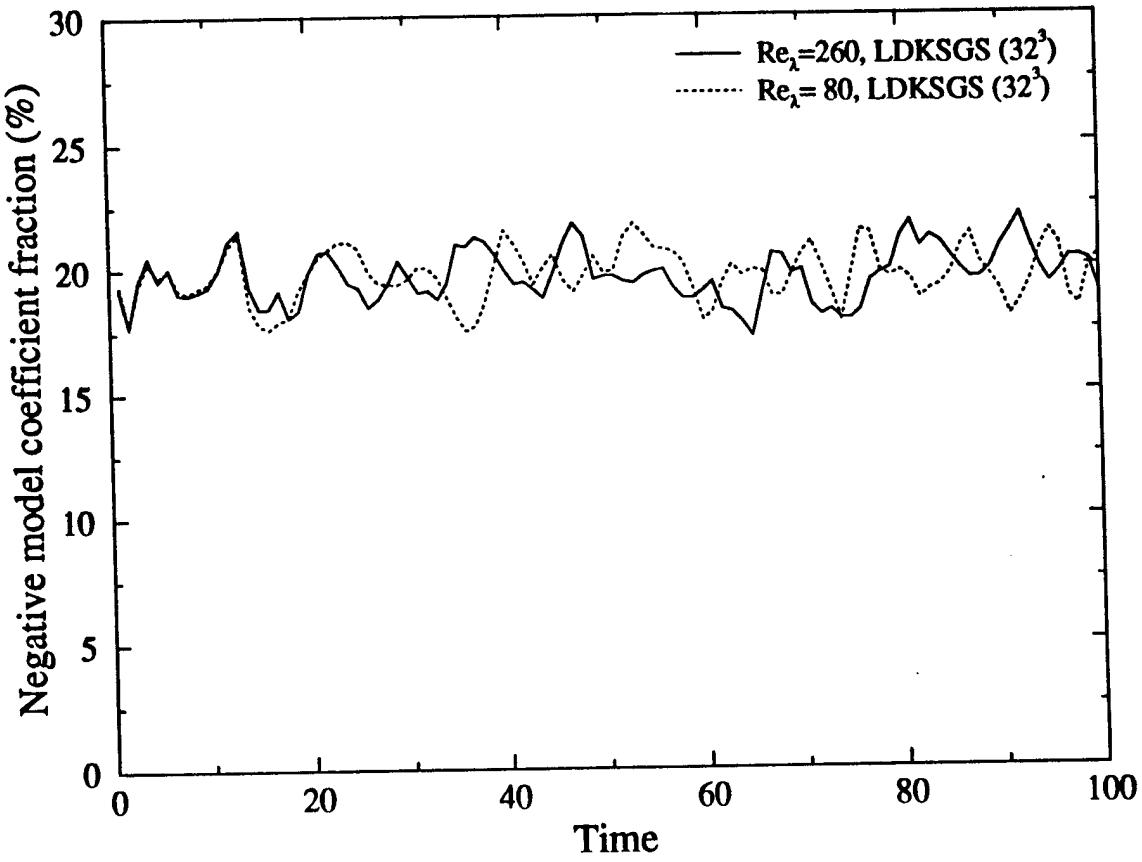
Re$_\lambda$=260, LDKSGS (32^3)
Re$_\lambda$= 80, LDKSGS (32^3)
Negative model coefficient fraction (%)
Time
0
5
10
15
20
25
30
0
20
40
60
80
100

Figure 23.

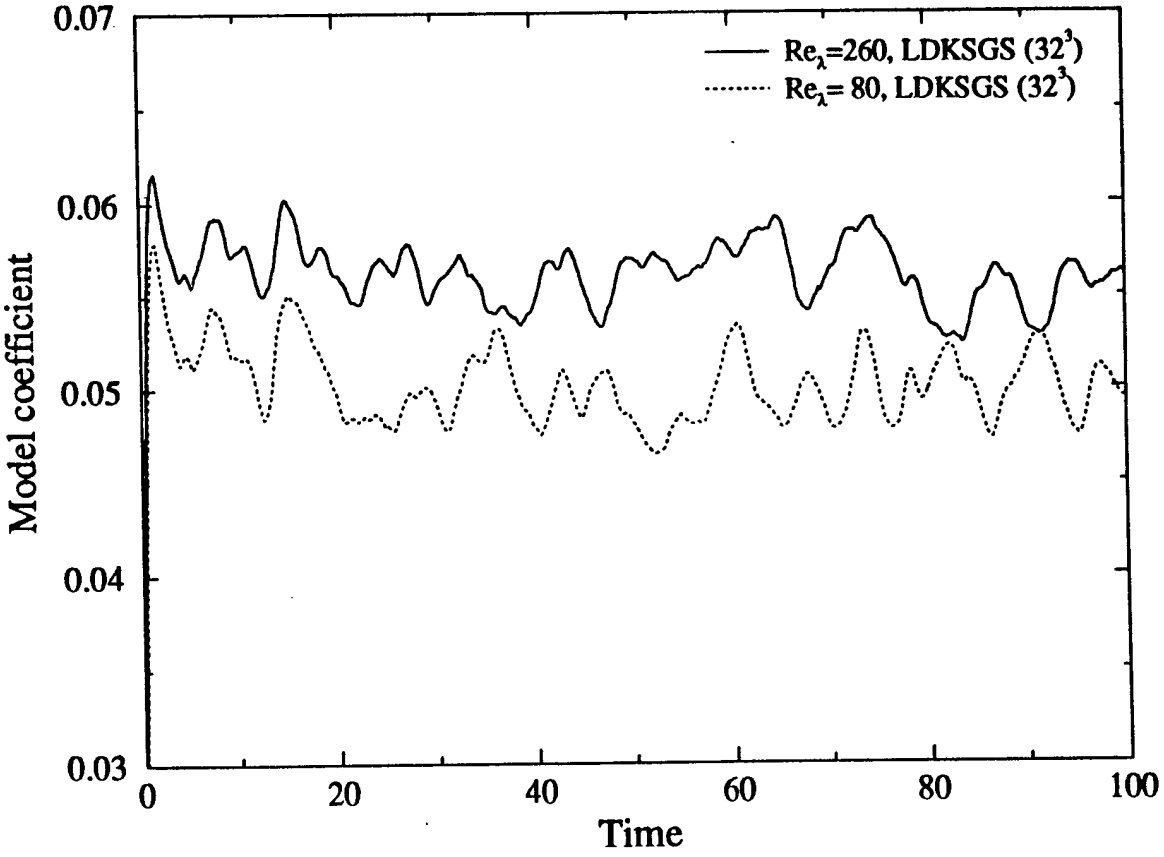
0.07
0.06
0.05
0.04
0.03
Model coefficient
0
20
40
60
80
100
Time
Re$_\lambda$=260, LDKSGS (32^3)
Re$_\lambda$= 80, LDKSGS (32^3)

Figure 24.

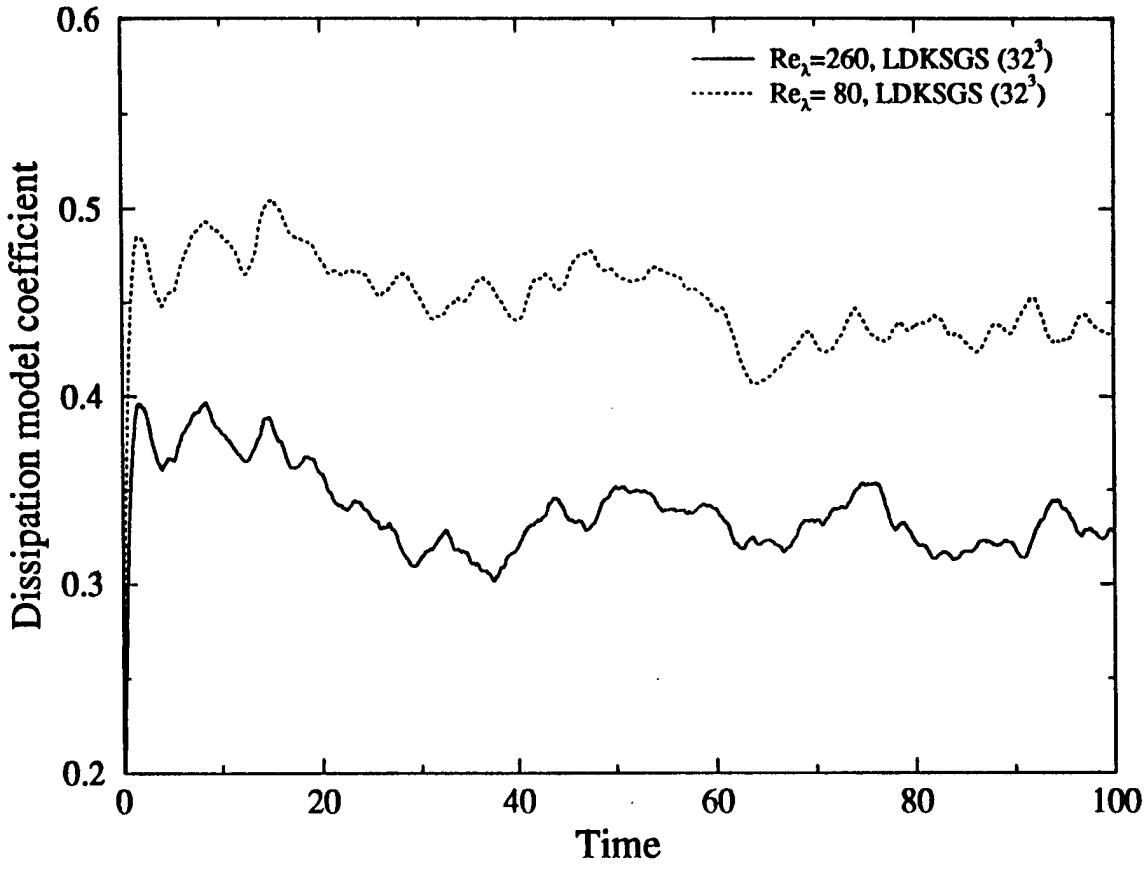
Dissipation model coefficient
0.6
0.5
0.4
0.3
0.2
0
20
40
60
80
100
Time
Re$_\lambda$=260, LDKSGS (32^3)
Re$_\lambda$= 80, LDKSGS (32^3)

Figure 25.

A NEW SEMI-IMPLICIT FRACTIONAL STEP METHOD FOR SIMULATION OF TURBULENT FLOWS ON A NON-STAGGERED GRID

V. K. Chakravarthy and S. Menon
School of Aerospace Engineering
Georgia Institute of Technology
Atlanta, Georgia 30332-0150

Preliminary Draft of Paper
for Submission to
The Journal of Computational Physics

July 1995

A new semi-implicit fractional step method for simulation of turbulent flows on a non-staggered grid.

V. K. Chakravarthy and Suresh Menon
School of Aerospace Engineering
Georgia Institute of Technology
Atlanta, Georgia.

Abstract

A method for solving Navier Stokes equations for reacting flows in the near incompressible Mach number limit is proposed and validated in this paper. A fractional step method often used in methods to simulate incompressible flows, is employed in the present formulation. An implicit scheme is used for time integration, which gives us a larger domain of stability. The convergence of the scheme is found to depend strongly on the efficiency of the method used to solve the elliptic equation for pressure. A multigrid scheme is used for achieving the required efficiency in the present formulation. The present method is found to be especially useful for application to Large Eddy Simulations. The variables used in such simulations are physical quantities convolved with some spatial filter and centered at the location where the corresponding filtered variable is defined. The use of a non-staggered grid, where all primitive variables are defined at the same physical location provides an unique location (at the grid node) of the filter for all the variables. The relative merits of this method over the existing methods that employ non-staggered grids, are indicated in this report and are proven using various test problems.

1. Introduction

A numerical method for solving three dimensional time dependent Navier-Stokes equations governing chemically reacting flows at low mach numbers is presented. At low speeds, acoustics have negligible effect on the fluid flow (and chemistry in case of chemically reacting flow fields). Chemical reactions in such flow fields essentially take place under isobaric conditions. The effect of combustion then, is felt as volumetric dilatation due to heat release and subsequent density variation. A method used by Mc.Murtry et al [1] for incorporating this effect into a flow field (that would be incompressible in the absence of heat release) is combined with a second order semi-implicit fractional step method formulated on a curvilinear non-staggered grid. Similar formulation for use in modeling of subsonic flows can be found in an article by Boris and Oran [2].

First proposed by Chorin [3] and Temam [4], the fractional step method has been modified many times because of it's initial shortcomings. Much of the work has been done on staggered grids. The physical locations where each of the variable is defined, varies from

method to method. A survey of these layout issues can be found in Yan Zang et al [5]. The present method defines all variables at the grid points and involves an upwind interpolation of velocities to half points on the grid (cell faces) and uses these interpolated values in the calculation of the source terms for the pressure Poisson equation (much like the way it is done by Yan Zang et al [5]). This makes it mimic the behavior of fractional step methods formulated on much used staggered grids. This prevents the pressure velocity decoupling and also enforces full mass conservation in the case of incompressible flows. The way in which volumetric dilatation due to heat release is accounted for, however makes the method non-conservative in case of chemically reacting flow simulations. This kind of layout leads to a reduction in terms of storage requirements for the metrics per node. Also the definition of all the primitive dependent variables at the same physical locations is advantageous in terms of analysis of the results obtained. Further, this layout is also preferable in terms of Large Eddy Simulation (LES). LES involves modeling of flow quantities that are convolved with a filter centered at the point where the quantities are defined. The information lost in the scales below the characteristic filter width is accounted for using a model. If a staggered grid layout is used, the velocities (contravariant or covariant) are defined at different locations which in a LES would imply that the filters needed for each of these velocity components are centered at different locations. This would need special attention in a LES. Since LES capability is the main requirement in the present study, a non-staggered grid is used.

The Poisson equation is solved using a multigrid scheme. Use of pseudocompressible methods along with an accelerating procedure such as a multigrid scheme would involve residual reduction in each of the coupled equations using the multigrid scheme. In the fractional step methods, however the multigrid scheme is necessary only for one elliptic equation. This leads to a substantial saving in terms of time for advancement of the solution. Unlike the methods based on block LU decomposition due to implicit treatment of diffusion terms [5], the present method treats implicitly also the nonlinear terms giving it better stability all the way to the inviscid limit. The memory storage efficiency, stability and accuracy of the method are established by simulation of various flows.

2. Low Mach number approximation of chemically reacting flow equations.

Consider the equations governing the flow a reacting perfect gas.

$$\frac{\partial \rho}{\partial t} + \frac{\partial}{\partial x_j}(\rho u_j) = 0$$

$$\rho \frac{Du_i}{Dt} = -\frac{\partial p}{\partial x_i} + \frac{\partial}{\partial x_j}(\tau_{ij})$$

$$\rho \frac{DE}{Dt} = -\frac{\partial (p u_i)}{\partial x_i} + \frac{\partial}{\partial x_j}(\tau_{ij} u_i) - \frac{\partial q_i}{\partial x_i} + Q$$

$$\frac{\partial C_\alpha}{\partial t}+\frac{\partial}{\partial x_j}(C_\alpha u_j)=R_\alpha+\frac{\partial}{\partial x_k}\left(D_\alpha\frac{\partial C_\alpha}{\partial x_k}\right)$$

where u_i represents the Cartesian velocity components, ρ is the fluid density, p is the pressure, τ_{ij} is the viscous stress tensor, q_i is the heat flux, Q is the heat source, C_α is the concentration of α^{th} species (Greek indices are used to denote properties of chemical species and are not tensor indices). R_α, D_α are the species production rate and species diffusion coefficient of α^{th} species. $E=e+0.5u_i u_i$, where e is the internal energy. These equations are conservation equations for mass, momentum, energy and chemical species respectively. These need to be supplemented with the equation of state relating density, temperature and pressure.

All the variables are put in dimensionless form by scaling with their reference quantities. The effect of compressibility is realized through a dimensionless parameter γM^2 (where M is the Mach number and γ is the ratio of specific heats). Assuming this to be small at low speeds and using perturbation analysis, we arrive at approximate governing equations for low speed reacting flow. Such an analysis was conducted by various researchers and we just give the final form of the equations without the actual analysis for brevity purposes. It is seen that all dependent variables appear only to lowest order of perturbation except for pressure, in which values upto two orders appear.

$$\frac{\partial \rho}{\partial t}+\frac{\partial}{\partial x_j}(\rho u_j)=0$$

$$\rho\frac{Du_i}{Dt}=-\frac{\partial p^{(1)}}{\partial x_i}+\frac{\partial}{\partial x_j}(\tau_{ij})$$

$$\frac{\partial p^{(0)}}{\partial x_k}=0$$

$$p^{(0)}=\rho T$$

$$\frac{\partial C_\alpha}{\partial t}+\frac{\partial}{\partial x_j}(C_\alpha u_j)=Da R_\alpha+\frac{1}{Pe}\frac{\partial^2 C_\alpha}{\partial x_k^2}$$

$$\frac{\partial u_i}{\partial x_i}=\frac{1}{\gamma p^{(0)}}\left(\frac{\gamma}{\mathrm{Pr\,Re}}\frac{\partial q_k}{\partial x_k}-\frac{\partial p^{(0)}}{\partial t}+CeQ\right)$$

where Pr, Re, Da and Pe are the Prandtl, Reynolds, Damkohler and Peclet numbers. Ce is reference heat release non-dimensionalized using reference quantities for velocity, length, density, temperature and C_v. This parameter needs to be small for the above approximation to be valid.

All dependent variables now represent lowest order values except pressure where the two order values are denoted by corresponding superscripts. The lowest order pressure as a result of lowest order approximation to momentum equation, is now constant in space but can vary in time. The first order pressure gradient enters the first order approximation of momentum equation. In this approximation, the speed of sound is infinite, so the thermodynamic pressure variations due to combustion are felt instantaneously making $p^{(0)}$constant. So combustion in the field is an isobaric process. The first order pressure is the dynamic pressure associated with the flow and has the sense of normal fluid stress as in incompressible flow fields. Q is the non-dimensional heat source and if this is zero, volumetric dilatation also reduces to zero. The temporal variation of thermodynamic pressure depends on whether combustion is a constant volume process (as in confined domains) or a constant pressure process (as in unconfined domains. The superscripts on first order pressure is dropped in following sections.

3.1 Review of fractional step methods.

This section briefly reviews the fractional step methods used to model incompressible flows. Fractional step methods are often preferred in the present day over other methods like pseudocompressiblity methods and vorticity-stream function methods because of their efficiency in terms of memory storage requirements and less complication in numerical implementation (see Quartepelle [6]), which is especially the case when using accelerating procedures like multigrid schemes. The advantages of this method have also been discussed to some extent by Yanenko [7]. However there still are a few shortcomings in this method that haven't been resolved. Some of them are listed here and are looked into in later sections. Similar analysis was conducted by Perot [8], especially for methods involving block LU decomposition due to implicit treatment of diffusion terms. Similar notation is used here.

Consider the incompressible Navier-Stokes equations in non-dimensional form (density = 1).

$$\frac{\partial u_i}{\partial x_i} = 0 \tag{1}$$

$$\frac{\partial u_i}{\partial t} + u_j \frac{\partial u_i}{\partial x_j} = -\frac{\partial p}{\partial x_i} + \frac{1}{\mathrm{Re}} \frac{\partial^2 u_i}{\partial x_k \partial x_k} \tag{2}$$

Temporal discretization of these equations usually involve explicit updating of convective terms and semi-implicit trapezoidal updating of diffusion terms. This produces a system of equations as follows.

$$D_i u_i^{n+1} = 0 \tag{3}$$

$$\frac{u_i^{n+1} - u_i^n}{\Delta t} + \left[1.5\, H_i(u_k^n) - 0.5\, H_i(u_k^{n-1})\right] = -G_i\, p + 0.5\mathrm{Re}^{-1} L(u_i^{n+1} + u_k^n) \tag{4}$$

H_i is the discrete convective operator, L is the discrete Laplacian operator G_i is the discrete gradient operator and D_i is the discrete divergence operator (not to be confused with the notation used for species diffusion coefficient previously). These can put in the following form.

$$\begin{bmatrix} A & G_i \\ D_i & 0 \end{bmatrix} \begin{bmatrix} u_i^{n+1} \\ p^{n+1} \end{bmatrix} = \begin{bmatrix} r_i \\ 0 \end{bmatrix} \tag{5}$$

where

$A = \frac{1}{\Delta t}\left[I - \frac{\Delta t}{2\mathrm{Re}} L\right]$, r_i contains the remainder of the terms which are explicitly known. This is usually factorized (to within an approximation) as

$$\begin{bmatrix} A & 0 \\ D_i & -\Delta t\, L \end{bmatrix} \begin{bmatrix} u_i^* \\ p^{n+1} \end{bmatrix} = \begin{bmatrix} r_i \\ 0 \end{bmatrix} \tag{6a}$$

$$\begin{bmatrix} I & \Delta t G_i \\ 0 & I \end{bmatrix} \begin{bmatrix} u_i^{n+1} \\ p^{n+1} \end{bmatrix} = \begin{bmatrix} u_i^* \\ p^{n+1} \end{bmatrix} \tag{6b}$$

In the above factorization , G_i is replaced by $A\,\Delta t\, G_i$. From the definition of A, it is seen that the error in factorization is of first order. This error tends to be diffusive and aids stability but needs to be avoided for time accurate calculations (Numerical dissipation should be minimized as much as possible in unsteady calculations). Taking divergence of the first vector equation in the second step, we arrive at a Poisson equation for pressure. This equation is

$$\frac{D_i u_i^*}{\Delta t} = -L\, p^{n+1} \tag{7}$$

The correct source term in Poisson equation for pressure should be divergence of the convective term in the momentum equation which is equal to the source term in the above equation to within a first order error. So the evolution of the pressure field is also first order accurate.

The first of the two shortcomings mentioned above, the error in factorization can be rectified to a certain extent. Several modifications have been proposed to overcome this problem. Maday et al [9] proposed a modification of r_i to explicitly account for the error through it's approximation in terms of known quantities. This approach has not been used much because of it's suspected stability properties. The second approach proposed by Perot [8] involves a different type of factorization of discrete time operator matrix acting on primitive variables. This approach leads to an equation for pressure that is not a Poisson equation but one of a higher order. In such a case, one needs to define a new pressure variable leading to a complicated pressure updating procedure.

The second of the issues that needs to be resolved appears more severe than the first one. The error in the source term is $\mathrm{Re}^{-1}\ (0.5\partial^2 u_i^* / \partial x_k^2)/\partial x_i$ and in the corrector step of the method leads to a first order error in velocity. Perot concludes that it is not possible to attain a higher order of accuracy for pressure in such formulations. However, as claimed by Temam [10], the first order error in pressure may not effect the orderof accuracy of the velocity field. This is due to the fact that the error term is usual small in most flow fields. It is suspected by the authors that, in flow fields with intense pressure gradients this error may be high enough to effect the accuracy of the velocity field as well. It is possible to define a new pressure variable (so called discrete pressure) to absorb the error and this has been used by Zang et al [5]. As pointed out previously by Perot [8], this however is not always possible and cannot be considered a permanent solution to the problem.

3.2 Second order fractional step method with trapezoidal updating.

In this section, a numerical method with implicit trapezoidal updating for equations governing reacting flows under zero Mach number approximation is presented. Consider first the conservation equations for mass and momentum. The species continuity equation is considered at the end of this section, rest of the equations in zero Mach number approximation are all algebraic and need no time integration.

$$\frac{\partial \rho}{\partial t} + u_j \frac{\partial \rho}{\partial x_j} + \rho \frac{\partial u_j}{\partial x_j} = 0 \tag{8}$$

$$\frac{\partial (\rho u_i)}{\partial t} + u_j \frac{\partial (\rho u_i)}{\partial x_j} + \rho u_i \frac{\partial u_j}{\partial x_j} = -\frac{\partial p}{\partial x_i} + \frac{\partial}{\partial x_j}(\tau_{ij}) \tag{9}$$

The volumetric dilatation is obtained in terms of an algebraic expression. For ease in further analysis, the following notation is used.

$$A = -u_j \frac{\partial \rho}{\partial x_j} - \rho \frac{\partial u_j}{\partial x_j}$$

$$B_i = -u_j \frac{\partial(\rho u_i)}{\partial x_j} - \rho u_i \frac{\partial u_j}{\partial x_j} + \frac{\partial}{\partial x_j}(\tau_{ij})$$

So the conservation equations now become

$$\frac{\partial \rho}{\partial t} = A \tag{10}$$

$$\frac{\partial(\rho u_i)}{\partial t} = B_i - \frac{\partial p}{\partial x_i} \tag{11}$$

A semi-implicit time integration scheme is used to advance the solution in time.

$$\frac{\rho^{n+1} - \rho^n}{\Delta t} = 0.5\left(A^n + A^{n+1}\right) \tag{12}$$

$$\frac{(\rho u_i)^{n+1} - (\rho u_i)^n}{\Delta t} = 0.5\left(B_i^n + B_i^{n+1}\right) - \frac{\partial p^{n+1/2}}{\partial x_i} \tag{13}$$

Following two step iterative solution procedure is proposed for converging the solution at each time step.

$$\frac{\rho^{n+1} - \rho^n}{\Delta t} = 0.5\left(A^n + A^{n+1}\right) \tag{14}$$

$$\frac{(\rho u_i)^* - (\rho u_i)^n}{\Delta t} = 0.5\left(B_i^n + B_i^{n+1}\right) \tag{15}$$

followed by

$$\frac{(\rho u_i)^{n+1} - (\rho u_i)^*}{\Delta t} = -\frac{\partial p^{n+1/2}}{\partial x_i} \tag{16}$$

Adding the two equations above, we can say that the numerical solution is second order accurate provided the pressure required in the second step is also atleast second order accurate. The equation for pressure is obtained by taking divergence of the second step of the split scheme.

$$\frac{\partial^2 p^{n+1/2}}{\partial x_k \partial x_k} = -\frac{1}{\Delta t}\frac{\partial}{\partial x_i}\left[(\rho u_i)^{n+1} - (\rho u_i)^*\right] \tag{17}$$

This equation needs to be solved before the second step of the solution procedure. In order to check the accuracy of this equation, we substitute for intermediate value of the momentum flux into it's place in the source term. Then the Poisson equation looks like

$$\frac{\partial^2 p^{n+1/2}}{\partial x_k \partial x_k} = -\frac{1}{\Delta t}\frac{\partial}{\partial x_i}\left[(\rho u_i)^{n+1} - (\rho u_i)^n\right] + 0.5\frac{\partial}{\partial x_i}\left(B_i^n + B_i^{n+1}\right) \tag{18}$$

This is an second order approximation to the following Poisson equation.

$$\frac{\partial^2 p}{\partial x_k \partial x_k} = -\frac{\partial^2 (\rho u_i)}{\partial x_i \partial t} + \frac{\partial B_i}{\partial x_i} \tag{19}$$

which is exact equation for pressure in continuous time domain. A genuinely second order scheme is obtained without any complicated pressure updating and also we only have a Poisson equation that needs to be solved unlike higher order equations that usually are obtained at this stage and need definition of new pressure variable. There is however an issue here that has previously been addressed by several researchers regarding the accuracy of the above approximation after spatial discretization in the fully incompressible case. The viscous stress term in the momentum equation for fully incompressible flows does not contribute to the source term of the Poisson equation since it is divergence free. This is because the Laplacian operator and the divergence operator commute. This however may not always be true in case of finite difference approximations to these operators, although the error involved is found to be usually very low (lower in order than the total truncation error in the scheme). But for some incompressible flow problems, the error involved could cause the unsteady solution may drift from actuality (non-periodic boundary conditions, high grid stretching , skewness of the grid are usually cited as sources of this type of error). In such cases, a new intermediate velocity variable is defined which is calculated without the viscous term. This new variable would then be different from the previously defined intermediate velocity variable and is used to calculate the source term for the Poisson equation. This source term doesn't involve the viscous term like in the continuum case. The issues regarding the Poisson solver are discussed in a later section.

In case of reacting flows, a species continuity equation also needs to be integrated in time. This is handled much the same way as the mass conservation equation, except that ρ is now replaced by C_α and the extra diffusion term in species equation is updated using a trapezoidal scheme.

3.3 Spatial discretization

A non-staggered grid layout is employed for spatial discretization. Although conservative forms are preferred, under the zero Mach number approximation, the nonlinear terms cannot be put in the conservation form. This is because the volumetric dilatation is

explicitly known as an algebraic expression. For cases without heat release however, the nonlinear terms can be put in conservative form. The non-conservative formulation necessary for the chemically reacting flows is discussed here.

Let us consider the terms in A. The volumetric dilatation is explicitly known. The other term is discretized as follows.

$$u_j \frac{\partial \rho}{\partial x_j} = u_j \frac{\partial \xi_k}{\partial x_j} \frac{\partial \rho}{\partial \xi_k}, \tag{20}$$

where ξ_k is the coordinate in the computational space. $\frac{\partial \xi_k}{\partial x_j}$ is the metric of transformation and is calculated with second order accuracy. The density gradient in the computational space is calculated using an upwind biased numerical approximation with upwinding based on the contra variant velocity $u_j \frac{\partial \xi_k}{\partial x_j}$.

Non diffusive part of B_i is written in terms on transformed coordinates as follows.

$$-u_j \frac{\partial \xi_k}{\partial x_j} \frac{\partial (\rho u_i)}{\partial \xi_k} - \rho u_i \frac{\partial u_j}{\partial x_j} \tag{21}$$

In the zero Mach number formulation, the volumetric dilatation is explicitly known. The derivative in the computational domain is evaluated again as an upwind biased third order finite difference approximation based on the sign of $u_j \frac{\partial \xi_k}{\partial x_j}$.

The diffusive part can be put in full conservation form as

$\frac{J}{\mathrm{Re}} \frac{\partial}{\partial \xi_k}\left(G_{kl} \frac{\partial u_i}{\partial \xi_l} \right)$, where J is the jacobian of the transformation. $J^{-1} = \det\left(\frac{\partial x_i}{\partial \xi_j} \right)$.

and G_{kl} is called the mesh skewness tensor given by $\frac{1}{J} \frac{\partial \xi_k}{\partial x_m} \frac{\partial \xi_l}{\partial x_m}$.

The second order 19 point generic stencil is used to discretize the Laplacian operator on the computational grid.

3.4 Poisson solver

The Poisson solver is implemented in full conservation form. This ensures full mass conservation in incompressible flows. For reacting flow calculations within the framework of zero Mach number approximation , as stated earlier full conservation form is not possible.

Special care needs to be taken with regards to pressure solvers when fractional step methods are used on non-staggered grids. Straight forward discretization of the equations often causes pressure velocity decoupling leading to checker board type high frequency oscillations of velocity and pressure [11]. A staggered grid layout is often preferred to circumvent this problem but this layout is more expensive in terms of storage requirements and is not completely without problems. Stencils for spatial discretization are to be chosen so as to achieve coupling of pressure and momentum equations.

The Poisson equation in curvilinear coordinates after discretization in space is

$$\frac{\partial}{\partial \xi_i}\left(G_{ij} \frac{\partial p}{\partial \xi_j} \right) = -\frac{1}{\Delta t} \frac{\partial}{\partial \xi_i} \left\{ \frac{1}{J} \frac{\partial \xi_i}{\partial x_j} \left[(\rho u_j)^{n+1} - (\rho u_j)^{*} \right] \right\}$$

Let $\frac{1}{J}\frac{\partial \xi_i}{\partial x_j}\left[(\rho u_j)^{n+1} - (\rho u_j)^{*}\right]$ be denoted by F_i. This is evaluated at the half points and needs the values of the metrics at the half points. The source term is now discretized as

$-\frac{1}{\Delta t}\left[(F_1)_{i+1/2,j,k} - (F_1)_{i-1/2,j,k} + (F_2)_{i,j+1/2,k} - (F_2)_{i,j-1/2,k} + (F_3)_{i,j,k+1/2} - (F_3)_{i,j,k-1/2} \right]$, where the indices outside of regular brackets denote the location in computational domain. Uniform computational mesh with unit spacing has been used here. F_i here is correction to the mass flux vector (across the surface when looked upon in the finite volume sense). In incompressible flows, the density is constant and u_i^{n+1} should be divergence free. So for this case, in solving the poisson equation, only the intermediate momentum term in the source term is considered. On solving the equation, we make the velocity at the advancing time step, divergence free in the fully conservative discrete sense.

The values of intermediate fluxes are needed at the half-points for the calculation of source term. Use of any symmetric interpolation scheme for this purpose, decouples the pressure and velocity fields. So an upwind biased QUICK interpolation scheme is used to obtain intermediate fluxes at the half points. This has been successfully used to obtain strong coupling by Yang et al [5].

The 19 point generic stencil is used for discretizing the Laplacian operator in the Poisson equation. A successive line over-relaxation (SLOR) scheme is used for the solution and a four level multigrid (MG) scheme is used to accelerate the convergence. The type of MG cycle is chosen based on the problem at hand.

When an accelerating procedure such as MG scheme are being used, simpler relaxation schemes such as point Jacobi or Gauss Seidel schemes are preferred because of their simplicity in implementation and easy vectorizability (or parallelizability). A SLOR is preferred here though because of it's high local convergence rate. The numerical method here involves global iteration because of it's implicit nature and this makes the efficiency of

the Poisson solver a very important factor towards total efficiency. It is found that, except for the initial stages of time advancement, the values of pressure from a sub-iteration form a very good estimate of the solution of Poisson equation at next sub-iteration. When such is the case, the MG cycle (necessary if one uses point Jacobi or Gauss-Seidel schemes) is not necessary, a couple of SLOR iterations on the finest grid level are enough to reach the solution. Further, SLOR schemes can fully vectorized at the expense of extra memory storage when required.

The spatial discretization stencils used here are found to yield very little artificial dissipation which is very desirable for accurate integration of time dependent flows. This is illustrated by simulating flows with known exact solutions. However one needs to ensure that the grid stretching is no more than 6-7%. If this is not the case, the derivatives in the computational domain used in the convective terms are computed using finite difference approximations with the stretching explicitly taken into account.

3.5 Boundary conditions

The velocity boundary conditions are specified as usual. At the inflow, the three velocity components are specified and at the outflow boundary, they are extrapolated from the interior. The intermediate velocity components are extrapolated to either of these boundaries. No slip condition is implemented at the walls and the intermediate velocity is extrapolated.

For the Poisson equation, it is not a necessity to implement boundary conditions. This is because, the extrapolation of intermediate velocities to the half points for calculation of source terms makes this formulation mimic the behavior of the staggered grid formulation (see Rosenfeld [12]). The issue of boundary conditions for pressure in staggered grid formulations where all pressure nodes are interior to the domain, has been discussed by Kim and Moin [13]. Gradient of pressure is equal to the value of intermediate velocity at each point and one may utilize this fact to implement a Neumann boundary condition at the boundary. Better ways of applying boundary conditions on non staggered grids are available [14] which are more expensive, but are not usually required except for in complex wall geometries.

3.6 Stability and efficiency of the numerical scheme

Stability in numerical schemes is governed by two factors. The first is the inviscid stability limit called the CFL condition. The second is the viscous stability limit which usually becomes restrictive near the boundaries and is expected to depend on the local shear stress. If the CFL number is defined as done by Yan Zang [5], the time integration was found to be stable upto a value of CFL as high as 2.5 in cases where viscous stability is not of concern (like problems with periodic or symmetric boundary conditions). However as pointed out by Choi and Moin [15], use of time steps equal to or more than the Kolmogorov time scale can lead to erroneous time history in case of direct numerical

simulation of turbulent flows. So the time step for each simulation is also restricted by the relevant physical time scales in the flow field.

This formulation needs storage of metrics and jacobian at the grid points and metrics at the half points. Including the mesh skewness tensor that has six independent components (because of symmetry), the storage requirement is 25 geometric variables per grid point.

The accuracy and stability in terms of CPU time requirements are illustrated by application of the method to various problems in the following sections.

4. Numerical results.

4.1 Multigrid Poisson Solver

The performance of the multigrid as against a single grid SLOR simulation is presented in Fig. 1. The convergence of the schemes is plotted against the CPU time required. The convergence is quantified by the L_∞ norm of the change in values after each iteration. In case of single grid simulations, the convergence is found to level off because of the persistent low wavenumber errors. The multigrid simulations on the other hand, is found to wipe out errors at all wavenumbers quite efficiently. The type of multigrid cycle that is most efficient, is found to depend strongly on the values of mesh skewness tensor and not so much on the initial conditions for the iteration. The convergence is found to vary with the type of boundary conditions (Neumann boundary conditions are found to sloe down the convergence). The type of MG cycle to be used for each simulation (geometry) is arrived at by experimentation.

4.2 Decaying vortices

The present numerical code is tested for accuracy using the analytical solution of two dimensional unsteady Navier-Stokes equations for the case of decaying vortices. This test case was used by Yan Zang [5] and several other researchers before to test their schemes. The exact solution is given by

$$u = -\cos(x)\sin(y)\,e^{-2t/\mathrm{Re}}$$

$$v = \sin(x)\cos(y)\,e^{-2t/\mathrm{Re}}$$

$$p = -\frac{1}{4}[\cos(2x)+\cos(2y)]e^{-4t/\mathrm{Re}}$$

A cubical domain is considered for the simulations. The initial solution is advanced for a non-dimensionless time of 20.0. This is done with various grid resolutions. This will demonstrate the final order of accuracy of the scheme. The maximum error in u velocity is plotted against the number of points used per 2π length in each direction, in Fig. 2. As

seen, the logarithmic plot has a slope less than 2.0 which indicates the second order of accuracy of the scheme.

4.3 Isotropic turbulence

A Direct numerical simulation (DNS) of isotropic turbulence was conducted on a 64x64x64 grid. Initialization was done using a power spectrum. The starting Reynolds number based on Taylor microscale was 32.0. The solution was advanced over a non-dimensional time of 17.0. The flow was found to be isotropic in course of the whole simulation. The flow field (energy spectrum) eventually becomes self-similar (as shown in Fig. 3.a and 3.b). The decay of kinetic energy in isotropic turbulence has been known to follow a power law with an exponent of about 1.3 to 1.4. Renormalization group theory due to Yakhot and Orszag [16] predicts a value of the exponent to be 1.33, while experiments due to Warhaft and Lumley [17] predict a value of 1.34. There is still no agreement about the correct value, but a value of 1.34 probably comes closest to being this value. In the present case, the decay rate exponent is expected to be between 1.32 and 1.41. The uncertainty in this prediction is due to the fact that, the state of the flow field at early stages of the simulation does not correspond to a state of fully developed turbulence. In fact, the turbulence may not even be realistic at these stages.

The finite difference methods are usually found to have numerical dissipation. This is due to the fact that the leading order term in the error due to upwind finite differencing often resembles terms that are responsible of dissipation in reality. This kind of error keeps reducing as the order of finite difference approximation is increased. So the present simulation has been conducted using different order upwind and central approximations to the convective term. The variation of kinetic energy as predicted by each of these is tabulated in Table.1. The corresponding values predicted using a spectral code have also been presented for comparison. It is found that the finite difference code with fifth or sixth order convective term is less dissipative than the spectral code. The third order upwind differencing of the convective term however leads to more dissipation. The spectral formulations usually have been found to be less dissipative than finite difference formulations. So a comparison mentioned above is a good test for the acceptability of present formulation for long time simulation of flow fields. Though third order upwind difference seems to cause excessive dissipation, the error involved is found to be very small and wouldn't affect the results substantially. So the third order convective term is retained for use in rest of the studies.

4.4 Laminar Jet

A Laminar circular jet was simulated using the present code. A 65 x 33 x 33 trapezoidal grid is used for this simulation. The flow in this case is axisymmetric. The farther the cross plane contours of any flow quantity are from axisymmetry, the more the error due to use of a non axisymmetric grid for an axisymmetric problem. Linear stretching was used in all three directions. The centerline velocity is found to decay as inverse of axial distance (corrected for inlet profile effects by making use of a virtual origin). The variation of

inverse of axial velocity with axial distance is shown in Fig. 4a. The velocity profiles downstream are found to be self similar when the steady state is reached. The profiles at various distances away from the nozzle and the analytical solution (found to fit with the experimental data very well) are shown in Fig. 4b. The momentum flux across the nozzle is is difficult to calculate exactly near the nozzle because of the use of very few points in the nozzle. The flux in the simulation can be calculated using the velocity field downstream. However the decay rate is predicted correctly and one can conclude that the momentum flux is conserved.

4.5 Mixing Layer

Stability and structural characteristics of the temporally evolving mixing layer are studied in this section. The case with hyperbolic tangent profile has been studied extensively by several researchers [18 , 19]. The disturbance is prescribed as a superposition of first few eigen modes (both 2D and 3D) and the amplitudes of each of these modes are specified. The eigen functions for this problem can be found in [19].

Linear growth rate of the first mode is studied as a function of amplitude of the first 2D mode. This eigen value problem has previously been studied by Michalke [19]. The amplification of first 2D mode is computed for different wavenumbers. The results are compared in Table. 2.

The structure of the roll up was studied for 2D and 3D modes. The contours of vorticity for the roll up due to 3D initial disturbance are plotted in Fig. 5a. Iso surfaces of vorticity magnitude are shown for the case of 3D mode in Fig. 5b.

With the initialization similar to that used by McMurtry [1] for the species concentrations in his study of low Mach number analysis of reacting mixing layers, the present code was used to study the effect of heat release on the flow field. Three cases with Ce = 0 , 5 and 10 were studied. It is found that heat release delays the roll up (for the reasons pointed out by McMurtry etal [1]). The mean velocity and temperature profiles are given in Fig 5c and 5d. The product formation profiles across the mixing layer are plotted in Fig 5e. All these simulations are at same values of parameters except for Ce and are conducted on a 32 x 32 x 32 grid. It is found that the product formation is hindered by heat release, which is in qualitative agreement with deductions of McMurtry etal [1]. The product formation is found also to depend strongly on the amplitudes of the initially prescribed disturbances. Quantitative comparison is hence not possible since the values of these amplitudes used by McMurtry etal [1] are unknown.

4.6.1 Couette flow

Direct numerical simulation of turbulent Couette flow at a Reynolds number of 5200 based on relative wall velocity and distance between the plates, was conducted on a 65 x 49 x 49 grid. Couette flow was chosen as a test problem for DNS of a wall bounded flow because of the inherent complexity of the wall driven flows over the pressure driven flows. Also Couette flow has received much attention recently as a problem used to study turbulence in wall bounded flows [20, 21, 22].

One other reason for choosing this problem is that the present DNS would serve to validate subgrid model for Large Eddy Simulation (LES). Large Eddy Simulations have needed special attention in the vicinity of the wall because of the near wall non-equilibrium structure. Problems like flow through a channel have received greater attention in this regard. The present study would concentrate on near wall behavior of wall driven shear flows. There however is also another interesting feature of the Couette flow. That is the existence of strong long range correlation in the flow direction especially near the core region. This is because of the long vortex streaks in the core region. The information regarding such turbulent structure is embedded in the second order velocity correlations. One would in reality need complicated theories like two point closure to study these structures. The question whether a single point closure like the present one equation LES be able to account for these features would be considered here.

The two point correlations depend on the length of the domain along the flow direction (in both experiments and numerical simulations). This differences in this length may to some extent explain the scatter of single point statistics like RMS values of velocities in the core region, between various simulations and experiments. Being the longest of all simulations performed in this study, the efficiency of the method can be deduced from this simulation. The code gives a performance of about 480 Mflops on Cray-C90 rated at 1 Gflop and advances 75 time steps in one minute. This gives a timing of 5.12 micro seconds per time step per grid point.

The results of the present DNS study (mean velocity profile and single point statistics) are presented in Fig. 6a and 6b along with experimental results and those from computations on a much finer grids. Fig. 6g shows the streamwise velocity variation along a plane normal to the mean flow. The turbulent bursts at distinct locations which are equally spaced near the wall can be seen in the picture. This suggests the existence of Λ - vortices even though the resolution is barely enough for a DNS. In Fig.6h, contours of vorticity magnitude near the wall are shown. There seem to be spots in the wall layer with intense vorticity magnitude. This is in agreement with the known fact that the near wall flow has coherent vortex structures of considerably higher vorticity than the surroundings. As far as the geometry of these structures is concerned, one would near much higher resolution for the simulation for prediction of correct shape and expanse of these structures.

4.6.2 LES Model

A one equation model with dynamic evaluation of model coefficients based on scale self similarity (proposed by Kim and Menon [23]) was used for the LES. This model has

shown good promise recently but needs critical evaluation for wall bounded flows. This model relies on the existence of a self similar range of scales in turbulence at the level of resolved scale. The self similar structure having strong scaling laws is a characteristic of scales at which the time scales are very small leading to equilibrium. This assumption is however not valid for the near wall regions where the flow has bursts of vortex structures and is in a state of non equilibrium. So use of this assumption in the near wall region leads to extremely high values of dissipation model coefficient. So we assume that the flow is in a state of equilibrium and has spectrum that is valid both in the inertial range and the dissipation range. This is very essential because the flow is well resolved to a scale pretty close the dissipation scale near the wall (for reason that involves proper resolution of the wall shear stress). The derivation of the proposed modification is given in the Appendix .

Fig. 6c and 6d have the results obtained from LES simulations at Re=5200 and 8200 conducted on a 49 x 33 x 33 grid. The results match closely to those obtained from DNS in case of 5200 Re case. The instantaneous values of model coefficients are shown in Fig 6e.

Fig. 6f shows the mean profiles of subgrid kinetic energy non-dimensionalized using wall friction velocity, for two different Re. At a given resolution, more energy would be found in the unresolved scale for a higher Reynolds number. It is seen that as the Re increases the subgrid kinetic energy increases rapidly. The component wise decomposition of subgrid kinetic energy is not possible. As a first approximation we can assume that the scales are isotropic and divide it equally. However factors like grid aspect ratio and local strain may in reality render this assumption invalid in reality.

4.7 Turbulent axisymmetric jet

The circular turbulent jet is a very good test problem for LES. Although of significant importance in terms real life applications, this problem has not received much attention in terms of LES in the past. This is because many models reduce to mixing length models for plane shear layers and using these problems as test cases leads to a model that would fail in flows in the next hierarchy of difficulty such as flows with axisymmetry and secondary flow patterns. Therefore to date, no turbulence model has been able to predict correctly the spreading rate of a circular jet without some corrections specific to this problem. The prediction of spreading rate is directly related to the way in which the production and dissipation terms are modeled. This would serve as an evaluation process for the dynamic evaluation of model coefficients.

A circular wall jet with parabolic mean velocity profile was simulated at a Reynolds number of 1000 (based on maximum mean inlet velocity and inlet diameter). The length in the axial direction upto which the simulation was conducted is 20 diameters. A 65x33x33 grid was made use of, in this simulation. The flow was forced at the inlet using five discrete Strouhal numbers. Each frequency was associated with a parabolic spatial mode of forcing for axial velocity with amplitude of 4.0%. This kind on inlet velocity

specification leads to a very slow growth of kinetic energy in the shear layer in axial direction. In reality, the RMS velocity should have much higher value near the wall of the nozzle as compared to the core unlike the present case where the maximum value is found at the centreline. As to the specifiation of the subgrid kinetic energy at the inlet, it is still an unresolved issue. For the present simulation, a value proportional to the kinetic energy of the forcing modes is used.

The centerline axial velocity decay with axial distance for this simulation is shown in Fig. 7a. The decay of RMS resolved scale velocity flucuations is plotted in Fig 7b. It is found that the axial velocity decay is inversely proportional to the axial distance which is in qualitative agreement with the experimental data. The turbulent kinetic energy decay is inversely proportional to the downstream distance once the self similar region is reached in experiments. A similar trend was predicted at the downstream end of the simulation. The velocity profiles at various downstream locations are shown in Fig 7c. The subgrid kinetic energy profiles at three locations that are not in the self similar region are shown in Fig 7d. It is found that the subgrid kinetic energy has a maximum value in the shear layer formed at a radial distance that is close to the radius of the nozzle. This is an indication that the shear layer has not collapsed as yet and hence we cannot expect self similarity at these locations.

Fig. 7e shows the vorticity distribution along the axial palne of the jet. The closed contours that are on either sides of the centerline indicate the presence of shear layer. A fully developed turbulent flow would not have such structures, instead one can expect these structures to have break up into smaller structures with no coherence and completely random when visualized. To show the extent of unsteadiness due to forcing, the radial velocity distribution on an axial plane is shown in Fig. 7f. As is seen, there is entrainment of the flow from the boundaries. The unsteady forcing seem to persist for a long time downstream. When a jet undergoes transition and becomes fully turbulent, the forcing is not of much consequence. The unsteadiness is used to excite some spatial modes that force a fast transition. Hence in the present case, Fig 7f. suggests that the jet needs to simulated for a larger downstream distance to achieve fully turbulent self similar structure of the flow.

While there is a qualitative agreement between the results from this simulation and the experimental results, the quantitative comparison is not yet possible. This is because a method of providing inlet conditions at the nozzle that correspond to realistic turbulence is not available as yet. The behavior of the model near the wall along which there is entrainment, is not completely understood. Further the flow at the jet boundary is found to be intermittent and this may require special attention in LES.

Conclusion

An implicit scheme has been proposed for use in time advancement of the solution of Navier Stokes equations on a non staggered grid. The accuracy of the scheme has been looked into by simulation of various laminar and turbulent flows. The stability of the

perturbation method in order to include effects of heat release was demonstrated by simulation of a reacting temporal mixing layer where the final temperature ratio between the maximum and the minimum values was found to be more than 2.5. This method would serve as a workbench for future work in LES of turbulent and reacting flows.

The LES model used in this study has been found to successfully work for the low Reynolds number wall bounded flows. The model performance at higher Re remains to be seen. The flow structure near the wall at higher Re is rather complicated and it may not be possible to capture all the physics in this region using a simple one equation LES. So the main issue would be to stabilize the simulation in the near wall region. This was very found to be very crucial near the wall in the jet simulation where the entraining flow is not necessarily turbulent.

The present model needs initialization of the subgrid kinetic energy at start. This issue is trivial in temporal problems as subgrid kinetic energy would evolve in time with the mean flow. In spatially evolving flows, the spatial evolution of the flow field greatly depends on the inflow conditions for the subgrid kinetic energy. The filtered velocity is also unsteady in such problems. This unsteadiness should be representative of the turbulence at the inlet. This issue is not restricted to the present model but also to the algebraic models that are often used for LES.

One other issue important towards the comprehensive development of an LES model is one of grid anisotropy. Very little work has been done in this area. Much of the work relied on use of either the RMS or the harmonic mean of the grid filter widths in each direction, as an effective isotropic filter width. Some corrections for the case of anisotropic grids was proposed by Scotty etal [24] based on theoretical analysis but has never been applied in an actual simulation to the best of the knowledge of the present authors. Work along this direction would be future direction of research.

References

1. P. A. McMurtry, W. -H. Jou, J. J. Riley and R. W. Metcalfe, AIAA Paper No. 85-0143 (1985).

2. E. S. Oran and J. P. Boris, Prog. Energy and Comb. Sci., **7**:1-72 (1981).

3. A. J. Chorin, Math. Comput. **22**, 745 (1968).

4. R. Temam, Arch. Rat. Mech. Anal. **32**, 377 (1969).

5. Yan Zang, Robert L. Street and Jeffrey R. Koseff, J. Comput. Phys. **114**, 18 (1994).

6. L. Quartepelle, Numerical Solution of the Incompressible Navier-Stokes Equations. (Birkhauser ISNM Vol **13**, 1993).

7. N. N. Yanenko, The Method of Fractional steps (Springer Verlag, New York, 1971).

8. J. B. Perot, J. Comput. Phys. **108**, 51 (1993).

9. Y. Maday, A. Patera and E. Ronquist, J. Sci. Comput. **5**, 263 (1990).

10. R. Temam, Theor. Comput. Fluid Dynamics.

11. S. V. Patankar, Numerical Heat Transfer and Fluid Flow (Hemisphere, New York, 1980).

12. M. Rosenfeld, D Kwak and M. Vinokur, J. Comput. Phys. **94**, 102 (1991).

13. J. Kim and P. Moin, J. Comput. Phys. **59**, 308 (1985).

14. S. Biringen and C. Cook, Numerical Heat Transfer, Vol **13**, 241 (1988).

15. H. Choi and P. Moin, J. Comput. Phys **113**, 1 (1994).

16. V. Yakhot and S. A. Orszag, J. Sci. Comput. **1**, 3 (1986a).

17. Warhaft and Lumley, J. Fluid Mechanics **88**, 659 (1978).

18. R. W. Metcalfe, S. A. Orszag, M. E. Brachet, S. Menon and J. J. Riley, J. Fluid Mechanics, Vol **1984**, 207 (1987).

19. A. Michalke, J. Fluid Mechanics **19**, 543 (1972)

20. K. Bech, N. Tillmark, H. Alfredsson and H. I. Andersson, J. Fluid Mechanics, Vol **286**, 191 (1995).

21. H. I. Andersson, K. H. Bech and R. Kristoferrson, Proc. R. Soc. London A, **438**, 477 (1992).

22. R. Krisofferson, K. H. Bech and H. I. Andersson, Appl. Sci. Research , **51**:337 (1993).

23. Kim and Menon, communicated to J. Fluid Mechanics.

24. A Scotti, C. Meneveau and D. K. Lilly, Phys. Fluids A, **5** (9), 2306 (1993).

25. Y. H. Pao, Phys. of Fluids **8**, 1063 (1965).

Appendix

We consider the spectrum deduced from experiments by Pao [25].

$E(k) = \alpha \varepsilon^{2/3} k^{-5/3} \exp\left[-\frac{3}{2}\alpha(k\eta)^{4/3}\right]$, where α is a constant with value around 1.5.

The subgrid scale dissipation for the spectral cutoff filter (with cotuff k_c)can now be calculated as

$$\varepsilon^{sgs} = \int_{k_c}^{\infty} 2\upsilon k^2 E(k)\,dk$$

$$= \int_{k_c}^{\infty} 2\alpha\upsilon\varepsilon^{2/3}k^{1/3}\exp\left[-\frac{3}{2}\alpha(k\eta)^{4/3}\right]dk$$

$$\varepsilon^{sgs} = \upsilon\varepsilon^{2/3}\eta^{-4/3}\exp\left[-\frac{3}{2}\alpha(k_c\eta)^{4/3}\right]$$

Now the total dissipation can be obtained in terms of subgrid kinetic energy and the resolved scale by integration of energy spectrum over unresolved scales as follows.

$$k^{sgs} = \int_{k_c}^{\infty} E(k)\,dk$$

On substituting the Kolmogorov form of the energy spectrum for the inertial range(since dissipative scales have very little contribution to the total energy), we get

$$\varepsilon = C_\varepsilon \frac{(k^{sgs})^{3/2}}{\Delta}, \text{ where } \Delta \approx \frac{1}{k_c}$$

On substituting this expression into the equation for subgrid dissipation and using the definition of Kolmogorov scale in terms of dissipation and viscosity, we can get an expression for subgrid dissipation. The filter that is used in the present simulation is a box filter whereas this derivation is for a spectral cuttoff filter. But as is usually known, the functional form of equations in LES do not change with filter type, only the model constants are different. So finally the subgrid dissipation can be written as

$$\varepsilon^{sgs} = C_\varepsilon \frac{(k^{sgs})^{3/2}}{\Delta}\exp\left(-C_\varepsilon' \frac{\upsilon}{\upsilon_t}\right)$$

Now the model coefficients correspond to a box filter. The first of the constants is evaluated dynamically while the second is put to 1.0 for the preliminary investigation. The form of the spectrum assumed is valid also for the inertial range and so this expression for dissipation can be used through out the domain. This would take care of the effects of the dissipation range wherever it is resolved.

Table 1.

Comparison of kinetic energy decay in isotropic turbulence simulated using the present code with various stencils for convective operator and a spectral code

time	spectral code	present code with 3rd order convective term	present code with 5rd order convective term	present code with 6rd order convective term
0.0	4.4869e-03	4.4869e-03	4.4869e-03	4.4869e-03
2.0	3.5626e-03	3.5593e-03	3.5724e-03	3.5756e-03
4.0	2.9195e-03	2.9152e-03	2.9283e-03	2.9325e-03
6.0	2.4517e-03	2.4466e-03	2.4575e-03	2.4622e-03
8.0	2.0995e-03	2.0930e-03	2.1016e-03	2.1065e-03

Table 2

Variation of amplification with wavenumber of a 2D disturbance in temporal mixing layer with hyperbolic tangent initial velocity profile

Wavenumber	Amplification (Michalke's computations)	Amplification (Computation with present code)
0.3	0.08654	0.08611
0.4446	0.09485	0.09466
0.6	0.08650	0.08639

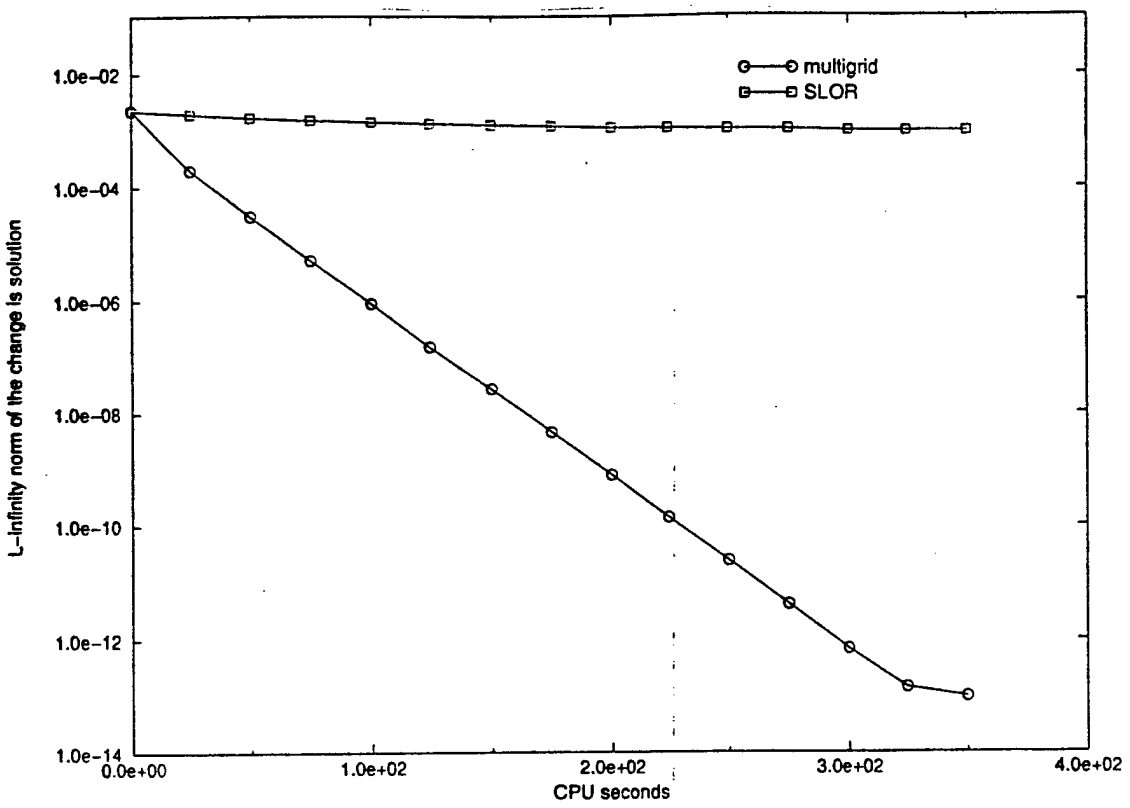

FIG. 1. Comparison of rate of convergence of multigrid scheme with regular SLOR scheme (when run on a SGI challenge workstation)

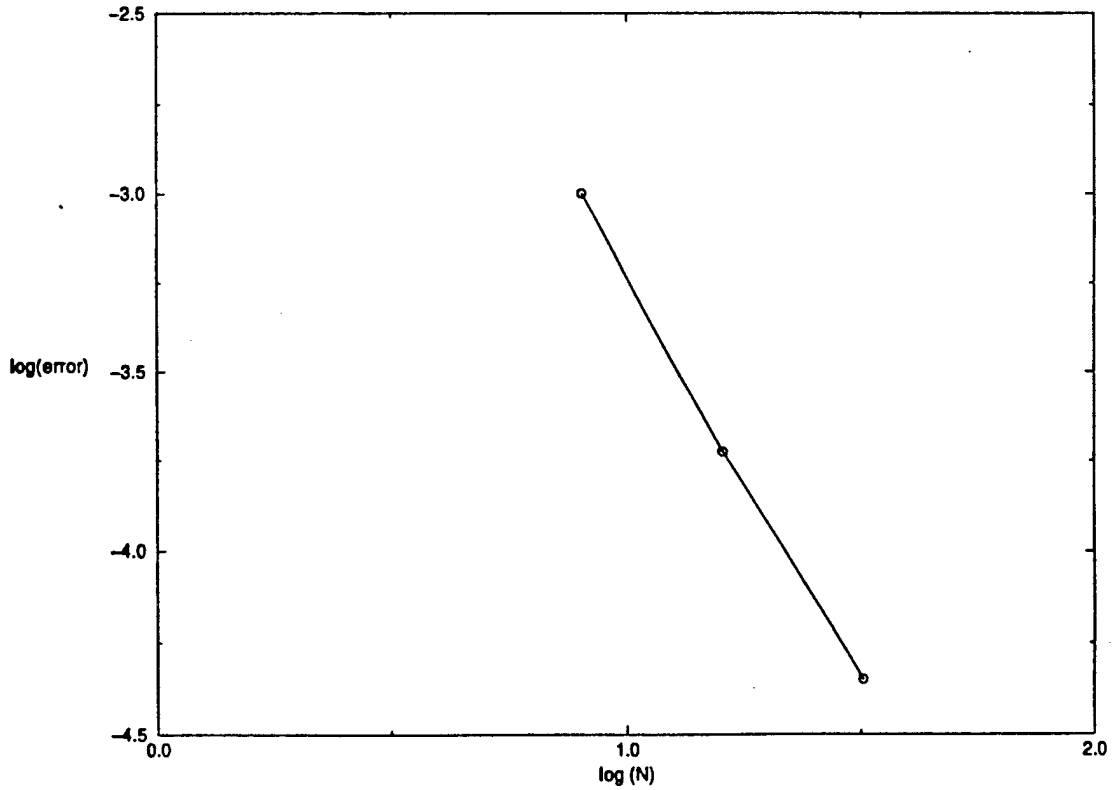

FIG. 2. Variation of maximum error in u with number of grid points used for the simulation (error against exact values computed after dimensionless time of 20.0)

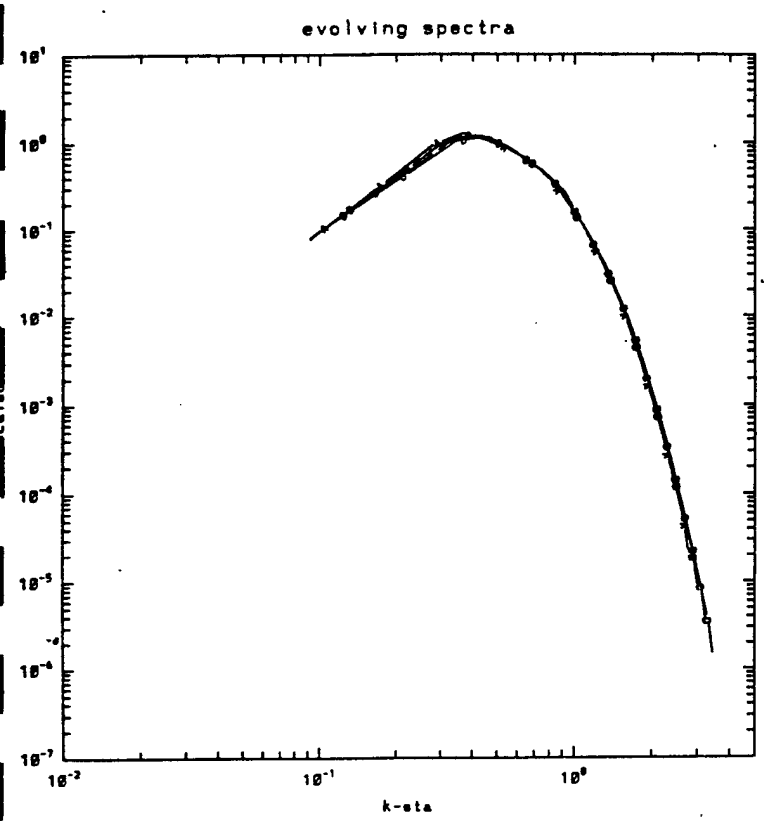

FIG. 3a. Self similarity of energy spectrum during final stages of decay (from nondimensional time of 11 to 17)

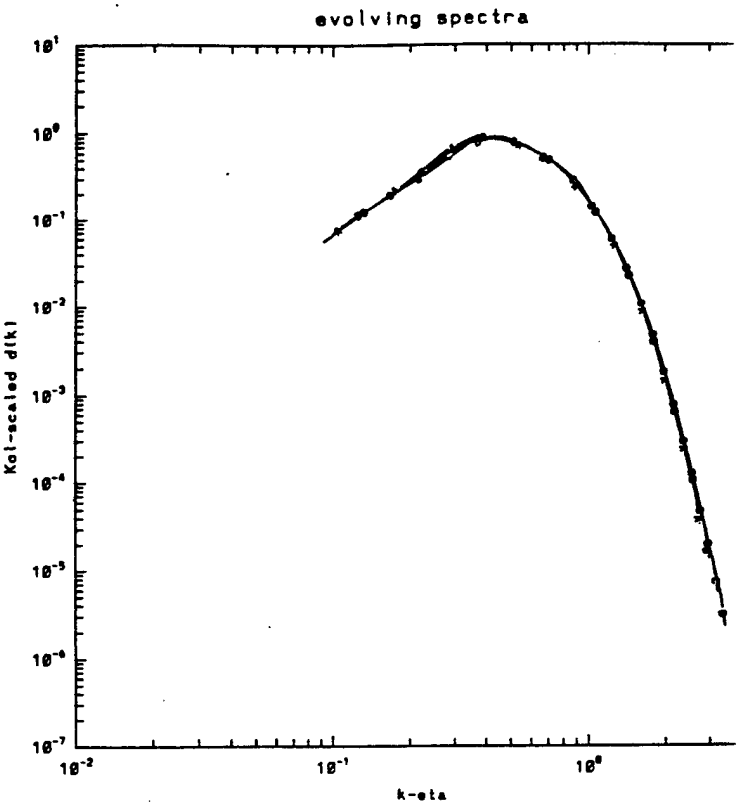

FIG. 3b. Self similarity of dissipation spectrum during final stages of decay (from nondimensional time of 11 to 17)

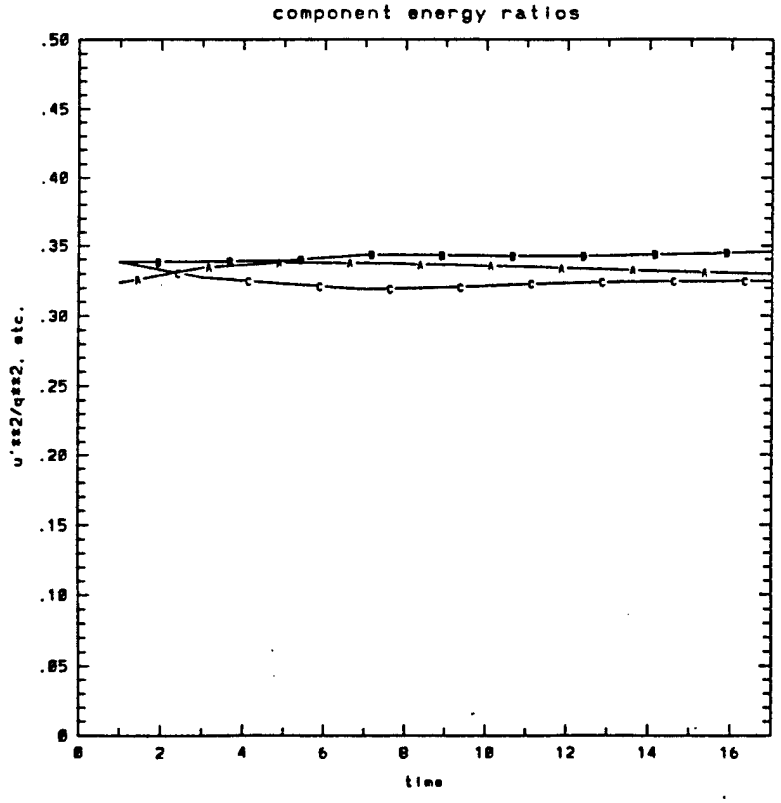

FIG. 3c. Component wise decomposition of kinetic energy

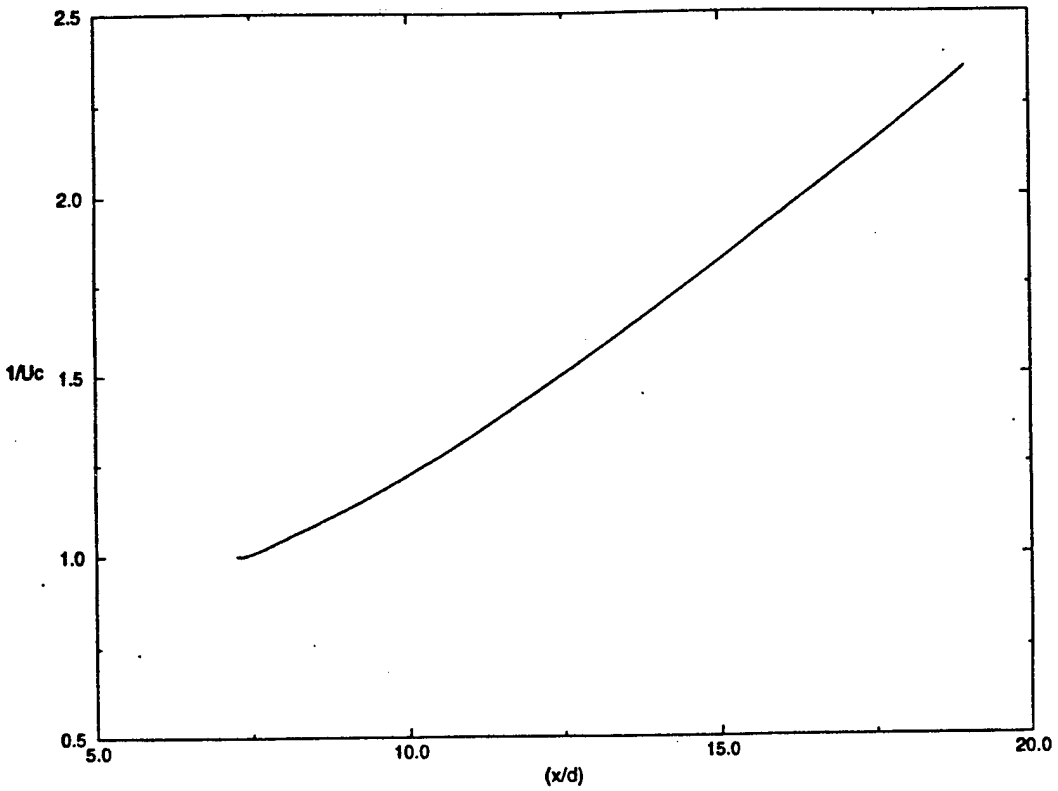

FIG. 4a. Centre line velocity decay as a function of downstream distance
(x is the distance from the virtual origin)

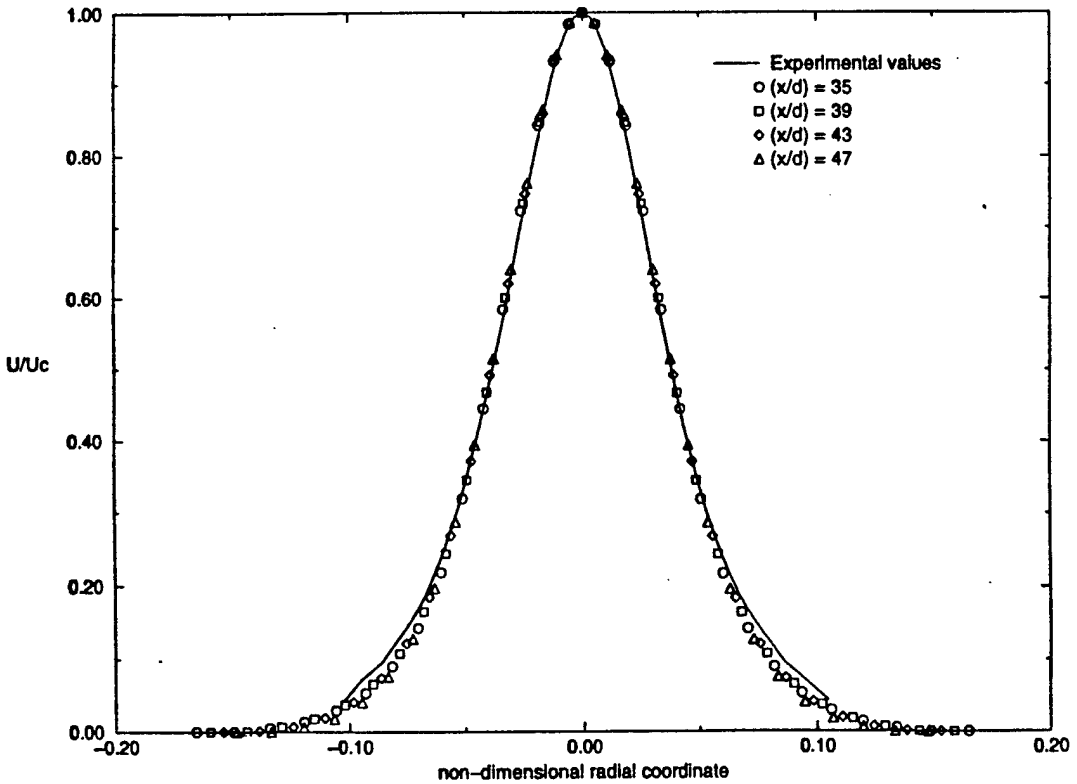

FIG. 4b. Velocity profiles at various downstream locations

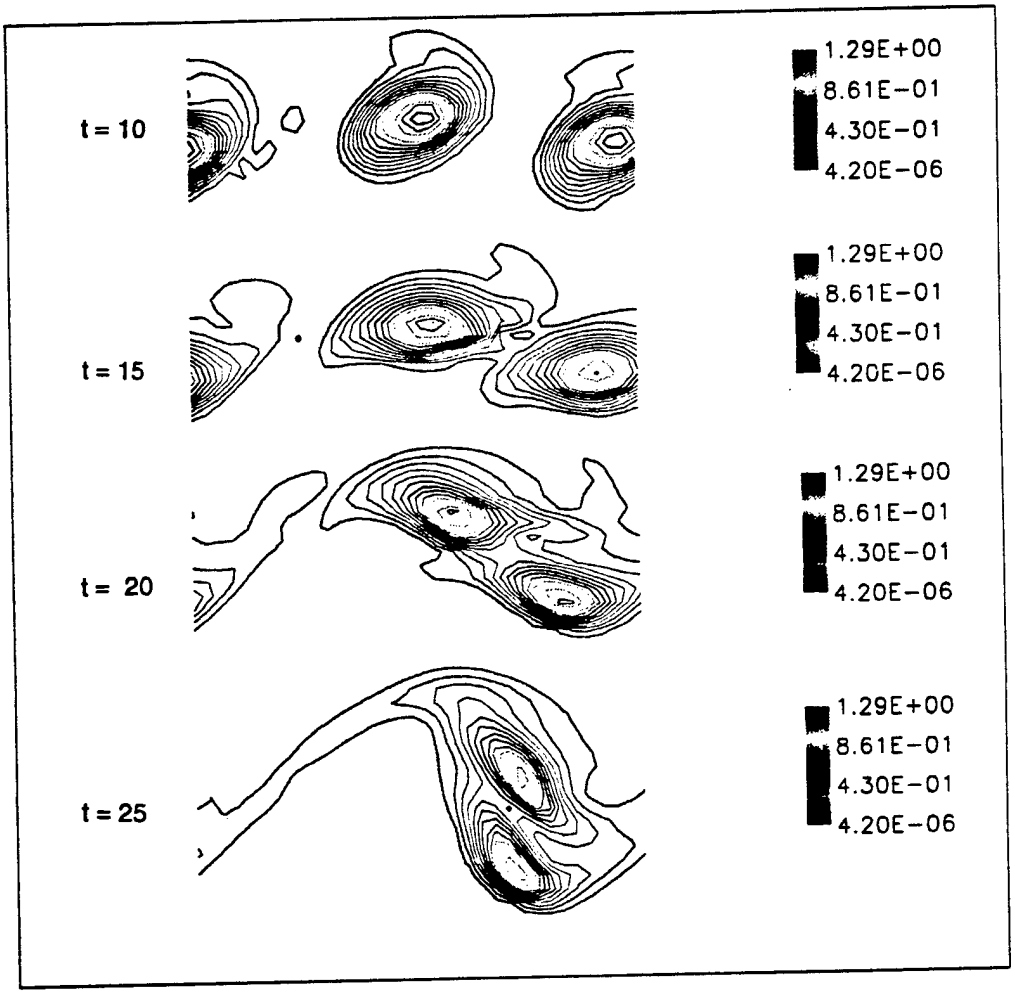

FIG. 5a. Contours of vorticity magnitude in a mixing layer with 3D initial disturbance

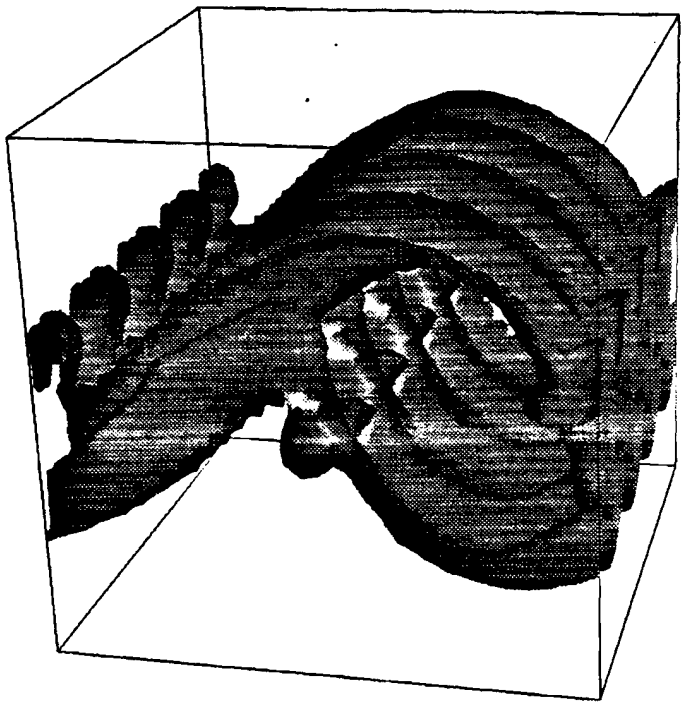

FIG. 5b. Isolevel surface of vorticity magnitude for a 3D roll up of mixing layer (t = 25.0)

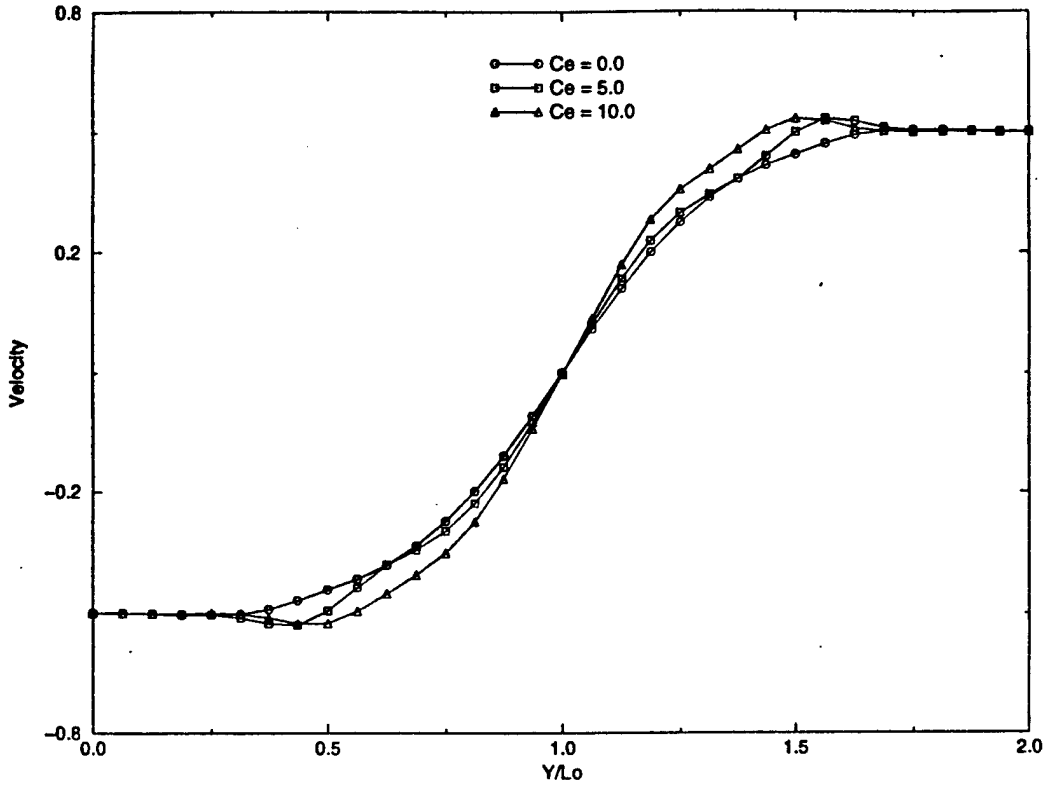

FIG. 5c. Velocity profile across the mixing layer
at t = 25.0

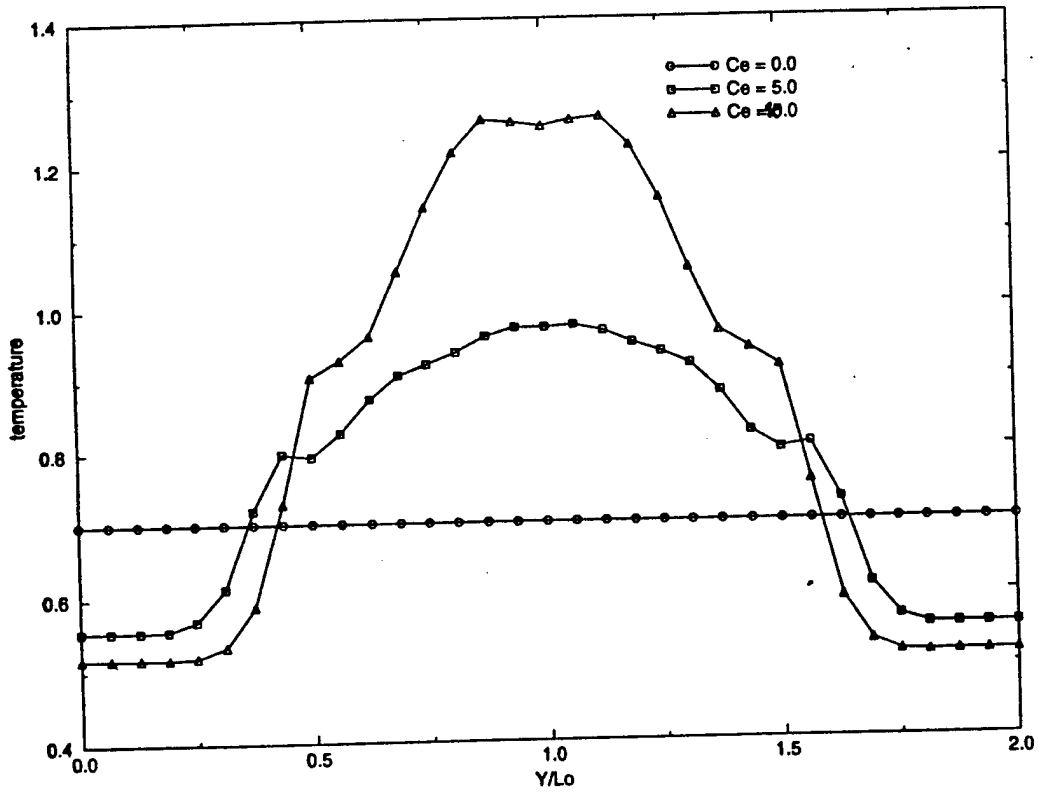

FIG. 5d. Average temperature profile across the mixing layer
at t = 25.0

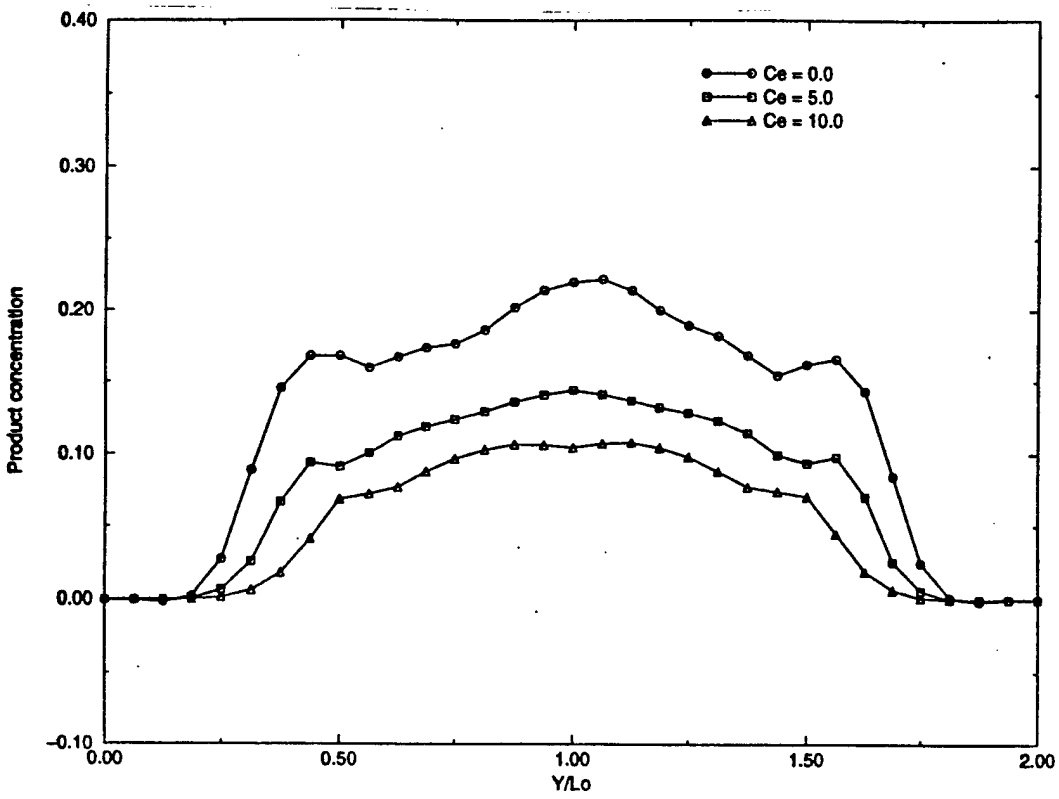

FIG. 5e. Average product concentration across the mixing layer at t = 25.0

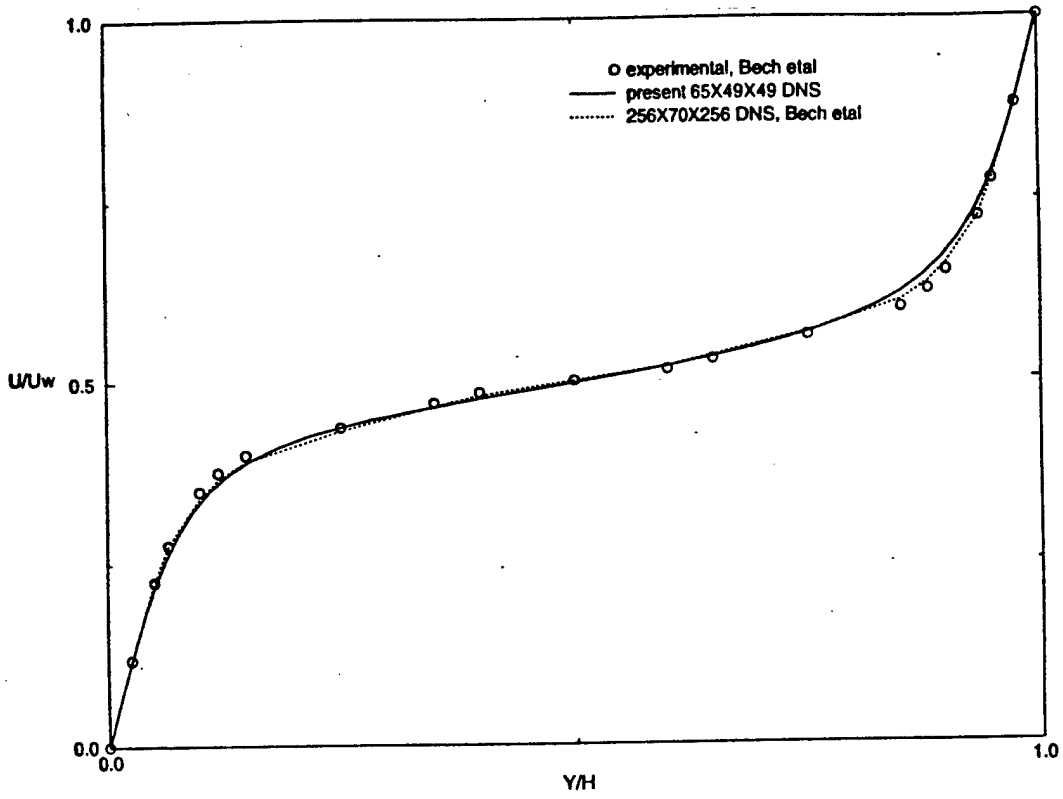

FIG. 6a. Mean velocity profile in Couette flow
Re = 5200

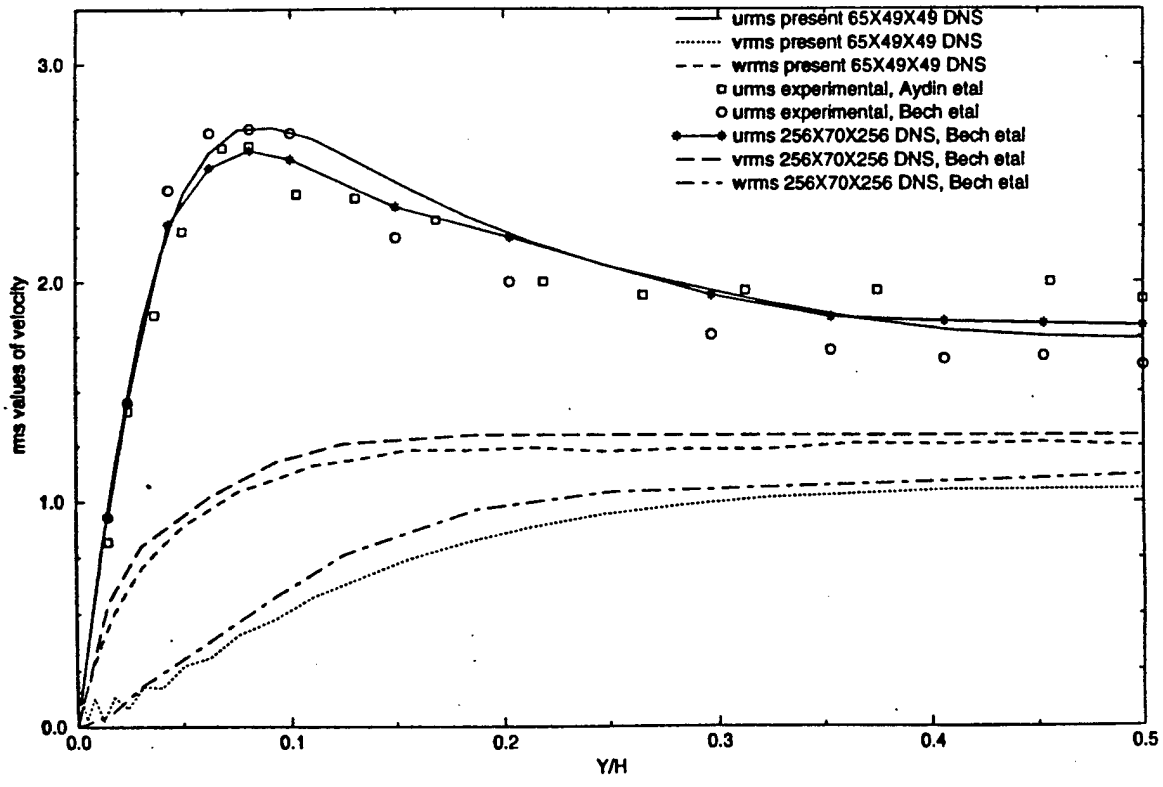

FIG. 6b. One point statistics in Couette flow (RMS values of fluctuating velocities)
All RMS values non-dimensionalized using u^*, all data collected at around Re of 5200

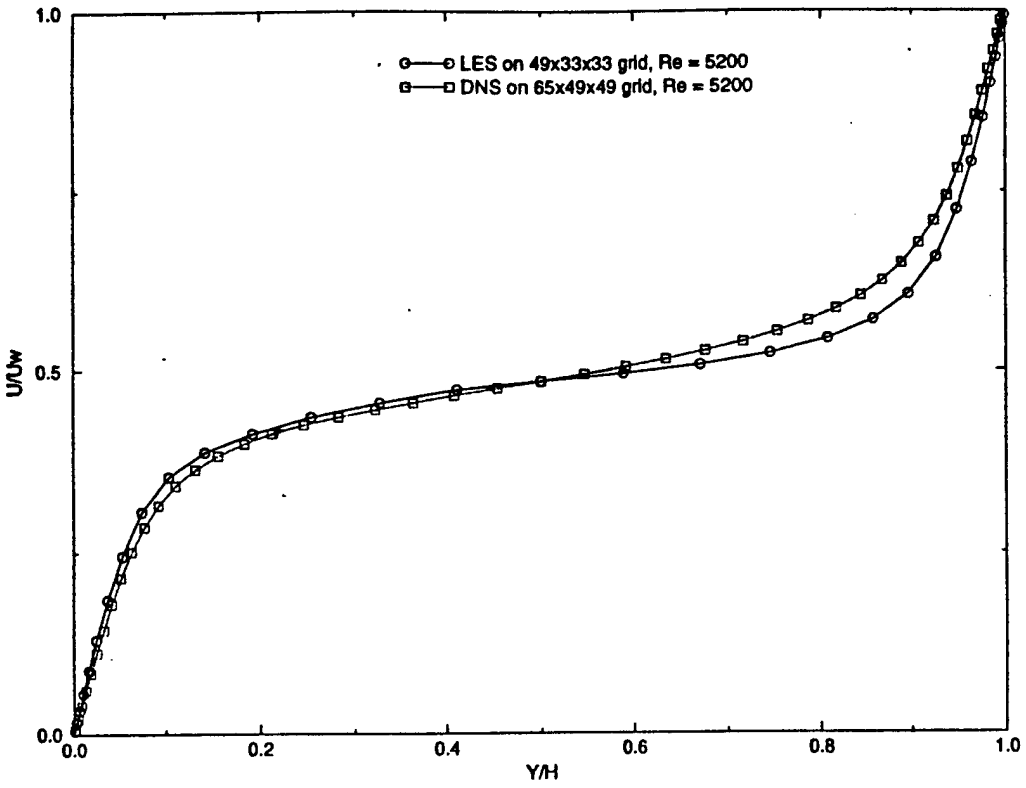

FIG. 6c. Comparison of DNS and LES mean velocity profiles

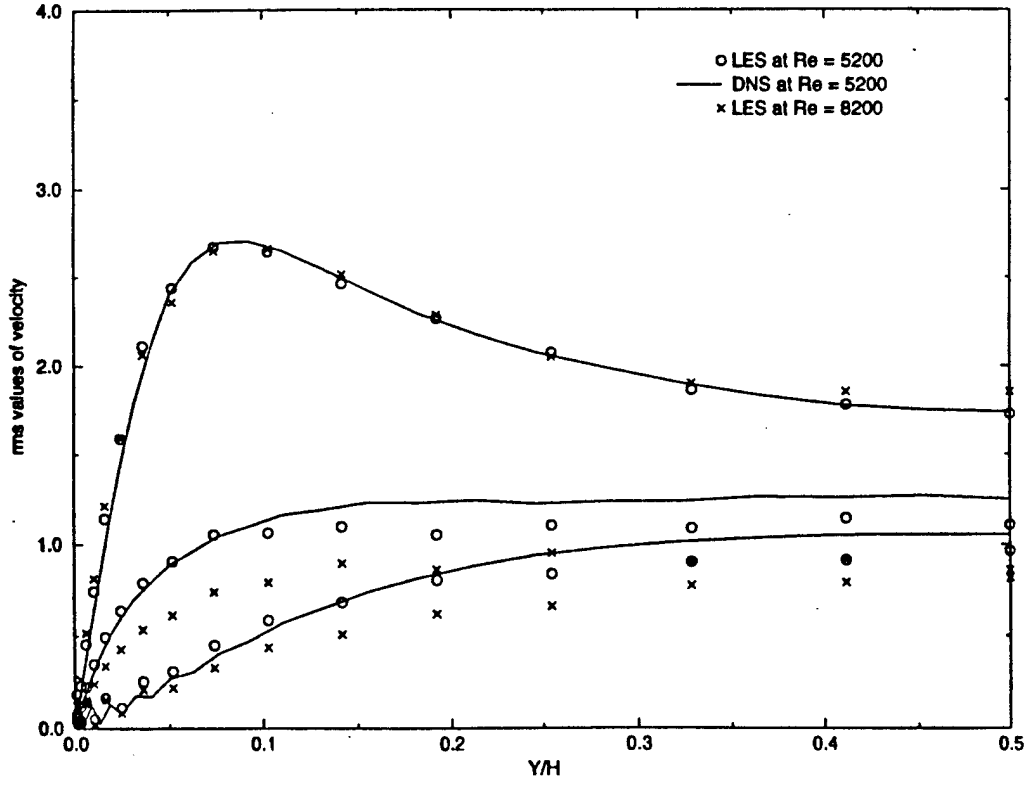

FIG. 6d. RMS values of velocities in Couette flow
All RMS values non-dimensionalized using u*

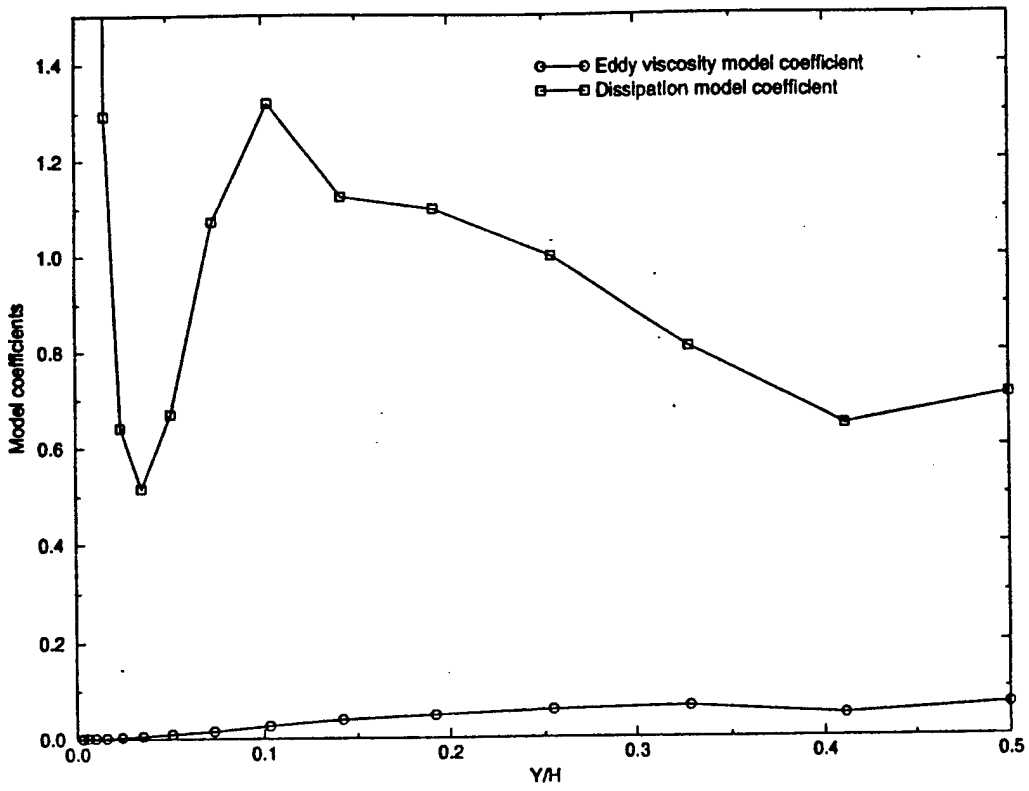

FIG. 6e. Variation of model coefficients along wall normal coordinate (instantaneous values)

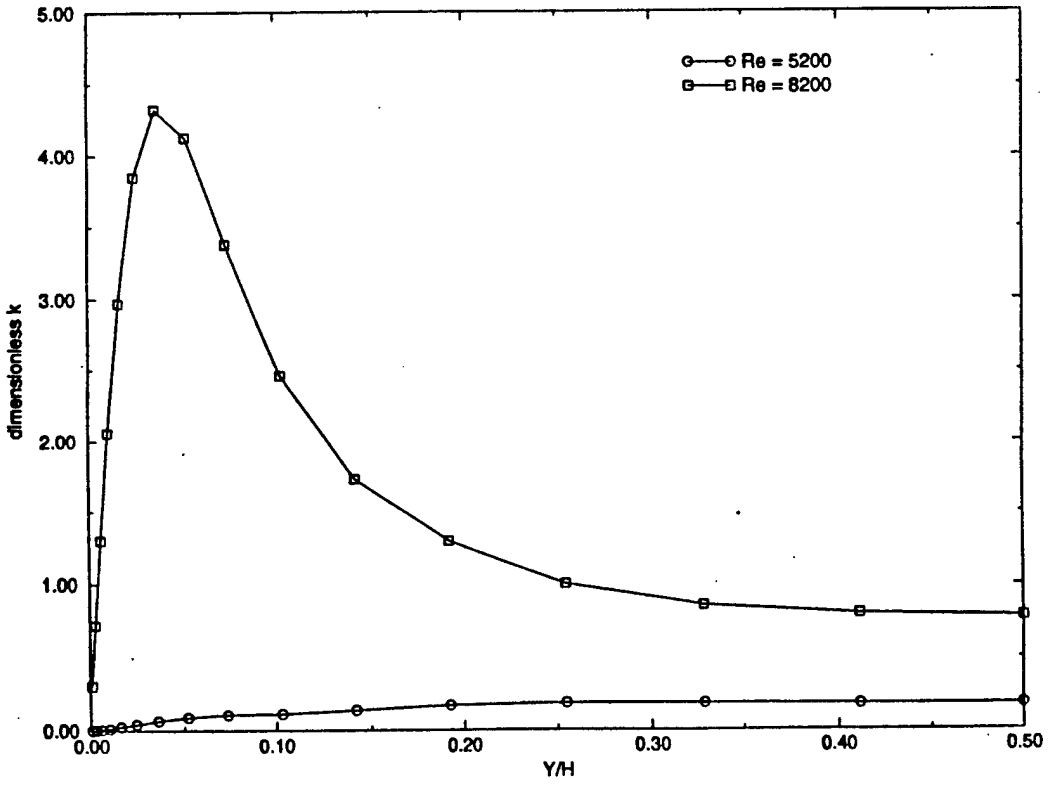

FIG. 6f. Mean subgrid kinetic energy profile (non–dimensionalized with square of u*)

FIG.6g. Streamwise velocity distribution in YZ plane of Couette flow
(wall velocity is in X direction and Y is the wall normal coordinate)

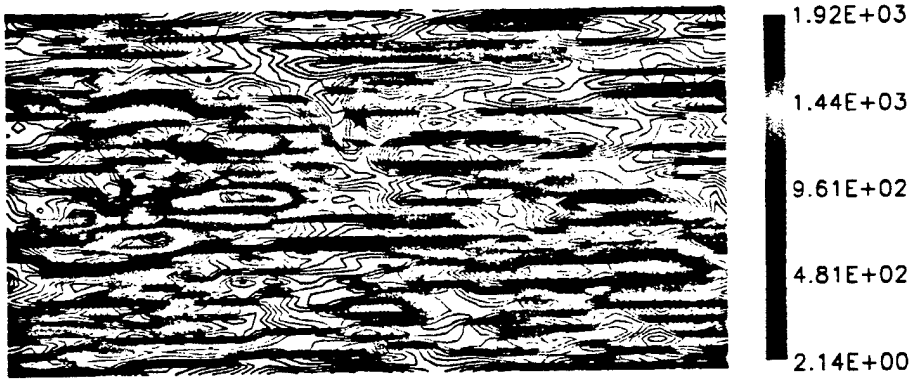

FIG.6h. Distribution of Vorticity magnitude in XZ plane of Couette flow
(wall velocity is in X direction and Y is the wall normal coordinate)

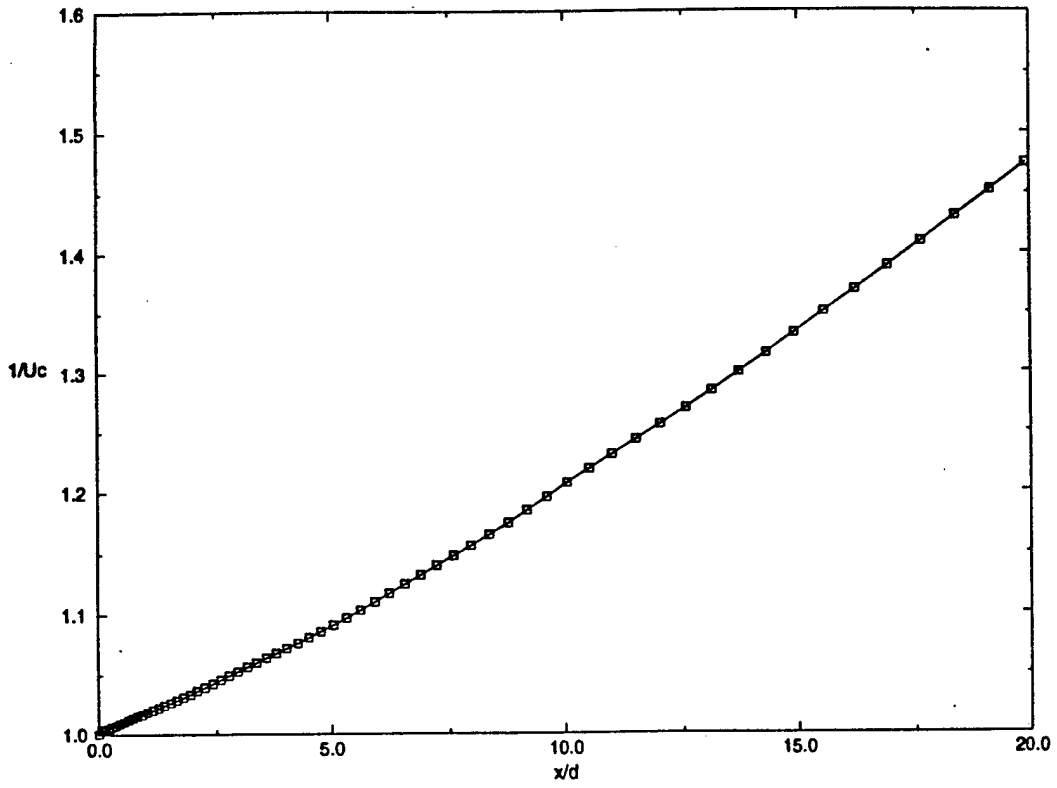

FIG. 7a. Centreline velocity decay in a turbulent axisymmetric jet
(Re = 1000 based on nozzle diameter and mean centreline velocity at the inlet)

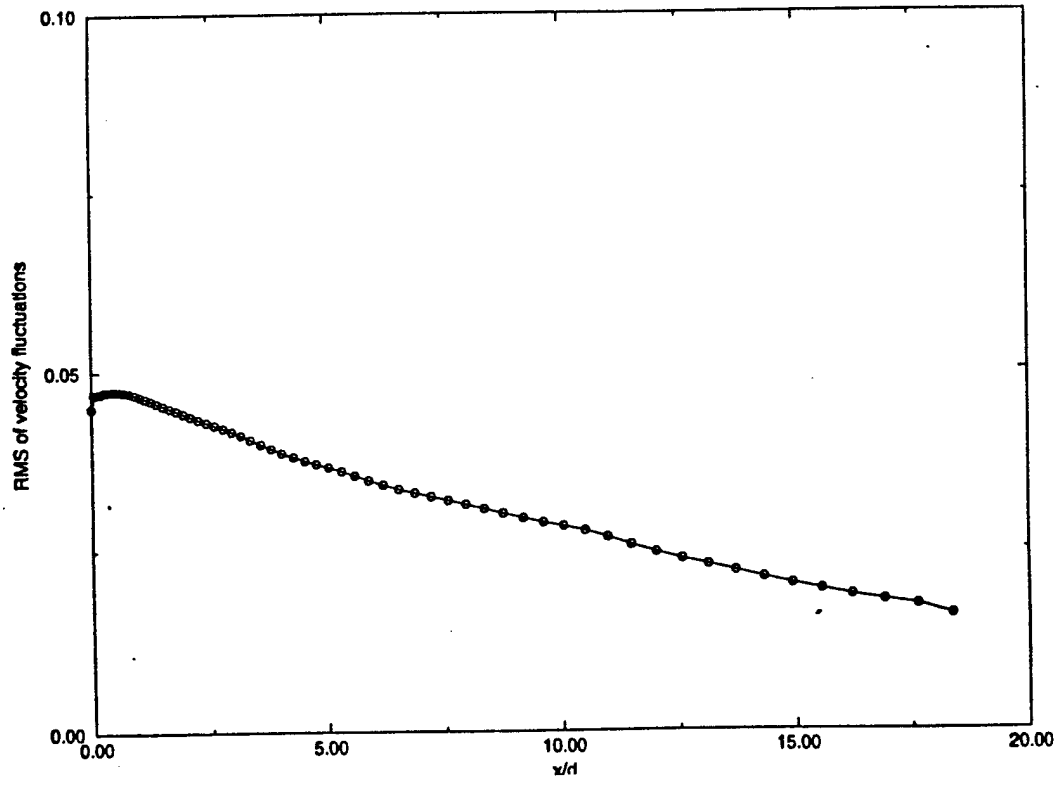

FIG. 7b. Axial variation of RMS resolved scale velocity fluctuations in a turbulent jet
(Re = 1000)

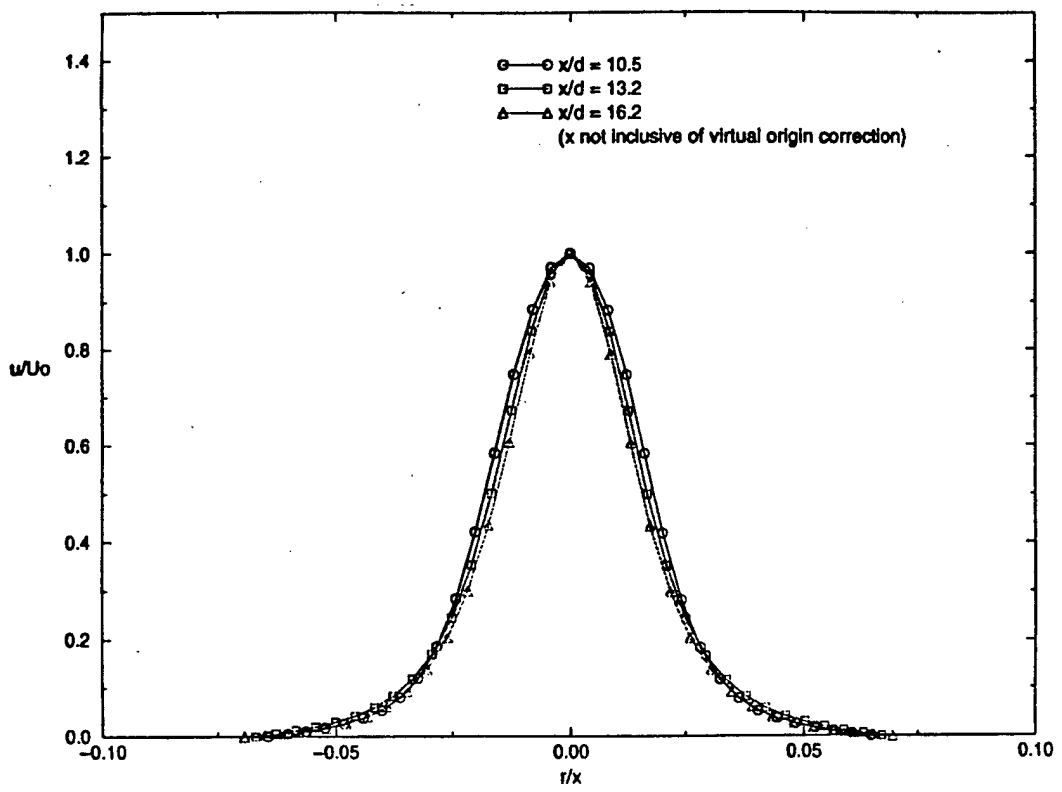

FIG. 7c. Velocity profiles in a turbulent circular jet
(Re = 1000)

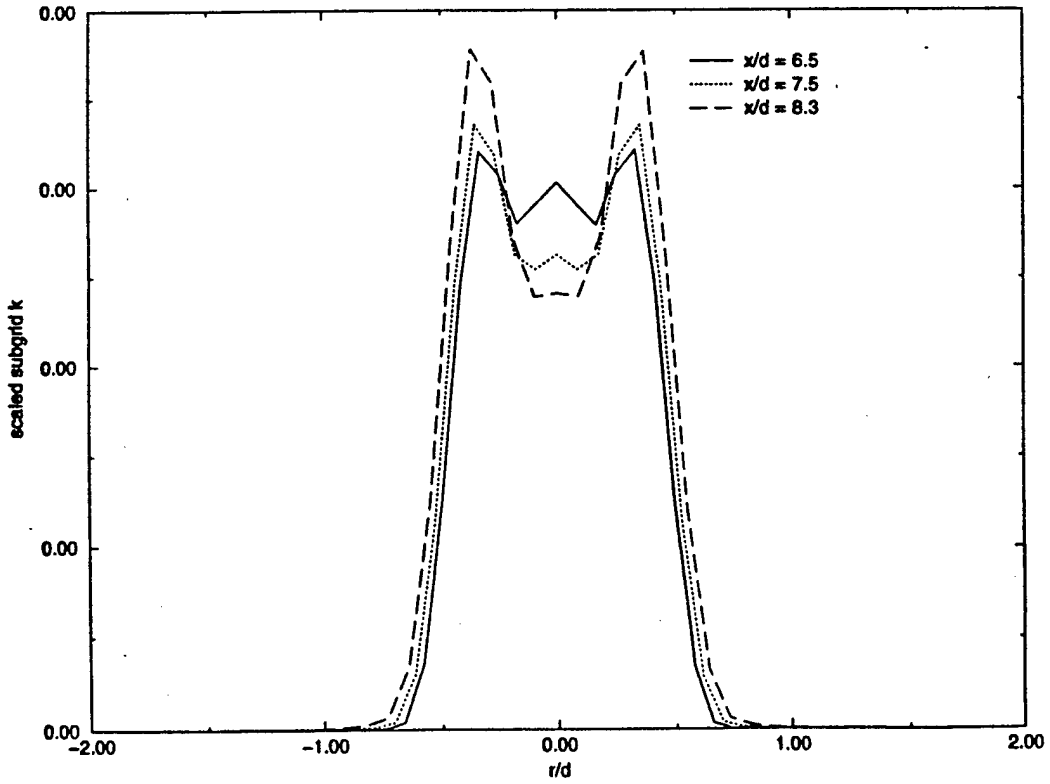

FIG. 7d. Mean subgrid kinetic energy profiles
(subgrid k scaled with square of centerline velocity)

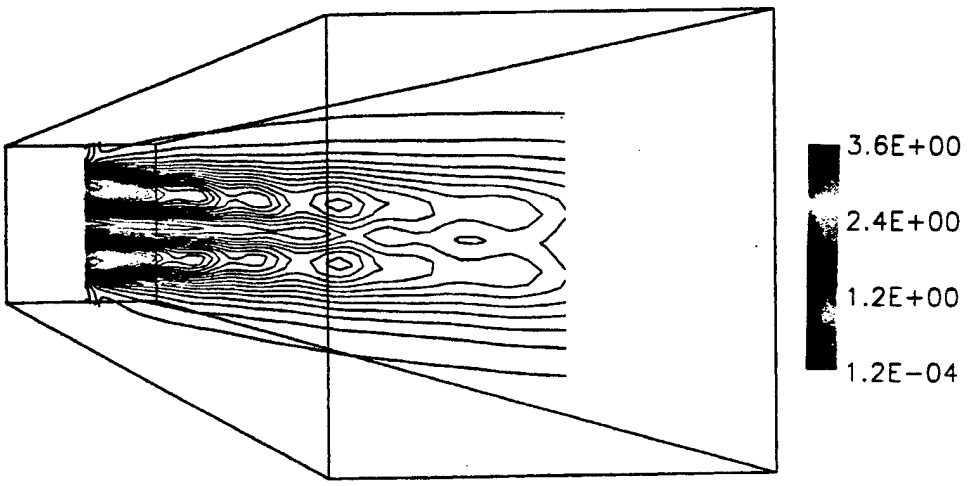

FIG.7e. Vorticity distribution in an axial plane of a turbulent jet

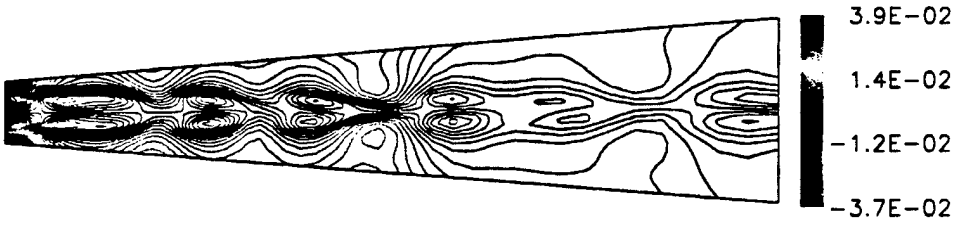

FIG.7f. Radial velocity distribution in an axial plane of a turbulent jet
(forced jet with entraining boundaries)

Draft Paper Submitted for Presentation at the
34th AIAA Aerospace Sciences Meeting and Exhibit
January 15-18, 1996

High Reynolds number flow simulations using the localized dynamic subgrid-scale model

Suresh Menon and Won-Wook Kim
School of Aerospace Engineering
Georgia Institute of Technology
Atlanta, Georgia
phone: (404) 853-9160
e-mail: menon@falcon.ae.gatech.edu

1. Introduction

The dynamic subgrid-scale (SGS) model, introduced by Germano *et al.* (1991), has been successfully applied to various types of flow fields (Moin *et al.*, 1991; Piomelli, 1993; Zang *et al.*, 1993; El-Hady *et al.*, 1994; Ghosal *et al.*, 1995). Two features of this model are typically emphasized in the literature. First, the model coefficient is determined as a part of the solution and therefore, this removes a major drawback of the earlier eddy viscosity type SGS models (e.g., Smagorinsky's (1963) model) which was their inability to model correctly the unresolved subgrid stresses in different types of turbulent flow fields with a single *universal* constant. Second, as a result of the dynamic evaluation, the model coefficient can become negative in certain regions of the flow field and thus, appears to have the capability to mimic backscatter of energy from the subgrid-scales to the resolved scales.

Although it has been shown that the Germano *et al.*'s model is superior to the conventional fixed-coefficient model, the dynamic method, as developed earlier, still has some drawbacks. These drawbacks originate from a weakness of the Smagorinsky's model used in Germano *et al.*'s dynamic model as well as from the mathematically inconsistent derivation and the ill-conditioning of the dynamic formulation itself. The Smagorinsky's time-independent, algebraic eddy viscosity model used in Germano *et al.*'s dynamic model is derived by assuming local equilibrium between the SGS energy production and dissipation rate. Thus, non-local and history effects of the turbulence evolution are completely neglected in this model. Also, as noted by the original authors, the dynamic model employing Germano *et al.*'s mathematical identity cannot guarantee stable numerical simulations. A popular approach to stabilize the simulations is spatial averaging of the model coefficient in directions of flow homogeneity. This has been quite successful in simple flows such as isotropic turbulence. However, since complex flows do not have any direction of flow homogeneity, more complex local averaging procedures are required and have been recently proposed (e.g., Zang *et al.*, 1993; Meneveau *et al.*, 1994; Kim and Menon, 1995). Although good results have been demonstrated using these methods, local-averaging approaches are still, in general, unacceptable because local-averaging is carried out only to avoid numerical instability, and has nothing to do with the dynamic method. Therefore, a truly robust dynamic model must be able to provide a stable and accurate solution using *local* values of the coefficient that vary both in time and space.

Recently, Kim and Menon (1995) developed a new localized dynamic formulation associated with the one-equation SGS model to avoid altogether local- or global-averaging and to remove the mathematical inconsistency and the ill-conditioning problem that occurs when employing Germano *et al.*'s

mathematical identity in the dynamic approach. This model provides a straightforward localized evaluation of the model coefficients and does not cause numerical instability. They applied the localized dynamic model to Taylor-Green vortex flows and show that this model predicts the turbulent flow field more accurately than the conventional dynamic models such as the dynamic algebraic SGS (DASGS) model and the local-averaged dynamic kinetic energy equation (DKSGS) model. The main objective of this paper is to further investigate the properties of the localized dynamic model and then, eventually, extend the model to high Reynolds number flows. The properties of the model have been studied in the theoretical point of view using realizability conditions and Galilean invariance and on practical grounds by applying it to Taylor-Green vortex flows, decaying and forced isotropic turbulence and turbulent mixing layers. The results are compared with predictions using experiments, direct numerical simulation and large-eddy simulations using the DASGS model and the local-averaged DKSGS model.

The numerical simulations were carried out using a finite-difference code that is second-order accurate in time and fifth-order (the convective terms) and sixth-order (the viscous terms) accurate in space using upwind-biased differences (Rai and Moin, 1991). Time-accurate solutions of the incompressible Navier-Stokes equations are obtained by the artificial compressibility approach (Chorin, 1967; Rogers *et al.*, 1991) which requires subiteration in pseudotime to get the divergence-free flow field. A significant acceleration of the convergence to a steady-state divergence-free solution in pseudotime is achieved by incorporating the full approximation scheme (FAS) multigrid concept proposed by Brandt (1981) Earlier (Menon and Yeung, 1994), this code was validated by carrying out DNS of decaying isotropic turbulence and comparing the resulting statistics with the predictions of a well known psuedo spectral code (Rogallo, 1981).

In the next section, various dynamic SGS models are described with the basic equations indicating their advantages and drawbacks. In section 3, we apply the localized model to Taylor-Green vortex flow, decaying and force isotropic turbulence and mixing layers. The results are briefly presented here. Future work is mentioned in section 4.

2. Dynamic subgrid-scale modeling

In physical space, the incompressible Navier-Stokes equations for LES are achieved by low-pass filtering of a computational mesh (hence, the characteristic length of this filter is $\overline{\Delta}$) as follows,

$$\frac{\partial \overline{u}_i}{\partial x_i} = 0 \tag{1}$$

$$\frac{\partial \overline{u}_i}{\partial t} + \overline{u}_j \frac{\partial \overline{u}_i}{\partial x_j} = -\frac{\partial}{\partial x_j}\left(\overline{p}\delta_{ij} + \tau_{ij}\right) + \nu \frac{\partial^2 \overline{u}_i}{\partial x_j \partial x_j} \tag{2}$$

where $\overline{u}_i(x_i, t)$ is the resolved velocity field and the SGS stress tensor τ_{ij} is defined as:

$$\tau_{ij} = \overline{u_i u_j} - \overline{u}_i \overline{u}_j. \tag{3}$$

In order to close equations (1) and (2), one needs to model τ_{ij} in terms of the resolved velocity field $\overline{u}_i$. Eddy viscosity model assumes proportionality between the anisotropic part of the SGS stress tensor, $\tau_{ij} - \frac{1}{3}\delta_{ij}\tau_{kk}$, and the resolved scale strain rate tensor, $\overline{S}_{ij}$:

$$\tau_{ij} - \tfrac{1}{3}\delta_{ij}\tau_{kk} = -2\nu_T \overline{S}_{ij} \tag{4}$$

where ν_T is the eddy viscosity and

$$\overline{S}_{ij} = \frac{1}{2}\left(\frac{\partial \overline{u}_i}{\partial x_j} + \frac{\partial \overline{u}_j}{\partial x_i}\right). \tag{5}$$

Simple dimensional arguments suggest that the eddy viscosity, ν_T, should be given by the product of a velocity scale and a length scale. In LES, the length scale is usually related to the filter width, however, various models differ in their prescription for the velocity scale. In Smagorinsky's (1963) model, an algebraically described velocity scale is obtained by assuming that an equilibrium exists between energy production and dissipation in the small scales. One-equation SGS model (Schumann, 1975; Yoshizawa, 1991; Menon *et al.*, 1994) solves a transport equation for the SGS kinetic energy to provide the velocity scale.

Dynamic SGS models have recently received the most attention. This type of model uses the eddy viscosity type model as a base model and incorporates the similarity concept (Bardina *et al.*, 1980; Liu *et al.*, 1994) to dynamically compute the model coefficients. To date, two typical dynamic models have been suggested. One is dynamic algebraic SGS model (Germano *et al.*, 1991) which is incorporated with Smagorinsky's model, and the other is dynamic one-equation SGS model (Ghosal *et al.*, 1995; Kim and Menon, 1995) based on the SGS kinetic energy.

2.1. Dynamic Algebraic Subgrid-Scale (DASGS) Model

The simplest model which predicts the global energy transfer with acceptable accuracy is the algebraic eddy viscosity model originally proposed by Smagorinsky (1963):

$$\tau_{ij} = -2c_A \overline{\Delta}^2 |\overline{S}| \overline{S}_{ij} + \tfrac{1}{3}\delta_{ij}\tau_{kk} \tag{6}$$

where, the model coefficient c_A is equivalent to the square of the Smagorinsky's constant, and $|\overline{S}| = (2\overline{S}_{ij}\overline{S}_{ij})^{\frac{1}{2}}$. c_A requires adjustment for different flows. A large number of studies have been devoted to fine-tuning c_A for various flows of interest. This problem was circumvented by using a dynamic procedure (Germano *et al.*, 1991) which implements a direct evaluation of c_A. In the dynamic modeling approach, a mathematical identity between the stresses resolved at the grid filter $\overline{\Delta}$ and a test filter $\hat{\Delta}$ (typically, $\hat{\Delta} = 2\overline{\Delta}$) is used to determine the model coefficient c_A. In the present study, we employ the top-hat filter for the test filtering which is considered appropriate for finite-difference methods in physical space. Thus if the application of the test filter on any variable ϕ is denoted by $\hat{\phi}$ or $<\phi>$, it can be shown that:

$$L_{ij} = T_{ij} - \hat{\tau}_{ij} = \left\langle \overline{u}_i \overline{u}_j \right\rangle - \hat{\overline{u}}_i \hat{\overline{u}}_j. \tag{7}$$

where,

$$T_{ij} = \left\langle u_i u_j \right\rangle - \hat{\overline{u}}_i \hat{\overline{u}}_j \tag{8}$$

is the SGS stress tensor defined at the test filter level. Assuming self-similarity of the subgrid stresses, one can model T_{ij} in the same way as τ_{ij}:

$$T_{ij} = -2c_A \hat{\Delta}^2 \left|\hat{\bar{S}}\right| \hat{\bar{S}}_{ij} + \tfrac{1}{3}\delta_{ij} T_{kk} \tag{9}$$

Combining (6), (7) and (9), an equation for c_A can be obtained:

$$L_{ij} - \tfrac{1}{3}\delta_{ij} L_{kk} = 2c_A M_{ij} \tag{10}$$

where

$$M_{ij} = -\left(\hat{\Delta}^2 \left|\hat{\bar{S}}\right| \hat{\bar{S}}_{ij} - \overline{\Delta^2 \left\langle |\bar{S}| \bar{S}_{ij} \right\rangle}\right). \tag{11}$$

Equation (10) is a set of five independent equations for one unknown c_A. To minimize the error that can occur solving this over-determined system, Lilly (1992) proposed a least square method which yields

$$c_A = \frac{1}{2} \frac{L_{ij} M_{ij}}{M_{ij} M_{ij}}. \tag{12}$$

While the Germano *et al.*'s dynamic model has been used successfully, some drawbacks of this model are worth noting. First, in spite of a large spatial variation of the model coefficient, it is taken out of the spatial-filtering operation, as shown in (10), as if it were a constant in space. Local values of the model coefficient as a function of space are then sought. This mathematical inconsistency decreases the accuracy of the dynamic model. Second, the resulting equation (12) for c_A is ill-conditioned because the denominator of this expression (i.e. M_{ij}) comes from the algebraic manipulation of two base models defined at different filtering levels and, hence, it can become very small causing numerical instability. These two drawbacks are directly related to the Germano *et al.*'s mathematical identity (7). Finally, another drawback is the prolonged occurrence of negative model coefficient in the flow field (negative model coefficient is possible since M_{ij} can become negative) which has also been shown to cause numerical instability (Ghosal *et al.*, 1993). This drawback appears to result from the nature of Smagorinsky's model used as a base model in the Germano *et al.*'s dynamic formulation. A possible resolution of all these deficiencies will be discussed in the following sections.

In this paper, we refer to the original Germano *et al.*'s dynamic formulation incorporated with Smagorinsky's model as the dynamic algebraic subgrid-scale (DASGS) model.

2.2. Dynamic k-Equation Subgrid-Scale (DKSGS) Model

A one-equation model for the subgrid-scale kinetic energy,

$$k_{sgs} = \tfrac{1}{2}\left(\overline{u_i^2} - \bar{u}_i^2\right), \tag{13}$$

in the following form (e.g. Yoshizawa, 1991),

$$\frac{\partial k_{sgs}}{\partial t} + \bar{u}_i \frac{\partial k_{sgs}}{\partial x_i} = -\tau_{ij} \frac{\partial \bar{u}_i}{\partial x_j} - \varepsilon + \frac{\partial}{\partial x_i}\left(\nu_T \frac{\partial k_{sgs}}{\partial x_i}\right) \tag{14}$$

has been studied recently (Menon and Yeung, 1994; Menon *et al.*, 1994). Here, the three terms on the right-hand-side of (14) represent, respectively, the production rate, the dissipation rate and the transport rate of k_{sgs}. The SGS stress tensor τ_{ij} is modeled in terms of the SGS eddy viscosity ν_T and k_{sgs} as:

$$\tau_{ij} = -2\nu_T \bar{S}_{ij} + \tfrac{2}{3}\delta_{ij} k_{sgs} \tag{15}$$

where

$$\nu_T = c_\epsilon k_{sgs}^{\frac{1}{2}} \bar{\Delta} \tag{16}$$

Here, c_ϵ is an adjustable coefficient that is determined dynamically, as shown below. As shown in (16), ν_T has the form which is used in a standard one-equation model for Reynolds-averaged Navier-Stokes computation. Equation (14) is closed by providing a model for the dissipation rate term, ε. Using simple scaling arguments, ε is usually modeled as,

$$\varepsilon = c_\epsilon \frac{k_{sgs}^{\frac{3}{2}}}{\bar{\Delta}}. \tag{17}$$

where, c_ϵ is another coefficient that is also obtained dynamically.

An important feature of this model is that no assumption of local equilibrium between the subgrid-scale energy production and dissipation rate has been made. That is, the direct computation of the subgrid-scale kinetic energy implemented in this model can account for some non-local and history effects which are completely neglected in the algebraic model described in section 2.1. Therefore, it is expected (and demonstrated in this paper) that this model will give better predictions of the SGS stresses than the algebraic model especially as the computation mesh becomes coarser.

The dynamic modeling method is applied to the *k*-equation subgrid-scale model to obtain appropriate values of the coefficients c_ϵ and c_ϵ. To implement this method, the turbulent kinetic energy at the test filter level is obtained from the trace of (7),

$$K = L_{ii}/2 + \hat{k}_{sgs}. \tag{18}$$

Using a procedure similar to that outlined in Section 2.1, an equation for c_ϵ can be derived:

$$L_{ij} - \tfrac{1}{3}\delta_{ij} L_{kk} = 2c_\epsilon N_{ij} \tag{19}$$

where

$$N_{ij} = -\left(\hat{\Delta} K^{\frac{1}{2}} \hat{\bar{S}}_{ij} - \bar{\Delta}\left\langle k_{sgs}^{\frac{1}{2}} \bar{S}_{ij} \right\rangle\right). \tag{20}$$

Since (19) has the same form as (10), c_ϵ can be determined in a similar manner using the least-square method:

$$c_\epsilon = \frac{1}{2}\frac{L_{ij} N_{ij}}{N_{ij} N_{ij}}. \tag{21}$$

A mathematical identity similar to (7) between the dissipation rate resolved at the grid filter level, ε, and the test filter level, E, can be obtained as,

$$F = E - \hat{\varepsilon} = \nu\left(\left\langle \frac{\partial \bar{u}_i}{\partial x_j}\frac{\partial \bar{u}_i}{\partial x_j}\right\rangle - \frac{\partial \hat{\bar{u}}_i}{\partial x_j}\frac{\partial \hat{\bar{u}}_i}{\partial x_j}\right). \tag{22}$$

where,

$$\varepsilon = \nu\left(\overline{\frac{\partial u_i}{\partial x_j}\frac{\partial u_i}{\partial x_j}} - \frac{\partial \bar{u}_i}{\partial x_j}\frac{\partial \bar{u}_i}{\partial x_j}\right) \tag{23}$$

$$E = \nu\left(\left\langle \overline{\frac{\partial u_i}{\partial x_j}\frac{\partial u_i}{\partial x_j}}\right\rangle - \frac{\partial \hat{\bar{u}}_i}{\partial x_j}\frac{\partial \hat{\bar{u}}_i}{\partial x_j}\right) \tag{24}$$

This identity is used to evaluate the dissipation rate model coefficient c_ε by employing the model for ε, (17), and the similar model for E at the test filter level,

$$F = c_\varepsilon\left(\frac{K^{\frac{3}{2}}}{\hat{\Delta}} - \left\langle\frac{k_{sgs}^{\frac{3}{2}}}{\bar{\Delta}}\right\rangle\right) \tag{25}$$

Note that (25) is a scalar equation for a single unknown and, hence, an *exact* value c_ε can be obtained without applying any approximation.

In this type of dynamic formulation, Germano *et al.*'s mathematical identity and its variant (22)) are still adopted. Hence, the mathematical inconsistent derivation and the ill-conditioning problem remain. The advantage of this model is that by introducing the k-equation SGS model as a basic model for the dynamic formulation the prolonged presence of negative model coefficient (i.e., c_ε) is no longer the source of numerical instability. Unfortunately, however, this formulation does generate another problem by introducing the identity (22). That is, the equation (25) for c_ε has the unphysical property of vanishing at high Reynolds numbers. This is due to the fact that the effective viscosity for E in (24) is not the same as the molecular viscosity for ε in (23). However, since E is the dissipation resolved at a scale larger than the scale at which ε is resolved, the effective viscosity for E should include the energy transfer (to the smaller scale) at that larger scale. The scale separation between E and ε increases as Reynolds number increases. Thus, as Reynolds number increases, the modeled expression for E, (24), becomes worse, resulting in poor prediction of the coefficient c_ε and, hence, the actual dissipation E. To resolve this problem, the molecular viscosity in (24) should be replaced by the effective viscosity for E which is larger than the molecular viscosity. However, deriving an expression for the effective viscosity is not feasible due to lack of information on the scale where the test-filter-level SGS kinetic energy is dissipated.

2.3 Localized Dynamic k-Equation Subgrid-Scale (LDKSGS) Model

Recently, Ghosal *et al.* (1995) developed the dynamic localization model based on the SGS kinetic energy, DLM(k), which is applicable to inhomogeneous flows. This model introduces a variational formulation to rigorously derive integral equations for the model coefficient as a function of position and time and is mathematically consistent. Also, by solving the integral equations iteratively, the numerical instability resulted from the ill-conditioning problem was effectively prevented (note that,

since this model use the SGS kinetic energy equation as a base model, the prolonged presence of negative model coefficient is not a source for numerical instability). However, this was achieved at an additional price (Carati et al. (1995) reported that DLM(k) required 67% more CPU time than the standard Smagorinsky's model while the conventional spatial-averaged dynamic model spent 4% more CPU time) due to the complicated and expensive procedure required to solve two more integral equations iteratively. This model has been tested in isotropic turbulence and in the flow over a backward-facing step and demonstrated its capability by showing a good agreement with experiments for both cases.

In this paper, we focus on the Kim and Menon's (1995) localized dynamic model which is a simple, mathematically-consistent and numerically-stable formulation. Before describing this model, some characteristic scales and flow properties at the grid and test filter level needs to be defined:

	Grid filter level		Test filter level		
	Dissipation range	Production range	Dissipation range		Production range
Characteristic length scale	Not available	$\overline{\Delta}$	Not available	Not available	$\hat{\Delta} = 2\overline{\Delta}$
Energy level	$\overline{u_i u_i}$	$\overline{\bar{u}_i \bar{u}_i}$	$\langle \overline{u_i u_i} \rangle$	$\langle \overline{\bar{u}_i \bar{u}_i} \rangle$	$\hat{\bar{u}}_i \hat{\bar{u}}_i$
Stress tensor	$\overline{u_i u_j}$	$\overline{\bar{u}_i \bar{u}_j}$	$\langle \overline{u_i u_j} \rangle$	$\langle \overline{\bar{u}_i \bar{u}_j} \rangle$	$\hat{\bar{u}}_i \hat{\bar{u}}_j$
Dissipation rate	$\overline{\frac{\partial u_i}{\partial x_j}\frac{\partial u_i}{\partial x_j}}$	$\frac{\partial \bar{u}_i}{\partial x_j}\frac{\partial \bar{u}_i}{\partial x_j}$	$\left\langle \overline{\frac{\partial u_i}{\partial x_j}\frac{\partial u_i}{\partial x_j}} \right\rangle$	$\left\langle \frac{\partial \bar{u}_i}{\partial x_j}\frac{\partial \bar{u}_i}{\partial x_j} \right\rangle$	$\frac{\partial \hat{\bar{u}}_i}{\partial x_j}\frac{\partial \hat{\bar{u}}_i}{\partial x_j}$
Strain rate tensor	Not available	$\bar{S}_{ij}$	Not available	Not available	$\hat{\bar{S}}_{ij}$
Effective viscosity	ν		ν	$\nu + \nu_T$	

The following discussion will attempt to demonstrate the new model using reasoning based in physical space (rather than in spectral space). At the grid filter level, there are two energy levels characterized by $\overline{u_i u_i}$ and $\overline{\bar{u}_i \bar{u}_i}$ (the factor ½ is neglected in the following discussion for brevity). The SGS kinetic energy k_{sgs} is then determined by the difference between these two energy levels, i.e., $2k_{sgs} = \overline{u_i u_i} - \overline{\bar{u}_i \bar{u}_i}$. Since the energy $\overline{\bar{u}_i \bar{u}_i}$ is resolved at the grid filter level, the only possible length scale characterizing this energy level is the grid resolution $\overline{\Delta}$. However, the characteristic length scale (say l^*) for the energy level $\overline{u_i u_i}$ is unknown. Since $\overline{u_i u_i} > \overline{\bar{u}_i \bar{u}_i}$, it can be deduced that the characteristic length scale for $\overline{u_i u_i}$ lies in the unresolved range of scales (i.e., $l^* < \overline{\Delta}$). It is clear that the production of SGS kinetic energy is characterized by the larger length scale than the dissipation of k_{sgs}. Hence, $\overline{\Delta}$ is related to the production mechanism of SGS kinetic energy while l^* is related to the dissipation mechanism. The separation between the scales where SGS kinetic energy is produced and where it is dissipated explains why the model for $\varepsilon \propto k_{sgs}^{3/2} / \overline{\Delta}$ is somewhat poor (i.e., the dissipation model has some scale gap between exact and modeled terms by using $\overline{\Delta}$ as a length scale). To properly model the production and the dissipation of SGS kinetic energy, it is necessary to have additional information on the energy transfers at these two length scales. However the information on the energy transfer characterized by the smaller scale (e.g., dissipation by the molecular viscosity) is not available. Therefore an additional assumption (similar to that used in the Reynolds-averaged Navier-Stokes computations) that the energy transfer which occurs at the smaller scale is essentially controlled by the energy transfer at the larger

scale and the energy determined by both energy transfers (e.g. k_{sgs}) is required. Finally, the length scale and strain rate tensor (to parameterize the energy transfer) of the larger scale and the energy determined by both energy transfers are sufficient to model not only the production rate of the SGS kinetic energy (or the SGS stress tensor on which the SGS kinetic energy production mechanism depends, e.g., the production rate of k_{sgs}, $\equiv -\tau_{ij}\overline{S}_{ij}$) but also the dissipation rate.

The definitions and relations employed at the grid filter level can be extended to the test filter level as long as the scales are defined in a similar manner. The energy level $\hat{\overline{u}}_i\hat{\overline{u}}_i$ is resolved at the test filter level and characterized by $\hat{\Delta}=2\overline{\Delta}$ whereas the characteristic length scale (say l^{**}) for the energy $\langle\overline{u_iu_i}\rangle$ is unknown, and again $\langle\overline{u_iu_i}\rangle > \hat{\overline{u}}_i\hat{\overline{u}}_i$ and $l^{**} < 2\overline{\Delta}$. However, at the test filter level, an additional scale can be defined. As the SGS kinetic energy, $2k_{sgs}=\overline{u_iu_i}-\overline{u}_i\overline{u}_i$, is obtained at the grid filter level by taking grid filtering to the total turbulent energy, u_iu_i, the similarly defined energy at the test filter level, $\langle\overline{u}_i\overline{u}_i\rangle-\hat{\overline{u}}_i\hat{\overline{u}}_i$, is obtained by taking test filtering to $\overline{u}_i\overline{u}_i$. This energy is dissipated at the scale characterized by the energy level $\langle\overline{u}_i\overline{u}_i\rangle$ while produced at the characteristic length scale $\hat{\Delta}=2\overline{\Delta}$ which is corresponding to the energy level $\hat{\overline{u}}_i\hat{\overline{u}}_i$ since $\langle\overline{u}_i\overline{u}_i\rangle > \hat{\overline{u}}_i\hat{\overline{u}}_i$. However, since this dissipative length scale lies in the resolved range of scales, the energy is dissipated due to the eddy viscosity as well as the molecular viscosity. Therefore, the effective viscosity is $(\nu+\nu_T)$.

Using the assumption and the parameters defined above, we obtain three different SGS stress tensors and dissipation rates, respectively, one at the grid filter level and the other two at the test filter level:

SGS stress tensor at the grid filter level,

$$\begin{aligned}\tau_{ij} &= \overline{u_iu_j}-\overline{u}_i\overline{u}_j \\ &= -2c_e\overline{\Delta}\left[\tfrac{1}{2}\left(\overline{u_iu_i}-\overline{u}_i\overline{u}_i\right)\right]^{\frac{1}{2}}\overline{S}_{ij}+\tfrac{2}{3}\delta_{ij}\left[\tfrac{1}{2}\left(\overline{u_iu_i}-\overline{u}_i\overline{u}_i\right)\right]\end{aligned} \tag{26a}$$

SGS stress tensors at the test filter level,

$$\begin{aligned}T_{ij} &= \langle\overline{u_iu_j}\rangle-\hat{\overline{u}}_i\hat{\overline{u}}_j \\ &= -2c_e\hat{\Delta}\left[\tfrac{1}{2}\left(\langle\overline{u_iu_i}\rangle-\hat{\overline{u}}_i\hat{\overline{u}}_i\right)\right]^{\frac{1}{2}}\hat{S}_{ij}+\tfrac{2}{3}\delta_{ij}\left[\tfrac{1}{2}\left(\langle\overline{u_iu_i}\rangle-\hat{\overline{u}}_i\hat{\overline{u}}_i\right)\right]\end{aligned} \tag{26b}$$

$$\begin{aligned}t_{ij} &= \langle\overline{u}_i\overline{u}_j\rangle-\hat{\overline{u}}_i\hat{\overline{u}}_j \\ &= -2c_e\hat{\Delta}\left[\tfrac{1}{2}\left(\langle\overline{u}_i\overline{u}_i\rangle-\hat{\overline{u}}_i\hat{\overline{u}}_i\right)\right]^{\frac{1}{2}}\hat{S}_{ij}+\tfrac{2}{3}\delta_{ij}\left[\tfrac{1}{2}\left(\langle\overline{u}_i\overline{u}_i\rangle-\hat{\overline{u}}_i\hat{\overline{u}}_i\right)\right]\end{aligned} \tag{26c}$$

dissipation rate at the grid filter level,

$$\begin{aligned}\varepsilon &= \nu\left(\overline{\frac{\partial u_i}{\partial x_j}\frac{\partial u_i}{\partial x_j}}-\frac{\partial\overline{u}_i}{\partial x_j}\frac{\partial\overline{u}_i}{\partial x_j}\right) \\ &= c_e\left[\tfrac{1}{2}\left(\overline{u_iu_i}-\overline{u}_i\overline{u}_i\right)\right]^{\frac{3}{2}}/\overline{\Delta}\end{aligned} \tag{27a}$$

dissipation rates at the test filter level,

$$E = \nu\left(\left\langle\overline{\frac{\partial u_i}{\partial x_j}\frac{\partial u_i}{\partial x_j}}\right\rangle - \frac{\partial\hat{\bar{u}}_i}{\partial x_j}\frac{\partial\hat{\bar{u}}_i}{\partial x_j}\right) = c_e\left[\tfrac{1}{2}\left(\langle\overline{u_iu_i}\rangle - \hat{\bar{u}}_i\hat{\bar{u}}_i\right)\right]^{\frac{3}{2}}/\hat{\Delta} \tag{27b}$$

$$e = (\nu+\nu_T)\left(\left\langle\frac{\partial\bar{u}_i}{\partial x_j}\frac{\partial\bar{u}_i}{\partial x_j}\right\rangle - \frac{\partial\hat{\bar{u}}_i}{\partial x_j}\frac{\partial\hat{\bar{u}}_i}{\partial x_j}\right) = c_e\left[\tfrac{1}{2}\left(\langle\bar{u}_i\bar{u}_i\rangle - \hat{\bar{u}}_i\hat{\bar{u}}_i\right)\right]^{\frac{3}{2}}/\hat{\Delta}. \tag{27c}$$

As long as both grid and test filter levels are located in the range where the similarity assumption is valid, c_t and c_e in (26) and (27) remain the same. Note that (26a) and (27a) represent, respectively, the original SGS stress tensor and the dissipation rate which must be modeled. These two expressions contain two unknown model coefficients. Previously (see section 2.2) the expressions for T_{ij} and E, (26b) and (27b), were adopted to dynamically determine these unknowns. However this procedure introduced additional unknowns, $\langle\overline{u_iu_j}\rangle$ and $\left\langle\overline{\frac{\partial u_i}{\partial x_j}\frac{\partial u_i}{\partial x_j}}\right\rangle$. Therefore, to close the model, the other independent relations (e.g. Germano *et al.*'s mathematical identity, (7), and its variant, (22)) were needed. These additionally introduced relations become the source of both the mathematical inconsistency and the ill-conditioning problems. In the Kim and Menon's (1995) model, they adopted the expressions for t_{ij} and e, (26c) and (27c), (which do not contain any additional unknowns) instead of T_{ij} and E, respectively. Therefore, the Germano *et al.*'s mathematical identity and its variant are no longer needed to close the model. Both c_t and c_e can be determined in the same manner as was done earlier for c_v and c_ε (in section 2.2). Thus,

$$c_t = \frac{1}{2}\frac{t_{ij}\sigma_{ij}}{\sigma_{ij}\sigma_{ij}} \tag{28}$$

where

$$\sigma_{ij} = -\hat{\Delta}\left[\tfrac{1}{2}\left(\langle\overline{u_iu_i}\rangle - \hat{\bar{u}}_i\hat{\bar{u}}_i\right)\right]^{\frac{1}{2}}\hat{\bar{S}}_{ij} \tag{29}$$

and,

$$c_e = \frac{(\nu+\nu_T)\left(\left\langle\overline{\frac{\partial u_i}{\partial x_j}\frac{\partial u_i}{\partial x_j}}\right\rangle - \frac{\partial\hat{\bar{u}}_i}{\partial x_j}\frac{\partial\hat{\bar{u}}_i}{\partial x_j}\right)}{\left[\tfrac{1}{2}\left(\langle\overline{u_iu_i}\rangle - \hat{\bar{u}}_i\hat{\bar{u}}_i\right)\right]^{\frac{3}{2}}/\hat{\Delta}}. \tag{30}$$

As shown, mathematically inconsistent procedure is not involved in this dynamic formulation. Furthermore, the denominators of (28) and (30) contain the energy information on the resolved scale which is well defined (note that in (12), (21) and (25), the denominators contain algebraically manipulated parameters, hence the resulting expressions were ill defined). Therefore, the ill-conditioning problem (observed in the dynamic models using the Germano *et al.*'s mathematical identity) is not considered serious here. Furthermore, the expression for c_e, (30), doesn't have the unphysical property of vanishing at high Reynolds numbers unlike (25) since the effective viscosity $(\nu+\nu_T)$ is used instead of just ν. The existence of the similarity between the SGS stress $\overline{u_iu_j} - \bar{u}_i\bar{u}_j$ and the resolved stress $\langle\overline{u_iu_j}\rangle - \hat{\bar{u}}_i\hat{\bar{u}}_j$ is supported by Liu *et al.*'s (1994) analysis of experimental data in the

far field of a round jet at a reasonably high Reynolds number ($Re_\lambda \approx 310$). In their work, a high correlation between the two stress tensors is obtained.

Before applying LDKSGS model to various flow fields of interest, it is worthwhile to examine basic properties of the model from a theoretical point of view. Recently, Vreman *et al.* (1994) argued that SGS models should share some basic properties with the exact SGS stress τ_{ij} to successfully predict this unresolved quantity. They presented three properties of τ_{ij} as a necessary condition that SGS models should fulfill. First, τ_{ij} is a symmetric tensor, therefore, the model of τ_{ij} should be symmetric. Second, the filtered Navier-Stokes equations are Galilean invariant. They should retain this property even after τ_{ij} is replaced by the model. The other property is that τ_{ij} is positive for positive filters (i.e., the filter kernel is positive over the domain applied). Therefore, the model of τ_{ij} is required to be positive as well, if positive filter is employed. Actually, the first requirement is true for all existing SGS models, however, the other two requirements need to be checked especially when a new SGS model is considered. We have proven that the LDKSGS model satisfies the Galilean invariance and the realizability requirements. However, we will briefly mention only about the realizability conditions (the other details will be presented in the final paper).

Using the inequalities given in Vreman *et al.* (1994), two realizability conditions for dynamically determined model coefficient are obtained;

$$\frac{k_{sgs}^{\frac{1}{2}}}{3\Delta\overline{S}_{nn}} \le c_I \le \frac{k_{sgs}^{\frac{1}{2}}}{3\Delta\overline{S}_{ll}}$$

$$-\frac{2}{\sqrt{3}}\frac{k_{sgs}^{\frac{1}{2}}}{\Delta|\overline{S}|} \le c_I \le \frac{2}{\sqrt{3}}\frac{k_{sgs}^{\frac{1}{2}}}{\Delta|\overline{S}|}$$

where $\overline{S}_{nn}$ and $\overline{S}_{ll}$ denote the smallest and the largest diagonal elements of the SGS stress, respectively and $|\overline{S}| = (2\overline{S}_{ij}\overline{S}_{ij})^{1/2}$. $\overline{S}_{nn}$ has negative sign and, hence, the lower bound for the first condition is also negative. The model coefficient c_I should satisfy these conditions for the LDKSGS model to become a realizable model of the SGS stress. Decaying isotropic turbulence is used for the numerical verification of these conditions. It is observed that more than 99.9% (for the 48^3 grid resolution), 99.8% (for the 32^3 grid resolution) and 99.6% (for the 24^3 grid resolution) of the grid points satisfy the both realizability conditions at the same time throughout the whole simulation. Therefore, it can be said that LDKSGS model satisfy the realizability conditions even in strict sense. Ghosal *et al.* reported that the DLM(k) model satisfy the realizability condition in about 95% of the grid points for the simulation of decaying isotropic turbulence using the 48^3 grid resolution. Thus, the DLM(k) is not quite realizable even for the simple isotropic turbulence.

3. Results and Discussion

The LDKSGS model was applied to Taylor-Green vortex flow, decaying and forced isotropic turbulence and temporally evolving mixing layers. These flows are briefly described and only typical results for each flow are presented. More detailed description of each test case and the other results will be given in the final paper.

3.1. Taylor-Green vortex flow

To evaluate the behavior of the dynamic SGS models, one popular approach is to compare the predicted LES results with the results of DNS prediction. However, since DNS require a significant amount of computer resources (both memory and execution time), it can be applied only to a limited low range of Reynolds numbers. This Reynolds number range can be increased by simulating a flow that has spatial symmetries (which are preserved in time as the flow evolves), because the information in a fractional part of the periodic box is sufficient to describe the whole flow field using these symmetries. This idea was exploited by Brachet *et al.* (1983) who simulated a Taylor-Green vortex flow and reduced the necessary memory by 1/64 compared with that required for a general non-symmetric periodic flow. In this work, simulation in the so-called impermeable box ($0 \le x,y,z \le \pi$) of the Taylor-Green vortex flow is carried out. The flow field develops from the initial condition:

$$u = \sin(x)\cos(y)\cos(z)$$
$$v = -\cos(x)\sin(y)\cos(z)$$
$$w = 0$$

At time $t = 0$, the flow is two-dimensional but becomes three-dimensional for all times $t > 0$. This flow is considered a simple flow field in which the generation of small scales and the resulting turbulence can be studied. In this study, an effectively 128^3 DNS in a 2π-box (actually simulated using 64^3 grid points in a π-box) has been carried out. The results were then used to evaluate the LES predictions (obtained using a coarse grid resolution). To evaluate the performance of the SGS models, the time evolution of the velocity-derivative (here, we use $\partial w/\partial z$) skewness S and flatness F factors computed from DNS and LES data are compared. The skewness and flatness factors are defined as follows:

$$S = \frac{\left\langle (\partial w/\partial z)^3 \right\rangle}{\left\langle (\partial w/\partial z)^2 \right\rangle^{\frac{3}{2}}}$$

$$F = \frac{\left\langle (\partial w/\partial z)^4 \right\rangle}{\left\langle (\partial w/\partial z)^2 \right\rangle^2}$$

Note that, here $\langle \cdot \rangle$ denote ensemble averaging instead of test filtering. Figure 1 shows the time evolution of the velocity derivative flatness computed from the filtered 128^3 DNS and the 32^3 LES. This figure clearly demonstrates the better prediction of the LDKSGS model than the other dynamic models tested.

3.2. Decaying isotropic turbulence

The experiment of decaying isotropic turbulence of Comte-Bellot and Corsin (1971) is simulated to demonstrate the capability of LDKSGS model in predicting the decay of the turbulent energy. Another reason of this test is to compare the results with those of Ghosal *et al.*'s DLM(k) (1993; 1995) which is the only existing localized dynamic model formulated without employing the *ad hoc* procedure. They simulated this experiment using 32^3 and 48^3 grid resolutions. In predicting the energy decaying rate, a good agreement with the experimental data was obtained using a 48^3 grid resolution (see Figure 1 in Ghosal *et al.*, 1995), however, relatively poor results were obtained using a 32^3 grid resolution (see Figure 1 in Ghosal *et al.*, 1993). This made them conclude that 48^3 grid points is the smallest possible resolution for LES since the 32^3 grid resolution is not fully consistent with the basic assumption of LES

that the resolved scales carry most of the energy. To investigate this issue, we computed the resolved energy at each grid resolution by numerically integrating the spectrum given by Comte-Bellot and Corsin(1971) between wavenumbers zero to the maximum wavenumber represented in the grid resolution:

Grid resolution	512^3	384^3	256^3	192^3	128^3	96^3	64^3	48^3	32^3	24^3	16^3	12^3	8^3
Resolved energy (%)	99.8	99.5	98.4	96.6	92.2	87.3	78.3	70.3	59.3	49.7	35.1	24.4	10.5

As shown, 32^3 and 48^3 grid resolutions are resolving not most of but a close amount (59.3% and 70.3%) of the energy. Strictly speaking, both resolutions are not fully consistent with the basic assumption of LES. They may lie in the range of very large eddy simulations (VLES) where much of the turbulent energy lies in the unresolved scales and model quantity becomes much more important. Therefore, the simulation of this experiment especially using the grid resolution coarser than 48^3 (i.e., the subgrid scales carry more than 30% of total turbulent kinetic energy) is a good test case in which the quality of the SGS model can be measured. For this purpose, three grid resolutions, 48^3, 32^3 and 24^3, are used for large eddy simulations implemented here. Figure 2 shows the decay of the resolved turbulent kinetic energy computed using the LDKSGS model at three grid resolutions, 48^3, 32^3 and 24^3. The results are compared with the predictions of volume-averaged DASGS model at the 48^3 grid resolution and the experimental data of Comte-Bellot and Corsin (1971). The predictions of both models are in good agreement with the experiment. As well known, the decay of the turbulent energy satisfy the power law, $E \sim (t^*)^{\alpha}$, in the asymptotic self-similar regime. The experimental data roughly confirms the existence of the power law by lying on a straight line on a log-log plot even though a limited number (three) of data raises some uncertainty. The decay exponent α is estimated by a least-square fit to each data as follows,

Grid resolution	Experiment	LDKSGS	DLM(k)	DASGS
48^3	-1.20	-1.17	-1.17	-1.20
32^3	-1.16	-1.13		
24^3	-1.12	-1.09		

Here, the value of α predicted by DLM(k) is used as given in Carati *et al.* (1995). These results confirm the agreement between the predictions of LES and the experiment. More importantly, the results of LDKSGS model at all three grid resolution used (even for 24^3 grid resolution where about a half of the turbulent kinetic energy is not resolved) show consistency in predicting the energy decay. This property of the model is a fascinating feature especially when the model is applied to complex and high Reynolds number flows where a lot of the turbulent energy lies in the unresolved scales.

3.3 Forced isotropic turbulence

A statistically stationary isotropic turbulence is simulated using a 32^3 grid resolution. The main purpose of this simulation is to show whether a low resolution LES using the LDKSGS model can reproduce the statistics of the large scale structures of a realistic, high Reynolds number turbulent field. The results is compared with the existing high resolution DNS data by Vincent and Meneguizzi (1991) and Jimenez *et al.* (1993).

A statistically stationary turbulent field is obtained by forcing the large scales as was done by Kerr (1985). In this study, the initial value of all Fourier modes with wave number components equal to 0 or 1 is kept fixed. The initial conditions are obtained by generating a random realization of the energy spectrum

$$E(k) = C\frac{k^4}{1+(k/k_0)^{5/3+4}}$$

with $k_0 = 1$ and C is a constant which normalize the initial total energy to be 0.5. Our simulation was run for 21 large-eddy turnover times. To ensure statistical independence, 25 fields were used for statistical analysis (i.e., the time interval between successive fields is almost one large eddy turnover time). In the simulation, an effective Taylor microscale Reynolds number $Re_\lambda = 116$ was achieved (where the *effective* attribute denotes the use of the eddy viscosity obtained from the SGS model in place of the molecular viscosity).

Figure 3 shows the probability distribution of velocity differences, $\delta u(r) = u(x+r) - u(r)$, for various values of r (note that all values of r used here are comparable with the inertial range scales). For generality, δu is normalized so that $\sigma^2 = <\delta u^2> = 1$. The LES results (using the LDKSGS model) clearly show that the continuous distribution changes from a non-Gaussian (which has the wings) to a Gaussian, as r increases. The same behavior of the distribution was observed in the high resolution DNS of Vincent and Meneguizzi (1991). In addition to the basic agreement regarding the development of the non-Gaussian statistics, the LES accurately predicts the probability for each bin. There is an agreement between the two distributions for $r = 0.39$ obtained from the LES and the DNS except for some deviation in the wing region. However, as is well known, the wings of the non-Gaussian distribution develop mainly due to small-scale fluctuations. Therefore, the deviation between the LES and the DNS results in the wings is somewhat natural.

The statistics of velocity and its derivatives are also investigated. While the statistics of velocity are the property of the large scales which is mostly resolved in LES, the statistics of velocity derivative are the property of the dissipation range scales which is not resolved by LES. Therefore, the direct comparison of LES and DNS using the statistics of velocity derivative may be meaningless. A more useful comparison can be achieved by filtering the DNS field down to the same resolution as LES. For the same grid resolution and flow conditions, the statistics of the LES and the filtered DNS should match well. However, the velocity derivative statistics of the filtered DNS data is not available, therefore, the DNS statistics of velocity derivative obtained from the full resolution simulation (shown in the table below) should be used only as a qualitative measure for the LES results. We computed the n-th moments of the velocity and its derivative distributions using

$$S_n = \frac{<x^n>}{<x^2>^{n/2}}$$

The results of this calculation is summarized in the following table,

	$\partial u/\partial x$				$\partial u/\partial y$				u	
	S_3	S_4	S_5	S_6	S_3	S_4	S_5	S_6	S_4	S_6
512^3 DNS	-0.525	6.1	-12.0	125		9.4		370	2.80	12.5
240^3 DNS	-0.5	5.9	-9	90	-0.04	8.0				
64^3 LES	-0.35				0.06	4.5				
32^3 LDKSGS	-0.332	3.59	-3.79	25.5	0.0092	4.90	0.0586	49.5	2.81	12.2
Gaussian	0.0	3.0	0.0	15.0	0.0	3.0	0.0	15.0	3.0	15.0

where the results of 512^3 DNS (Re_λ =168.1), 240^3 DNS (Re_λ =150), and 64^3 LES are obtained from Jimenez *et al.* (1993), Vincent and Meneguizzi (1991), and Briscolini and Santangelo (1994), respectively. 64^3 LES was implemented using Kraichnan's eddy viscosity defined in the spectral space.

3.4 Temporal mixing layers

The LDKSGS model is applied to simulate the temporally evolving turbulent mixing layer. In this simulation, the LDKSGS model response to the evolution of coherent structures is investigated. We adopt the initial conditions used in Comte *et al.* (1991). The basic velocity profile is defined by

$$u_0(y) = U \tanh(2y/\delta_i)$$

where δ_i is the initial vorticity thickness. This unidirectional basic flow is superimposed by the 3-dimensional, of kinetic energy $10^{-4}U^2$, random perturbations whose spectra are broad-banded. For the numerical implementation, periodic boundary conditions are applied in the streamwise and spanwise directions, and, slip-wall boundary conditions in the transverse direction. The computational domain is cubic, with a side length chosen equal to 4 times of the most unstable streamwise wavelength which is predicted by the inviscid linear-stability theory to be $7.07\delta_i$. An initial Reynolds number is $\mathrm{Re} = U\delta_i/\nu = 100$ and the flow is simulated up to $t = 120\delta_i/U$ using a 32^3 grid resolution.

The following sequence of the temporal evolution of the mixing layer was observed. First, the mixing layer shows the roll-up of the spanwise vorticity, resulting in 4 rollers. Subsequently, pairing of these rollers is observed. After final pairing is accomplished, complicated structures of the flow are generated showing a highly 3-dimensional nature. Spanwise vorticity isosurfaces in Figure 4. show the typical sequence of changes in coherent structures. At t=40 (top), two rollers appear as a result of the first pairing. At this instant, coherent structures are in a very ordered form. At t=80 (middle), the flow starts to generate the complicated structures and becomes 3-dimensional. At the last instant of the simulation (bottom) coherent structures become totally 3-dimensional. The dynamically determined model coefficients (shown as contours) are not correlated with the coherent structures at t=40 since the coherent structures are still laminar at that instant. After t=80, as the coherent structures generate 3-dimensional complicated structures, the model coefficient are highly correlated with these turbulent-like structures.

Figure 5. shows a time evolution of the dynamically determined model coefficient. In the actual simulations, the local values of the coefficients were employed. However, to see the behavior of the coefficients more clearly, the volume-averaged values are presented here. The time dependent behavior of the model coefficient confirms the findings shown in Figure 4. During the early stages of evolution, when the mixing layer is highly organized and primarily 2-dimensional, the model coefficients remains very small. When the structures become more 3-dimensional and generate small-scale turbulence (at t=80), the model coefficients increase rapidly.

4. Future work to be included in the final paper

We have demonstrated the capability of the LDKSGS model in predicting the SGS stress more accurately than the other dynamic models tested here. More importantly, this model appeals to have a promising potential for the application to the high Reynolds number flows by behaving quite well in the low-resolution simulations. This issue will be further investigated in the final paper.

Acknowledgments

This work is supported by the Office of Naval Research under Grant No. N00014-93-0342. Computing time was provided by the Numerical Aerodynamic Simulation (NAS) at NASA Ames Research Center and is gratefully acknowledged.

References

Brachet, M. E., Meiron, D. I., Orszag, S. A., Nickel, B. G., Morf, R. H. & Frisch, U. 1983 Small-scale structure of the Taylor Green Vortex. *J. Fluid Mech.* **130**, 411.

Brandt, A. 1981 Guide to multigrid development. In *Lecture Notes in Mathematics* **960**, 220. Springer-Verlag Berlin.

Briscolini, M. & Santangelo, P. 1994 The non-Gaussian statistics of the velocity field in low-resolution large-eddy simulations of homogeneous turbulence. *J. Fluid Mech.* **270**, 199.

Chorin, A. J. 1967 A numerical method for solving incompressible viscous flow problems. *J. Comput. Phys.* **2**,12.

Carati, D., Ghosal, S. & Moin, P. 1995 On the representation of backscatter in dynamic localization models. *Phys. Fluids* **7**, 606.

Comte, P., Fouillet, Y., Gonze, M.-A., Lesieur, M., Metais, O. & Normand, X. 1991 Generation of coherent structures in free shear layers. In *Turbulence and Coherent Structures*, Kluwer Academic Publishers (ed. O. Metais & M. Lesieur), p. 45.

El-Hady, N. M., Zang, T. A. & Piomelli, U. 1994 Application of the dynamic subgrid-scale model to axisymmetric transitional boundary layer at high speed. *Phys. Fluids* **6**, 1299.

Germano, M., Piomelli, U., Moin, P. & Cabot, W. H. 1991 A dynamic subgrid-scale eddy viscosity model. *Phys. Fluids* A **3**, 1760.

Ghosal, S., Lund, T. S. & Moin, P. 1993 A local dynamic model for large eddy simulation. *CTR Annual Research Briefs* 1992, p. 3.

Ghosal, S., Lund, T. S., Moin, P. & Akselvoll, K. 1995 A dynamic localization model for large-eddy simulation of turbulent flows. *J. Fluid Mech.* **289**, 229.

Jimenez, J., Wray, A. A., Saffman, P. S. & Rogallo, R. S. The structure of intense vorticity in isotropic turbulence. *J. Fluid Mech.* **255**, 65.

Kerr, R. M. 1985 Higher order derivative correlations and the alignment of small-scale structures in isotropic numerical turbulence. *J. Fluid Mech.* **153**, 31.

Kim, W.-W. & Menon, S. 1995 A new dynamic one-equation subgrid-scale model for large eddy simulations. *AIAA 33rd Aerospace Sciences Mtg, Reno, NV.*

Lilly, D. K. 1992 A proposed modification of the Germano subgrid-scale closure method. *Phys. Fluids* **4**, 633.

Liu, S., Meneveau, C. & Katz, J. 1994 On the properties of similarity subgrid-scale models as deduced from measurements in a turbulent jet. *J. Fluid Mech.* **275**, 83.

Meneveau, C., Lund, T. S. & Cabot, W. 1994 A Lagrangian dynamic subgrid-scale model of turbulence. *Proc. CTR Summer Program* 1994, p. 271.

Menon, S. & Yeung, P.-K. 1994 Analysis of subgrid models using direct and large-eddy simulations of isotropic turbulence. *Proc. AGARD 74th Fluid Dynamics Symp. on Application of Direct and Large Eddy Simulation to Transition and Turbulence, AGARD-CP-551*, p. 10-1.

Menon, S., Yeung, P.-K. & Kim, W.-W. 1994 Effect of subgrid models on the computed interscale energy transfer in isotropic turbulence. *AIAA 25th Fluid Dynamics Conf. Colorado Springs, CO.*

Moin, P., Squires, K., Cabot, W. & Lee, S. 1991 A dynamic subgrid-scale model for compressible turbulence and scalar transport. *Phys. Fluids* A **3**, 2746.

Piomelli, U. 1993 High Reynolds number calculations using the dynamic subgrid-scale stress model. *Phys. Fluids* A **5**, 1484.

Rai, M. M. & Moin, P. 1991 Direct simulations of turbulent flow using finite-difference schemes. *J. Comput. Phys.* **96**, 15.

Rogallo, R. S. 1981 Numerical experiments in homogeneous turbulence. *NASA Tech. Memo.* 81315.

Rogers, S. E., Kwak, D. & Kiris, C. 1991 Steady and unsteady solutions of the incompressible Navier-Stokes equations. *AIAA J.* **29**, 603.

Schumann, U. 1975 Subgrid scale model for finite difference simulations of turbulent flows in plane channels and annuli. *J. Comput. Phys.* **18**, 376.

Smagorinsky, J. 1963 General circulation experiments with the primitive equations. I. The basic experiment. *Month. Wea. Rev.* **91**, 99.

Speziale, C. G. 1985 Galilean invariance of subgrid-scale stress models in the large-eddy simulation of turbulence. *J. Fluid Mech.* **156**, 55.

Vincent, A. & Meneguzzi, M. 1991 The spatial structure and statistical properties of homogeneous turbulence. *J. Fluid Mech.* **225**, 1.

Vreman, B., Geurts, B. & Kuerten, H. 1994 Realizability conditions for the turbulent stress tensor in large-eddy simulation. *J. Fluid Mech.* **278**, 351.

Yoshizawa, A. 1991 Eddy-viscosity-type subgrid-scale model with a variable Smagorinsky coefficient and its relationship with the one-equation model in Large eddy simulation. *Phys. Fluids* A **3**, 2007.

Zang, Y., Street, R. L. & Koseff, J. R. 1993 A dynamic mixed subgrid-scale model and its application to turbulent recirculating flows. *Phys. Fluids* A **5**, 3186.

FIGURE CAPTIONS

Figure 1. Temporal evolution of velocity derivative flatness computed from 32^3 LES using 3 different SGS models, compared with filtered 128^3 DNS.

Figure 2. Temporal evolution of turbulent kinetic energy in isotropic turbulence resolved at 3 different grid resolutions, compared with experiment by Comte-Bellot and Corsin (1971).

Figure 3. Probability distribution of normalized velocity difference for 5 different scales r, compared with high resolution DNS by Vincent and Meneguizzi (1991).

Figure 4. Spanwise vorticity isosurfaces and dynamically evaluated model coefficient contours computed from 32^3 LES using LDKSGS at t=40 (top), t=80 (middle), and t=120 (bottom).

Figure 5. Temporal evolution of model coefficient computed from 32^3 LES using LDKSGS model.

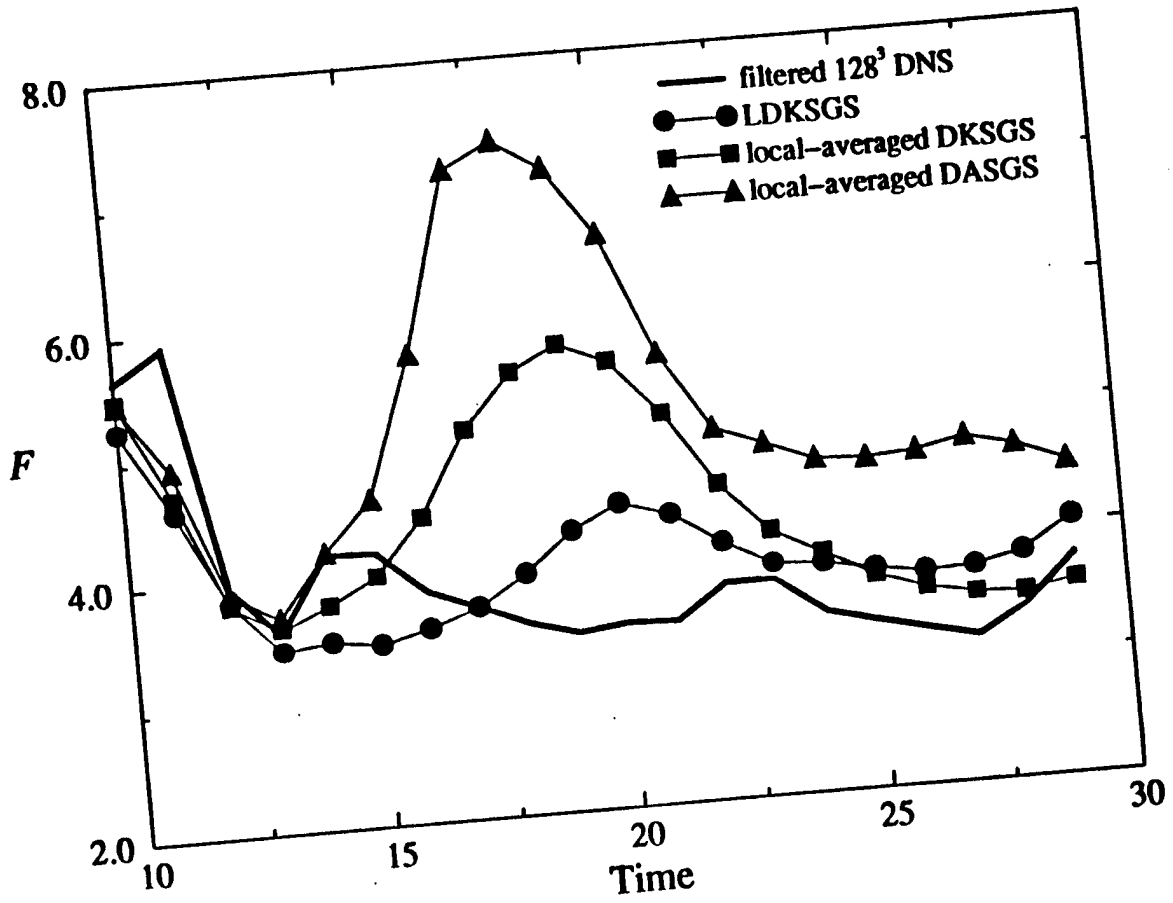
filtered 128³ DNS
LDKSGS
local–averaged DKSGS
local–averaged DASGS
8.0
6.0
4.0
2.0
F
10
15
20
25
30
Time

Figure 1

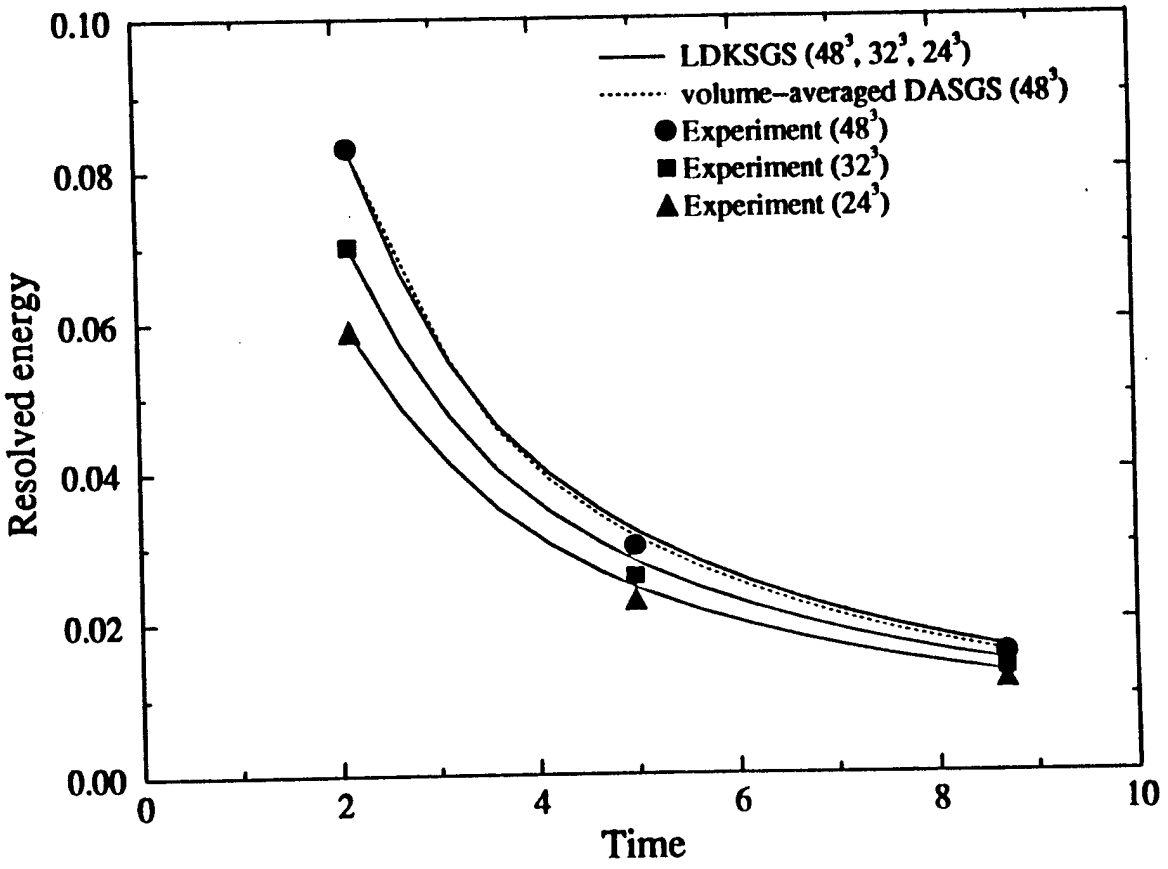
LDKSGS (48^3, 32^3, 24^3)
volume–averaged DASGS (48^3)
Experiment (48^3)
Experiment (32^3)
Experiment (24^3)
Resolved energy
Time
0.00
0.02
0.04
0.06
0.08
0.10
0
2
4
6
8
10

Figure 2.

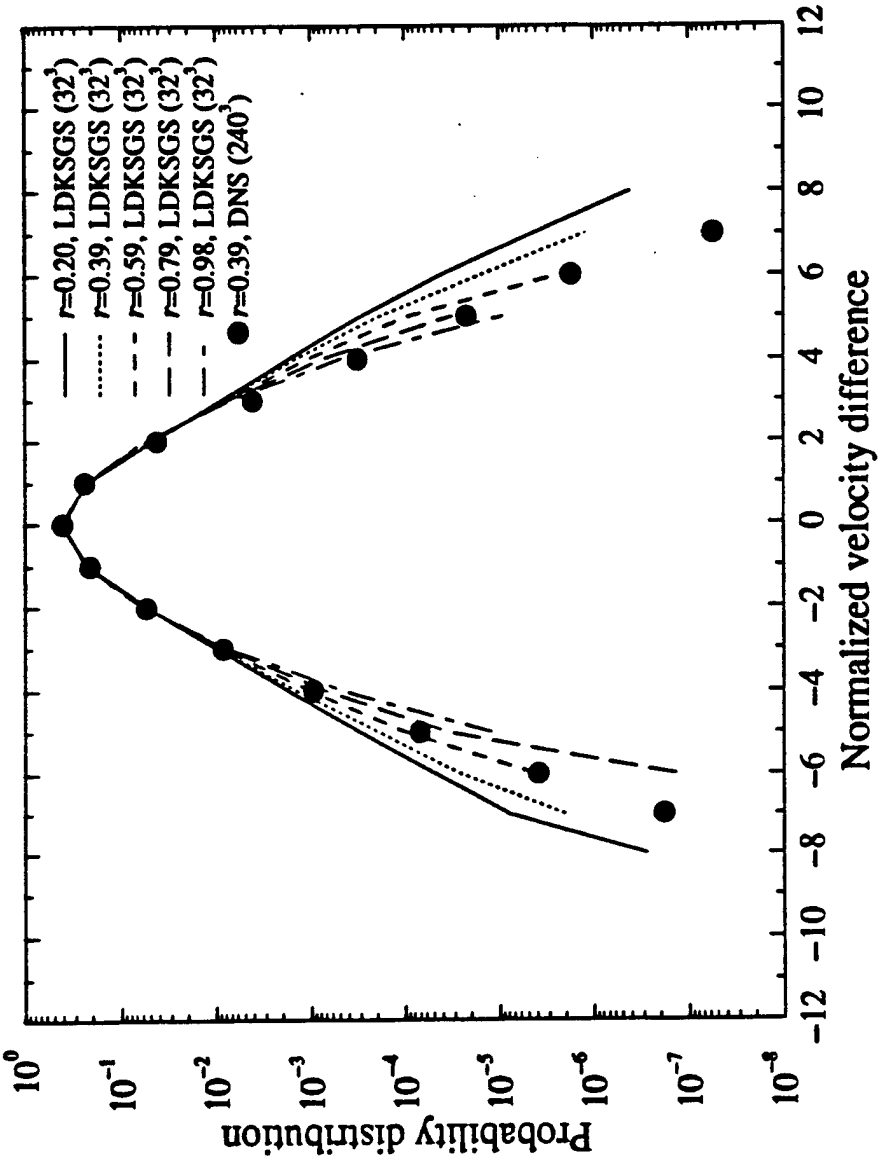
Probability distribution
Normalized velocity difference
r=0.20, LDKSGS (32³)
r=0.39, LDKSGS (32³)
r=0.59, LDKSGS (32³)
r=0.79, LDKSGS (32³)
r=0.98, LDKSGS (32³)
r=0.39, DNS (240³)
10⁰
10⁻¹
10⁻²
10⁻³
10⁻⁴
10⁻⁵
10⁻⁶
10⁻⁷
10⁻⁸
−12 −10 −8 −6 −4 −2 0 2 4 6 8 10 12

Figure 3.

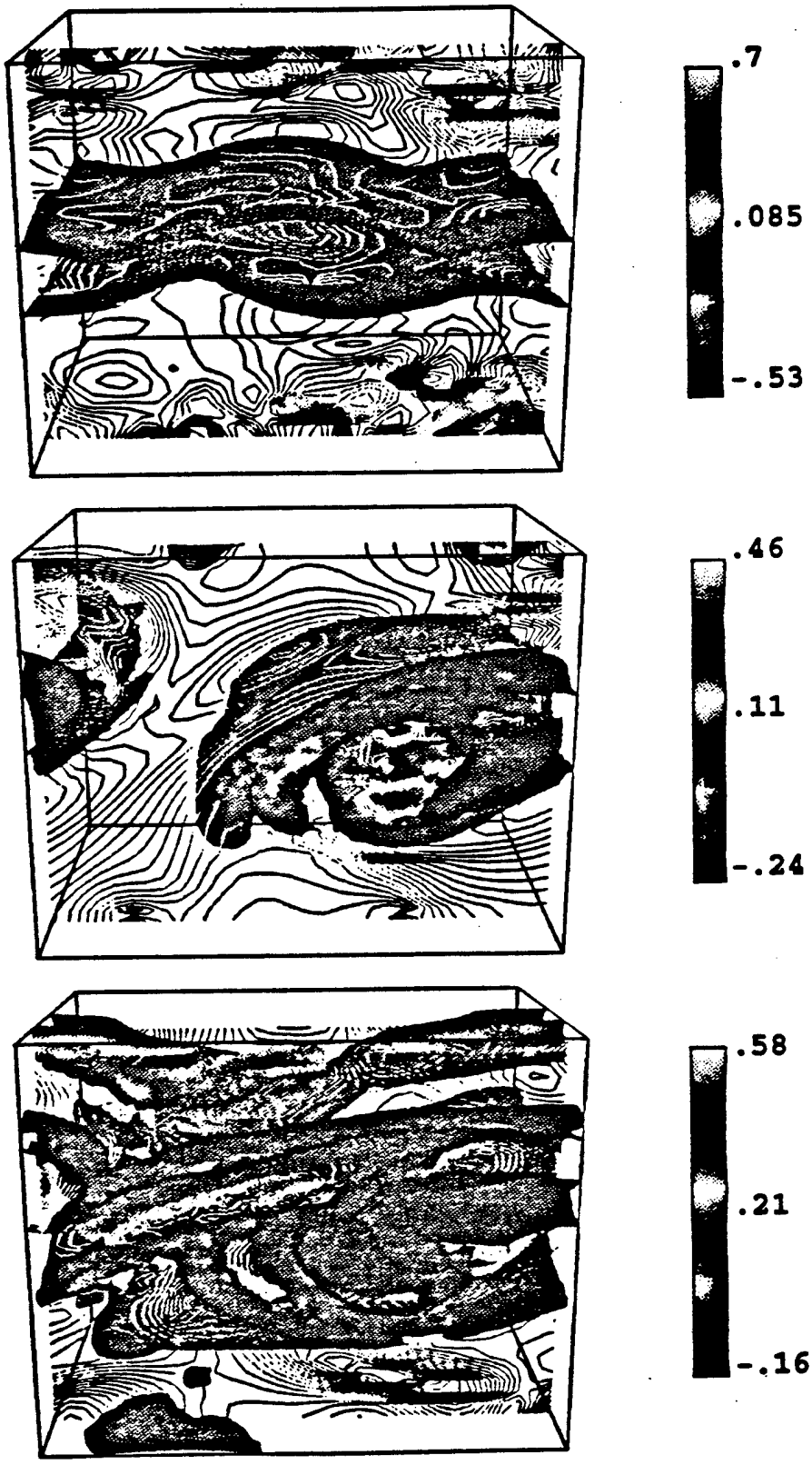

Figure 4.

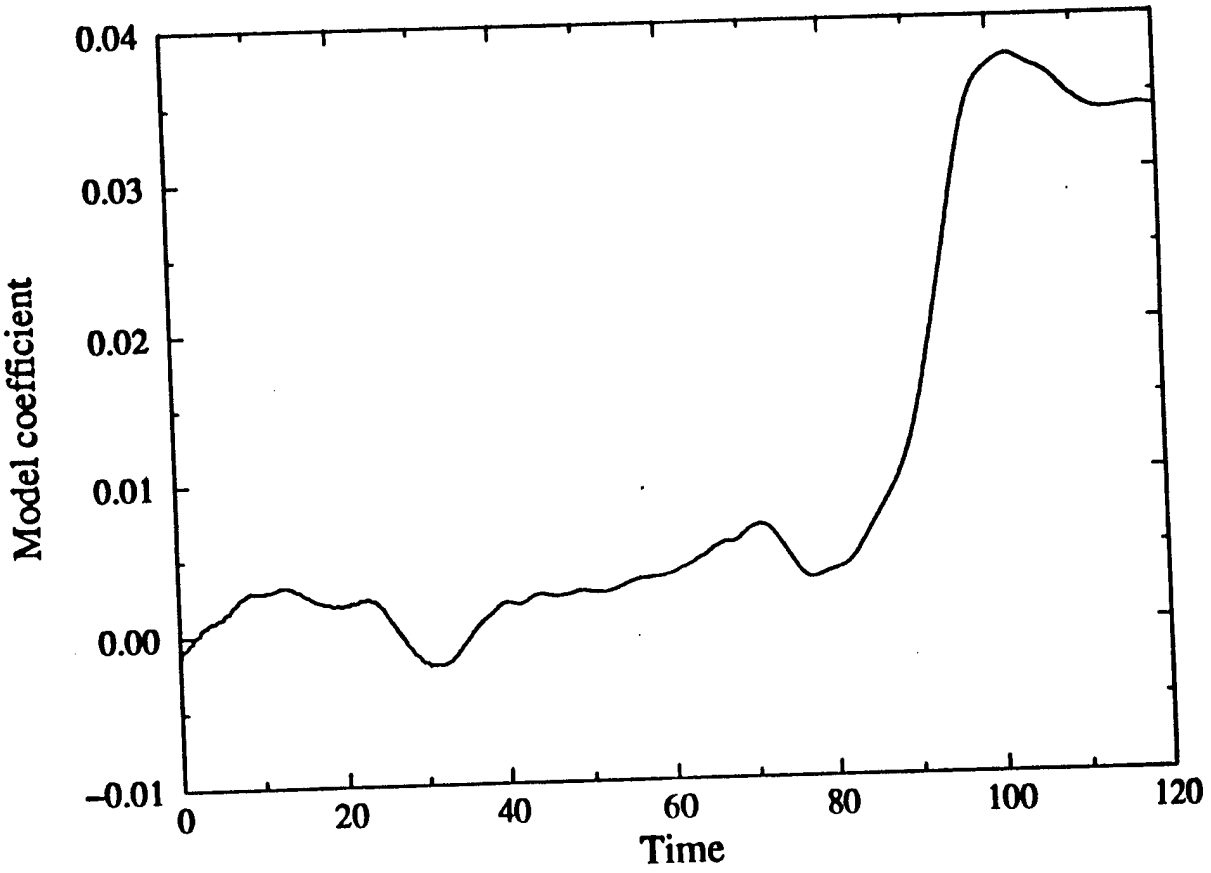
0.04
0.03
0.02
0.01
0.00
−0.01
Model coefficient
0
20
40
60
80
100
120
Time

Figure 5.

EFFECT OF SUBGRID MODELS ON THE COMPUTED INTERSCALE ENERGY TRANSFER IN ISOTROPIC TURBULENCE

S. Menon, P.-K. Yeung and W.-W. Kim
School of Aerospace Engineering
Georgia Institute of Technology
Atlanta, Georgia 30332-0150

(404)-853-9160
menon@falcon.ae.gatech.edu

Submitted to

Computers and Fluids
February 1995

EFFECT OF SUBGRID MODELS ON THE COMPUTED INTERSCALE ENERGY TRANSFER IN ISOTROPIC TURBULENCE

S. Menon, P.-K. Yeung and W.-W. Kim

School of Aerospace Engineering

Georgia Institute of Technology

Atlanta, Georgia

ABSTRACT

Direct and large eddy simulations of forced and decaying isotropic turbulence have been performed to investigate the behavior of subgrid models. Various subgrid models have been analyzed (i.e., Smagorinsky's eddy viscosity model, dynamic eddy viscosity model, dynamic one-equation model for the subgrid kinetic energy and scale-similarity model). *A priori* analysis showed that the subgrid stress and the subgrid energy flux predicted by the scale similarity model, and subgrid kinetic energy model (with fixed coefficients) correlate reasonably well with exact data, while the Smagorinsky's eddy viscosity model showed relatively poor agreement. However, the correlation for the scale similarity model decreased much more rapidly with decrease in grid resolution when compared to the subgrid kinetic energy model. The subgrid models were then used to carry out large-eddy simulations for a range of Reynolds number. It was determined that the dissipation was modeled poorly and that correlations with exact results were quite low for all models where no dynamic procedure was employed. When dynamic evaluation was incorporated, the correlation improved significantly. The dynamic subgrid kinetic energy model showed consistently a higher correlation for a range of Reynolds number when compared to the dynamic eddy viscosity model. These results demonstrate the capabilities of the dynamic one-equation model.

1. INTRODUCTION

Large-eddy simulation (LES) methods are currently being used to simulate a variety of flow problems. For such methods to perform adequately, subgrid models that faithfully represent the effects of the unresolved subgrid scales (SGS) on the resolved motion have to be developed and validated. The capability of the subgrid models can be determined by carrying out LES and comparing the predicted results (typically, ensemble or time-averaged properties) with experimental data. Good agreement would demonstrate the capability and validity of the chosen subgrid model. However, this approach does not provide any means to improve the subgrid model if poor agreement with experimental data occurs. Alternatively, the subgrid model(s) can be evaluated using direct numerical simulation (DNS) data, and then the subgrid model(s) can be used in an LES of the same flow field, by using coarse grids.

Comparison of the LES results with the DNS data can then be used to determine the validity of the model. This approach, however, also has problems. Models validated using low Reynolds number DNS data (for simple flows) invariably show poor agreement with data when used to simulate high Reynolds number, complex flows.

In recent years, studies have identified some inherent limitations of subgrid models currently being employed for LES. For example, it has been shown that the 'constant' in the popular eddy viscosity model of Smagorinsky has to be fine-tuned for every flow of interest. This problem was circumvented recently by using a dynamic procedure [1] which allows a direct evaluation of the constant as a part of the solution. The dynamic model has proven quite versatile, and results show that it can model correctly the behavior of subgrid stresses both near and away from the wall, and has a capability to model backscatter [1,2]. However, even this model has some problems. Namely, the evaluation of the 'constant' can result in numerical problems. Methods to address this limitation have been developed [2-4].

For LES of high Reynolds number flows, the typical grid resolution possible (due to computer resource limitations) can be quite coarse. In this case, a large dynamic range of scales, including 'energy containing' scales of motion, can remain unresolved. It is not clear if eddy viscosity-type subgrid models will be able to model accurately the effects of these unresolved scales. Since a significant amount of turbulent kinetic energy may be present in the subgrid scales, the assumption of balance between the energy production and the dissipation rate (an assumption implicit in the formulation of the eddy viscosity models) may be violated. Furthermore, reverse cascade of energy (the so-called backscatter) from the subgrid scales to the resolved scales could become significant, and anisotropy effects in the unresolved scales may have to be taken into account. Higher order models, such as the one-equation model studied here, may be required to take these features into account.

In this paper, the effects of the form of the chosen subgrid model on the energy transfer process between the resolved and unresolved scales in LES, will be investigated. The results of DNS and LES of forced and decaying isotropic turbulence is analyzed in both physical and spectral space. The goal of this research is to develop methods to analyze subgrid models without using any DNS information. This would enable investigation of the validity and the applicability of subgrid models in more complex flows which cannot be computed using DNS techniques.

2. NUMERICAL METHODS AND SUBGRID MODELS

Two simulation codes have been used in this research. A well-known pseudo-spectral code of Rogallo [5] has been used to obtain high resolution DNS data. However, no LES has been performed using this code. To carry out both LES and DNS, a finite-difference, Navier-Stokes solver, which is fifth-order accurate in space and second-order

accurate in time, is used. The numerical algorithm is based on the artificial compressibility method. To obtain time-accuracy at each time step, pseudo time iterations are carried out using a multigrid technique until the incompressibility condition has been met. The Kolmogorov-scaled energy and dissipation spectra obtained using the finite-difference code, were compared to the results obtained using the psuedo-spectral code. Very good agreement over nearly the entire wavenumber space was obtained [6]. Detailed evaluations of the various statistical quantities (such as the dissipation rate, skewness, etc.) also showed that the physical space code is capable of reproducing statistics very similar to those obtained by the spectral code.

Decaying and forced isotropic turbulence data obtained on both 64^3 and 128^3 grid resolutions have been employed for analysis. For the decaying case, the hydrodynamic field is allowed to evolve until a "realistic", self-similar state has been reached. This developed isotropic state is characterized by Kolmogorov similarity in the high wavenumber energy spectrum, power law decay of energy, and non-Gaussian velocity gradients. The decaying turbulence DNS data used in this paper is approximately at a Taylor-scale Reynolds number Re_λ of 20 (obtained on a 128^3 grid) and 10 (obtained on a 64^3 grid). DNS data at a Re_λ of around 90 obtained (on a 128^3 grid) using stochastic forcing [7], is also used for some analysis.

2.1. Subgrid Modeling in Physical Space

In physical space, the incompressible Navier-Stokes equations are filtered using a spatial filter of characteristic width Δ (typically, the grid resolution) resulting in the filtered LES equations:

$$\frac{\partial \bar{u}_i}{\partial x_i} = 0 \tag{1a}$$

$$\frac{\partial \bar{u}_i}{\partial t} + \bar{u}_j \frac{\partial \bar{u}_i}{\partial x_j} = -\frac{\partial}{\partial x_j}\left[\frac{\bar{p}}{\rho}\delta_{ij} + \tau_{ij}\right] + \nu \nabla^2 \bar{u}_i \tag{1b}$$

where $\bar{u}_i(\mathbf{x}, t)$ is the resolved velocity field, p and ρ are, respectively, the pressure and density, and ν is the kinematic viscosity. Here, the bar over the flow variable indicates the effect of the filtering process. The subgrid scale stress tensor τ_{ij} is defined as: $\tau_{ij} = \overline{u_i u_j} - \bar{u}_i \bar{u}_j$ and must be modeled. It has been shown [8] that proper choice of the filtering process is essential to maintain model consistency. Various types of filtering processes have been studied in the past [8,9] such as, the top hat, the Gaussian, and the Fourier cutoff filters. In the present study, we employ the top hat filter which is considered appropriate for finite-difference methods.

The goal of SGS modeling is to represent the SGS stress τ_{ij} in terms of the resolved field $\bar{u}_i(\mathbf{x}, t)$ in such a manner

that the modeled SGS stresses represent, as much as possible, the exact stresses. In addition, the energy flux to the unresolved scales given by $E(\Delta) = -\tau_{ij}\bar{S}_{ij}$ must also be modeled reasonably well by the subgrid model. These issues will be addressed in this study.

2.1.1. Smagorinsk's Eddy Viscosity Model

The most popular subgrid model is the algebraic eddy viscosity model originally proposed by Smagorinsky:

$$\tau_{ij} - \frac{1}{3}\delta_{ij}\tau_{kk} = -2\nu_t \bar{S}_{ij} \tag{2}$$

where, $\nu_T = C\Delta^2 |S|$ is the subgrid eddy viscosity, C is constant,

$$\bar{S}_{ij} = \frac{1}{2}\left(\frac{\partial \bar{u}_i}{\partial x_j} + \frac{\partial \bar{u}_j}{\partial x_i}\right) \tag{3}$$

is the resolved rate-of-strain tensor, and $|\bar{S}| = |2\bar{S}_{ij}\bar{S}_{ij}|^{1/2}$. As noted above, the 'constant' C has to be adjusted for different flows. For decaying isotropic turbulence, a value of $C = 0.03$ has been suggested by Lilly [10], and is used here.

This model is denoted Model A for subsequent discussions.

2.1.2. Dynamic Eddy Viscosity Model

In the dynamic modeling approach [1], a mathematical identity between the stresses resolved at the grid scale filter Δ and a test filter $<\Delta>$ (typically, $\approx 2\Delta$) is used to determine the model coefficient C as a part of the simulation. Thus, if the application of the test filter on any variable $\bar{\phi}$ is denoted by $<\bar{\phi}>$, it can be shown that:

$$L_{ij} = T_{ij} - <\tau_{ij}> = <\overline{\bar{u}_i\bar{u}_j}> - <\bar{u}_i><\bar{u}_j> \tag{4}$$

Here, $T_{ij} = <\overline{\bar{u}_i\bar{u}_j}> - <\bar{u}_i><\bar{u}_j>$ is defined using the test filter. Assuming that T_{ij} is similar to τ_{ij} results in an expression for T_{ij} as:

$$T_{ij} - \frac{1}{3}\delta_{ij}T_{kk} = -2\nu_T <\bar{\bar{S}}_{ij}> \tag{5}$$

where, $\nu_T = C<\Delta>^2 |<\bar{S}>|$. Combining Eqs. (2), (4) and (5), an equation for C can be obtained:

$$L_{ij} - \frac{1}{3}\delta_{ij}L_{kk} = 2CM_{ij} \tag{6}$$

where

$$M_{ij} = -\left[<\Delta>^2 |<\bar{S}>| <\overline{S_{ij}}> - \Delta^2 <|\bar{S}| \overline{S_{ij}}> \right] \tag{7}$$

Equation (6) is a set of five independant equations for one unknown C. To minimize the error from solving this overdetermined system, Lilly [11] proposed a least square method which yields

$$C = \frac{1}{2} \frac{L_{ij} M_{ij}}{M_{ij} M_{ij}} \tag{8}$$

Studies [12] have shown that the numerical value of C obtained from Eq. (8) can vary widely (and change sign) in the flow field. In addition, the denominator in Eq. (8) can become zero in some places. All these effects can (and do) result in numerical instability. Various methods have been proposed to resolve this problem. Typically, spatial averaging (usually only in the direction of flow homogeneity) is performed for both the numerator and denominator in Eq. (8). For homogeneous, isotropic turbulence averaging can be implemented over the entire computational domain. Thus, in the present implementation of the dynamic model, C is a function of time only.

This model is denoted Model B for subsequent discussions.

2.1.3. Subgrid Kinetic Energy Model

A one-equation model for the subgrid kinetic energy $k_{sgs} = \frac{1}{2}\left[\overline{u_i^2} - \bar{u}_i^2 \right]$, in the following form:

$$\frac{\partial k_{sgs}}{\partial t} + \bar{u}_i \frac{\partial k_{sgs}}{\partial x_i} = -\tau_{ij} \frac{\partial \bar{u}_i}{\partial x_j} - C_\varepsilon \frac{k_{sgs}^{3/2}}{\Delta} + \frac{\partial}{\partial x_i} \left[\frac{\nu_k}{\sigma_k} \frac{\partial k_{sgs}}{\partial x_i} \right] \tag{9}$$

has also been studied. Here, the three terms on the right-hand side of Eq. (9) represent, respectively, production, dissipation, and transport of the subgrid kinetic energy. The subgrid stresses τ_{ij} are modeled in terms of the SGS eddy viscosity ν_k as:

$$\tau_{ij} = -2\nu_k \bar{S}_{ij} + \frac{2}{3} k_{sgs} \delta_{ij} \tag{10}$$

where the SGS eddy viscosity is $\nu_k = C_k \sqrt{k_{sgs}}\, \Delta$. The constants are chosen, based on earlier study [13], to be $C_k = 0.09$, $C_\varepsilon = 0.916$ and $\sigma_k = 1.0$.

An important feature of this model is that no assumption of local balance between the subgrid scale energy production and dissipation rate has been made. Therefore, it is expected that this model would be much better than the algebraic eddy viscosity model in regions where local balance is violated. The results of this study (described

below) clearly show this capability.

To investigate the behavior of the k_{sgs} model, the exact production, the dissipation, and the transport terms were computed by filtering the DNS data, and then correlated with the model terms in Eq. (9). The results (not shown) showed that the transport and the production terms in the model equation were correlated quite well with the exact terms (with a correlation greater that 0.6). However, the dissipation term was poorly correlated. This result agreed with the earlier observation that the dissipation model needs further improvement. This has been addressed using a dynamic procedure, which is outlined below.

This model is denoted Model C for subsequent discussions.

2.1.4. Dynamic Subgrid Kinetic Energy Model

The dynamic approach can be used to obtain appropriate values of the coefficients C_k and C_ε. To implement this method, the kinetic energy at the test filter level is obtained by using the trace of Eq. (4): $K = L_{ii}/2 + \langle k \rangle$. Using a procedure similar to that outlined in Section 2.1.2, equations for both C_k and C_ε can be derived:

$$L_{ij} - \frac{1}{3}\delta_{ij}L_{kk} = -C_k\left[\langle\Delta\rangle K^{1/2}\langle\overline{S_{ij}}\rangle - \Delta\langle k^{1/2}\overline{S_{ij}}\rangle\right] \tag{11}$$

$$\nu\left[\left\langle\frac{\partial\overline{u_i}}{\partial x_j}\frac{\partial\overline{u_i}}{\partial x_j}\right\rangle - \frac{\partial\langle\overline{u_i}\rangle}{\partial x_j}\frac{\partial\langle\overline{u_i}\rangle}{\partial x_j}\right] = C_\varepsilon\left[\frac{K^{3/2}}{\langle\Delta\rangle} - \frac{\langle k^{3/2}\rangle}{\Delta}\right] \tag{12}$$

Note that, Eq. (12) is a scalar equation for a single unknown and, thus, the exact value of C_ε can be obtained without applying the least square method.

This model is denoted Model D for subsequent discussion.

2.1.5. Stochastic Backscatter Model

If subgrid scales contain energy-containing eddies, then backscatter of energy from the subgrid scales to the resolved scales may occur. Analysis of DNS data has shown that backscatter occurs over a significant portion of the grid points [14]. Furthermore, earlier studies [15,16] have shown that the forward scatter (by the eddy viscosity term) and the backscatter are two distinct processes and, therefore, the two effects must be modeled separately. Using the results of Chasnov [15], a phenomenological model for stochastic backscatter was derived earlier [17] by assuming that the backscatter effect can be modeled by a random force which satisfies certain constraints. The

resulting form of the backscatter contribution to the subgrid stress model can be written as:

$$\tau_{ij}^{bs} = C_{bs} \prod \frac{\Delta^2}{\sqrt{\Delta t}} |\bar{S}| \bar{S}_{ij}^{1/2} \tag{13}$$

Here, C_{bs} is a constant of order unity (here, $C_{bs} = 0.1$), Δt is the time step of the LES, and $\prod$ is a random number with zero mean and unit variance. This term, Eq. (13), can be added to any model for the forward scatter, i.e., Eq. (2) or (10). In the present study, the backscatter effects were investigated in conjunction with the k_{sgs} model (Model C) given in Section 2.1.3.

This combined model is denoted Model E for subsequent discussions.

2.1.6. Scale Similarity Model

A scale similarity model was recently proposed by Liu et al.[9] based on *a priori* analysis of high Re_λ (= 310) experimental data for a turbulent jet. This model is of the form:

$$\tau_{ij} = C_L f(I_{LS}) L_{ij} \tag{14}$$

where the stress $L_{ij} = <\bar{u}_i \bar{u}_j> - <\bar{u}_i><\bar{u}_j>$ can be computed entirely from the resolved velocity field. Also, $f(I_{LS})$ is a scalar function defined below. The constant C_L was determined to be 0.45 using the high Re_λ data [9]. This model is similar to the scale similarity model proposed earlier by Bardina [18], and it can be shown that the energy flux to the subgrid scale $E_L = -L_{ij}\bar{S}_{ij}$ will exhibit both positive (forward scatter) and negative (backscatter) in the flow. However, it has been noted earlier [9,18] and in the present study, that this backscatter (which may not be real) can result in numerical instability. Hence, to control the backscatter, a scalar function $f(I_{LS})$ is defined in terms of I_{LS}, a dimensionless invariant:

$$I_{LS} = -\frac{L_{mn}\bar{S}_{mn}}{\sqrt{L_{ij}L_{ij}}\sqrt{\bar{S}_{ij}\bar{S}_{ij}}} \tag{15}$$

Here, I_{LS} represents the alignment between L_{ij} and $\bar{S}_{ij}$. Various forms of the scalar function $f(I_{LS})$ were proposed by Liu et al.[9], but their validity in LES has not been investigated. Furthermore, the experimental data was a two-dimensional slice of the flow field and Liu et al.[9] had to make some assumptions to determine the contribution from the third dimension. In the present study, *a priori* analysis of DNS results and LES results, was carried out to evaluate this model. Various forms of backscatter control were also studied. However, for LES, $f(I_{LS})$ was chosen following the earlier suggestion [9] such that $f(I_{LS}) = \left[1 - \exp(-10 I_{LS}^2)\right]$, if $I_{LS} \geq 0$, and $f(I_{LS}) = 0$, if $I_{LS} < 0$.

For subsequent discussion, the scale-similarity model without backscatter control (i.e. with $f(I_{LS}) = 1$) is denoted **Model F1** and with backscatter control is denoted **Model F2**.

During the study of high Reynolds number (e.g., $Re_\lambda = 100$) decaying turbulence, it was observed that the LES with the Model F2 would become numerically unstable. Therefore, some simulations were carried out using a mixed model which involved combining the eddy viscosity model, Model A with Model F2. This type of model is similar to the mixed model proposed earlier [18].

The mixed scale similarity model is denoted Model F3 for subsequent discussion.

2.2. Subgrid Modeling in Fourier Space

The Fourier space representation of the Navier-Stokes equations may be written as:

$$\left[\frac{\partial}{\partial t} + \nu k^2\right] u_n(\mathbf{k}) = N_n(\mathbf{k}) \tag{16}$$

where $u_n(\mathbf{k})$ is the velocity field in the Fourier space at a wavenumber mode $\mathbf{k}$ (of magnitude k), and $N_n(\mathbf{k})$ is the nonlinear term which includes the effects of advection, pressure and incompressibility [6].

In Fourier space, the various terms in the above equation can be decomposed into "resolved" and "subgrid" components in the wavenumber space by introducing a wavenumber cutoff at k_c. For example, the nonlinear term may be decomposed into [6,19]:

$$N_n(\mathbf{k}) = N_n(\mathbf{k}\,|\,k_c) + N_n^s(\mathbf{k}\,|\,k_c) \quad (k \le k_c) \tag{17}$$

The resolved nonlinear term, $N_n(\mathbf{k}\,|\,k_c)$, represents contributions from those triad interactions that couple a resolved mode $k \le k_c$ to two other resolved modes p and $k-p$ (i.e., with both $\mathbf{p}$ and $\mathbf{k}-\mathbf{p}$ in the resolved range below k_c). On the other hand, the rest of the triad interactions, which couple the resolved modes to subgrid modes (with at least one of $\mathbf{p}$ and $\mathbf{k}-\mathbf{p}$ in the subgrid range $k > k_c$), are represented by the subgrid nonlinear term, $N_n^s(\mathbf{k}\,|\,k_c)$.

Energy transfer between different scales is represented by triadic interactions. The total (rate of) energy transfer to a Fourier mode $\mathbf{k}$, due to its interactions with the subgrid scales, is given by $T^s(\mathbf{k}\,|\,k_c) = \mathrm{Re}\left[u_n^*(\mathbf{k}) N_n(\mathbf{k}\,|\,k_c)\right]$, where the asterisk denotes complex conjugate and Re indicates the real part. The subgrid transfer spectrum function is then given by:

$$T^s(k\,|\,k_c) = \sum_{k-\frac{\Delta k}{2} \le |k'| < k+\frac{\Delta k}{2}} T^s(k'\,|\,k_c) \tag{18}$$

Here, $T^s(k\,|\,k_c)$ is a function of wavenumber magnitude k only, and the shell thickness Δk is taken as unity for convenience. Summation over spectral shells, denoted by $\sum_{\Delta k}$ for short, is also used in the formation of the energy spectrum function $E(k)$ from the energy of discrete Fourier modes: $E(k) = \frac{1}{2}\sum_{\Delta k} u_n(\mathbf{k}')\, u_n^*(\mathbf{k}')$. The energy spectrum $E^L(k)$ of the resolved scales (i.e., for $k \le k_c$, signified by superscript L) at wavenumber k evolves by:

$$\frac{\partial}{\partial t} E^L(k) = -2\nu k^2 E^L(k) + T(k\,|\,k_c) + T^s(k\,|\,k_c) \tag{19}$$

where $T(k\,|\,k_c)$ represents energy transfer from interactions with resolved scales only, and $T^s(k\,|\,k_c)$ represents interactions with subgrid modes which must be modeled in an LES.

2.2.1. Spectral Eddy Viscosity Model

A spectral subgrid eddy viscosity can be defined as [19]:

$$\nu_e(k\,|\,k_c) = -\frac{T^s(k\,|\,k_c)}{2k^2 E^L(k)}, \quad k \le k_c \tag{20}$$

The corresponding modeled, subgrid nonlinear term is given by: $N_n^{sm}(\mathbf{k}\,|\,k_c) = -\nu_e(k\,|\,k_c)\, k^2\, u_n(\mathbf{k})$, and the modeled subgrid transfer is $T^{sm}(\mathbf{k}\,|\,k_c) = \mathrm{Re}\left[u_n^*(\mathbf{k})\, N_n^{sm}(\mathbf{k}\,|\,k_c)\right]$.

It can be shown that this spectral, eddy viscosity model accounts for the total energy transfer to a spectral shell correctly [6]. However, this model assumes that energy and energy transfer have the same form of distribution within a given spectral shell. In other words, energy and energy transfer are assumed to be entirely in phase with each other in wavenumber space. This assumption, of course, deviates from the exact spectral equations.

3. RESULTS AND DISCUSSIONS

In this section, the results of the analysis in both the spectral and physical space is discussed.

3.1. Spectral Space Analysis

Energy transfer information extracted from the DNS data was analyzed to determine the effect of a variable cutoff wavenumber k_c on energy transfer between the resolved (in an LES sense, $k \le k_c$) and subgrid ($k \ge k_c$) scale ranges.

The SGS eddy viscosity (Eq. 20) and the subgrid energy transfer $T^s(k \mid k_c)$ computed using the DNS data for decaying isotropic turbulence (at $Re_\lambda \approx 20$) are shown in Figs. 1a and 1b, respectively. It can be seen that the SGS eddy viscosity takes negative, albeit, small values at low k/k_c for relatively high values of the cutoff wavenumber. This indicates that the SGS energy transfer $T^s(k \mid k_c)$ takes on positive values - representing a non-negligible backscatter of energy from the subgrid scales to the resolved scales. The eddy viscosity displays a cusp-like behavior at resolved wavenumbers approaching k_c, consistent with the results of Domaradzki [19] at higher Reynolds number. The formation of these cusps may be understood in terms of the local nature of energy transfer in turbulence. An active, forward-cascading transfer of energy occurring between scales close to k_c causes a large and negative value of $T^s(k \mid k_c)$ and, hence, a large and positive SGS eddy viscosity. The strength of this local transfer, which is evident in Fig. 1b, depends, of course, on the energy in scales of size in the order of $1/k_c$ and, hence, weakens with increasing k_c.

In Fig. 1a, it may be seen that the SGS eddy viscosity at the lowest cutoff wavenumber k_c=10.5 (line A) has a much greater value than the data at higher spectral cutoffs. This is a consequence of the subgrid transfer taking on a more local character as the spectral cutoff is moved to lower wavenumbers. That is, energy transfer between the largest scales and the subgrid scales becomes much more significant if the subgrid range is expanded to include the intermediate scales that are closer to the largest scales. The upturn in line A at the low wavenumber end is partly a result of the fall-off in the energy spectrum as the low wavenumber limit is approached.

The data obtained using the forced isotropic turbulence data was also analyzed and discussed earlier [6]. The results showed that the cusp-like behavior of the SGS eddy viscosity near k_c is preserved, although, more pronounced than for decaying turbulence. The influence of k_c on the magnitudes of the SGS eddy viscosity and subgrid transfer near k_c is qualitatively similar to decaying isotropic turbulence.

To assess the performance of the SGS eddy viscosity model (Eq. 20), an important criterion is how well the energy transfer is predicted in physical space. The Fourier space considerations illustrated by Eq. 19, indicate, (in homogeneous turbulence) that the space average of the energy transfer is reproduced exactly by this model. However, incorrect phase information in Fourier space translates to deviations from exact values at each grid point in physical space. A quantitative measure of model accuracy is the correlation coefficient between the exact and modeled SGS transfer in physical space, denoted by $T^s(\mathbf{x} \mid k_c)$ and $T^m(\mathbf{x} \mid k_c)$, respectively. This correlation coefficient, $\rho(T^s, T^m)$, which is computed over all grid points in physical space, is shown in Fig. 2a as a function of the cutoff wavenumber k_c. Also shown, is the corresponding correlation coefficient, averaged over the coordinate components, between the exact and modeled SGS nonlinear terms, denoted by $\rho(N^s, N^m)$.

Several observations may be made in Fig. 2a. First, for all of the quantities considered, model performance improves steadily with increasing cutoff wavenumber. This is clearly consistent with the general expectation that SGS models should improve if a wider range of scales are resolved in an LES by increasing the number of grid points, leaving only the smallest scales to be modeled. Second, except at low cutoff wavenumbers, the nonlinear term is predicted more accurately than the energy transfer. Since in physical space this (subgrid) transfer is given by the dot product between the resolved velocity vector and the subgrid nonlinear vector, we may conclude that the alignment between these vectors is not well predicted. Third, the model produces better agreement with DNS data in the decaying case compared to the forced case. This is not surprising, since the artificial forcing has a distorting effect on energy transfer, especially at the large scales, which generally dominate the correlation coefficients.

The scale similarity model (Model F1) was also studied in the Fourier space. Since two filter operations are required to evaluate this model, two cutoff wave numbers are defined as k_{c1} and k_{c2}, where $k_{c2} < k_{c1}$. Using the decaying turbulence data obtained on the 128^3 grid (for which, $k_{max} = 60$), the correlation of the exact subgrid stress τ_{ij} with the modeled subgrid stress (Eq. 14, with $f(I_{LS}) = 1$) was carried out. Figure 2b shows the correlation $\rho(\tau_{xx}, L_{xx})$ as a function of the ratio k_{c2}/k_{c1} for a range of values of k_{c1} and k_{c2}. This figure shows that for a fixed value of k_{c1}, the correlation decreases rapidly with decrease in the test cutoff wavenumber k_{c2}. Note that $k_{c2}/k_{c1} = 0.5$ is equivalent, in phyiscal space, to a ratio between the test filter 2Δ and the grid filter Δ. Thus, it can be seen that there is a significant reduction in the correlation when the grid filter Δ (or equivalently, k_{c1}) is decreased. This implies that the scale similarity model prediction becomes quite poor as the grid is coarsened.

It has been observed in the present study and also noted earlier [9] that the scale similarity model can predict both forward- and backscatter. However, it is possible that the backscatter predicted by this model is not realistic. To determine this, the correlation between the negative values of the exact subgrid stresses and the scale similarity model was computed as a function of k_{c1} and k_{c2}. The results (not shown) indicate that for a fixed value of k_{c1}, a high correlation is observed only when k_{c2} is close to k_{c1}. The correlation was always lower than the correlation shown in Fig. 2b indicating that the negative parts are relatively less correlated. In addition, with decrease in k_{c1}, the correlation of the backscatter part dropped rapidly. These results suggest that the backscatter modeled by the scale similarity model is somewhat realistic, however, when the grid is coarsened (or $k_{c2} \ll k_{c1}$), a significant portion of the modeled backscatter could be non-physical.

The spectral space analysis method was then used to analyze the behavior of some of the subgrid models. Figure 3a shows the Kolmogorov scaled energy spectra for the 64^3 DNS, and for the 32^3 and 16^3 LES using the k_{sgs} model with stochastic backscatter (Model E), and the scale-similarity model (Model F2) at a time $t = 12$ which corresponds

to around 21.7 large-eddy turnover time. The LES simulations were performed by first filtering the 64^3 initial field (i.e., at $t = 0$) in *physical space* into the LES grid using the top hat filter. Thus, at $t = 0$, all the initial fields were highly correlated in the physical space. (Results of the physical space analysis will be discussed in the next section). However, in Fourier space, due to the form of the transfer function for the top hat filter, the initial energy spectra will be quite different for the direct and large eddy simulations. This should show up in the eventual evolution of the flow field when analyzed in the Fourier space. However, if the simulations are self consistent, the Kolmogorov scaled spectra should exhibit similarity, as seen in Fig. 3a.

Figure 3b shows the energy spectra (normalized by the kinetic energy) as a function of wavenumber. The disagreements between DNS and LES results are more apparent in this figure. The normalized energy spectra obtained using LES predict a higher peak energy at a lower wavenumber when compared to DNS data. Both models E and F2 predict nearly the same peak value (about 25 percent higher than exact) and location with 32^3 resolution. However, as the grid is coarsened, the k_{sgs} model shows an energy peak larger than the similarity model. Further, near $k = k_{max}$, the energy in the high wavenumbers is much lower for the LES.

The dissipation spectra (not shown) peaks at larger wavenumbers (by a factor of 2) and all the data shows similar trends. However, since energy is lower near $k = k_{max}$, the LES results predict lower dissipation when compared to the DNS results. These results suggest that the dissipation modeled by the subgrid models is insufficient and needs to be improved.

The energy transfer in the spectral space was also analyzed using the LES data. Using the DNS and LES fields shown in Fig. 3, the spectral eddy viscosity and the subgrid transfer at a cutoff wavenumber $k_c = 10$ was computed and is shown in Figs. 4a and 4b, respectively. Note that for the DNS, $k_{max} = 30$, while for the LES, $k_{max} = 15$. Therefore, a k_c of 10 is in the range of resolved scales for all the simulations. Figure 4a shows that the spectral eddy viscosity behavior in all cases is nearly identical suggesting that the LES models are behaving quite well. However, this is somewhat misleading. Figure 4b shows that at $k/k_c \rightarrow 1$ both models E and F2 predict lower negative values for the subgrid transfer $T^v(k|k_c)$. A low value for the transfer would result in a lower peak in the eddy viscosity. However, less energy is being transferred to the subgrid scales, as seen in Fig. 3. Therefore, the combination of low (negative) value of $T^v(k|k_c)$ and lower $E^L(k)$ near k_c, results in an eddy viscosity (from Eq. 20) that appears to agree with the *a priori* results.

3.2. Physical Space Analysis

The analysis in the physical space was carried out using methods that attempted to quantify the behavior of the models in terms of the resolution of the large-scale structures, and the correlation between the exact and the modeled stresses and energy flux to the subgrid scales. Although the *a priori* analysis was carried out on all the DNS data sets, only representative results are discussed below.

Figure 5a shows contours of the subgrid energy flux ($E(\Delta) = -\tau_{ij}\bar{S}_{ij}$) to the subgrid scales on a 32^3 grid obtained by filtering the 128^3 forced stationary turbulence data. This result is compared to the prediction by the k_{sgs} model without backscatter (Model C, Fig. 5b) and the scale similarity models, Model F1 (Fig. 5c) and Model F2 (Fig. 5d). The contour interval is the same for all figures, and an arbitrary (but same) slice of the 3D field is shown. Comparison with the exact results (Fig. 5a) shows that there is significant similarity in regions with high positive transfer. However, only Model F1 (Fig. 5c) is capable of resolving regions with backscatter, although, the peak negative value is over 35% lower than in the exact case. The peak positive value also is not predicted very well. Model C is predicting a maximum level nearly 60% lower than the exact value while Model F1 is predicting peak level around 35% lower without backscatter control. With backscatter control, Model F2 predicts a peak level around 42% lower. These results suggest that even when there is similarity between the resolved structures, the peak values predicted by subgrid models can be quite different from the exact values.

To further quantify the differences and the similarities between the model predictions and the exact values, the subgrid stress and the energy transfer correlations were computed. The stress correlation data indicates that the correlation decreases with an increase in filter width for all cases. Figure 6a shows the average correlation for the isotropic components of the subgrid stress tensor (i.e., τ_{ii}) as a function of filter width. The correlation for the similarity models (Models F1 and F2) decreases rapidly with increase in filter size when compared to other models. When backscatter control was imposed (Model F2), the correlation was lower. This suggests that some of the backscatter intrinsic in the scale-similarity model may be realistic and this result is consistent with the data obtained earlier [9]. The eddy viscosity model of Smagorinsky (Model A) consistently showed the lowest correlation, as seen in earlier studies. On the other hand, the k_{sgs} model (Model C) showed a relatively high correlation for the stresses with only a weak dependence on the filter width. However, note that the high correlation is observed for the k_{sgs} model only for the isotropic stress components by virtue of the definition, Eq. (10). The correlation for the off-diagonal stress components was found to be quite low. Correlation analysis of the energy flux ($=-\tau_{ij}\bar{S}_{ij}$) is more relevant for present analysis and is discussed in more details below.

Figure 6b shows the energy flux correlation for the models shown in Fig. 6a, and Fig. 6c shows the energy flux

correlation for the models at two different Reynolds numbers. Note that the higher Reynolds number case is obtained using stochastic forcing and therefore, direct comparison of the forced and decaying turbulence cases is not intended in this figure. As noted earlier, the energy flux to the unresolved scales is defined as $E(\Delta) = -\tau_{ij}\bar{S}_{ij}$ at a filter width Δ for the exact energy flux. For the subgrid models, τ_{ij} is replaced by the appropriate model. For small values of Δ/η, where η is the Kolmogorov scale, the correlation for the scale similarity models (Model F1 and F2) is much higher than for the other models. The correlation decreases with increase in filter width for both Reynolds number with the largest decrease seen for the similarity models. On the other hand, the one-equation model (Model C) shows only a weak dependance on the filter width and Reynolds number. This suggests that the subgrid kinetic energy model may have good potential for application in coarse grid LES.

The decrease in the subgrid stress and energy transfer correlation for the similarity models with increase in filter width can be understood by noting that this model was developed based on analysis of very high Re_λ experimental data with at least a decade of wavenumbers in the inertial range. For the present DNS data, there is no appreciable inertial range, and this situation is even worse for the low Re_λ case. Furthermore, the model assumes that there is similarity between the stresses resolved at 2Δ grid and the stresses resolved at the Δ grid. In the present case, as the filter width increases (or as the grid coarsens), this assumption breaks down.

Since the ensemble-averaged value of the energy flux $<E(\Delta)>$ should be of the order of the dissipation rate ε, a comparison was carried out for all the models studied here. The results (not shown) indicate that all models predicted values lower than the dissipation rate computed from the exact field. However, the predicted $<E(\Delta)>$ was of the same order as the dissipation rate. This agreed with the earlier observations [9]. The energy flux at scales larger than Δ is also of interest. For example, it was shown [9] that the energy flux at a scale 2Δ can be represented from the 'local' and 'not-so-local' contributions. Using the Germano identity, the energy flux at 2Δ can be written as: $E(2\Delta) = -(L_{ij}<\bar{S}>_{ij} + <\tau>_{ij}<\bar{S}>_{ij})$. The first term on the right-hand side of the above expression represents the 'local' transfer of energy flux from large scales to scales between Δ and 2Δ, while the second term represents the energy transfer to the scales smaller than Δ. A correlation between these two terms was computed for various filter width. The results (again, not shown for brevity) indicate a very high correlation around 0.8, and since $E(2\Delta)$ was always positive, this suggests that both the energy fluxes were forward scattered. A similar high correlation and behavior was observed by Liu et al.[9].

The coefficient C_L in Models F1 and F2 was determined by assuming that the correct amount of dissipation must be predicted by the model. Thus, $C_L = <\tau_{ij}\bar{S}_{ij}>/<f(I_{LS})L_{ij}\bar{S}_{ij}>$ where $<>$ denotes ensemble averaging. A value of around 0.45±0.15 was estimated for the high Reynolds number experimental data [9]. For the correlation analysis

shown in Fig. 6a-c, $C_L = 0.45$ was employed. Since, in the present study, a significant variation in the correlation was observed as a function of both the filter width and Re_λ, this coefficient was recomputed using the above noted relation. Figure 6d shows the variation of C_L as a function of filter width and Re_λ. The results suggest that this coefficient increases with increase in filter width and decrease in Re_λ. However, for small filter widths, the predicted value is well within the range of the value determined experimentally [9] in high Re_λ flows. The large variation in the value of C_L may be an artifact of the limited range of scales resolved in the present DNS data and the problems with the similarity model (discussed above) when the grid is coarsened. This issue needs further study.

A priori analysis of the DNS data at $Re_\lambda \approx 10$ was also carried out since this data is used for comparison with LES predictions (as discussed in Fig. 3). Comparison of the flow structures, and the stress and energy flux correlations showed a picture very similar to that seen at the higher Re_λ (and therefore, is not shown).

The subgrid models were implemented in LES using 32^3 and 16^3 grid resolutions. For LES, the flow field was initialized by the filtered initial field for the 64^3 DNS. Hence, at $t = 0$ the physical space fields were highly correlated (although, in the Fourier space there was quite a bit of discrepancy, see Fig. 3). However, the results showed that as time evolved, the DNS and LES became highly uncorrelated.

To analyze the LES results, the DNS data obtained on the 64^3 grid resolution, and the LES data obtained on the 32^3 grid were filtered to the 16^3 grid. The energy flux predicted from these two simulations at the 16^3 grid resolution was then compared to the model prediction in the actual 16^3 grid LES. The results showed that all the models predicted very poor correlation (less than 0.1) when the 16^3 grid LES was compared to the filtered DNS data set at the same grid level. The comparison between the two LES showed that the energy transfer correlation for the scale similarity models (F1 and F2) was very low (around 0.12), while the k_{sgs} model (Model E) predicted a relatively higher value of around 0.35. This again suggests that when coarse grids are employed in LES, the k_{sgs} model appears to behave much better.

To visualize these results, Fig. 7a shows the contours of the energy transfer computed on the 16^3 grid by filtering the 64^3 DNS data. Figure 7b shows the contours (using the same contour interval as in Fig. 7a) of the *a priori* prediction by the k_{sgs} model (Model C) on the 16^3 grid using the same DNS data. Clearly, there is quite a good correlation between the two figures (as seen in Figs. 6a and 6b).

Figure 8a shows the contours of the energy transfer computed on the 16^3 by filtering the results of the 32^3 grid LES

(using the Model C). Finally, Fig. 8b shows the energy transfer on the 16^3 grid obtained by carrying out LES using Model C in that grid. If the subgrid model was accurate, then all these figures should be highly correlated. As noted above, although the *a priori* correlation was high (Figs. 7a and 7b), the correlation obtained using LES data was quite low (Figs. 8a and 8b). However, it is worth noting these results were much better than the results obtained using Models A and F2 (not shown).

Figure 9a summarizes the above results for a range of Reynolds number. The computed correlation in the 16^3 grid for the various models is plotted as a function of the initial Reynolds number. The data shows that the correlation for all models is much lower in LES than in the *a priori* analysis. Furthermore, with increase in Re_λ, the correlation for all the models decreases, indicating a serious problem with the dissipation modeling. With backscatter modeling (Model E), a slightly higher value of the correlation was obtained when compared to the model without backscatter (Model C). This small change does not justify the inclusion of the backscatter term. However, this issue will be revisited at a later stage.

The above study showed that, although the one-equation model had some potential for application as a subgrid model, it still had some major problems. To determine if these problems could be removed, a series of calculations were carried out using the dynamic versions of the eddy viscosity model (Model B) and the dynamic one-equation model (Model D). The results obtained from these simulations were much more encouraging. To evaluate the self consistency of the dynamic models, the LES results obtained on the 32^3 grid were compared to the LES results obtained on the 16^3 grid. The flow fields from these two simulations can be related through the mathematical identity, Eq. (4). Thus, the modeled quantity $<\overline{u_i u_j}>$ obtained from the two data sets must be identical if the subgrid model has performed correctly at the two grid level.

Figure 9b shows the average value of the correlation for the anisotropic components of $<\overline{u_i u_j}>$ as a function of the Reynolds number. Clearly, the correlation is very high for both the dynamic models with values consistently in the 0.85-0.97 range. However, with increase in Reynolds number, the correlation for the dynamic eddy viscosity model decreases while the dynamic one-equation model maintains a high value. This result suggests that models that do not make the assumption of local equilibrium between energy production and dissipation rate (e.g., Model D) are superior to algebraic eddy viscosity type models (e.g., Model B). This result is very important since this implies that such models may be applicable for LES of high Reynolds number flows using relatively coarse grids (grid resolution restrictions are typically imposed due to computer resource limitations).

Figure 10a shows the variation of the dynamically evaluated constants (i.e., C, C_k, and C_ϵ) with time during the

simulation for $Re_{\lambda_o} = 100$. Figure 10b shows the variation of the constants with the Reynolds number. The model coefficients go through changes in the early stages of the turbulent flow development. However, as a realistic decaying isotropic field develops, the coefficients reach an asymptotic state. Also, the values of the coefficients at this asymptotic state are almost independent of Reynolds number (Fig. 10b), except for C_ϵ in Model D which is sensitive to both grid resolution and Reynolds number. The values of the constants are in good agreement with earlier results. For example, the Smagorinsky's constant C_S (which is the square-root of the dynamic model coefficient C) is around 0.165 which is quite close to 0.17, suggested by Lilly [10] for homogeneous, isotropic turbulence with cut-off in the inertial range.

4. CONCLUSIONS

Direct and large eddy simulations of forced and decaying isotropic turbulence have been performed using a pseudospectral and a finite-difference code. Subgrid models that include a one-equation subgrid kinetic energy model with and without a stochastic backscatter forcing term and a new scale similarity model, have been analyzed in both the Fourier space and physical space using high resolution DNS data. The spectral space analysis showed that energy transfer across the cutoff wavenumber k_c is dominated by local interaction. Correlation analysis of the modeled (by a spectral eddy viscosity) and exact nonlinear terms, and the subgrid energy transfer in physical space showed very low values. The correlation of the scale similarity model was much higher, however, the correlation decreased with decrease in the test cutoff wave number (k_{c2}). This suggests that as the grid becomes coarse (i.e. Δ is large), the scale similarity model becomes less reliable.

In physical space, *a priori* analysis of the stress and energy transfer correlation between the exact value and the modeled terms was carried out for a range of Re_λ. Results show that the stress and energy flux predicted by subgrid models C and F2 correlates reasonably well with the DNS data, with the scale similarity model showing very high correlation for reasonable grid resolution. However, with decrease in grid resolution, the scale similarity model (Model F2) becomes more uncorrelated when compared to the kinetic energy model (Model C). This result is consistent with the observation made in the spectral space.

When the subgrid models (with fixed coefficients) were used for LES, correlation with the DNS results was very low. This suggests that the results of *a priori* analysis cannot be used to predict the behavior of the subgrid models in actual LES. The analysis of the LES data obtained on very coarse grids showed that the scale similarity model behaves very poorly when compared to the k_{sgs} model, which consistently showed relatively higher (albiet, low) correlation. These results suggest that the scale similarity model can be used only for relatively fine grid resolution, whereas, the kinetic energy model may be useful even in coarse grids. However, it was determined that to improve

the one-equation model, the dissipation term has to be modeled more accurately.

To determine the performance of dynamic models, two models (the dynamic eddy viscosity model and the dynamic one-equation model) were implemented and LES was carried out for a range of Reynolds number. The correlation analysis of these simulations was carried out without using any DNS information. It was shown that both models consistently indicated a very high correlation even in coarse grids. However, with increase in Reynolds number, the correlation for the dynamic eddy viscosity model decreased while for the dynamic one-equation model there was not much change. This showed that models that do not assume local balance between the energy production and dissipation rate (as Model D) have a much better potential for modeling subgrid stresses in coarse grids even at relatively high Reynolds number. Furthermore, the application of the dynamic procedure to the one-equation model appears to have improved the modeled dissipation term in the original equation.

ACKNOWLEDGMENTS

This work is supported by the Office of Naval Research under Grant No. N00014-93-1-0342. Computing time was provided by the Numerical Aerodynamic Simulation (NAS) at NASA Ames Research Center and is gratefully acknowledged.

REFERENCES

1. Germano, M., Piomelli, U., Moin, P., and Cabot, W. H., "A Dynamic Subgrid-Scale Eddy Viscosity Model," *Phys. Fluids A*, 3, 1760 (1991).

2. Moin, P., Carati, D., Lund, T., Ghosal, S., and Akselvoll, K., "Developments and Applications of Dynamic Models for Large Eddy Simulations of Complex Flows," *Proceedings of the 74th AGARD/FDP Symposium on "Application of Direct and Large Eddy Simulation to Transition and Turbulence"*, AGARD CP-551, (1995).

3. Piomelli, U., and Liu, J., "Large-Eddy Simulations of Rotating Channel Flows Using a Localized Dynamic Model," *Proceedings of the 74th AGARD/FDP Symposium on "Application of Direct and Large Eddy Simulation to Transition and Turbulence"*, AGARD CP-551, (1995).

4. Ghosal, S. Lund, T. S., and Moin, P., "A Local Dynamic Model for Large Eddy Simulations," *Annual Research Briefs-1992*, Center for Turbulence Research, Stanford University/NASA Ames, pp. 3-25, (1993).

5. Rogallo, R. S., "Numerical Experiments in Homogeneous Turbulence," NASA TM 81315, (1981).

6. Menon, S. and Yeung. P.-K., "Analysis of Subgrid Models Using Direct and Large Eddy Simulations of Isotropic Turbulence," *Proceedings of the 74th AGARD/FDP Symposium on "Application of Direct and Large Eddy Simulation to Transition and Turbulence"*, AGARD CP-551, (1995).

7. Eswaran, V. and Pope, S.B., "An Examination of Forcing in Direct Numerical Simulations of Turbulence," *Comput. & Fluids*, **16**, 257 (1988).

8. Piomelli, U., Moin, P., and Ferziger, J.H., "Model Consistency in Large Eddy Simulation of Turbulent Channel Flows," *Phys. Fluids*, **31**, 1884 (1988).

9. Liu, S., Meneveau, C., and Katz, J., "On the Properties of Similarity Subgrid-scale Models as Deduced from Measurements in a Turbulent Jet," *J. Fluid Mech.*, **275**, 83 (1994).

10. Lilly, D. K., "On the Application of the Eddy Viscosity Concept in the Inertial Sub-Range of Turbulence," NCAR Manuscript 123, (1966).

11. Lilly, D. K., "A Proposed Modification of the Germano Subgrid-Scale Closure Model," *Phys. Fluids*, **4**, 633 (1992).

12. Zang, Y., Street, R. L., and Koseff, J.R., "Application of a Dynamic Subgrid Scale Model to Turbulent Recirculating Flows," in *Annual Research Briefs-1992*, Center for Turbulence Research, Stanford University/NASA Ames, (1993).

13. Yoshizawa, A., "Bridging between Eddy-viscosity-type and Second-order Models using a Two-Scale DIA", Ninth Symposium on "Turbulent Shear Flows", Kyoto, Japan, August, (1993).

14. Piomelli, U., Cabot, W.H., Moin, P., and Lee, S., "Subgrid-scale Backscatter in Turbulent and Transitional Flows," *Phys. Fluids A*, **3**, 1766 (1991).

15. Chasnov, J. R., "Simulation of the Kolmogorov Inertial Subrange Using an Improved Subgrid Model," *Phys. Fluids A*, **3**, 188 (1991).

16. Leith, C.E., "Stochastic Backscatter in a Subgrid-scale Model: Plane Shear Mixing Layer," *Phys. Fluids A*, 2, 297 (1990).

17. Menon, S., "A Numerical Study of Secondary Fuel Injection Control of Combustion Instability in a Ramjet", AIAA Paper No. 92-0777, (1992).

18. Bardina, J., Ferziger, J.H., and Reynolds, W.C., "Improved Subgrid Scale Models for Large Eddy Simulations," AIAA Paper 90-1357, (1980).

19. Domaradzki, J. A., Liu, W., and Brachet, M. E., "An Analysis of Subgrid Scale Interactions in Numerically Simulated Isotropic Turbulence," *Phys. Fluids A*, 5, 1747 (1993).

LIST OF FIGURES

Fig. 1. The subgrid eddy viscosity and subgrid energy transfer computed from decaying isotropic turbulence DNS data for various values of k_c. Curves A-D are for k_c=10.5, 15.5, 30.5 and 48.5, respectively. a) Subgrid eddy viscosity, $\nu_e(k|k_c)$; b) subgrid energy transfer, $T^s(k|k_c)$.

Fig. 2. Correlation between the exact and modeled quantities computed in physical space. a) Spectral eddy viscosity model. Curves A and B are for decaying turbulence while curves C and D are for the forced case. b) Scale similarity model (Model F1).

Fig. 3. Comparison of the energy spectra for DNS and LES with various subgrid models at Re_λ=10. a) Kolmogorov scaled energy spectra; b) normalized energy spectra.

Fig. 4. The subgrid eddy viscosity and subgrid energy transfer computed from DNS and LES data for k_c=10.5. Curve A: 32^3 LES, Model E; curve B: 32^3 LES, Model F2; curve C: 64^3 DNS. a) Subgrid eddy viscosity, $\nu_e(k|k_c)$; b) subgrid energy transfer, $T^s(k|k_c)$.

Fig. 5. Comparison of the contours of subgrid energy transfer for forced DNS data (Re_λ=90) and subgrid model predictions on 32^3 grid. Same contour interval and locations shown for all cases. Solid contours indicate forward scatter and dotted contours indicate backscatter. a) Exact energy transfer from DNS data; b) energy transfer predicted by Model C; c) energy transfer predicted by Model F1; d) energy transfer predicted by Model F2.

Fig. 6. Correlation between exact and modeled subgrid stress and energy transfer computed from 128^3 decaying turbulence DNS data. a) Stress correlation at Re_λ=20; b) energy transfer correlation at Re_λ=20; c) energy transfer correlation at Re_λ=20 and 90; d) variation of C_L (Model F1 and F2).

Fig. 7. Comparison of the exact and modeled subgrid energy transfer resolved on a 16^3 grid obtained using 64^3 decaying isotropic turbulence DNS data. Same contour interval and location shown. a) Exact energy transfer from DNS data; b) modeled energy transfer by Model C.

Fig. 8. Comparison of the subgrid energy transfer predicted by LES using Model C on a 16^3 grid. Same contour interval and location shown as in FIG. 7. a) Energy transfer predicted using 32^3 LES data; b) energy transfer modeled by Model C in 16^3 LES.

Fig. 9. Variation of subgrid energy transfer correlation with Re_λ. Correlation computed on 16^3 grid. a) Subgrid models with fixed coefficients; b) dynamic subgrid models.

Fig. 10. The variation of the coefficients with time and Re_λ for the dynamic models. a) Variation with time; b) variation with Re_λ.

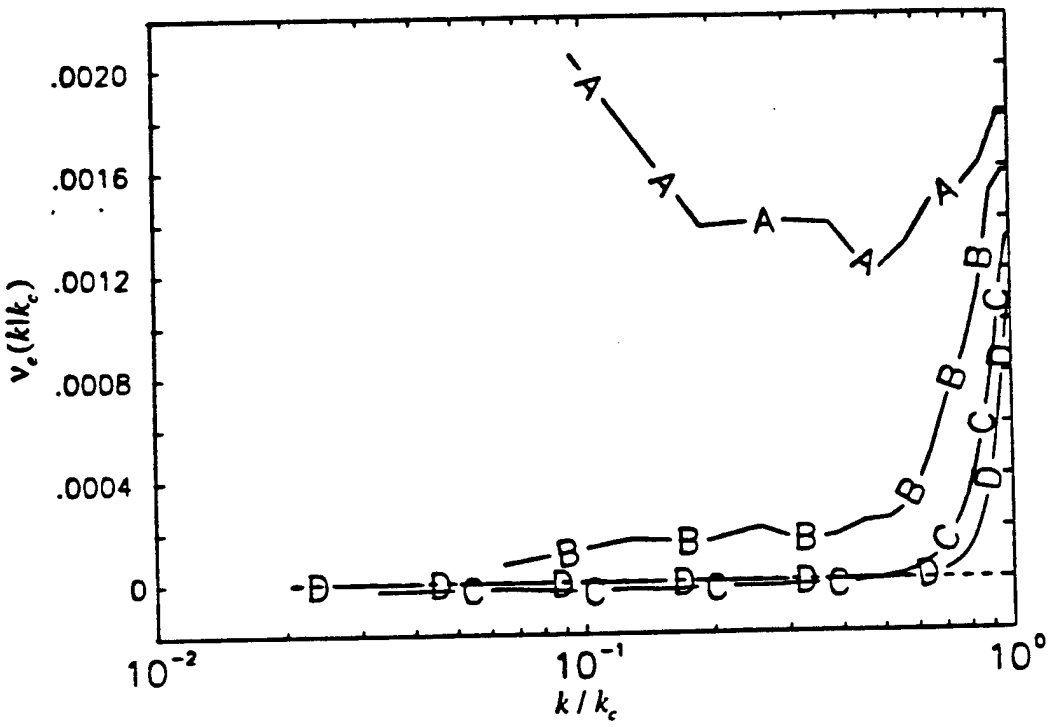
.0020
.0016
.0012
.0008
.0004
0
$\nu_e(k/k_c)$
10^{-2}
10^{-1}
10^{0}
k/k_c

a)

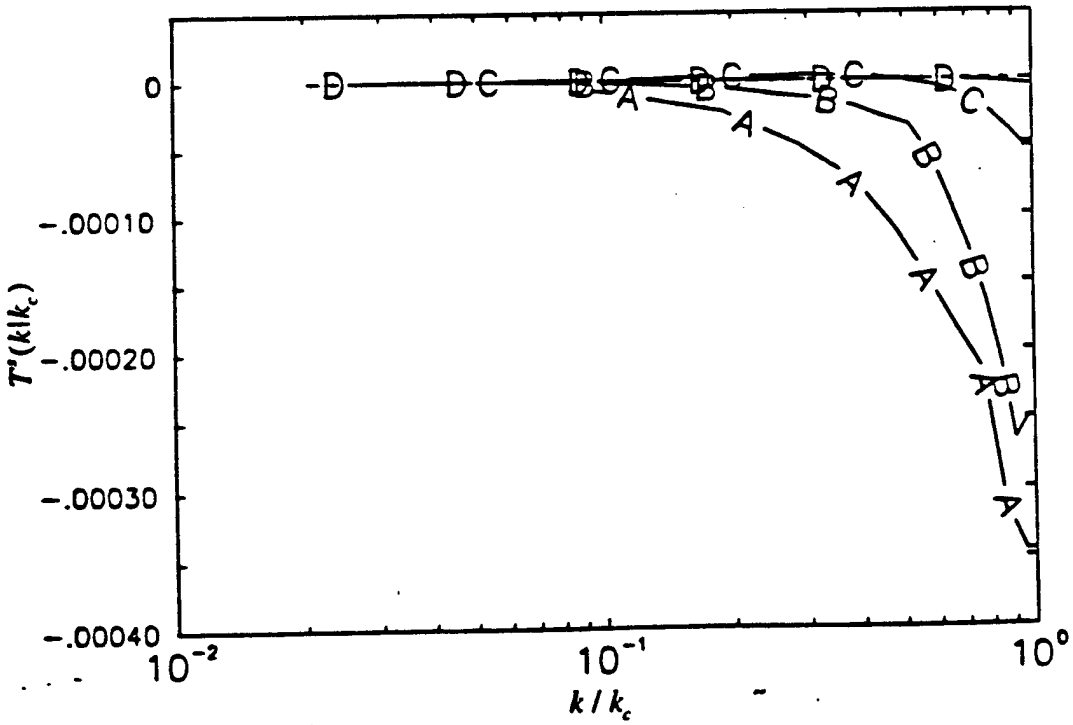
0
−.00010
−.00020
−.00030
−.00040
$T'(k/k_c)$
10^{-2}
10^{-1}
10^{0}
k/k_c

b)

Figure 1

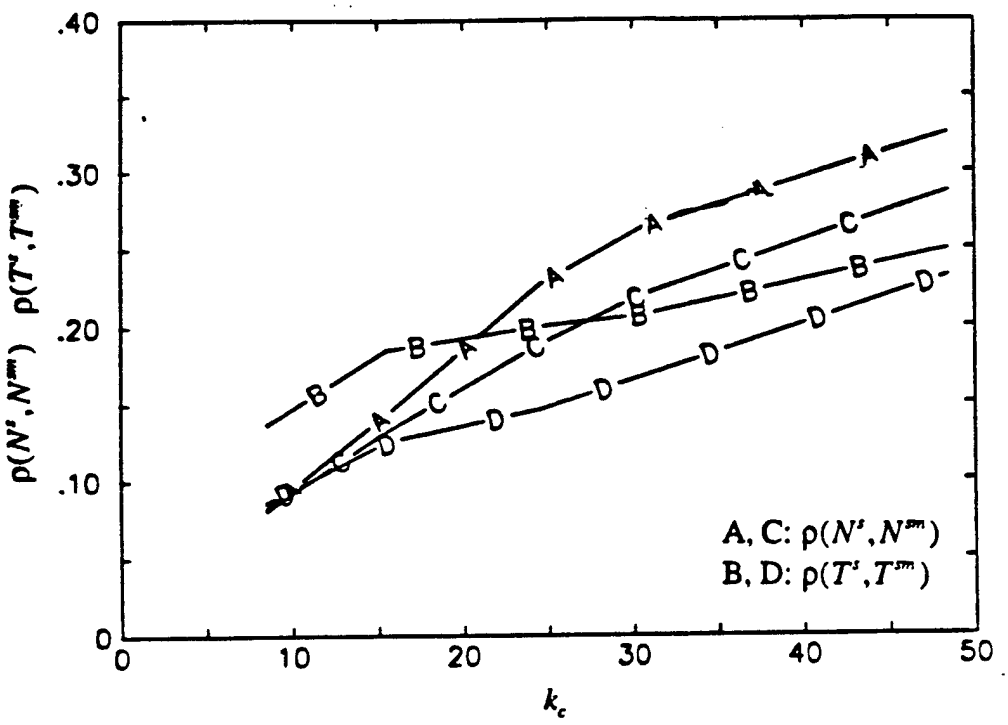
.40
.30
.20
.10
0
0
10
20
30
40
50
k_c
$\rho(N^s, N^{sm})$ $\rho(T^s, T^{sm})$
A, C: $\rho(N^s, N^{sm})$
B, D: $\rho(T^s, T^{sm})$

a)

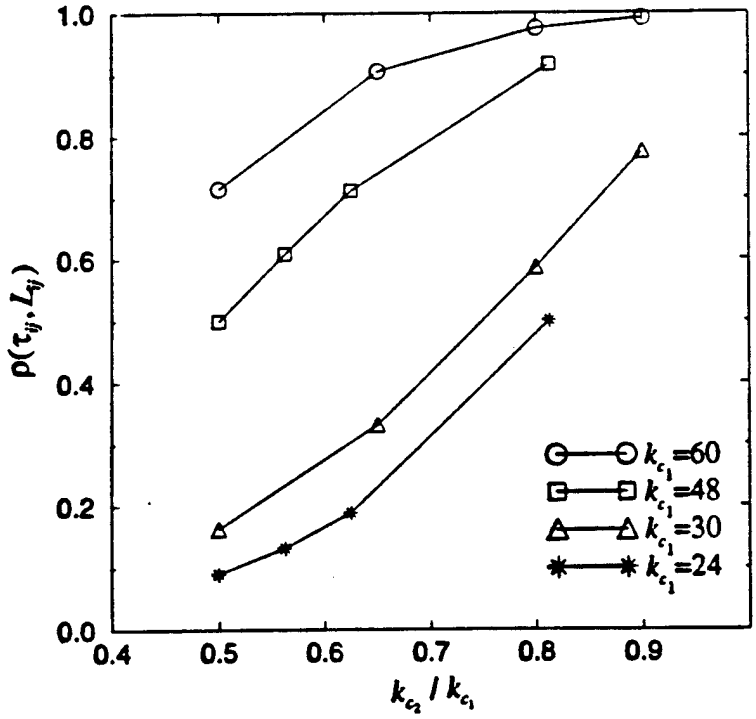
1.0
0.8
0.6
0.4
0.2
0.0
0.4
0.5
0.6
0.7
0.8
0.9
k_{c_2} / k_{c_1}
$\rho(\tau_{ij}, L_{ij})$
k_{c_1}=60
k_{c_1}=48
k_{c_1}=30
k_{c_1}=24

b)

Figure 2

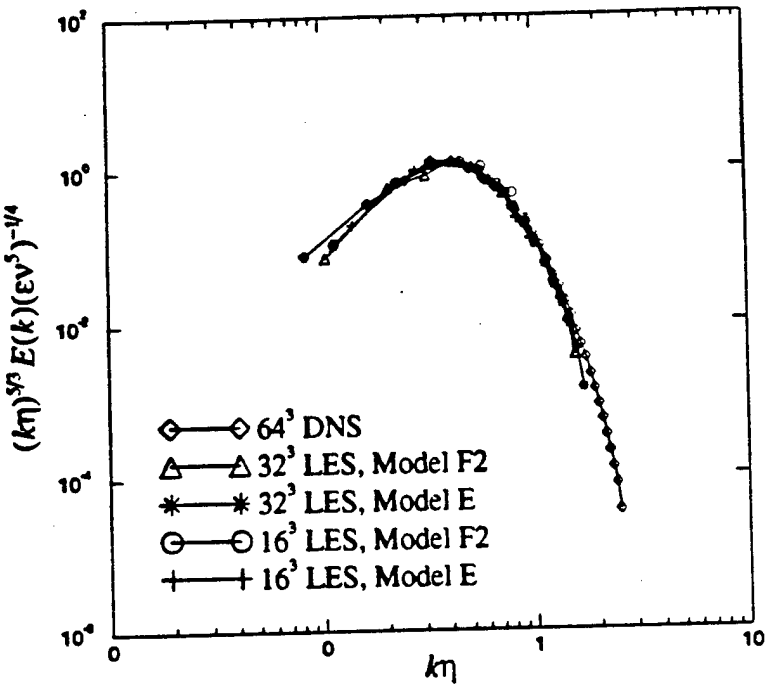
$(k\eta)^{5/3} E(k)(\epsilon\nu^5)^{-1/4}$
$k\eta$
64^3 DNS
32^3 LES, Model F2
32^3 LES, Model E
16^3 LES, Model F2
16^3 LES, Model E

a)

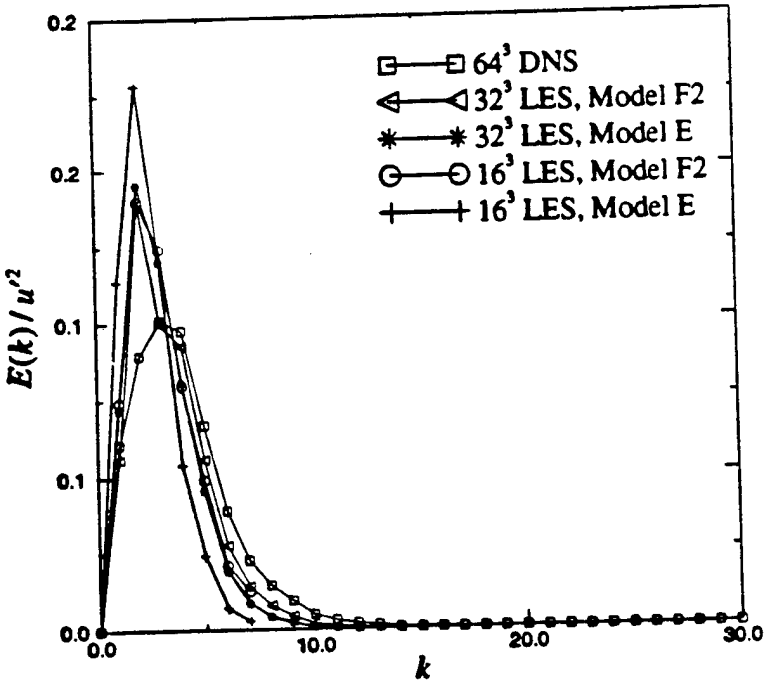
$E(k)/u'^2$
k
64^3 DNS
32^3 LES, Model F2
32^3 LES, Model E
16^3 LES, Model F2
16^3 LES, Model E

b)

Figure 3

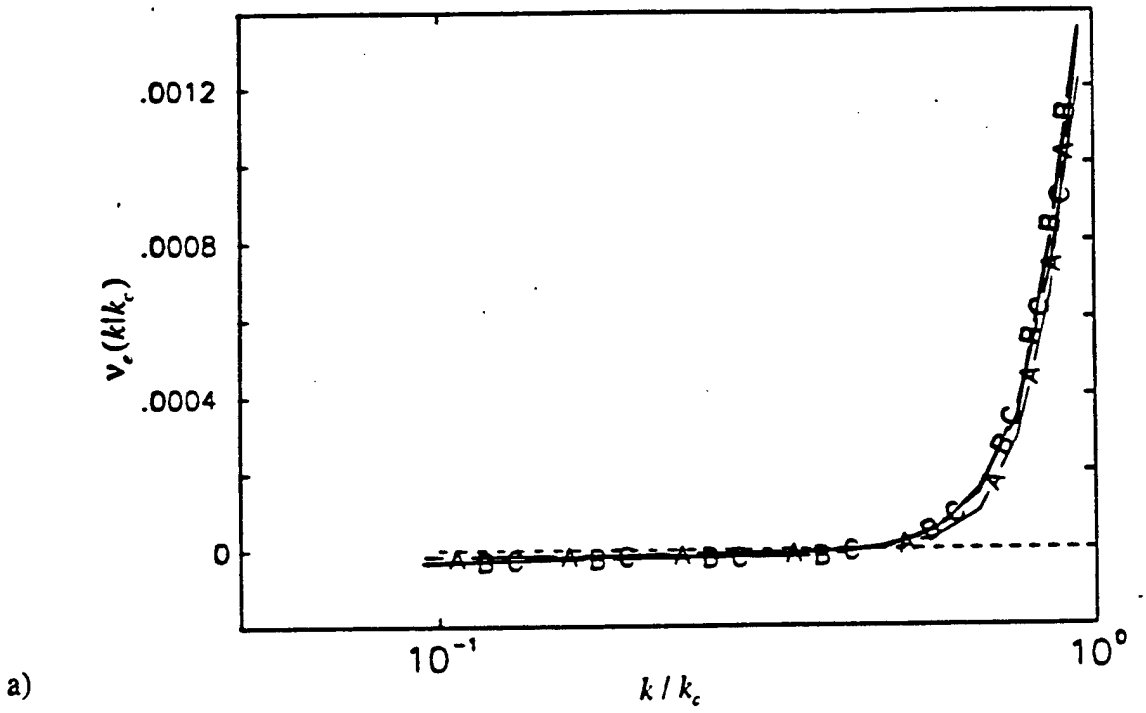
.0012
.0008
.0004
0
$\nu_e(k/k_c)$
10^{-1}
10^{0}
k/k_c

a)

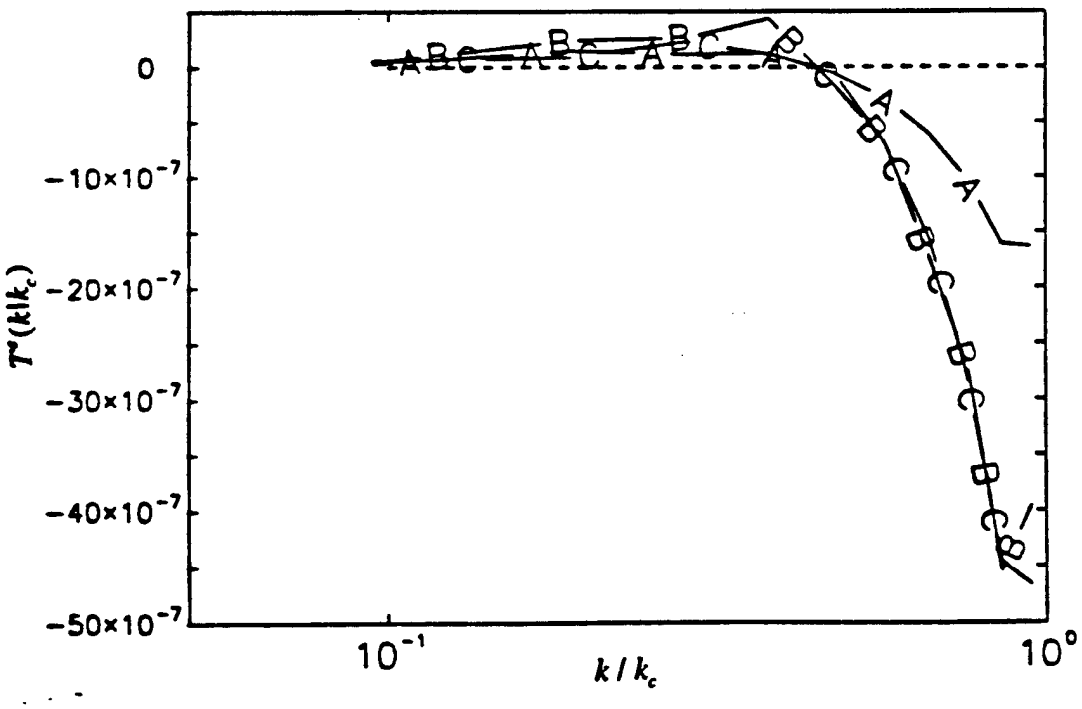
0
-10×10^{-7}
-20×10^{-7}
-30×10^{-7}
-40×10^{-7}
-50×10^{-7}
$T'(k/k_c)$
A
10^{-1}
10^{0}
k/k_c

b)

Figure 4

a)

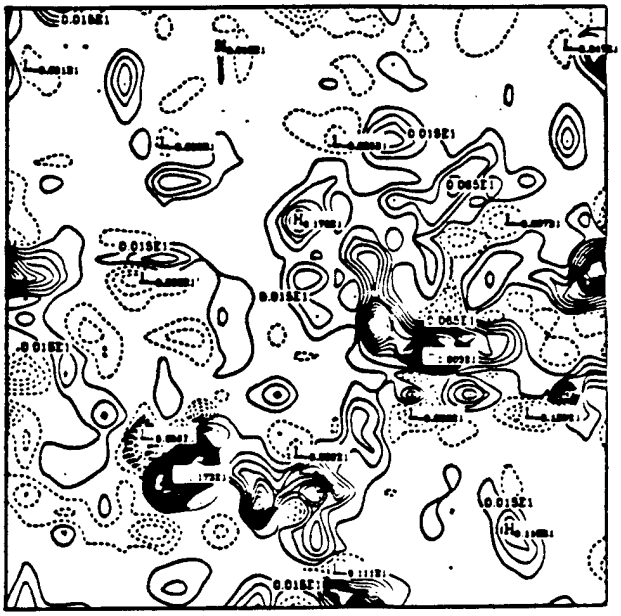

b)

Figure 5

c)

d)

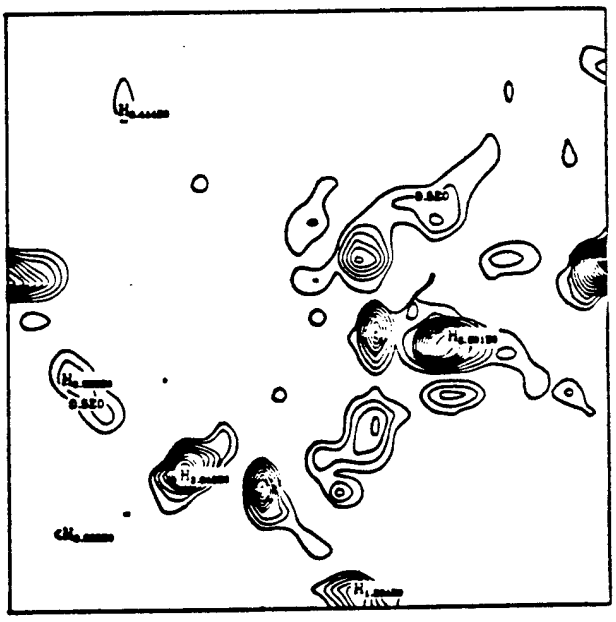

Figure 5 (cont.)

a)

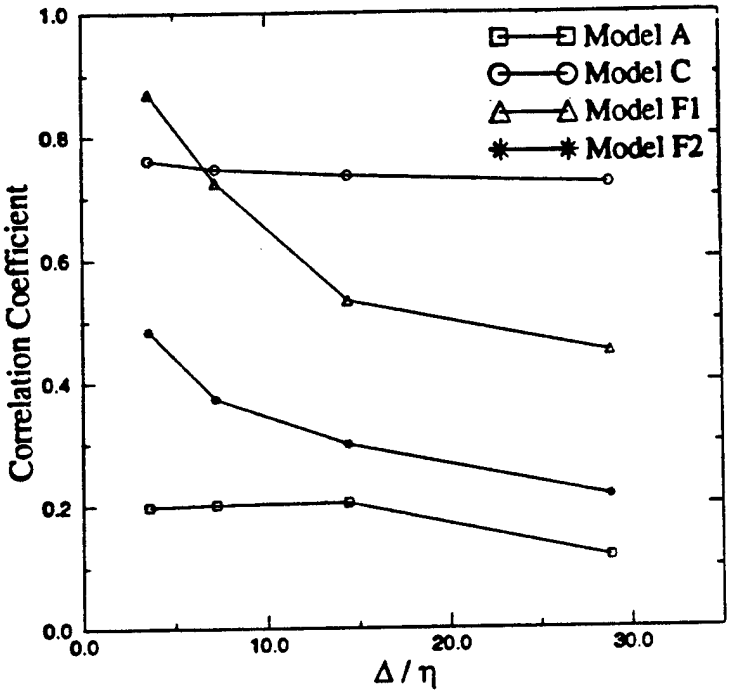
Model A
Model C
Model F1
Model F2
Correlation Coefficient
1.0
0.8
0.6
0.4
0.2
0.0
0.0
10.0
20.0
30.0
Δ / η

b)

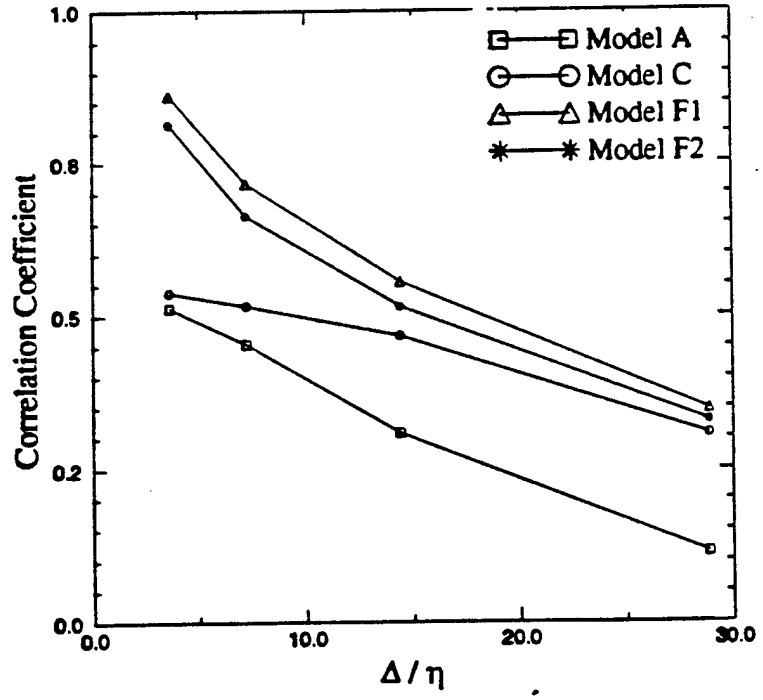
Model A
Model C
Model F1
Model F2
Correlation Coefficient
1.0
0.8
0.5
0.2
0.0
0.0
10.0
20.0
30.0
Δ / η

Figure 6

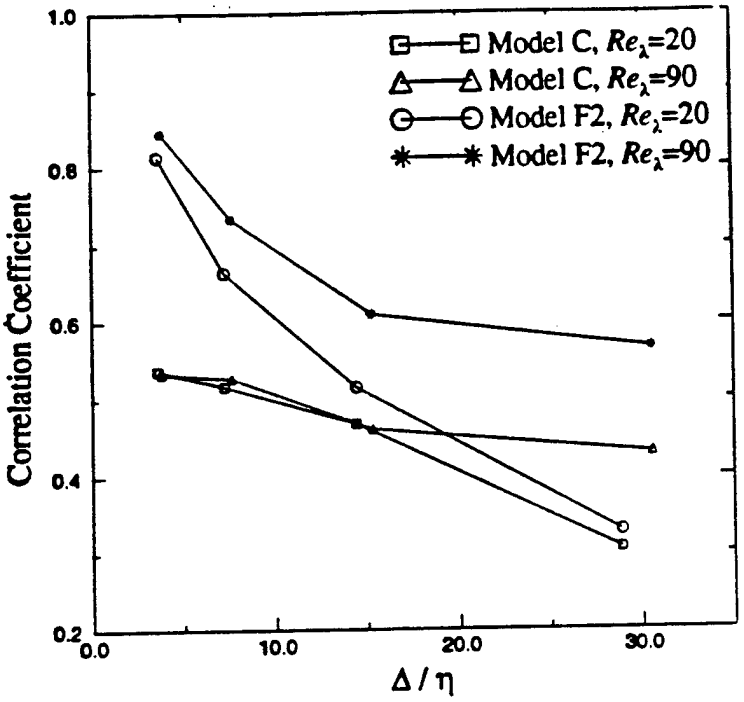

c)

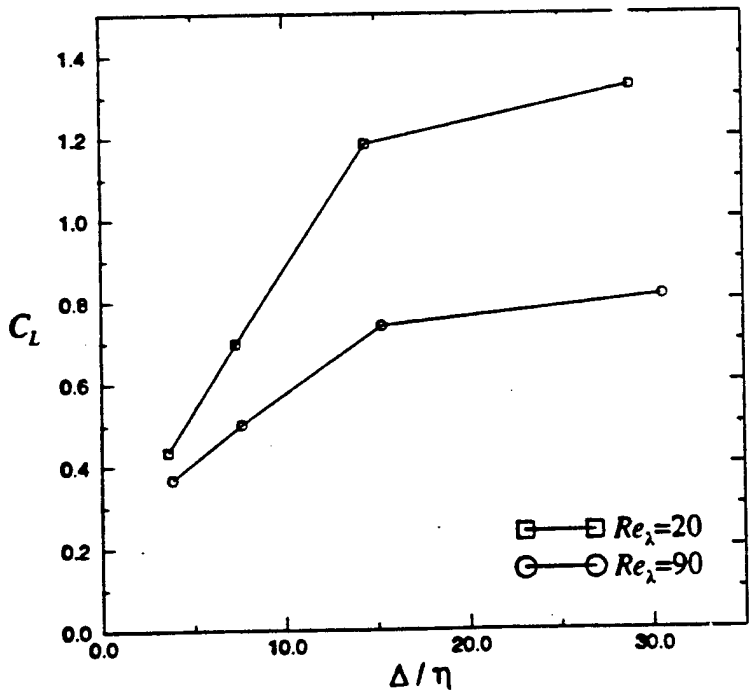

d)

Figure 6 (cont.)

a)

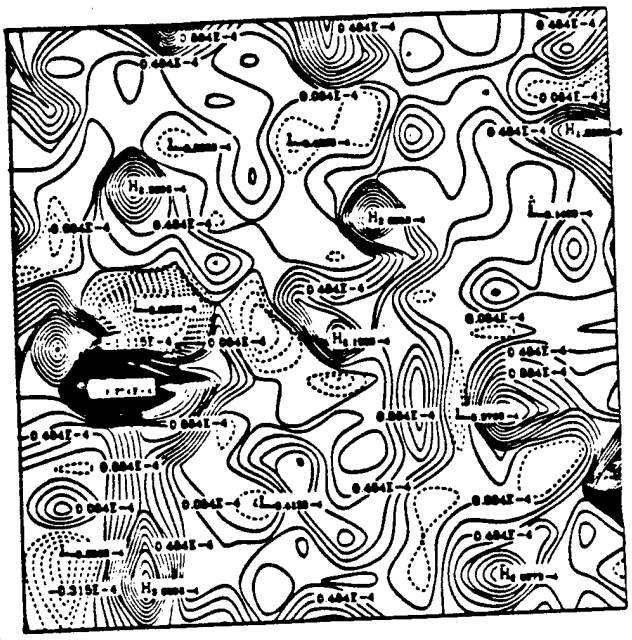

b)

Figure 7

a)

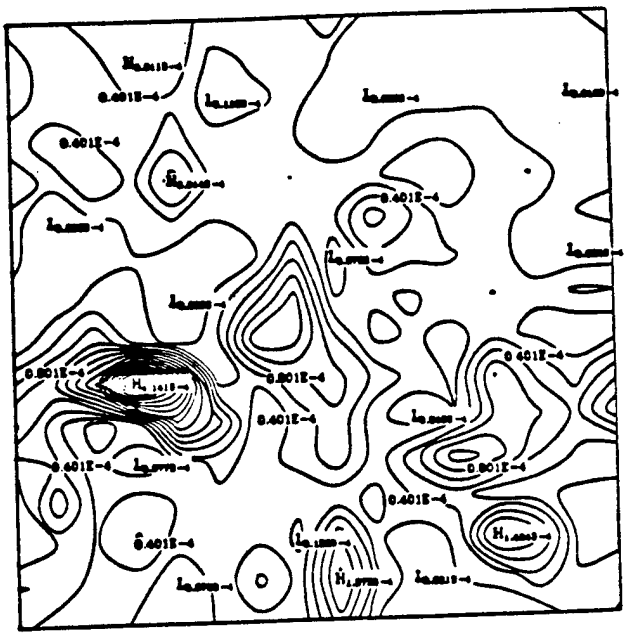

b)

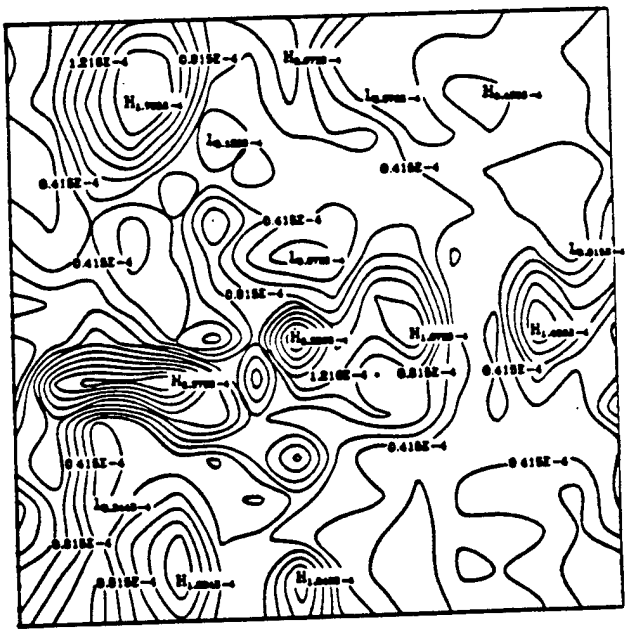

Figure 8

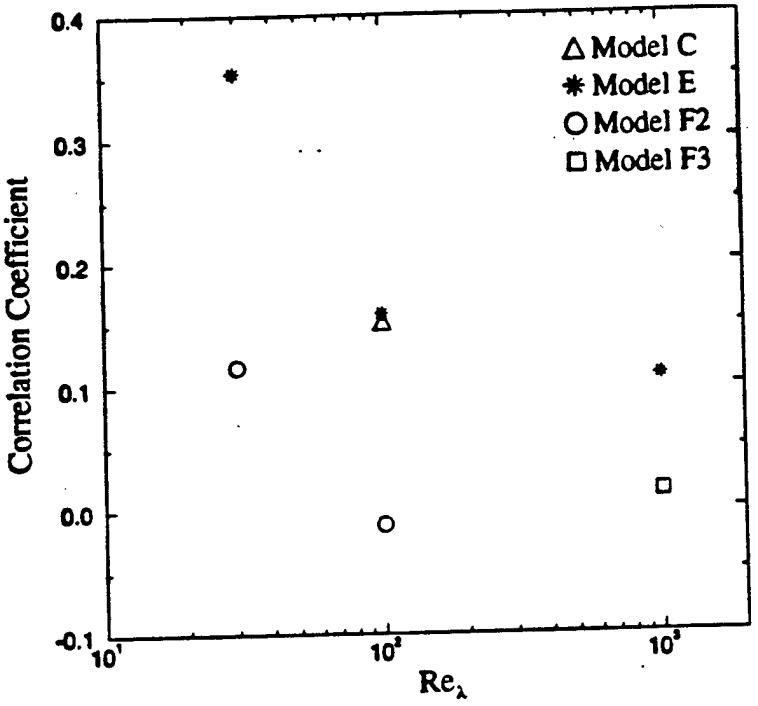
Model C
Model E
Model F2
Model F3
Correlation Coefficient
0.4
0.3
0.2
0.1
0.0
-0.1
10^1
10^2
10^3
Re_λ

a)

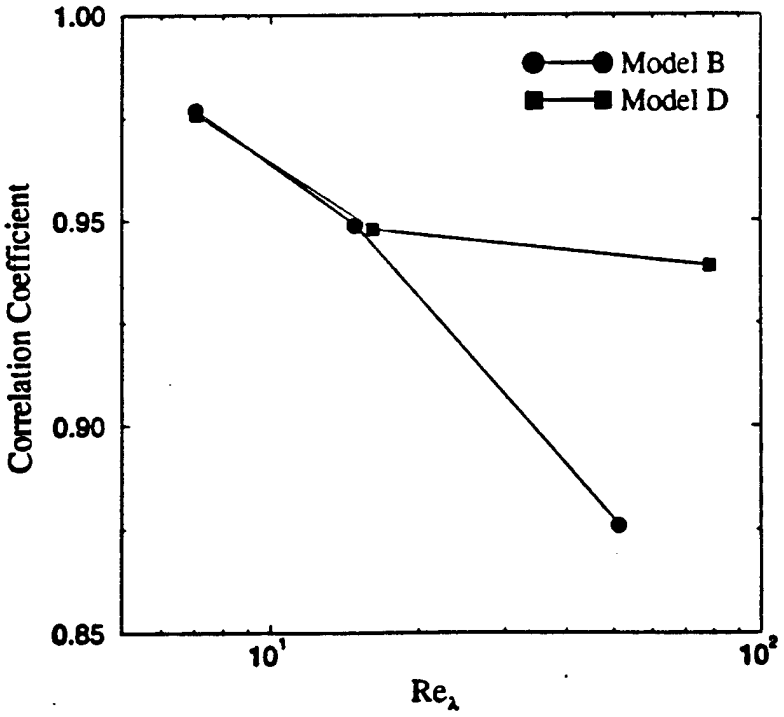
Model B
Model D
Correlation Coefficient
1.00
0.95
0.90
0.85
10^1
10^2
Re_λ

b)

Figure 9

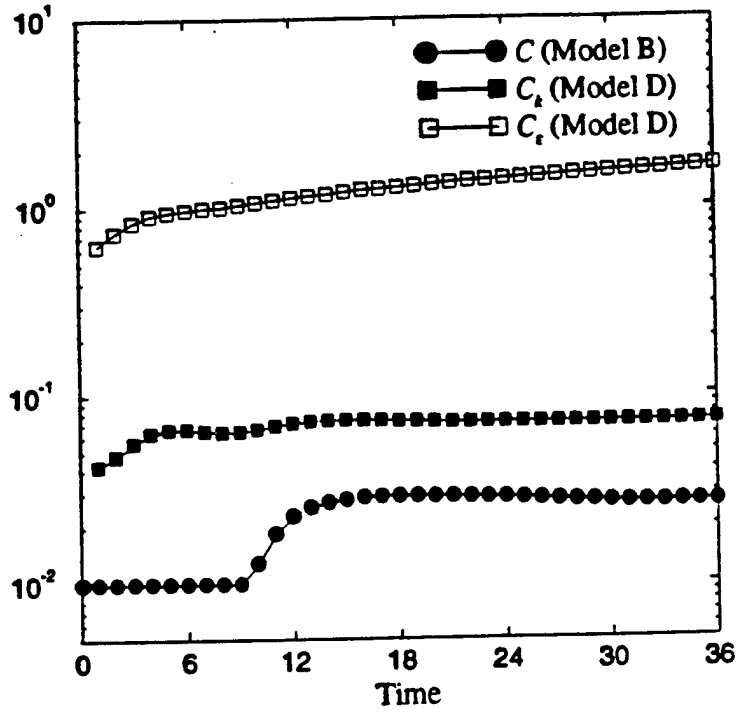
10^1
10^0
10^{-1}
10^{-2}
C (Model B)
C_k (Model D)
C_ε (Model D)
0
6
12
18
24
30
36
Time

a)

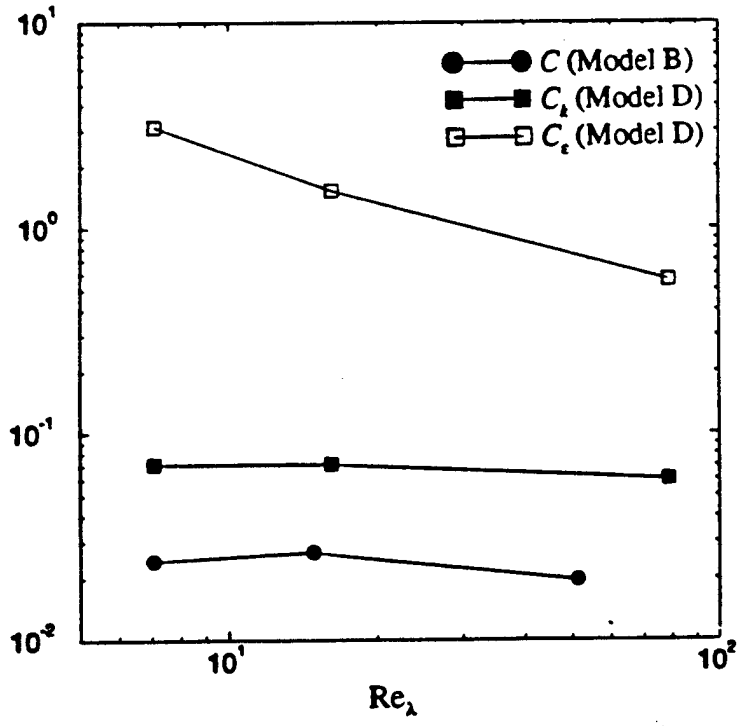
10^1
10^0
10^{-1}
10^{-2}
C (Model B)
C_k (Model D)
C_ε (Model D)
10^1
10^2
Re_λ

b)

Figure 10

AIAA 95-0356
A New Dynamic One-Equation Subgrid-Scale Model for Large Eddy Simulations

Won-Wook Kim
Suresh Menon
School of Aerospace Engineering
Georgia Institute of Technology
Atlanta, Georgia

33rd Aerospace Sciences Meeting and Exhibit
January 9-12, 1995 / Reno, NV

A NEW DYNAMIC ONE-EQUATION SUBGRID-SCALE MODEL FOR LARGE EDDY SIMULATIONS

Won-Wook Kim* and Suresh Menon**
School of Aerospace Engineering
Georgia Institute of Technology

Abstract

A new formulation of the local dynamic model associated with the subgrid-scale (SGS) kinetic energy equation closure (local dynamic *k*-equation subgrid-scale; LDKSGS) has been tested. The results are compared with direct numerical simulation (DNS), Germano *et al.*'s (1991) dynamic algebraic subgrid-scale (DASGS) model and a locally averaged (based on vortical structure) dynamic *k*-equation subgrid-scale (DKSGS) model which has been introduced by the present authors. Basic properties of the model have been studied using Taylor-Green vortex flows. By preserving the almost exact spatial locality, the local dynamic one-equation model predicts the turbulent flow field more accurately than the other models tested. In addition, this model has proven to be efficient with lower computational cost than the locally averaged DKSGS model. Further study is underway to investigate the robustness of this new local dynamic model by applying it to more complex flows, such as a rearward facing step.

1. Introduction

The dynamic SGS model, introduced by Germano *et al.*, has been successfully applied to various types of flow fields (see Moin *et al.*, 1994 for a recent review). Two desirable features of this model are emphasized. Firstly, the model coefficient is neither prescribed *a priori* nor remains a constant, rather, it is determined as a part of the solution. This model removed a major drawback of the earlier eddy viscosity type SGS models which was their inability to model correctly the unresolved subgrid stresses in different types of turbulent flow fields with a single *universal* constant. Secondly, as a result of the dynamic evaluation, the model coefficient can become negative in certain regions of the flow field and thus, appears to have the capability to mimic backscatter of energy from the subgrid-scales to the resolved scales.

Although it has been shown that this model is superior to the conventional fixed-coefficient model, the dynamic method still has some drawbacks. These drawbacks appear to originate from a weakness of the Smagorinsky model used in Germano *et al.*'s dynamic model as well as from the mathematically inconsistent derivation and the ill-conditioning of the dynamic formulation itself. The Smagorinsky's time-independent, algebraic eddy viscosity model used in Germano *et al.*'s dynamic model is derived by assuming local equilibrium between the SGS energy production and dissipation rate. Thus, non-local and history effects of the turbulence evolution are completely neglected in this model. In this work, we use a transport equation for the subgrid-scale kinetic energy coupled with the dynamic formulation. The direct computation of the SGS kinetic energy implemented in this model is expected to account for the local details of the flow structure and the turbulence development history. It is well known that the dynamic model employing Germano *et al.*'s mathematical identity cannot guarantee stable numerical simulations. One possible (and the most popular) way to stabilize the simulations is achieved by spatial averaging of the model coefficient in directions of flow homogeneity. In this work, we develop a generally applicable averaging scheme applied over local structures defined in terms of vorticity rather than directions of homogeneity.

Although the above noted local averaging method and other similar methods (e.g., Meneveau *et al.*, 1994) have shown good results, this local averaging approach is still, in general, unacceptable because local averaging is carried out only to avoid numerical instability, and has nothing to do with the dynamic method. Therefore, a truly robust dynamic model must be able to provide a stable and accurate solution using local values of the coefficient that vary both in space and time. In the present study, the mathematical inconsistency and the ill-conditioning problem that occurs when employing Germano *et al.*'s mathematical identity in the dynamic approach is eliminated by introducing a new local dynamic formulation associated with the one-equation SGS model. This model provides a straightforward localized evaluation of the model coefficients and does not cause numerical instability.

In this paper, two dynamic models based on the one-equation SGS closure (DKSGS and LDKSGS) and Germano *et al.*'s DASGS model are evaluated by comparing results with high resolution DNS data from Taylor-Green vortex flow.

2. Subgrid-scale modeling

In physical space, the incompressible Navier-Stokes equations are filtered using a spatial filter of characteristic width $\overline{\Delta}$ (typically, the grid resolution) resulting in the filtered LES equations:

$$\frac{\partial \overline{u}_i}{\partial x_j} = 0 \tag{1}$$

$$\frac{\partial \overline{u}_i}{\partial t} + \overline{u}_j \frac{\partial \overline{u}_i}{\partial x_j} = -\frac{\partial}{\partial x_j}\left(\overline{p}\delta_{ij} + \tau_{ij}\right) + \nu \frac{\partial^2 \overline{u}_i}{\partial x_j \partial x_j} \tag{2}$$

where $\overline{u}_i(x_i, t)$ is the resolved velocity field and the subgrid-scale (SGS) stress tensor τ_{ij} is defined as: $\tau_{ij} = \overline{u_i u_j} - \overline{u}_i \overline{u}_j$. It has been shown that the proper choice of filter is essential to maintain model consistency (Piomelli *et al.*, 1988). Various types of filtering processes have been studied in the past, such as

* Graduate Research Assistant, Student Member AIAA.
** Associate Professor, Senior Member AIAA.

top-hat, Gaussian and Fourier cut-off (Liu *et al.*, 1993; Piomelli *et al.*, 1988). In the present study, we employ the top-hat filter which is considered appropriate for finite-difference methods.

2.1. *Dynamic Algebraic Subgrid-Scale (DASGS) Model*

Currently, the most popular subgrid-scale model is the algebraic eddy viscosity model originally proposed by Smagorinsky (1963);

$$\tau_{ij} = -2\nu_T \overline{S}_{ij} + \tfrac{1}{3}\delta_{ij}\tau_{kk} \tag{3}$$

where, $\nu_T = c_s^2 \overline{\Delta}^2 |\overline{S}|$ is the subgrid eddy viscosity, c_s is the Smagorinsky's constant,

$$\overline{S}_{ij} = \frac{1}{2}\left(\frac{\partial \overline{u}_i}{\partial x_j} + \frac{\partial \overline{u}_j}{\partial x_i}\right) \tag{4}$$

is the resolved scale strain rate tensor and $|\overline{S}| = (2\overline{S}_{ij}\overline{S}_{ij})^{\frac{1}{2}}$. The *constant* c_s requires adjustment for different flows. A large number of studies have been devoted to fine-tuning c_s for various flows of interest. This problem was circumvented recently by using a dynamic procedure (Germano *et al.*, 1991) which implements a direct evaluation of the model coefficient, c_s^2. In the dynamic modeling approach, a mathematical identity between the stresses resolved at the grid scale filter $\overline{\Delta}$ and a test filter $\hat{\Delta}$ (typically, $\hat{\Delta} = 2\overline{\Delta}$) is used to determine the model coefficient c_s^2. Thus if the application of the test filter on any variable ϕ is denoted by $\hat{\phi}$ or $<\phi>$, it can be shown that:

$$L_{ij} = T_{ij} - \hat{\tau}_{ij} = \left\langle \overline{u}_i \overline{u}_j \right\rangle - \hat{\overline{u}}_i \hat{\overline{u}}_j . \tag{5}$$

Here, $T_{ij} = \left\langle \overline{u}_i \overline{u}_j \right\rangle - \hat{\overline{u}}_i \hat{\overline{u}}_j$ is defined using the test filter. Assuming self-similarity of the subgrid stresses, one can model T_{ij} in the same way as τ_{ij}:

$$T_{ij} = -2\nu_T \hat{\overline{S}}_{ij} + \tfrac{1}{3}\delta_{ij} T_{kk} \tag{6}$$

where $\nu_T = c_s^2 \hat{\Delta}^2 |\hat{\overline{S}}|$. Combining Eqs. (3), (5) and (6), an equation for c_s^2 can be obtained:

$$L_{ij} - \tfrac{1}{3}\delta_{ij} L_{kk} = 2c_s^2 M_{ij} \tag{7}$$

where

$$M_{ij} = -\left(\hat{\Delta}^2 |\hat{\overline{S}}| \hat{\overline{S}}_{ij} - \overline{\Delta}^2 \left\langle |\overline{S}| \overline{S}_{ij} \right\rangle\right). \tag{8}$$

Eq. (7) is a set of five independent equations for one unknown c_s^2. To minimize the error that can occur solving this over-determined system, Lilly (1992) proposed a least square method which yields

$$c_s^2 = \frac{1}{2}\frac{L_{ij} M_{ij}}{M_{ij} M_{ij}}. \tag{9}$$

In this paper, we refer to this original formulation of the dynamic modeling coupled with Smagorinsky model as the dynamic algebraic subgrid-scale (DASGS) model.

2.2. *Dynamic k-Equation Subgrid-Scale (DKSGS) Model*

A one-equation model for the subgrid-scale kinetic energy, $k_{sgs} = \frac{1}{2}\left(\overline{u_i^2} - \overline{u}_i^2\right)$, in the following form (e.g. Yoshizawa, 1993),

$$\frac{\partial k_{sgs}}{\partial t} + \overline{u}_i \frac{\partial k_{sgs}}{\partial x_i} = -\tau_{ij}\frac{\partial \overline{u}_i}{\partial x_j} - \varepsilon + \frac{\partial}{\partial x_i}\left(\nu_T \frac{\partial k_{sgs}}{\partial x_i}\right) \tag{10}$$

has been studied recently (Menon and Yeung, 1994; Menon *et al.*, 1994). Here the three terms on the right-hand-side of Eq. (10) represent, respectively, the production rate, the dissipation rate and the transport rate of k_{sgs}. The subgrid stresses τ_{ij} are modeled in terms of the SGS eddy viscosity ν_T as:

$$\tau_{ij} = -2\nu_T \overline{S}_{ij} + \tfrac{2}{3}\delta_{ij} k_{sgs}, \tag{11}$$

where,

$$\nu_T = c_\nu k_{sgs}^{\frac{1}{2}} \overline{\Delta}. \tag{12}$$

As shown Eq. (12), ν_T has the form which is used in standard one-equation models of turbulence. Eq. (10) is closed by providing a model for the dissipation rate term, ε. By simple scaling arguments, ε is usually modeled as,

$$\varepsilon = c_\varepsilon \frac{k_{sgs}^{\frac{3}{2}}}{\overline{\Delta}}. \tag{13}$$

An important feature of this model is that no assumption of local equilibrium between the subgrid-scale energy production and dissipation rate has been made. That is, the direct computation of the subgrid-scale kinetic energy implemented in this model can account for some non-local and history effects which are completely neglected in the algebraic model described in section 2.1. Therefore, it is expected that this model will give better predictions of the eddy viscosity than the algebraic model.

In the present study, we apply the dynamic modeling method to the k-equation subgrid-scale model to obtain appropriate values of the coefficients c_ν and c_ε. To implement this method, the turbulent kinetic energy at the test filter level is obtained from the trace of Eq. (5), $K = L_{kk}/2 + \hat{k}_{sgs}$. Using a procedure similar to that outlined in Section 2.1, an equation for c_ν can be derived:

$$L_{ij} - \tfrac{1}{3}\delta_{ij} L_{kk} = 2c_\nu M_{ij} \tag{14}$$

where

$$M_{ij} = -\left(\hat{\Delta}\hat{K}^{\frac{1}{2}}\hat{\overline{S}}_{ij} - \overline{\Delta}\left\langle k_{sgs}^{\frac{1}{2}} \overline{S}_{ij} \right\rangle\right). \tag{15}$$

Eq. (14) has the same form as Eq. (7), so c_ν can be determined in a similar manner using the least-square method:

$$c_\nu = \frac{1}{2}\frac{L_{ij} M_{ij}}{M_{ij} M_{ij}}. \tag{16}$$

A mathematical identity similar to Eq. (5) between the dissipation rate resolved at the grid scale filter level,

$\varepsilon = \nu\left(\overline{\frac{\partial u_i}{\partial x_j}\frac{\partial u_i}{\partial x_j}} - \frac{\partial \overline{u}_i}{\partial x_j}\frac{\partial \overline{u}_i}{\partial x_j}\right)$, and the test filter level, $E = \nu\left(\left\langle\overline{\frac{\partial u_i}{\partial x_j}\frac{\partial u_i}{\partial x_j}}\right\rangle - \frac{\partial \hat{\overline{u}}_i}{\partial x_j}\frac{\partial \hat{\overline{u}}_i}{\partial x_j}\right)$, can be obtained as,

$$F = E - \hat{\varepsilon} = \nu\left(\left\langle\frac{\partial \overline{u}_i}{\partial x_j}\frac{\partial \overline{u}_i}{\partial x_j}\right\rangle - \frac{\partial \hat{\overline{u}}_i}{\partial x_j}\frac{\partial \hat{\overline{u}}_i}{\partial x_j}\right). \quad (17)$$

This identity is used to evaluate the dissipation rate model coefficient c_ε,

$$F = c_\varepsilon G \quad (18)$$

where,

$$G = \left(\frac{\hat{K}^{\frac{3}{2}}}{\Delta} - \left\langle\frac{k_{sgs}^{\frac{3}{2}}}{\Delta}\right\rangle\right). \quad (19)$$

Note that Eq. (18) is a scalar equation for a single unknown and, hence, the exact value c_ε can be obtained without applying the least square method

$$c_\varepsilon = \frac{F}{G}. \quad (20)$$

2.3. Local averaging of model coefficients

It has been reported by many authors that the evaluation of the coefficient in Germano *et al.*'s (1991) dynamic model can result in numerical instability. The sources of instability appear to be the ill-conditioning of the model coefficient (because the denominator of the expression for the model coefficient becomes very small at some points in the flow) and the prolonged presence of negative model coefficients at some locations. This problem has been circumvented by spatially averaging the expression for the model coefficient in directions of flow homogeneity (Germano *et al.*, 1991). Recently, Meneveau *et al.* (1994) suggested an averaging scheme applied along particle trajectories rather than directions of homogeneity. This model is based on the hypothesis that the SGS model coefficient at a given point should depend in some way on the history of the flow along the trajectory leading to that point because turbulent eddies are expected to evolve along this pathline. This model is superior to the conventional spatial-averaging schemes in that it retains some local details of the flow structure and the turbulence development history, both of which are ignored in the conventional averaging schemes.

In this study, a new and simple local averaging technique has been developed. This technique is based on the assumption that the main dynamic mechanism determining the local property of the turbulent flow occurs inside local structures. It seems natural to define these local structures in terms of vorticity since turbulent flow is characterized by random three-dimensional vorticity fluctuations. In the present study, to carry out local averaging based on the extraction of local vortical structures, a cubic box with 9^3 grid points is chosen surrounding a given point in the flow field, and the location of the maximum vorticity magnitude is determined. The local structure is then identified by determining all the grid points within the control volume where the vorticity-magnitude is greater than 25% of the maximum. The model coefficients are computed by volume averaging inside this local structure. As a result of this local averaging procedure, the model coefficients vary from point-to-point. This variation is smooth so that no numerical oscillation occurs.

Although the behavior of the above noted locally averaged dynamic one-equation model is reasonable (as discussed below), the concept of local averaging (whether based on local structures or direction of homogeneity) is still an artifact that is employed primarily to avoid the numerical instability. Furthermore, the local averaging method is inconsistent with the dynamic procedure. A true dynamic model should evaluate the model coefficients locally without any *ad hoc* averaging. In the following section, we describe a new dynamic model that does not employ averaging, and where the coefficients are used locally without causing numerical instability.

2.4. Local Dynamic k-Equation Subgrid-Scale (LDKSGS) Model

While Germano *et al.*'s formulation for the dynamic model has been used widely and successfully, it still has some problems. Firstly, in spite of large spatial variation of the model coefficient's value, it is taken out of the filtering operation as if it were a constant. Local values of the model coefficient are then determined as a function of position. This mathematical inconsistency can decrease the accuracy of the dynamic model. Secondly, *ad hoc* spatial averaging has been adopted, without any physical justification, for the purpose of stabilizing a numerical simulation of the model. It has subsequently been shown by Ghosal *et al.* (1993) that, for flows with directions of homogeneity, the solution for the model coefficient obtained using this seemingly *ad hoc* averaging operation is the same as that obtained from a more rigorous variational formulation of the dynamic model. While this averaging scheme proved to be effective in controlling possible instabilities and led to accurate results, it prevents the dynamic model from possessing straightforward localization. Ghosal *et al.* (1993) also proposed a local dynamic model which seems to be applicable to inhomogeneous flows. However this model was implemented in a complicated manner by employing the original Germano *et al.*'s dynamic model with two integral equations obtained from a variational formulation (which are solved by an expensive iterative procedure) and one auxiliary transport equation for subgrid-scale kinetic energy that is used to constrain the Smagorinsky's model coefficient.

We propose a different approach to dynamic modeling associated with the one-equation SGS model in order to eliminate the deficiencies of Germano *et al.*'s formulation described above. Consider some scales related to different energy levels as follows:

	Grid filter level		Test filter level		
Energy level	$\overline{u_i u_i}$	$\overline{\bar{u}_i \bar{u}_i}$	$\langle u_i u_i \rangle$	$\langle \overline{u_i u_i} \rangle$	$\hat{\bar{u}}_i \hat{\bar{u}}_i$
Stress tensor	$\overline{u_i u_j}$	$\overline{\bar{u}_i \bar{u}_j}$	$\langle u_i u_j \rangle$	$\langle \overline{u_i u_j} \rangle$	$\hat{\bar{u}}_i \hat{\bar{u}}_j$
Dissipation rate level	$\overline{\frac{\partial u_i}{\partial x_j}\frac{\partial u_i}{\partial x_j}}$	$\frac{\partial \bar{u}_i}{\partial x_j}\frac{\partial \bar{u}_i}{\partial x_j}$	$\left\langle \frac{\partial u_i}{\partial x_j}\frac{\partial u_i}{\partial x_j} \right\rangle$	$\left\langle \frac{\partial \bar{u}_i}{\partial x_j}\frac{\partial \bar{u}_i}{\partial x_j} \right\rangle$	$\frac{\partial \hat{\bar{u}}_i}{\partial x_j}\frac{\partial \hat{\bar{u}}_i}{\partial x_j}$
Length scale	Not available	$\bar{\Delta}$	Not available	Not available	$\hat{\Delta}$
Strain rate	Not available	$\lvert \bar{S} \rvert$	Not available	Not available	$\lvert \hat{\bar{S}} \rvert$

At the grid filter level, there are two energy levels characterized by the filtered kinetic energy $\overline{u_i u_i}$ and the resolved kinetic energy $\bar{u}_i \bar{u}_i$ (the factor $\frac{1}{2}$ is neglected in the following discussion for brevity). The SGS kinetic energy k_{sgs} is then determined by the difference between these two energy levels, i.e., $2k_{sgs} = \overline{u_i u_i} - \bar{u}_i \bar{u}_i$. Since the energy $\bar{u}_i \bar{u}_i$ is resolved on the grid scale $\bar{\Delta}$, the characteristic length scale for this energy is $\bar{\Delta}$. However, the characteristic length scale (say λ) for the energy level $\overline{u_i u_i}$ is unknown and furthermore, since $\overline{u_i u_i} > \bar{u}_i \bar{u}_i$ and $\overline{u_i u_i}$ contains the SGS kinetic energy, it is clear that $\lambda < \bar{\Delta}$. Thus, the characteristic length scale for the energy $\overline{u_i u_i}$ lies in the unresolved range of scales. Whereas $\bar{\Delta}$ is related to the production rate of SGS kinetic energy, λ is related to the dissipation rate. The separation between the scales where SGS kinetic energy is produced and where it is dissipated explains why the model for $\varepsilon \propto k_{sgs}^{3/2} / \bar{\Delta}$ is somewhat poor. Clearly, for proper modeling of the production and dissipation of SGS kinetic energy, it is necessary to have additional information on the energy transfer occurring at these two length scales. However the information on the smaller scale is not available. Therefore an additional assumption (similar to that used in the standard k-equation model) that the energy transfer rate which occurs at the smaller scale is essentially determined by the rate of the larger scale, and the energy determined by both energy transfers is required. Finally, the length scale and strain rate of the larger scale, and the energy level difference are needed to model not only the production rate of the SGS kinetic energy (or the SGS stress tensor on which the SGS kinetic energy production mechanism depends) but also the dissipation rate.

The definitions and relations obtained on the grid filter level can be extended to the test filter level as long as the scales are defined in a similar manner. As in the above discussion, the energy level $\hat{\bar{u}}_i \hat{\bar{u}}_i$ is resolved at the test filter level ($2\bar{\Delta}$) whereas the characteristic length scale (say $\hat{\lambda}$) for the energy $\langle \overline{u_i u_i} \rangle$ is unknown, and again $\langle \overline{u_i u_i} \rangle > \hat{\bar{u}}_i \hat{\bar{u}}_i$ and $\hat{\lambda} < 2\bar{\Delta}$. However, at the test filter level, an additional similarly-defined length scale is available. This scale (say δ) related to the energy level $\langle \bar{u}_i \bar{u}_i \rangle$, which can be computed, is larger than $\hat{\lambda}$.

We can consider three different SGS stress tensors and dissipation rates, one at the grid filter level and the other two at the test filter level:

$$\begin{aligned} \tau_{ij} &= \overline{u_i u_j} - \bar{u}_i \bar{u}_j \\ &= 2c_t \bar{\Delta} \left[\tfrac{1}{2} \left(\overline{u_i u_i} - \bar{u}_i \bar{u}_i \right) \right]^{\frac{1}{2}} \bar{S}_{ij} + \tfrac{2}{3} \delta_{ij} \left[\tfrac{1}{2} \left(\overline{u_i u_i} - \bar{u}_i \bar{u}_i \right) \right] \end{aligned} \tag{21a}$$

$$\begin{aligned} T_{ij} &= \langle \overline{u_i u_j} \rangle - \hat{\bar{u}}_i \hat{\bar{u}}_j \\ &= -2c_t \hat{\Delta} \left[\tfrac{1}{2} \left(\langle \overline{u_i u_i} \rangle - \hat{\bar{u}}_i \hat{\bar{u}}_i \right) \right]^{\frac{1}{2}} \hat{S}_{ij} + \tfrac{2}{3} \delta_{ij} \left[\tfrac{1}{2} \left(\langle \overline{u_i u_i} \rangle - \hat{\bar{u}}_i \hat{\bar{u}}_i \right) \right] \end{aligned} \tag{21b}$$

$$\begin{aligned} t_{ij} &= \langle \bar{u}_i \bar{u}_j \rangle - \hat{\bar{u}}_i \hat{\bar{u}}_j \\ &= 2c_t \hat{\Delta} \left[\tfrac{1}{2} \left(\langle \bar{u}_i \bar{u}_i \rangle - \hat{\bar{u}}_i \hat{\bar{u}}_i \right) \right]^{\frac{1}{2}} \hat{S}_{ij} + \tfrac{2}{3} \delta_{ij} \left[\tfrac{1}{2} \left(\langle \bar{u}_i \bar{u}_i \rangle - \hat{\bar{u}}_i \hat{\bar{u}}_i \right) \right] \end{aligned} \tag{21c}$$

$$\begin{aligned} \varepsilon &= \nu \left(\overline{\frac{\partial u_i}{\partial x_j} \frac{\partial u_i}{\partial x_j}} - \frac{\partial \bar{u}_i}{\partial x_j} \frac{\partial \bar{u}_i}{\partial x_j} \right) \\ &= c_\varepsilon \left[\tfrac{1}{2} \left(\overline{u_i u_i} - \bar{u}_i \bar{u}_i \right) \right]^{\frac{3}{2}} / \bar{\Delta} \end{aligned} \tag{22a}$$

$$\begin{aligned} E &= \nu \left(\left\langle \overline{\frac{\partial u_i}{\partial x_j} \frac{\partial u_i}{\partial x_j}} \right\rangle - \frac{\partial \hat{\bar{u}}_i}{\partial x_j} \frac{\partial \hat{\bar{u}}_i}{\partial x_j} \right) \\ &= c_\varepsilon \left[\tfrac{1}{2} \left(\langle \overline{u_i u_i} \rangle - \hat{\bar{u}}_i \hat{\bar{u}}_i \right) \right]^{\frac{3}{2}} / \hat{\Delta} \end{aligned} \tag{22b}$$

$$\begin{aligned} e &= \nu \left(\left\langle \frac{\partial \bar{u}_i}{\partial x_j} \frac{\partial \bar{u}_i}{\partial x_j} \right\rangle - \frac{\partial \hat{\bar{u}}_i}{\partial x_j} \frac{\partial \hat{\bar{u}}_i}{\partial x_j} \right). \\ &= c_\varepsilon \left[\tfrac{1}{2} \left(\langle \bar{u}_i \bar{u}_i \rangle - \hat{\bar{u}}_i \hat{\bar{u}}_i \right) \right]^{\frac{3}{2}} / \hat{\Delta} \end{aligned} \tag{22c}$$

As long as the cut-off is located inside the range where the scale similarity assumption is valid, c_t and c_ε in Eqs. (21) and (22) remain the same. Note that τ_{ij} and ε are the actual models implemented in the simulation. These two expressions contain two unknown model coefficients. Previously (see section 2.3) we adopted the expressions for T_{ij} and E to dynamically determine these unknowns. However this procedure introduced additional unknowns, $\langle \overline{u_i u_j} \rangle$ and $\left\langle \frac{\partial \bar{u}_i}{\partial x_j} \frac{\partial \bar{u}_i}{\partial x_j} \right\rangle$. Therefore, to close the model, one other independent relation (e.g. Germano *et al.*'s mathematical identity) is needed. At present we use the expressions for t_{ij} and e (instead of T_{ij} and E) which do not contain any additional unknowns. Then, both c_t and c_ε can be determined in the same manner as was done for c_ν and c_ε:

$$c_t = \frac{1}{2} \frac{t_{ij} \sigma_{ij}}{\sigma_{ij} \sigma_{ij}} \tag{23}$$

where

$$\sigma_{ij} = -\hat{\Delta}\left[\tfrac{1}{2}\left(\left(\overline{u_i u_i}\right) - \hat{\bar{u}}_i \hat{\bar{u}}_i\right)\right]^{\frac{1}{2}} \hat{\bar{S}}_{ij} \tag{24}$$

$$c_s = \frac{\sqrt{\left(\left\langle \frac{\partial \bar{u}_i}{\partial x_j}\frac{\partial \bar{u}_i}{\partial x_j}\right\rangle - \frac{\partial \hat{\bar{u}}_i}{\partial x_j}\frac{\partial \hat{\bar{u}}_i}{\partial x_j}\right)}}{\left[\tfrac{1}{2}\left(\left(\overline{u_i u_i}\right) - \hat{\bar{u}}_i \hat{\bar{u}}_i\right)\right]^{\frac{1}{2}} / \hat{\Delta}}. \tag{25}$$

The denominators of Eqs. (23) and (25) contain the energy information on the resolved scale which is always non-zero. Therefore, the ill-conditioning problem (observed in Germano *et al.*'s dynamic model) is not considered serious here. This local dynamic model is expected to be valid where Germano *et al.*'s model is valid since both use the same scale similarity assumption. The existence of the similarity between the SGS stress $\overline{u_i u_j} - \overline{u}_i \overline{u}_j$ and the resolved stress $\left\langle \overline{u_i u_j} \right\rangle - \hat{\bar{u}}_i \hat{\bar{u}}_j$ is supported by Liu *et al.*'s (1994) analysis using experimental data in the far field of a round jet at a reasonably high Reynolds number. In this work, a high correlation between the two stress tensors is obtained. The proposed new dynamic model is more effective in actual numerical implementation, cheaper in computational cost and appears more robust than both the averaging approach and Ghosal *et al.*'s inhomogeneous version of Germano *et al.*'s dynamic model.

3. Numerical method and application

In this section, we briefly describe the numerical method employed to solve the incompressible Navier-Stokes equations and the test case used to evaluate the proposed dynamic models.

3.1. Numerical method

To date, the most reliable simulations of turbulent flow have been performed with spectral methods because of the extremely high accuracy of these methods. However, spectral methods are difficult to use in complex geometries. They are also relatively complicated and are not the prevailing methods in existing application codes. Unlike spectral methods, finite-difference methods are simple to implement and are common in current application codes. The major shortcoming of finite-difference methods is that their accuracy level is inadequate for turbulence simulations. Rai and Moin (1991) suggested the high-order accurate upwind-biased method as a good candidate for direct simulations of turbulent flows associated with complex geometry. In this work, we use the non-staggered grid approach and simulations have been carried out using second-order accuracy in time and fifth-order (the convective terms) and sixth-order (the viscous terms) accuracy in space. This code was validated (Menon and Yeung, 1994; Menon *et al.*, 1994) by carrying out direct numerical simulations (DNS) of decaying isotropic turbulence and comparing the resulting statistics with the predictions of a well-known pseudo spectral code (Rogallo, 1981).

Time-accurate solutions of the incompressible Navier-Stokes equations are obtained by the artificial compressibility approach originally proposed by Chorin (1967). The basic idea behind artificial compressibility is to introduce a pseudo-time equation for the pressure through the continuity equation. The introduction of artificial compressibility alters the type of the system of incompressible equations to have properties similar to that of compressible flow and allows the extension of the well developed algorithms of compressible flow to incompressible problems. Originally, artificial compressibility was used for steady-state solutions. The time-accurate solution capability is obtained here by adding a pseudo-time derivative of the primitive variables to each corresponding equation (Rogers *et al.*, 1991). The artificial compressibility approach is applied only to the pseudo-time and the physical time behavior is not influenced as long as the solution converges to a *steady-state* for each physical time level.

The integration in pseudo-time is carried out by an explicit method based on a Runge-Kutta time-stepping scheme. At present, a 5-step scheme has been employed to obtain the maximum CFL number. Local time-steps (in pseudo-time), determined by the local stability limit, are also adopted to accelerate the convergence to a steady-state solution. A further significant improvement in convergence is achieved by incorporating the full approximation scheme (FAS) multigrid concept proposed by Brandt (1981). A typical convergence history is shown in Figure 1, comparing a two level multigrid to a single grid solution. The code has the capability of using up to 4 multigrid levels.

3.2. Application to Taylor-Green vortex flow

To evaluate the behavior of the dynamic SGS models, we need to compare the predicted LES results with the results of DNS. However, since DNS require a significant amount of computer resources (both memory and execution time), it can be applied only to a limited range of Reynolds numbers. This Reynolds number range can be increased by simulating a flow that has spatial symmetries (which are preserved in time as the flow evolves), because the information in a fractional part of the periodic box is sufficient to describe the whole flow field using these symmetries. This idea was exploited by Brachet *et al.* (1983) who simulated a Taylor-Green vortex flow and reduced the necessary memory by 1/64 compared with that required for a general non-symmetric periodic flow. In this work, we also simulated the so-called impermeable box ($0 \le x,y,z \le \pi$) of the Taylor-Green vortex flow that develops from the following initial condition:

$$u = \sin(x)\cos(y)\cos(z)$$
$$v = -\cos(x)\sin(y)\cos(z)$$
$$w = 0$$

At time $t=0$, the flow is two-dimensional but becomes three-dimensional for all times $t>0$. This flow is considered as a simple system in which the generation of small scales and the resulting turbulence can be studied.

4. Results and Discussion

Typical results are described below to highlight the behavior of the SGS models. We begin the study by carrying out high resolution DNS which are then used to evaluate the LES. Figure 2 shows the unscaled energy and dissipation spectra for a effectively 128^3 DNS data at $t=29$. At this time, the Taylor microscale Reynolds number Re_λ is approximately 32. In the range of wave numbers $k \le 10$, the energy spectrum conforms to the inertial $k^{-5/3}$ law with the dissipation spectrum having a peak at $k \approx 10$. At this resolution and for the chosen initial Re=1000,

the energy containing range and the dissipation range have a significant overlap (at very high Re, this should separate widely). This is similar to the results of Domaradzki *et al.* (1993) which were obtained at $Re_\lambda \approx 70$. Thus, the Reynolds number used in this simulation is just high enough to capture the beginnings of the inertial range dynamics but too low to separate it from the effects of the dissipation range dynamics.

Figure 3 shows the Kolmogorov scaled energy transfer for the 128^3 DNS, and for 64^3 and 32^3 LES using the DKSGS model with local averaging and the DASGS model with constrained local averaging at t=29. All LES simulations were performed by first filtering the 128^3 DNS flow field into the LES grid using the top-hat filter at t=9. Thus, at t=9, all flow variables (e.g., velocities and pressure) were highly correlated in the physical space. As observed in other studies, the subsequent evolution of the flow field in the LES simulation will not remain correlated with DNS data. Therefore, point-to-point correlation between the energy transfer predicted by DNS and the energy transfer predicted by LES is expected to be low. However, if the dynamic models guarantee the self-consistency of the LES, then it is expected that the Kolmogorov-scaled spectra computed in DNS and LES will be similar. This is observed and is presented in Figure 3.

To determine whether the flow fields in consecutive resolutions have some similarity, which is the basic assumption adopted in the dynamic modeling formulation using two filter levels, we investigate the relative behavior of two energy transfers (the production and dissipation rates of the SGS kinetic energy) related to each resolution. The energy transfer appears an appropriate choice to check the similarity, since the property of the turbulence is determined by the energy cascade mechanism. In particular, the relative behavior of the production and dissipation rates of the SGS kinetic energy, which are related to the different scales, is expected to represent this energy cascade in some scale range. Figure 4 shows the ratio between these two energy transfers at three different resolutions (64^3, 32^3 and 16^3) as computed from the 128^3 DNS data. For the 64^3 LES using the dynamic model, the information from the 32^3 grid level is needed for test filter level information. Further the information on the 16^3 grid level is used in the 32^3 LES. According to this figure, we have similar energy transfers between 32^3 and 16^3 grid levels (the ratios remain in the same range). However, it is observed that there are different energy transfer mechanisms between 64^3 and 32^3 grid levels. This means that the similarity law is not valid in the 64^3 simulation, especially after $t \approx 19$. Hence LES using dynamic models is expected to give poor results at this resolution and time range.

To evaluate the performance of the SGS models, we compare the time evolution of the velocity-derivative (here, we use $\partial w/\partial z$), skewness S, and flatness F, factors computed from DNS and LES data. The skewness and flatness are defined as follows (Vincent and Meneguzzi, 1991):

$$S = \frac{\left\langle (\partial w/\partial z)^3 \right\rangle}{\left\langle (\partial w/\partial z)^2 \right\rangle^{\frac{3}{2}}}$$

$$F = \frac{\left\langle (\partial w/\partial z)^4 \right\rangle}{\left\langle (\partial w/\partial z)^2 \right\rangle^{2}}$$

Note that $\langle \cdot \rangle$ denote ensemble averaging instead of test filtering here. Figures 5 and 6 show, respectively, the skewness and flatness evolution on the 64^3 grid level as a function of time. This grid level has the cut-off wave number at $k \approx 30$ which is located inside the dissipation range (see Figure 2). Actually, in simulations at this resolution, the role of the SGS models is not important because a significant dissipation scales are resolved even without the models. Without any obvious superiority, all SGS models contribute in a favorable way by pushing the low resolution simulations to represent the higher resolution results. It can be seen from both figures that the curves for 64^3 LES are always located between the curves for 128^3 and 64^3 DNS. As noted previously, all LES results begin to deviate from the 128^3 DNS results after t=21.

In figure 7, the modeled production and dissipation rates are compared to the exact values computed from the DNS data. While the production rates are reasonably modeled, there is relatively poor agreement between the exact and the modeled dissipation rates.

Figure 8 and 9 show the velocity derivative skewness and flatness computed from the 32^3 LES. There is now a clear difference in the results of different models; the one-equation model is behaving better than the algebraic model. More interestingly, it can be seen that the local dynamic model predicts a more realistic flow field than the locally averaged dynamic model.

The reason for the difference in predictions between the locally averaged DKSGS and LDKSGS is addressed in Figure 10. The LDKSGS model shows an improved prediction of the energy transfer, especially for dissipation prediction. These improvements seem to originate from the fact that, in the LDKSGS model, the turbulent intermittency effects can be retained by not employing spatial averaging. Since the dissipation mechanism is dominated by the scales smaller than the scales determining the production, it has a higher level of intermittency than the production mechanism. Therefore, LDKSGS can improve the prediction of the dissipation significantly.

Figures 11 and 12 show the temporal variation of the various dynamically determined coefficients. In the actual simulations, the local values of the coefficients (obtained locally as in LDKSGS model or by local averaging as in the DKSGS and DASGS models) were employed. However, to simplify comparisons, the global coefficients (obtained by averaging over the whole flow field) are shown in Figures 11 and 12. It was observed during the simulations, that the model coefficients can become locally negative. In the LES using the locally averaged (DKSGS) and local (LDKSGS) one-equation models, negative coefficients (i.e. $c_\nu < 0$ and $c_\epsilon < 0$) do not cause numerical instability (note that $k_{sgs} \geq 0$ always for these cases). However, LES using the DASGS model becomes unstable when $c_S^2 < 0$. Therefore, the DASGS model constrained the coefficients to non-negative values (constrained local averaging). This

demonstrates that the DASGS model is more restrictive when using local coefficients.

When the model coefficients become negative (e.g., $c_v < 0$ and $c_l < 0$), the model backscatters. To estimate this backscatter, we require information about the energy contained within the subgrid-scale. Thus when the subgrid kinetic energy vanishes, backscatter should vanish. This is automatically satisfied with one-equation models since the eddy viscosity is modeled in terms of the subgrid kinetic energy whereas in the algebraic model, backscatter may occur (due to $c_s^2 < 0$) thereby resulting in numerical instability. Another interesting observation from Figures 11 and 12 is that the coefficient computed using the LDKSGS model are usually smaller in magnitude than the coefficients computed using the locally averaged model (DKSGS). For the LDKSGS model, this is due to the local value of the coefficient becoming negative in increased regions of the flow and lowers the average value. The variation of the dissipation model coefficient is similar for both one-equation models at 64^3 resolution. However, their values at the 32^3 grid level differ significantly.

5. Conclusions

A new formulation of the local dynamic model associated with the SGS kinetic energy equation closure has been tested. The results are compared with those from DNS, Germano *et al.*'s DASGS model and locally averaged (based on vortical structure) DKSGS model, which has been introduced by the present authors. Basic properties of the model have been studied using Taylor-Green vortex flows. By preserving the almost exact spatial locality, the local dynamic one-equation model predicts the turbulent flow field more accurately than the other models tested. Also, this model has proven to be very efficient in actual numerical implementations with lower computational cost than the locally averaged DKSGS model. We stress that the detailed study of similarity in consecutive resolutions (which is the base of dynamic modeling approaches using two filter levels) should be carried out to address the limit of dynamic models. In this study, we demonstrated that the ratio of the production and dissipation rates of the SGS kinetic energy is one way to check this similarity property.

Acknowledgments

This work is supported by the Office of Naval Research under Grant No. N00014-93-0342. Computing time was provided by the Numerical Aerodynamic Simulation (NAS) at NASA Ames Research Center and is gratefully acknowledged.

References

M. E. Brachet, D. I. Meiron, S. A. Orszag, B. G. Nickel, R. H. Morf and U. Frisch (1983), "Small-scale structure of the Taylor Green Vortex," J. Fluid Mech. 130, 411.

A. Brandt (1981), "Guide to multigrid development," in *Lecture Notes in Mathematics* 960, 220, Springer-Verlag Berlin.

A. J. Chorin (1967), "A numerical method for solving incompressible viscous flow problems," J. Comput. Phys. 2,12.

J. A. Domaradzki, W. Liu, and M. E. Brachet (1993), "An analysis of subgrid-scale interactions in numerically simulated isotropic turbulence," Phys. Fluids A 5, 1747.

M. Germano, U. Piomelli, P. Moin, and W. H. Cabot (1991), "A dynamic subgrid-scale eddy viscosity model," Phys. Fluids A 3, 1760.

S. Ghosal, T. S. Lund and P. Moin (1993), "A local dynamic model for Large eddy simulation," in Center for Turbulence Research Annual Research Briefs 1992, p. 3.

D. K. Lilly (1992), "A proposed modification of the Germano subgrid-scale closure method," Phys. Fluids 4, 633.

S. Liu, C. Meneveau and J. Katz (1994), "On the properties of similarity subgrid-scale models as deduced from measurements in a turbulent jet," J. Fluid Mech. 275, 83.

C. Meneveau, T. S. Lund and W. Cabot (1994), "A Lagrangian dynamic subgrid-scale model of turbulence," in Center for Turbulence Research Proceedings of the Summer Program 1994, p. 1.

S. Menon and P.-K. Yeung (1994), "Analysis of subgrid models using direct and large-eddy simulations of isotropic turbulence," presented at the 74th AGARD/FDP Symposium on Application of Direct and Large Eddy Simulation to Transition and Turbulence, Chania, Greece, April 18-21, 1994.

S. Menon, P.-K. Yeung and W.-W. Kim (1994), "Effect of subgrid models on the computed interscale energy transfer in isotropic turbulence," presented at the 25th AIAA Fluid Dynamics Conference, Colorado Springs, CO, June 20-23, 1994.

P. Moin, D. Carati, T. Lund, S. Ghosal, and K. Akselvoll (1994), "Developments and applications of dynamic models for large eddy simulation of complex flows," presented at the 74th AGARD/FDP Symposium on Application of Direct and Large Eddy Simulation to Transition and Turbulence, Chania, Greece, April 18-21, 1994.

U. Piomelli, P. Moin and J. H. Ferziger (1988), "Model consistency in large eddy simulation of turbulent channel flows," Phys. Fluids 31, 1884.

M. M. Rai and P. Moin (1991), "Direct simulations of turbulent flow using finite-difference schemes," J. Comput. Phys. 96, 15.

R. S. Rogallo (1981), "Numerical experiments in homogeneous turbulence," NASA Tech. Memo. 81315.

S. E. Rogers, D. Kwak, and C. Kiris (1991), "Steady and unsteady solutions of the incompressible Navier-Stokes equations," AIAA J. 29, 603.

A. Vincent and M. Meneguzzi (1991), "The spatial structure and statistical properties of homogeneous turbulence," J. Fluid Mech. 225, 1.

A. Yoshizawa (1993), "Bridging between eddy-viscosity-type and second-order models using a two-scale DIA," presented at the 9th symposium on Turbulent Shear Flows, Kyoto, Japan, August 16-18, 1993.

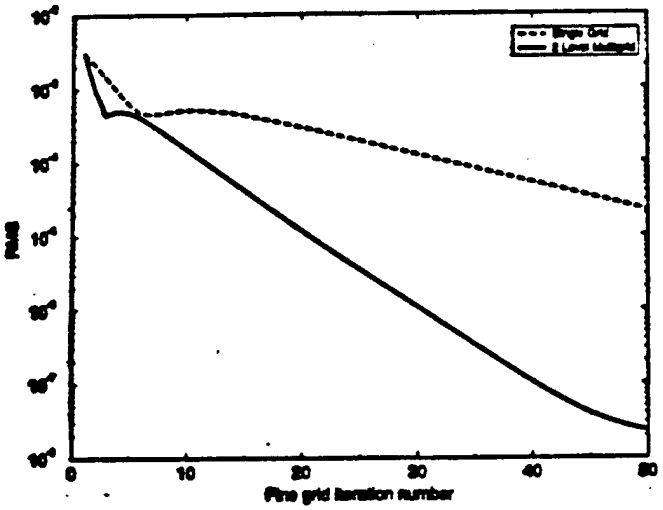

Figure 1. Convergence history during one physical time step on a 64^3 grid, plotted as root-mean-square of residuals (RMS) vs. fine grid iteration number.

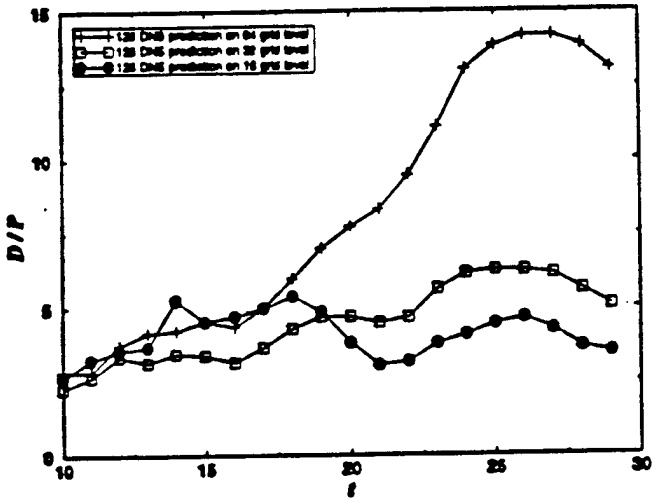

Figure 2. Unscaled spectra of the energy (E) and the dissipation (D) computed from 128^3 DNS data at t=29.

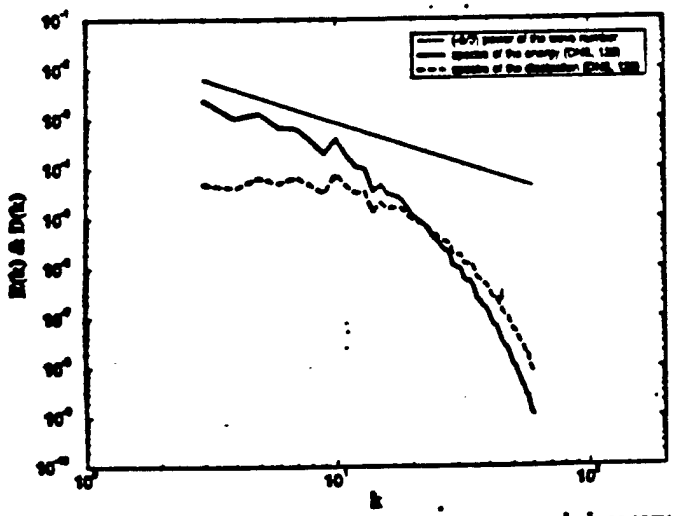

Figure 3. Comparison of the Kolmogorov scaled energy spectra for DNS and LES with various dynamic SGS models at t=29.

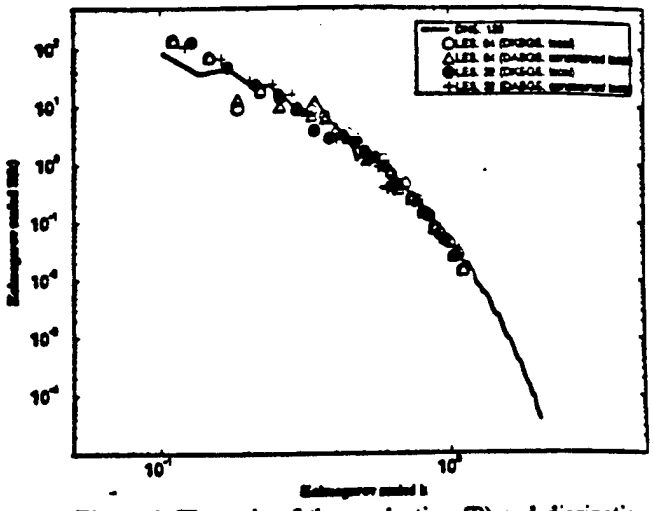

Figure 4. The ratio of the production (P) and dissipation (D) rates of the SGS kinetic energy computed from 128^3 DNS data.

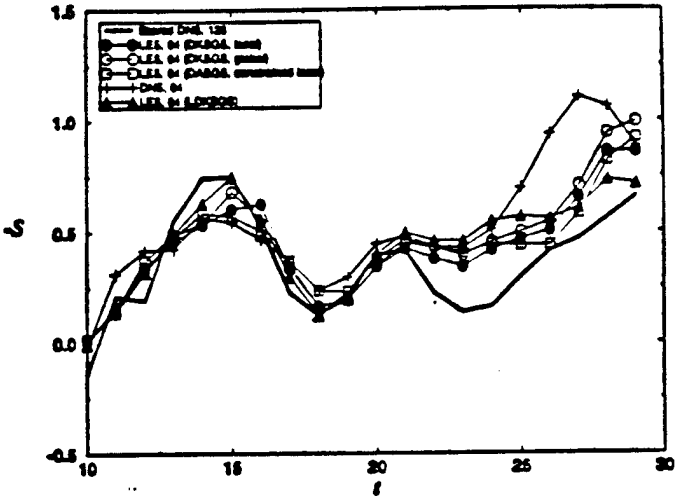

Figure 5. Comparison of the velocity-derivative skewness factor (S) for DNS and LES with various dynamic SGS models on a 64^3 grid.

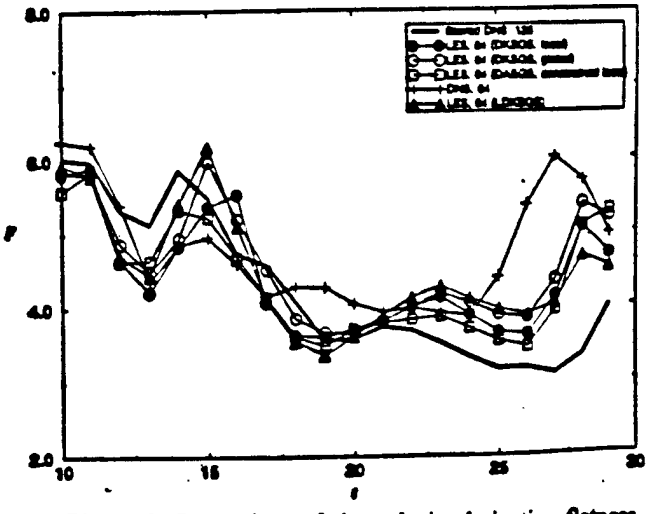

Figure 6. Comparison of the velocity-derivative flatness factor (F) for DNS and LES with various dynamic SGS models on a 64^3 grid.

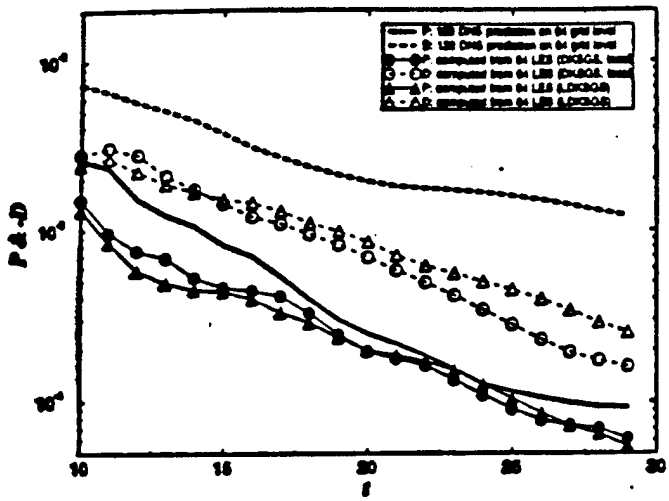

Figure 7. Comparison of the production (P) and dissipation (D) rates of the SGS kinetic energy for DNS and LES with various dynamic SGS models on a 64^3 grid.

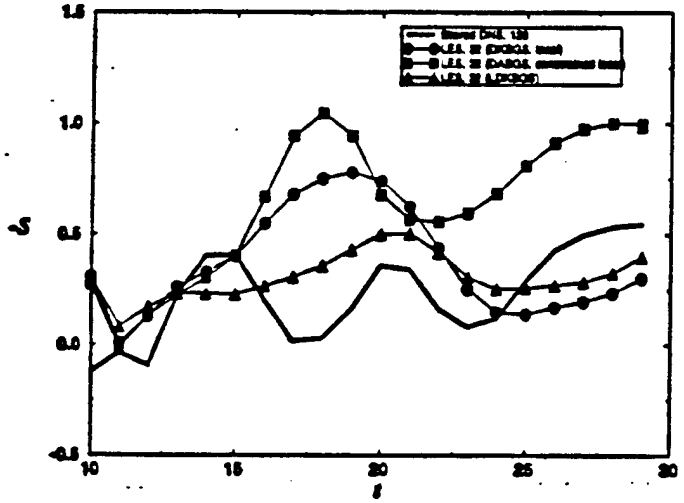

Figure 8. Comparison of the velocity-derivative skewness factor (S) for DNS and LES with various dynamic SGS models on a 32^3 grid.

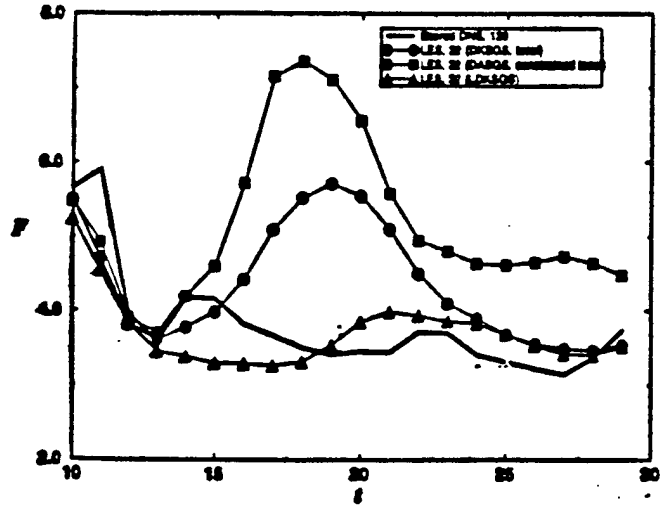

Figure 9. Comparison of the velocity-derivative flatness factor (F) for DNS and LES with various dynamic SGS models on a 32^3 grid.

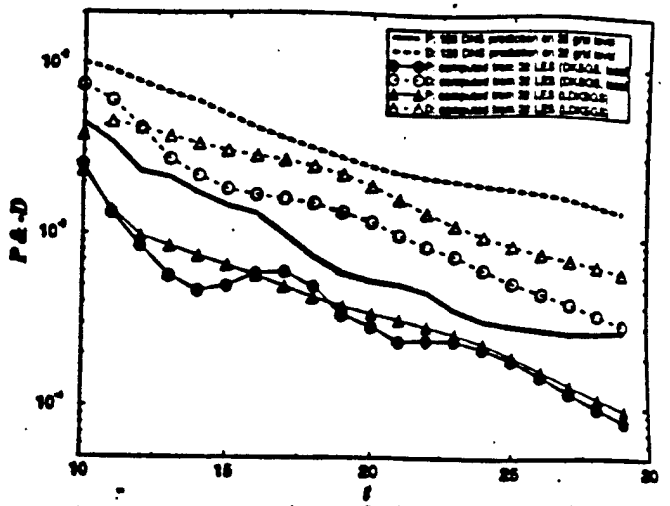

Figure 10. Comparison of the production (P) and dissipation (D) rates of the SGS kinetic energy for DNS and LES with various dynamic SGS models on a 32^3 grid.

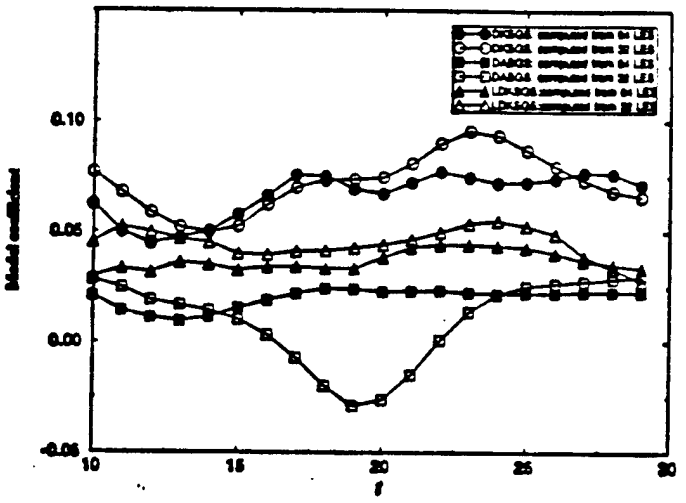

Figure 11. The time evolution of the model coefficients for dynamic SGS models.

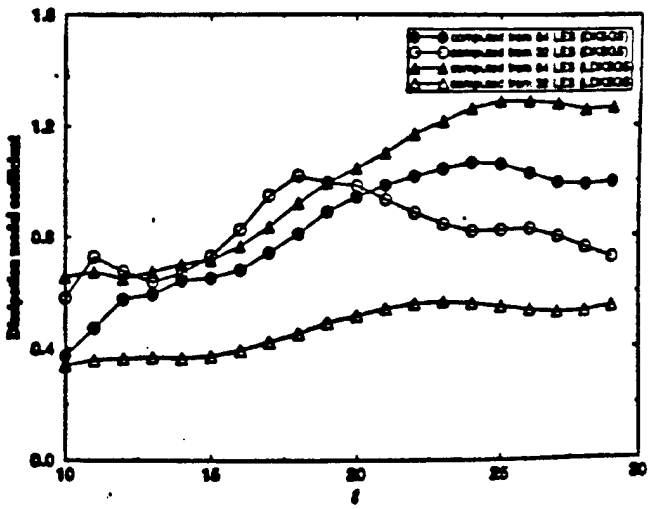

Figure 12. The time evolution of the dissipation model coefficients for dynamic one-equation SGS models.